PhD Thesis

Josephson junctions, quantum interference devices and applications in the field of dark matter search

Alessandro Giordano

Contents

3 Double and triple-barrier Josephson junctions

4 I-V characteristics for triple-barrier Josephson junction

5 Semi-classical and quantum analysis of the one-junction and two-junction interferometer

6   Application of SQUIDs in Dark Matter search

Conclusions   165

Bibliography   168

Acknowledgements   178

Introduction

In this PhD Thesis, I and my supervisor, Prof. Roberto De Luca, have analyzed some particular superconducting devices, the Josephson Junctions and the SQUIDs (Superconducting Quantum Interference Devices), from a semi-classical and quantum mechanical point of view. With the collaboration of some Russian professors, i. e. the Professors Larisa Zherikhina and Andrej Tshovrebov of the Lebedev Institute of RAS (Russian Academy of Sciences), in Moscow, Russia and the Prof. George Izmailov of the MAI (Moscow Aviation Institute), also in Moscow. Application of these devices (in particular of SQUIDs) as detectors of Dark Matter has been considered.

We first describe our theoretical activity about Josephson Junctions and SQUIDs, and then we underline the role of SQUIDs as detectors of Dark Matter, in some particular applications that we have considered.

We start with the microscopic analysis of a linear chain of N superconductors, for which we have considered interactions between first neighbouring sites. In the particular case of N = 2 coupled superconductors, so that they form a Josephson Junction, we have obtained the same relations characterizing the Feynman model, which describes, from a quantum mechanical point of view, this system. The results confirm the validity of Ohta's semi-classical model, that represents the extension of Feynman's model to a Josephson junction connected to an external f.e.m. source.

We have then analysed the theoretical properties of the Double Barrier Josephson Junction (DBJJ) and the Triple Barrier Josephson Junction (TBJJ).

For the DBJJ, a three layer superconducting system, in which the intermediate layer is considered as a pure quantum system, we have considered non-homogeneous couplings between the superconducting layers 1-2 and 2-3. The coupling constant between the superconducting layers 1-3 is taken to be small compared to the first ones.

For the TBJJ, a four layer superconducting system, in which the inner two superconducting layers are treated as pure quantum mechanical systems, the coupling constants between the layers 1-2, 2-3 and 3-4 are different, so also in this case we have non-homogeneous couplings, and the coupling constants between 1-3 and 2-4 are considered smaller than the previous ones. For sake of simplicity, we take the superconducting phase difference of the inner layers 2 and 3 equal to zero. Under these hypotheses, by using Ohta's semi-classical model, we have obtained the current phase relation (CPR) for these systems. It is seen that these devices are different from the sinusoidal one, characterizing the simple Josephson Junction (SJJ), and is in good agreement both with the theoretical results obtained by Brinkmann, based on a microscopic approach, and also with the experimental results found by Nevirkovets et al. The latter results are based on the observation of the Shapiro steps, and the analysis of their amplitudes as a function of the applied voltage.

The voltage- current characteristics of a TBJJ, with the previously considered properties, have been analytically and numerically studied, both in the case of homogeneous coupling between all the superconducting layers and also in the non-homogeneous one. In the homogeneous case, and considering also a constant bias of electric current, the voltage-current characteristic of a TBJJ has an analytic form very similar to the one of a SJJ, despite a TBJJ has a non-canonical CPR. Of course, in the case of a TBJJ, we have an opportune value of the constant of normalization for the current, which is different from the corresponding value for a SJJ.

However, in the case of inhomogeneous coupling between different layers in the TBJJ, we obtain a deviation from this behaviour. In the presence of a radio frequency radiation, integer and fractional Shapiro steps are predicted, whose amplitudes, calculated in the homogeneous case, are a clear indication of the non-canonical CPR of these systems.

After these theoretical remarks about Josephson Junctions, we describe a mechanical analogy between a Josephson Junction and a simple pendulum, in the over-damped limit. This condition, in the case of a simple pendulum, indicates that the medium is characterized by a large value of the coefficient of viscosity, while, in the case of a Josephson Junction, denotes negligible capacitive effects between the two superconducting electrodes. In this situation, we have found that the dynamical equation of a simple pendulum is formally equivalent to the one of a Josephson Junction. This mechanical analogy can also be used for didactical purposes in order to grasp further information about the voltage- current relation of over-damping Josephson Junctions.

A further topic treated in the present work has been the semi-classical and quantum analysis of one-junction and two-junction quantum interference devices. These systems consist of a superconducting loop interrupted by one or two Josephson junctions. Starting from a review of the semi-classical and quantum properties of one-junction interference devices, we have extended our analysis to two-junction interferometers. In particular, we have determined the Hamiltonian function for this system in the semi-classical limit, and the Hamiltonian operator in the corresponding quantum case limited to a Hilbert space spanned by the flux number kets $|0\rangle$ and $|1\rangle$. In the condition of a negligible value of the superconducting loop inductance, we have also calculated, in the quantum regime, the energy and the electric current for these two representative states.

As for the second part of the PhD thesis accomplished with the collaboration of the Russian professors mentioned before, the application of superconductor devices, in particular of SQUIDs, as detectors of Dark Matter has been analysed. In this way, an introduction of the problem of Dark Matter in the modern cosmology has been given. In particular, two important experiments for the registration of Dark Matter particles, one based on Josephson Junctions and the other one based on the use of SQUID, have been analysed. The first experiment uses a multi-channel detector, made up by a set of weakly coupled superconductors, so that they form a system of Josephson Junctions, displaced in the geometrical form of a matrix. The second experiment is a system made up by a paramagnetic calorimeter connected with a SQUID, by which it is possible to register the rate of interaction of Dark Matter particles, and also the energy release with the atoms of the material. In fact, there are several modes of operation of this experimental apparatus, and in particular we have focused on the dual channel mode of operation, in order to reduce the lepton background noise corresponding to the registration process.

After these considerations, we have dedicated to the analysis of the possible creation of a magnetic moment for Dark Matter particles: if they possess this magnetic moment they can electromagnetically interact with the common matter, and we have calculated that the cross section of this interaction is 9 orders of magnitude larger than the contact interaction with the atomic nucleus.

We have also overviewed a theoretical model exploring the possibility that Dark Matter and Dark Energy are two aspects of the same Cosmological Essence, defined "Dark Substance". According to this theoretical model, Dark Energy represents the unperturbed state of Dark Substance, while Dark Matter particles play the role of swings or perturbations of it. These perturbations will be stable if all their decay channels are blocked, and also, more interestingly for our case, if they are in their

state of lowest relative energy minimum, where they coincide with the particles we can experimentally register. In fact, the potential energy of the perturbed state of Dark Substance presents some positions of relative minimum, which act as traps for its metastable excited states.

In these positions of relative minimum, the Dark matter particles are in an excited state, so instable, while in the lowest position of relative minimum they are stable, and so do not decay, according to the main property of Dark Matter particles. On the other hand, the position of absolute minimum is occupied by Dark Energy, as in this theoretical model Dark Energy represents the unperturbed state of Dark Substance.

We have finally described two types of experimental systems, which are suitable for Dark Matter registration in the two cases considered above. In particular, for the registration of Dark Matter into the form of particles, we propose use of a SQUID-paramagnetic absorber, while for the registration of a flux of Dark Matter, or equivalently, according to the theoretical model of Dark Substance, of a corpuscular flux of Dark Energy, we propose use of a SQUID-magnetostrictor.

Chapter 1

From microscopic to macroscopic description of Josephson dynamics

In this chapter we consider a theoretical model, based on quantum mechanics, of the Josephson dynamics. In particular, we analyse an array of N coupled superconductors, in which we consider only the interaction between nearest neighbour sites. By using some properties of the quantum operators algebra, and the Heisenberg picture in quantum mechanics, we obtain a particular set of linear differential equations. With opportune considerations, we can adapt this description to only two coupled superconductors, and so we finally obtain two differential linear equations, which are similar to those derived by Feynman in his celebrated model for Josephson junctions.

1.1 Introduction

The dynamics of two weakly-coupled superconductors was first predicted by Josephson in 1963 [1]. Successively, a simple and celebrated model of a Josephson junction (JJ) was proposed by Feynman [2]. Even though Feynman's description of a JJ is useful in considering a two-level quantum system in which the interacting condensates are not perturbed by an external classical system, the case in which an external voltage source is applied across the JJ has been fully taken into account by Ohta [3]. In this respect, an analysis taking from a microscopic Hamiltonian to the Feynman equations for a Josephson junction is still lacking. More recently, after the discovery of high-temperature superconductors [4], models of one-dimensional arrays of Josephson junctions [5-7] have been widely adopted in the study of the physical properties of granular superconducting systems.

In the present chapter we perform a microscopic analysis of N coupled superconductors in which nearest-neighbour interactions are present. We define the dynamics of the order parameter of each superconducting element by recurring to the Heisenberg picture for fermionic operators. In this way, a set of coupled ordinary differential equations (ODEs) is obtained. When specializing this system of ODEs to only two coupled superconductors, Feynman's model can be obtained. These results confirm the correspondence between the microscopic picture proposed in the present chapter and, by generalizing to a non-isolated JJ, the semi-classical analysis given by Ohta. In this way, further generalization of Ohta's model to multi-barrier Josephson junctions [8] based on the semi-classical analysis can be retained to agree with a strict microscopic description of these types of junctions, lately proposed for application in fabricating innovative quantum interference devices [9-10].

1.2 Feynman's model

In this section, we consider Feynman's model and Ohta's semi-classical model [2], [3], for the description of the dynamics of a Josephson Junction JJ, (i.e. a system made up by two weakly coupled superconductors, S_1 *and* S_2), that is based on the Josephson's equations:

$$I = I_{J,0} sen\varphi$$
$$V = \frac{\Phi_0}{2\pi} \frac{d\varphi}{dt}$$
(1.1)

where I is the superconducting current flowing through the insulating barrier, $I_{J,0}$ being its maximum value, $\varphi = \theta_2 - \theta_1$ is the superconducting phase difference across the JJ, in which θ_1 and θ_2 are the superconducting phases of the k-th electrode, V is the voltage drop through the JJ, and $\Phi_0 = \frac{h}{2e}$ is the elementary flux quantum, expressed as the ratio of Planck's constant h, and of the absolute value of the Cooper pair charge *2e*.

We start by noticing that the superconducting phases θ_1 and θ_2 are defined in the wave functions of the considered superconductors:

$$\psi_1 = \sqrt{N_1} e^{-i\theta_1} \;\; ; \;\; \psi_2 = \sqrt{N_2} e^{-i\theta_2},$$
(1.2)

where N_k is the number density of Cooper pairs. We can sketch a Josephson junction in the next figure 1.1.
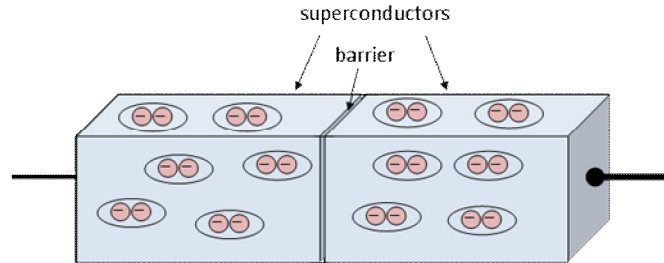
Figure 1.1. *A Josephson junction. This device is made up by two pieces of superconducting materials, separated by a very thin insulating barrier.*

The Feynman's model [2] is a pure quantum mechanics model, which is able [11] to derive only the first of the equations (1.1), the so called Current-Phase Relation (CPR), but it is not able to derive the second one, that is called Voltage-Frequency Relation (VFR). In fact, it does not provide a consistent account of the external bias circuit, which has a parallel connection with the JJ, as shown in figure 1.2.

This drawback was solved by Ohta [2], [3], who introduced a semi-classical model based on a rigorous quantum derivation, in which an additional term, due to energy contribution of the external classical circuit biasing the JJ, is added. Let us consider, the analytic description of these two models.

Starting with Feynman's model, which is, as just said, a quantum mechanical model, we can describe [11] the dynamics of JJ by using the Schroedinger equation:

$$i\hbar \frac{\partial \psi}{\partial t} = \hat{H}_0 \psi ,$$

(1.3)

where $\psi = \begin{pmatrix} \psi_1 \\ \psi_2 \end{pmatrix}$ and ψ_1 and ψ_2 have been defined in equation (1.2).
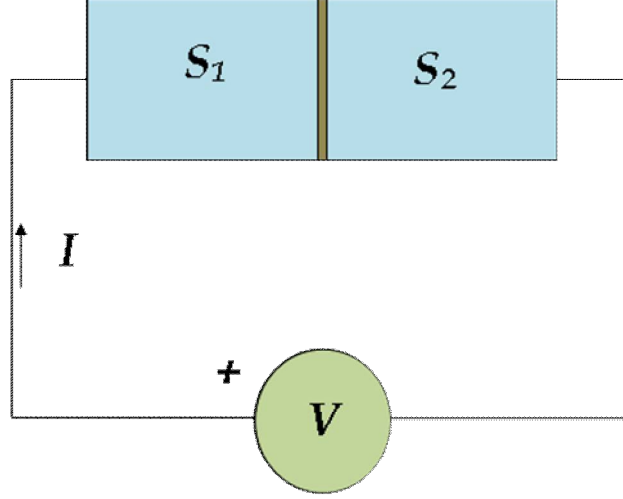
Figure 1.2. *A schematic representation of Josephson junction with both electrodes connected to an external classical circuit.*

We can calculate the matrix expression of the Hamiltonian operator $\hat{H}_0$; it is made up by the summation of three terms:

$$\hat{H}_0 = \hat{H}_1 + \hat{H}_2 + \hat{H}_K ,$$

(1.4)

where $\hat{H}_1 = E_1 |\psi_1\rangle\langle\psi_1|$ is the Hamiltonian operator of the superconductor 1, $\hat{H}_2 = E_2 |\psi_2\rangle\langle\psi_2|$ is the Hamiltonian operator of the superconductor 2, and $\hat{H}_K = -K(|\psi_1\rangle\langle\psi_2| + |\psi_2\rangle\langle\psi_1|)$ is the Hamiltonian operator describing the interaction between the two superconductors. By considering that the vectors $|\psi_1\rangle$ and $|\psi_2\rangle$ constitute an orthonormal set, we know that:

$$\langle\psi_i|\psi_j\rangle = \delta_{i,j} = \begin{cases} 1 & for\ i = j \\ 0 & for\ i \neq j \end{cases}$$

(1.5)

So, if we calculate the matrix elements of the operator $\hat{H}_0$:

$$(\hat{H}_0)_{ij} = \langle\psi_i|\hat{H}_0|\psi_j\rangle = \begin{cases} E_i & for\ i = j \\ -K & for\ i \neq j \end{cases}$$

we get:

$$\hat{H}_0 = \begin{pmatrix} E_1 & -K \\ -K & E_2 \end{pmatrix} . \qquad (1.6)$$

By now substituting (1.6) in (1.3), and making the matrix product, we have:

$$i\hbar \frac{\partial}{\partial t}\begin{pmatrix} \psi_1 \\ \psi_2 \end{pmatrix} = \begin{pmatrix} E_1 & -K \\ -K & E_2 \end{pmatrix}\begin{pmatrix} \psi_1 \\ \psi_2 \end{pmatrix} \Rightarrow$$

$$\begin{cases} i\hbar \dfrac{\partial \psi_1}{\partial t} = E_1\psi_1 - K\psi_2 \\[2mm] i\hbar \dfrac{\partial \psi_2}{\partial t} = E_2\psi_2 - K\psi_1 \end{cases} \qquad (1.7)$$

If we express the scalar wave functions as in (1.2), we get, from the first equation:

$$\frac{i\hbar}{2\sqrt{N_1}}\frac{dN_1}{dt}e^{-i\theta_1} + \sqrt{N_1}e^{-i\theta_1}\hbar\frac{d\theta_1}{dt} = E_1\sqrt{N_1}e^{-i\theta_1} - K\sqrt{N_2}e^{-i\theta_2} .$$

If we now multiply both members by $\dfrac{e^{i\theta_1}}{\sqrt{N_1}}$, we obtain:

$$\hbar\frac{d\theta_1}{dt} + \frac{i\hbar}{2N_1}\frac{dN_1}{dt} = E_1 - K\sqrt{\frac{N_2}{N_1}}e^{-i\varphi} , \qquad (1.8)$$

where $\varphi = \theta_2 - \theta_1$ is the superconducting phase difference. By doing the same for the second equation, in particular, by multiplying both members of the second equation by $\dfrac{e^{i\theta_2}}{\sqrt{N_2}}$, we obtain:

$$\hbar\frac{d\theta_2}{dt} + \frac{i\hbar}{2N_2}\frac{dN_2}{dt} = E_2 - K\sqrt{\frac{N_1}{N_2}}e^{i\varphi} . \qquad (1.9)$$

By expressing $e^{i\phi} = \cos\phi + i\sin\phi$, from (1.8), we get:

$$\hbar\frac{d\theta_1}{dt} + \frac{i\hbar}{2N_1}\frac{dN_1}{dt} = E_1 - K\sqrt{\frac{N_2}{N_1}}\cos\varphi - i\left(-K\sqrt{\frac{N_2}{N_1}}\right)\sin\varphi . \qquad (1.10)$$

So, equating the real and the imaginary part of both members of this expression, we get:

$$\hbar \frac{d\theta_1}{dt} = E_1 - K \sqrt{\frac{N_2}{N_1}} \cos\varphi$$

$$\frac{\hbar}{2N_1} \frac{dN_1}{dt} = K \sqrt{\frac{N_2}{N_1}} \sin\varphi$$

In the same way, from the expression:

$$\hbar \frac{d\theta_2}{dt} + \frac{i\hbar}{2N_2} \frac{dN_2}{dt} = E_2 - K \sqrt{\frac{N_1}{N_2}} \cos\varphi + i\left(-K \sqrt{\frac{N_1}{N_2}}\right) \sin\varphi \qquad (1.11)$$

we get:

$$\hbar \frac{d\theta_2}{dt} = E_2 - K \sqrt{\frac{N_1}{N_2}} \cos\varphi$$

$$\frac{\hbar}{2N_2} \frac{dN_2}{dt} = -K \sqrt{\frac{N_1}{N_2}} \sin\varphi$$

Therefore, we obtain:

$$\frac{dN_2}{dt} = -\frac{2KN_2}{\hbar} \sqrt{\frac{N_1}{N_2}} \sin\varphi = -\frac{2K}{\hbar} \sqrt{N_1 N_2} \sin\varphi = -\frac{dN_1}{dt}.$$

The relation $\frac{dN_2}{dt} = -\frac{dN_1}{dt} = -\frac{2K}{\hbar} \sqrt{N_1 N_2} \sin\varphi$ satisfies the principle of charge conservation, since we can interpret the term $-2eN_i$ with $i = 1, 2$ as the electric charge density for unitary volume inside the i-th superconductor, and so the time variation of it represents the electric current flowing from a superconductor to the other one. Therefore, by multiplying the equation $\frac{dN_2}{dt} = -\frac{2K}{\hbar} \sqrt{N_1 N_2} \sin\varphi$ by the term -2e in both members, we obtain:

$$I = I_{j,0} \sin\varphi,$$

where $I = \frac{d(-2eN_2)}{dt}$ which is the electric current, made up by Cooper pairs, flowing between the superconductors, and $I_{J,0} = \frac{4eK}{\hbar} \sqrt{N_1 N_2}$.

In this way, we notice that, by using the Feynman model, we have obtained the first Josephson equation, i.e. the CPR. This means that the Feynman model is able to describe the CPR of a Josephson junction.

As far as the second Josephson equation (i.e. the VFR) is concerned, we can consider that, by subtracting from the expression of $\hbar \frac{d\theta_2}{dt}$ the one of $\hbar \frac{d\theta_1}{dt}$ and by doing calculations, we get:

$$\hbar\frac{d}{dt}(\theta_2 - \theta_1) = E_2 - K\sqrt{\frac{N_1}{N_2}}\cos\varphi - \left(E_1 - K\sqrt{\frac{N_2}{N_1}}\cos\varphi\right) \Rightarrow$$

$$\hbar\frac{d}{dt}(\theta_2 - \theta_1) = (E_2 - E_1) - K\left(\sqrt{\frac{N_1}{N_2}} - \sqrt{\frac{N_2}{N_1}}\right)\cos\varphi.$$

By taking $\phi = \theta_2 - \theta_1$ and $E_2 - E_1 = 2eV$ we finally obtain:

$$\frac{d\phi}{dt} = \frac{2eV}{\hbar} - \frac{K}{\hbar}\left(\sqrt{\frac{N_1}{N_2}} - \sqrt{\frac{N_2}{N_1}}\right)\cos\varphi. \tag{1.12}$$

In order to obtain from this equation the VFR, we must have that $N_1 = N_2$; this latter relation, however, is not consistent with conservation of electric charge $\dot{N}_1 + \dot{N}_2 = 0$. Therefore, we may conclude that the Feynman model does not provide a proof of the strict voltage-frequency Josephson relation (VFR). The importance of Feynman model, however, rests in the fact that a single JJ can be considered, at least in first approximation, as an isolated quantum system, which verifies the current-phase relation (CPR). Furthermore, Feynman's model can be applied to any weakly coupled two-level quantum system as long as it does not interact with the classical world.

1.3 Ohta's semi-classical model

In his important work [3], Ohta stated that he had long been puzzled by the fact that one could not achieve a strict VFR by means of the Feynman model. He thus developed a rigorous semi-classical analysis which took into account the contribution due to the external circuit. We shall here give a simplified account [11] of the more complete analysis given by Ohta.
Starting from quantum mechanical considerations, Ohta first recovered Feynman's Hamiltonian.
However, considering the classical nature of the problem (the system made up by the external circuit and the JJ), Ohta projected Feynman results onto the classical world. A way to do this is to consider the classically observable energy:

$$H_0 = \langle\psi|\hat{H}_0|\psi\rangle. \tag{1.13}$$

Carrying out the calculations, we find:

$$H_0 = \begin{pmatrix}\psi_1^* & \psi_2^*\end{pmatrix}\begin{pmatrix}E_1 & -K \\ -K & E_2\end{pmatrix}\begin{pmatrix}\psi_1 \\ \psi_2\end{pmatrix} = E_1\psi_1^*\psi_1 - K\psi_1^*\psi_2 - K\psi_1\psi_2^* + E_2\psi_2^*\psi_2 = E_1|\psi_1|^2 + E_2|\psi_2|^2 - K\psi_1^*\psi_2$$

$$- K\psi_1\psi_2^* = E_1 N_1 + E_2 N_2 - K\sqrt{N_1 N_2}e^{-i(\theta_2-\theta_1)} - K\sqrt{N_1 N_2}e^{i(\theta_2-\theta_1)} = E_1 N_1 + E_2 N_2 - 2K\sqrt{N_1 N_2}\left(\frac{e^{i(\theta_2-\theta_1)} + e^{-i(\theta_2-\theta_1)}}{2}\right).$$

So, we get:

$$H_0 = E_1 N_1 + E_2 N_2 - 2K\sqrt{N_1 N_2}\cos(\theta_2 - \theta_1). \tag{1.14}$$

This is only one portion of the classical Hamiltonian related to the whole system in figure 1.2. The remaining portion is given by the energy provided by the circuit, which can be written as

$W = \int IV dt$, typical form of an electromagnetic energy. In this way, the classical complete Hamiltonian can be written as follows:

$$H = H_0 - W = E_1 N_1 + E_2 N_2 - 2K\sqrt{N_1 N_2}\cos(\theta_2 - \theta_1) - W . \tag{1.15}$$

The minus sign near the expression for W is due to the fact that it represents an energy transferred from the external environment to the system.

The transition to the classical world is, in this way, complete so that a solution to the problem by classical mechanics can be found. First, let us note that θ_k and $\hbar N_k$ are conjugate variables (angle-action variables, for $k = 1, 2$). Hamilton's equations thus give:

$$\hbar \dot{N}_k = -\frac{\partial H}{\partial \theta_k} \tag{1.16a}$$

$$\dot{\theta}_k = \frac{1}{\hbar}\frac{\partial H}{\partial N_k} \tag{1.16b}$$

for $k = 1, 2$, where the dot represents the time derivative.

By now defining the coupling energy as $E_C = -2K\sqrt{N_1 N_2}\cos(\theta_2 - \theta_1)$, and by setting

$$E_R = E_C - W , \tag{1.17}$$

we may rewrite the above equations as follows:

$$\hbar N_k = -\frac{\partial E_R}{\partial \theta_k} \tag{1.18a}$$

$$\dot{\theta}_k = \frac{E_k}{\hbar} + \frac{1}{\hbar}\frac{\partial E_R}{\partial N_k} \tag{1.18b}$$

for $k = 1, 2$. Let us now consider the time derivative of E_R; by using the theorem of total differential we get:

$$\dot{E}_R = \sum_{k=1}^{2}\left(\frac{\partial E_R}{\partial N_k}\dot{N}_k + \frac{\partial E_R}{\partial \theta_k}\dot{\theta}_k\right). \tag{1.19}$$

By using the relations (1.18a) and (1.18b), we obtain:

$$\dot{E}_R = \sum_{k=1}^{2}\frac{\partial E_R}{\partial N_k}\left(-\frac{1}{\hbar}\frac{\partial E_R}{\partial \theta_k}\right) + \frac{\partial E_R}{\partial \theta_k}\left(\frac{E_k}{\hbar} + \frac{1}{\hbar}\frac{\partial E_R}{\partial N_k}\right) = \sum_{k=1}^{2}\frac{\partial E_R}{\partial \theta_k}\frac{E_k}{\hbar} = \sum_{k=1}^{2}(-\hbar\dot{N}_k)\frac{E_k}{\hbar} .$$

So we get:

$$\dot{E}_R = \sum_{k=1}^{2}(-\dot{N}_k E_k) = -(E_1\dot{N}_1 + E_2\dot{N}_2) \ .$$

If we set $E_1 = -eV$ and $E_2 = eV$, so that $E_2 - E_1 = 2eV$, we find:

$$E_R = \int \dot{E}_R dt = \int -(E_1\dot{N}_1 + E_2\dot{N}_2) = -\int (E_1\dot{N}_1 + E_2\dot{N}_2)dt = -eV\int (\dot{N}_2 - \dot{N}_1)dt \ . \qquad (1.20)$$

Let us now consider the Josephson Junction to be in a thermal bath, which is the condition indicating that the temperature is uniform and constant in all the thermodynamic system considered, so that $\dot{N}_1 = \dot{N}_2 = 0$. In this way, the charge conservation relation $\dot{N}_1 + \dot{N}_2 = 0$ becomes a trivial identity and the function E_R is seen to be zero. We may also notice that, for constant values of E_1 and E_2, the Hamiltonian H is a constant of motion, so that the energy of the system is conserved. By using these results, in particular the relation (1.18b), we have:

$$\dot{\theta}_k = \frac{E_k}{\hbar} \qquad (1.21)$$

for k = 1, 2. This relation leads directly to the VFR, in fact, by knowing that $\dot{\theta}_2 - \dot{\theta}_1 = \dfrac{E_2 - E_1}{\hbar} = \dfrac{2eV}{\hbar}$ and by denoting by $\varphi = \theta_2 - \theta_1$ the difference between the superconducting phases of the electrodes in the Josephson Junction, we obtain:

$$\dot{\varphi} = \frac{2eV}{\hbar} \ . \qquad (1.22)$$

The above expression is the strict form of the VFR sought.

In addition, if we look in details at the condition of thermal bath, according to which $E_R = 0 \Rightarrow \dot{E}_R = 0$, we have:

$$\dot{E}_C = \dot{W} \Rightarrow 2(\dot{\theta}_2 - \dot{\theta}_1)K\sqrt{N_1 N_2}\sin(\theta_2 - \theta_1) = IV$$

By using the relation (1.22) we get:

$$I = \frac{4eK}{\hbar}\sqrt{N_1 N_2}\sin\varphi \ . \qquad (1.23)$$

Equation(1.23) is just the CPR for a Josephson Junction, expressed in the relation (1.1).

1.4 *N* coupled superconductors

In order to prove that Feynman model indeed follows from a microscopic analysis of the superconducting system, we can start by considering [12] the Hamiltonian operator $\hat{H}$ for an array of *N* nearest neighbour superconductors:

$$\hat{H} = \sum_{i,\sigma} \varepsilon_i \hat{c}_{i,\sigma}^+ \hat{c}_{i,\sigma} + \sum_i (\Delta_i \hat{c}_{i,\downarrow}^+ \hat{c}_{i,\uparrow}^+ + h.c.) - \sum_{i,\sigma} (K_{i,i+1} \hat{c}_{i+1,\sigma}^+ \hat{c}_{i,\sigma} + h.c.), \qquad (1.24)$$

where $i = 1, 2, \ldots, N$ is the index labelling the superconductors, σ is the spin index, which assumes only the two values $\uparrow, \downarrow$ (spin up and spin down), $K_{i,i+1}$ is the coupling constant between the superconductors i and i+1, which describes the electromagnetic interaction between two electrons, each one in a different site (*i* or i +1), $\hat{c}$ *and* $\hat{c}^+$ are the operators of destruction and creation, and h.c. stands for hermitian conjugate. For example, the hermitian conjugate of the operator $\Delta_i \hat{c}_{i,\downarrow}^+ \hat{c}_{i,\uparrow}^+$ is the operator $\Delta_i^* \hat{c}_{i,\uparrow} \hat{c}_{i,\downarrow}$, in which, by the symbol * we denote the complex conjugate of a function or of a constant. In the same way, the hermitian conjugate of the operator $K_{i,i+1} \hat{c}_{i+1,\sigma}^+ \hat{c}_{i,\sigma}$ is the operator: $K_{i,i+1}^* \hat{c}_{i,\sigma}^+ \hat{c}_{i+1,\sigma}$. In these expressions we have also considered the term Δ_i, defined in the following way :

$$\Delta_i = \left\langle \hat{c}_{i,\uparrow} \hat{c}_{i,\downarrow} \right\rangle . \qquad (1.25)$$

The quantity Δ_i is thus the time dependent expectation value of the product of two destruction operators. This quantity can be identified with the order parameter, being it proportional to the numerical density of Cooper pairs.
We can sketch this system, and the interactions among its superconductors in the next figure 1.3.
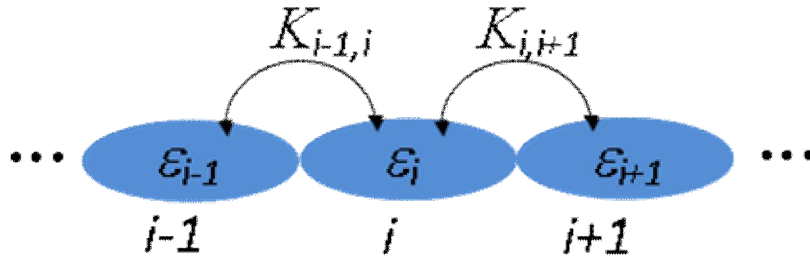
Figure 1.3. *Schematic representation of a one-dimensional array of weakly coupled superconducting islands. The coupling constant between the adjacent sites i and i+1 is denoted by $K_{i,i+1}$.*

The Hamiltonian operator written in (1.24), which can act on the superconducting wave function of a single electron on the site *i*, for $i = 1, 2, \ldots, N$, is made up by the sum of three terms (that are three summations).
The first term, $\hat{H}_0 = \sum_{i,\sigma} \varepsilon_i \hat{c}_{i,\sigma}^+ \hat{c}_{i,\sigma}$, as usual, describes the kinetic properties of electrons. The scalar quantity ε_i is the energy of an electron; so the analytic expression of $\hat{H}_0$ represents the total kinetic energy of the electrons present on the *N* superconductors.
The second term, denoted as $\hat{H}_S$, describes the coupling potential energy of a single pair of electrons, both present on the same superconductor, represented by the index *i*, (it's well known, in the theory of superconductivity, that these electrons, through their electromagnetic interaction with

the ions of lattice, become a Cooper pair). By carrying out the summation on all the N superconductors, we get all the possible interactions between the electrons present on each of these superconductors, as represented by the analytic expression of H_S.

The third term, denoted as $\hat{H}_K$, describes the interaction potential energy between electrons on next neighbouring superconductors. In the analytic expression of $\hat{H}_K$, we notice that $K_{i,i+1}$ is the coupling constant between two next neighbouring superconductors (i and $i+1$), the operator $\hat{c}_{i+1,\sigma}^+$ creates an electron on the superconductor $i+1$, and the operator $\hat{c}_{i,\sigma}$ destroys an electron on the superconductor i; in the same way, the hermitian conjugated operator h.c., defined before in expression (1.24), destroys an electron on the site $i+1$ and creates it on the site i. So, an electron is induced to pass (or we may say to jump) from a superconductor to the next one, and for this reason, the term $\hat{H}_K$ can be defined "hopping term". It is interesting to notice that one could arrive to a similar analytic expression of the Hamiltonian by considering a Fermi- Hubbard model with an attractive interaction [13], and also by a mean-field approximation giving the definition of the order parameter in (1.25).

Once we have described [12] the analytic properties of the Hamiltonian operator $\hat{H}$, let us consider the time evolution of the function Δ_i, which, as just considered, can be interpreted as the wave function ψ_i of the superconducting state on the site i. In order to analyse the time evolution of this quantity, for which :

$$i\hbar \frac{\partial}{\partial t} \hat{c}_{i,\sigma} = \left[\hat{c}_{i,\sigma}, \hat{H} \right]. \tag{1.26}$$

For sake of simplicity, we can denote the symbol $\dfrac{\partial}{\partial t}$ as ∂_t.

The fermionic operators $\hat{c}_{i,\sigma}$ obey to the following anti-commutation rules:

$$\left\{ \hat{c}_{i,\sigma}, \hat{c}_{j,\sigma'} \right\} = 0 \;\; ; \;\; \left\{ \hat{c}_{i\sigma}, \hat{c}_{j,\sigma'}^+ \right\} = \delta_{ij}\delta_{\sigma\sigma'} \;\; ; \;\; \left\{ \hat{c}_{i,\sigma}^+, \hat{c}_{j,\sigma'}^+ \right\} = 0 . \tag{1.27}$$

So, we get:

$$i\hbar \partial_t \psi_i = i\hbar \partial_t \left\langle \hat{c}_{i,\uparrow} \hat{c}_{i,\downarrow} \right\rangle = i\hbar \left\langle \left[\hat{c}_{i,\uparrow}, \hat{H} \right] \hat{c}_{i,\downarrow} \right\rangle + i\hbar \left\langle \hat{c}_{i,\uparrow} \left[\hat{c}_{i,\downarrow}, \hat{H} \right] \right\rangle . \tag{1.28}$$

By using the relations (1.27), and the property:

$$\left[\hat{A}, \hat{B}\hat{C} \right] = \left\{ \hat{A}, \hat{B} \right\} \hat{C} - \hat{B} \left\{ \hat{A}, \hat{C} \right\}$$

we can calculate the two terms $\left[\hat{c}_{i,\uparrow}, \hat{H} \right]$ and $\left[\hat{c}_{i,\downarrow}, \hat{H} \right]$.

Therefore, knowing that $\hat{H} = \hat{H}_0 + \hat{H}_S + \hat{H}_K$ we get:

$$\left[\hat{c}_{i,\sigma}, \hat{H}_0 \right] = \varepsilon_i \hat{c}_{i,\sigma} \;\; ; \;\; \left[\hat{c}_{i,\sigma}, \hat{H}_S \right] = \psi_i (\hat{c}_{i,\uparrow}^+ \delta_{\sigma,\downarrow} - \hat{c}_{i,\downarrow}^+ \delta_{\sigma,\uparrow}) \;\; ; \;\; \left[\hat{c}_{i,\sigma}, \hat{H}_K \right] = -K_{i-1,i} \hat{c}_{i-1,\sigma} - K_{i+1,i} \hat{c}_{i+1,\sigma} \tag{1.29}$$

where $\sigma = \uparrow, \downarrow$.

By using these results for the operators of commutation, and by doing all the calculations, inside (1.28), if we consider the operators

$$\hat{n}_i = \hat{c}_{i,\uparrow}^+ \hat{c}_{i,\uparrow} = \hat{c}_{i,\downarrow}^+ \hat{c}_{i,\downarrow} \tag{1.30}$$

and the functions

$$\Phi_i = \langle \hat{c}_{i,\uparrow} \hat{c}_{i+1,\downarrow} \rangle + \langle \hat{c}_{i+1,\uparrow} \hat{c}_{i,\downarrow} \rangle \tag{1.31}$$

we get the equations:

$$i\hbar \partial_t \psi_i = 2\varepsilon_i \psi_i + \left[1 - 2\langle \hat{n}_i \rangle\right] \psi_i - K_{i-1,i} \Phi_{i-1} - K_{i+1,i} \Phi_i. \tag{1.32}$$

In all these expressions $i = 1, 2, \ldots, N$. In order to define the complete dynamics of the system of the N differential equations in (1.32), we need to define the time evolution of the functions defined in (1.31), and so we calculate:

$$i\hbar \partial_t \Phi_i = \langle \left[\hat{c}_{i,\uparrow}, \hat{H}\right] \hat{c}_{1+1,\downarrow} \rangle + \langle \hat{c}_{i,\uparrow} \left[\hat{c}_{i+1,\downarrow}, \hat{H}\right] \rangle + \langle \left[\hat{c}_{i+1,\uparrow}, \hat{H}\right] \hat{c}_{i,\downarrow} \rangle + \langle \hat{c}_{i+1,\uparrow} \left[\hat{c}_{i,\downarrow}, \hat{H}\right] \rangle. \tag{1.33}$$

By using the relations (1.29), and by getting out all the calculations, we obtain:

$$i\hbar \partial_t \Phi_i = (\varepsilon_i + \varepsilon_{i+1})\Phi_i - (M_i + 2K_{i,i+1})\psi_i - (M_i^* + 2K_{i+1,i})\psi_{i+1} - K_{i-1,i}\Lambda_i - K_{i+2,i+1}\Lambda_{i+1} \tag{1.34}$$

where we have defined the following functions:

$$\begin{aligned}
M_i &= \langle \hat{c}_{i,\uparrow}^+ \hat{c}_{i+1,\uparrow} \rangle + \langle \hat{c}_{i,\downarrow}^+ \hat{c}_{i+1,\downarrow} \rangle \\
M_i^* &= \langle \hat{c}_{i+1,\uparrow}^+ \hat{c}_{i,\uparrow} \rangle + \langle \hat{c}_{i+1,\downarrow}^+ \hat{c}_{i,\downarrow} \rangle
\end{aligned} \tag{1.35}$$

and the function Λ_i as follows:

$$\Lambda_i = \langle \hat{c}_{i+1,\uparrow} \hat{c}_{i-1,\downarrow} \rangle + \langle \hat{c}_{i-1,\uparrow} \hat{c}_{i+1,\downarrow} \rangle. \tag{1.36}$$

According to our hypothesis of interactions only between first neighbouring sites, the next neighbouring sites are uncorrelated, and so we have $\Lambda_i = 0$. In this way, equations (1.20) and (1.22) suffice to describe the dynamics of the system of N coupled superconductors.

In the following section we shall consider the application of these results to the case of 2 coupled superconductors, which form the so called Josephson Junction, and we solve, by using some approximations, the equations (1.20) and so also the equations (1.22).

1.5 Two coupled superconductors: a Josephson Junction

In the case of only two coupled superconductors ($N = 2$), we may rewrite [12] equations (1.32) and (1.34) by considering $i = 1, 2$. We can also show that the expectation value of the number operator $\hat{n} = \hat{c}_{i,\uparrow}^{+}\hat{c}_{i,\uparrow} = \hat{c}_{i,\downarrow}^{+}\hat{c}_{i,\downarrow}$ is $\langle n \rangle = \dfrac{1}{2}$. In fact, we can consider that electrons are fermions, so they obey to the Fermi-Dirac statistics, that is: $f(E) = \dfrac{1}{1 + e^{\frac{E - \mu}{k_B T}}}$; as the chemical potential μ is very close to Fermi energy E_F, and the most sensible electrons to the interaction with phonons (so that Cooper pairs are formed) are the ones whose energy is closest to the Fermi energy E_F, we notice that, for these electrons:

$$f(E) \cong f(E_F) = \frac{1}{2}. \tag{1.37}$$

It is known that the Fermi-Dirac statistics represents the number of fermions per unitary volume, in an unitary range of energy values, we notice that this number is $\dfrac{1}{2}$. As the expectation value of the number operator equals to the number of particles which are present in a well defined state (0 or 1, according to Pauli Exclusion Principle), it can be considered equals to the number of electrons represented by the Fermi-Dirac statistics, $f(E_F) = \dfrac{1}{2}$.

So, we may set

$$\langle n \rangle = \langle n_1 \rangle = \langle n_2 \rangle = \frac{1}{2}. \tag{1.38}$$

Thus, in the case of $N = 2$ coupled superconductors, we have, from equations (1.32) and (1.34):

$$\begin{cases} i\hbar\partial_t\psi_1 = 2\varepsilon_1\psi_1 + \psi_1(1 - 2\frac{1}{2}) - K_0\Phi_0 - K_{2,1}\Phi_1 \\ i\hbar\partial_t\Phi_1 = (\varepsilon_1 + \varepsilon_2)\Phi_1 - (M_1 + 2K_{1,2})\psi_1 - (M_1^* + 2K_{2,1})\psi_2 \\ i\hbar\partial_t\psi_2 = 2\varepsilon_2\psi_2 - K_1\Phi_1 - K_{3,2}\Phi_2 \end{cases}$$

As we are only considering two superconductors, we have: $K_{3,2} = 0$. We can also set $K_{1,2} = K_{2,1} = K$, and make use of the simplifying hypothesis by which $M_1^* = M_1$, so that M_1 is a real function of time. In this way, the previous set of differential equations can be simplified as follows:

$$\begin{cases} i\hbar\partial_t\psi_1 = 2\varepsilon_1\psi_1 - K\phi_1 \\ i\hbar\partial_t\phi_1 = (\varepsilon_1 + \varepsilon_2)\phi_1 - 2(K + \frac{M_1}{2})(\psi_1 + \psi_2) \\ i\hbar\partial_t\psi_2 = 2\varepsilon_2\psi_2 - K\phi_1 \end{cases} \tag{1.39}$$

In order to solve [5] the two differential equations for ψ_1 and ψ_2, we can solve the differential equation for ϕ_1; so, substituting the analytic expression obtained for ϕ_1 inside the differential equations for ψ_1 and ψ_2, we can solve them. As for the solution of the differential equation for ϕ_1, we can, first of all, set:

$$\tilde{K} = K + \frac{M_1}{2}; \quad \varepsilon_1 = \varepsilon - eV; \quad \varepsilon_2 = \varepsilon + eV \qquad (1.40)$$

So we have:

$$\varepsilon_1 + \varepsilon_2 = \varepsilon.$$

In this way, the differential equation for ϕ_1 can be rewritten in the more simplified form:

$$i\hbar \partial_t \phi_1 = 2\varepsilon \phi_1 - 2\tilde{K}(\psi_1 + \psi_2). \qquad (1.41)$$

Being it a linear differential equation, we know that its more general solution can be expressed as the sum of the solution of its homogeneous associated differential equation, and of a particular solution of (1.41). The associated homogeneous differential equation is:

$$(i\hbar \partial_t - 2\varepsilon)\phi_{1,H} = 0,$$

its solution being:

$$\phi_{1,H}(t) = \phi_1(0)\exp(-\frac{2i\varepsilon}{\hbar}t). \qquad (1.42)$$

In order to find the particular solution of (1.41), we can use the method of Green function:

$$\phi_{1,P}(t) = -2\tilde{K}\int_{-\infty}^{+\infty} \chi(t - t')\big[\psi_1(t') + \psi_2(t')\big]dt' \qquad (1.43)$$

in which $\chi(t)$ is the Green function, or also called the kernel function, and must satisfy this differential equation:

$$(i\hbar \partial_t - 2\varepsilon)\chi(t) = \delta(t) \qquad (1.44)$$

where $\delta(t)$ is the Dirac distribution function, so defined:

$$\delta(t) = \begin{cases} +\infty & for \ t = 0 \\ 0 & for \ t \neq 0 \end{cases} \qquad (1.45)$$

In fact, if we substitute the expression (1.43) in (1.41), and, by using the expression (1.32), we do all the calculations, we find this result:

$$(i\hbar\partial_t - 2\varepsilon)\phi_{1,P} = -2\tilde{K}\int_{-\infty}^{+\infty}\delta(t-t')\big[\psi_1(t') + \psi_2(t')\big]dt' = -2\tilde{K}(\psi_1(t) + \psi_2(t)),$$

where, in the latter equation, we have used the property (1.45) of Dirac distribution function. Having found that (1.43) is a particular solution of (1.41), we must determine the analytic expression of the function $\chi(t)$; it can be expressed in the factorized form:

$$\chi(t) = A(t)\theta(t) \tag{1.46}$$

where $\theta(t)$ is the Heaviside unitary step function, so defined:

$$\theta(t) = \begin{cases} 1 & for\ t \geq 0 \\ 0 & for\ t < 0 \end{cases}$$

The reason why we use this function, inside the expression (1.46), is that $\chi(t)$ represents the response of the system to an external interaction, represented by the function (1.45); in particular, this response starts at $t \geq 0$, and it is zero before, i. e., for t < 0. Therefore, by inserting the expression (1.46) inside (1.44), and by doing the opportune calculations, we get:

$$\theta(t)\big[i\hbar\partial_t A(t)\big] - 2\varepsilon\theta(t)A(t) + i\hbar A(t)\partial_t\theta(t) = \delta(t) \Rightarrow$$
$$\theta(t)\big[i\hbar\partial_t A(t) - 2\varepsilon A(t)\big] = \big[1 - i\hbar A(0)\big]\delta(t) \tag{1.47}$$

In this expression we have used the result:

$$\frac{d\theta(t)}{dt} = \delta(t) \tag{1.48}$$

so that $i\hbar A(t)\dfrac{d\theta}{dt} = i\hbar A(t)\delta(t)$, and, by using the property of δ (t) that, for $t \neq 0$ is equals to 0, we have:

$$i\hbar A(t)\delta(t) = i\hbar A(0)\delta(t).$$

As $A(0)$ is an arbitrary constant, we can take:

$$A(0) = -\frac{i}{\hbar}.$$

So, the equation (1.24) becomes:

$$\theta(t)\big[i\hbar\partial_t A(t) - 2\varepsilon A(t)\big] = 0.$$

Knowing that, for $t \geq 0$ $\theta(t) = 1$, we get:

$$(i\hbar\partial_t - 2\varepsilon)A(t) = 0 \tag{1.49}$$

and its solution is:

$$A(t) = -\frac{i}{\hbar}\exp(-\frac{2i\varepsilon}{\hbar}t) \; .$$

Therefore:

$$\chi(t-t^{'}) = -\frac{i}{\hbar}\theta(t-t^{'})\exp\left[-\frac{2i\varepsilon}{\hbar}(t-t^{'})\right] \tag{1.50}$$

and

$$\phi_{1,P}(t) = \frac{2i\widetilde{K}}{\hbar}\int_{-\infty}^{+\infty}\theta(t-t^{'})\exp\left[-\frac{2i\varepsilon}{\hbar}(t-t^{'})\right]dt^{'} \; . \tag{1.51}$$

As we have just said, the most general solution of (1.51) is given by the sum of the solution of the homogeneous associated differential equation, and of the particular solution considered:

$$\phi_1(t) = \phi_{1,H}(t) + \phi_{1,P}(t). \tag{1.52}$$

For ranges of time $t \gg 0$ we can consider negligible the term $\phi_{1,H}(t)$, and so we can approximate the solution with $\phi_{1,P}(t) \Rightarrow \phi_1(t) = \phi_{1,P}(t)$ for $t \gg 0$. In order to simplify the expression (1.51), we can, first of all, notice that for $t - t^{'} > 0 \Rightarrow t > t^{'}$ we have:

$$\theta(t-t^{'}) = 1,$$

while for $t - t^{'} < 0$ we have: $\theta(t-t^{'}) = 0$. Therefore, we can rewrite the (1.51) in the following way:

$$\phi_1(t) = \frac{2i\widetilde{K}}{\hbar}\int_{-\infty}^{t}\left[\psi_1(t^{'}) + \psi_2(t^{'})\right]\exp\left[-\frac{2i\varepsilon}{\hbar}(t-t^{'})\right]dt^{'} \; . \tag{1.53}$$

To further simplify this expression, we can operate [12] the following change of variables:

$$\varepsilon = \varepsilon' - i\frac{\gamma}{2}. \tag{1.54}$$

So, in the expression of the exponential function, we get:

$$\exp\left[-\frac{2i\varepsilon}{\hbar}(t-t^{'})\right] \rightarrow \exp\left[-\frac{2i\varepsilon'}{\hbar}(t-t^{'})\right]\exp\left[-\frac{\gamma}{\hbar}(t-t^{'})\right].$$

In this way the expression (1.53) becomes:

$$\phi_1(t) = \frac{2i\widetilde{K}}{\hbar}\int_{-\infty}^{t}\left[\psi_1(t^{'}) + \psi_2(t^{'})\right]\exp\left[-\frac{2i\varepsilon}{\hbar}(t-t^{'})\right]\exp\left[-\frac{\gamma}{\hbar}(t-t^{'})\right]dt^{'} \tag{1.55}$$

where we have considered $\varepsilon' = \varepsilon$ for sake of simplicity. The position (1.54) allows the introduction of a cut-off time t^* in the expression (1.55). In fact, for t^* sufficiently close to t, we may set:

$$\phi_1(t) = \frac{2i\widetilde{K}}{\hbar} \int_{-\infty}^{t^*} \left[\psi_1(t') + \psi_2(t')\right] \exp\left[-\frac{2i\varepsilon}{\hbar}(t-t')\right] \exp\left[-\frac{\gamma}{\hbar}(t-t')\right] dt' +$$

$$\frac{2i\widetilde{K}}{\hbar} \int_{t^*}^{t} \left[\psi_1(t') + \psi_2(t')\right] \exp\left[-\frac{2i\varepsilon}{\hbar}(t-t')\right] \exp\left[-\frac{\gamma}{\hbar}(t-t')\right] dt' \cong$$

$$\frac{2i\widetilde{K}}{\hbar} \int_{t^*}^{t} \left[\psi_1(t') + \psi_2(t')\right] \exp\left[-\frac{2i\varepsilon}{\hbar}(t-t')\right] \exp\left[-\frac{\gamma}{\hbar}(t-t')\right] dt'$$

where we can consider negligible the first integral, because for t' comprised between $-\infty$ and t^* we have:

$$\exp\left[-\frac{\gamma}{\hbar}(t-t')\right] << 1$$

so that the first integral tends towards zero.

Assuming now that $\psi_1(t)$ and $\psi_2(t)$ are slowly varying functions in the interval $\left[t^*, t\right]$, we get:

$$\phi_1(t) \cong \frac{2i\widetilde{K}}{\hbar} \left[\psi_1(t) + \psi_2(t)\right] \int_{t^*}^{t} \exp\left[-\frac{2i\varepsilon}{\hbar}(t-t')\right] \exp\left[-\frac{\gamma}{\hbar}(t-t')\right] dt' . \qquad (1.56)$$

In this way, we can calculate the integral considered in (1.56) as follows

$$\int_{t^*}^{t} \exp\left[-\frac{2i\varepsilon}{\hbar}(t-t')\right] \exp\left[-\frac{\gamma}{\hbar}(t-t')\right] dt' \cong \int_{t^*}^{t} \exp\left[-\frac{2i\varepsilon}{\hbar}(t-t')\right] \exp\left(-\frac{1}{\hbar}\right) dt' .$$

In fact, as t' is very close to t^*, it is possible to approximate $t-t'$ with $t-t^* = \mu$, and we can set:

$$\gamma \cong \frac{A}{\mu} \Rightarrow \exp\left[-\frac{\gamma}{\hbar}(t-t')\right] \cong \exp\left[-\frac{A}{\hbar}\frac{1}{\mu}\mu\right] = \exp\left[-\frac{A}{\hbar}\right].$$

The relation $\gamma \cong \frac{A}{\mu}$, with A a constant of order one, follows from the fact that γ is the potential interaction energy between two electrons, one on the site i, and the other one on the site $i +1$, which decays in a characteristic time μ. We can also consider that the interaction energy γ is usually less than the energy ε of an electron on the site i; in reality it happens that the electrons forming a Cooper pair, and belonging to different first neighbour sites, tend to pass on the same site, so to lead to the creation of Cooper pairs on the same superconductor site. In this way, we can say that expression (1.55) indicates the sum of the kinetic energy of the electron (represented by ε_i), plus the interaction energy γ of the same electron with the external environment, that in this case is the next-neighbour superconductor, is the total energy of the electron. The factor 2 in (1.55) is taken in order to simplify the calculations in expression (1.56).

Coming back to the calculation of integral in (1.56), we may consider that the term $\exp\left[-\dfrac{A}{\hbar}\right]$ can be directly inserted inside the constant $\widetilde{K}$. In this way, we can calculate the integral as follows:

$$\int_{t^*}^{t} \exp\left[-\frac{2i\varepsilon}{\hbar}(t-t')\right] = \frac{\hbar}{2i\varepsilon}\left[\exp\left[-\frac{2i\varepsilon}{\hbar}(t-t')\right]\right]_{t'=t^*}^{t} = \frac{\hbar}{2i\varepsilon}\left[1-\exp\left[-\frac{2i\varepsilon}{\hbar}(t-t^*)\right]\right].$$

By noticing that $t-t^* = \mu \ll 1$, we can approximate the exponential term as:

$$\exp\left[-\frac{2i\varepsilon}{\hbar}\mu\right] \cong 1 - \frac{2i\varepsilon}{\hbar}\mu + \frac{1}{2}\left(\frac{2i\varepsilon}{\hbar}\mu\right)^2$$

having considered the Taylor series expansion of $e^{-x} \cong 1 - x + \dfrac{x^2}{2}$ valid for x $\ll$ 1. In this way, considering the expression (1.56), we get:

$$\phi_1(t) \cong \frac{2i\widetilde{K}}{\varepsilon}\left[\psi_1(t) + \psi_2(t)\right]\frac{\hbar}{2i\varepsilon}\left[1 - 1 + \frac{2i\varepsilon}{\hbar}\mu - \frac{1}{2}\left(\frac{2i\varepsilon}{\hbar}\mu\right)^2\right] =$$

$$\frac{\widetilde{K}}{\varepsilon}\left[\psi_1(t) + \psi_2(t)\right]\frac{2i\varepsilon}{\hbar}\mu\left[1 - \frac{i\varepsilon\mu}{\hbar}\right] = \frac{2i\mu}{\hbar}\widetilde{K}\left(1 - \frac{i\varepsilon\mu}{\hbar}\right)\left[\psi_1(t) + \psi_2(t)\right]$$

If we substitute this expression obtained for $\phi_1(t)$ inside the two differential equations for ψ_1 and ψ_2, in the expression (1.39), we get for ψ_1:

$$i\hbar\partial_t\psi_1 = 2\varepsilon_1\psi_1 - \frac{2iK\widetilde{K}}{\hbar}\mu\left(1 - \frac{i\varepsilon\mu}{\hbar}\right)\left[\psi_1(t) + \psi_2(t)\right]. \qquad (1.57)$$

By setting:

$$\Sigma = \frac{2iK\widetilde{K}}{\hbar}\mu\left(1 - \frac{i\varepsilon\mu}{\hbar}\right) \qquad (1.58)$$

we get:

$$i\hbar\partial_t\psi_1 = 2\varepsilon_1\psi_1 - \Sigma\psi_1 - \Sigma\psi_2 \Rightarrow \quad i\hbar\partial_t\psi_1 = (2\varepsilon_1 - \Sigma)\psi_1(t) - \Sigma\psi_2(t).$$

In the same way, we get, for ψ_2:

$$i\hbar\partial_t\psi_2 = (2\varepsilon_2 - \Sigma)\psi_2 - \Sigma\psi_1.$$

By now setting

$$2\varepsilon_i = E_i, \quad (i = 1, 2)$$

where E_i can be interpreted as the energy of the Cooper pair (so a system of two electrons) on the superconductor i, we obtain the following form for the differential equations:

$$\begin{cases} i\hbar\partial_t\psi_1 = (E_1 - \Sigma)\psi_1 - \Sigma\psi_2 \\ i\hbar\partial_t\psi_2 = (E_2 - \Sigma)\psi_2 - \Sigma\psi_1 \end{cases} \tag{1.59}$$

In order to obtain an Hamiltonian system, as in the case of Feynman's celebrated model of Josephson Junctions, we can consider that in (1.58) there is a real part, defined as Σ_R, and an imaginary part, defined as Σ_I. In this respect, we notice that the quantity $\Sigma_R = \dfrac{2\varepsilon K \widetilde{K}\mu^2}{\hbar^2}$ is a real parameter, describing the interaction energy between two Cooper pairs on different superconducting sites. In fact, we know that Σ_R is proportional to $\mu \propto \dfrac{1}{\gamma}$, where γ, defined in expression (1.54), is, as just considered, the potential energy between two electrons on different first neighbour sites. By considering the quantities $\widetilde{E}_k = E_k - \Sigma_R$, which are the effective energies of a Cooper pair on the site $k = 1, 2$, we get:

$$\begin{cases} i\hbar\partial_t\psi_1 = \widetilde{E}_1\psi_1 - \Sigma_R\psi_2 \\ i\hbar\partial_t\psi_2 = \widetilde{E}_2\psi_2 - \Sigma_R\psi_1 \end{cases} \tag{1.60}$$

These differential equations are similar to the ones obtained by Feynman in his celebrated model of a Josephson junction. At the end of this chapter we may notice that, in deriving equation (1.60), we have made use of a formal solution of Φ_1 in terms of ψ_1 and ψ_2, as expressed in relations (1.39). If we carry out the same kind of analysis for more than two coupled superconductors, we can obtain the extension of Feynman's and Ohta's models to multi-barrier Josephson junctions, already proposed by De Luca and Romeo in reference [14], which is, as just remarked in the introduction, in good agreement with a strict microscopic description of these types of devices.

1.6 Conclusions

We have considered a microscopic description of N coupled superconductors in which nearest-neighbour interactions are present. Starting from the time evolution of the fermionic operators $\hat{c}$ and $\hat{c}^+$ in the Heisenberg picture, we obtain a set of coupled ordinary differential equations for the order parameters Δ_i.

Since the main aim of the present analysis is to show that Feynman's model for a single Josephson junction can be justified by a microscopic model, we have specifically written the resulting system of differential equations in the case of two coupled superconductors. In this simple case Feynman's model is obtained. In this way, one can argue that there exists a strict correspondence between the microscopic picture described in the present work and the semi-classical analysis proposed by Feynman and successively refined by Ohta. Therefore, generalizations of Ohta's model to multi-barrier Josephson junctions [8] based on the semi-classical analysis developed by the latter authors can be retained to agree with a strict microscopic description of these systems.

Chapter 2

Mechanical analogue of an over-damped Josephson junction

An over-damped pendulum can be adopted as a mechanical analog of an over-damped Josephson junction. The basic equations leading to the driving torque versus the time average of the angular frequency are studied. The mechanical analog can be used to provide additional insight into the current-voltage characteristics of over-damped Josephson junctions.

2.1 Introduction

In 1973 B. D. Josephson received the Nobel Prize for having predicted the so called d. c. and a. c. Josephson effects [1] in a superconducting device that was named after him: the Josephson junction (JJ). A JJ consists of two weakly coupled superconductors. The dynamics of the superconducting phase difference φ across the junction is described by the following equations [15]:

$$I = I_{J,0} \sin \varphi \qquad\qquad (2.1a)$$

$$\frac{d\varphi}{dt} = \frac{2eV}{\hbar} \qquad\qquad (2.1b)$$

where I is the current flowing through the junction ($I_{J,0}$ being the maximum value that can flow inside the zero-voltage state), $\hbar = h/2\pi$, h being Planck's constant, and V is the voltage across the two superconductors.

In the d. c. Josephson effect a non-dissipative current can be seen to flow at zero voltage, as it can be shown by setting $V=0$ in (2.1b), so that $\varphi = \text{constant}$. In this way, $I_{J,0}$ represents the maximum value of I flowing in the junction in the zero-voltage state.

In the a. c. Josephson effect, the voltage across the JJ is kept at a fixed non-zero value V_0. Integrating both sides of Eq. (2.1b) we obtain $\varphi(t) = (2e/\hbar)V_0 t + \varphi_0$ where φ_0 is the constant of integration. Therefore the current I is seen to oscillate at a frequency $\omega_J = (2e/\hbar)V_0$.

Alternative derivations of equations (2.1a-b) have been also proposed by Feynman [2] and by Ohta [3], as we have seen in the preceding chapter. In the Feynman model a JJ is described as a weakly coupled two-level quantum system. Ohta noticed that Feynman model did not include an additional term due to energy contribution of the external classical circuit biasing the Josephson junction. The latter author therefore introduced a semi-classical model based on a rigorous quantum derivation to attain full agreement between equations (2.1a-b) and the corresponding final equations obtained by means of his valuable semi-classical analysis.

In order to describe the dynamics of the superconducting phase difference φ in an over-damped JJ, a Resistively Shunted Junction model can be adopted [15].
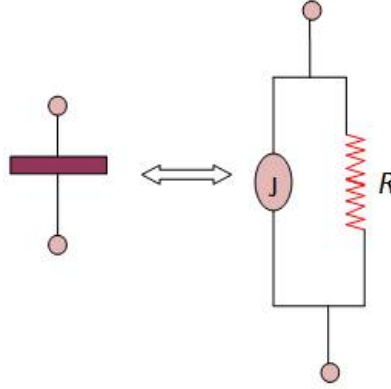
Figure 2.1. *Resistively Shunted Model for a Josephson junction. The junction on the left is described by a parallel connection of a resistor with resistance R and an ideal Josephson element J. In the latter a current $I = I_{J,0} \sin \varphi$ can flow.*

In this model a purely superconducting element carrying a current I expressed in terms of φ as in Eq. (2.1a) is placed in parallel with a resistor of resistance R, as shown in fig. 1. By injecting a current I_B in the system and by invoking charge conservation, we may write:

$$\frac{V}{R} + I_{J,0} \sin \varphi = I_B \qquad (2.2)$$

where V is the voltage across the JJ. By expressing V in terms of φ as in Eq. (1b) and by introducing the dimensionless quantities $i_B = \dfrac{I_B}{I_{J,0}}$ and $\tau = \dfrac{2\pi R I_{J,0}}{\Phi_0} t$ we may rewrite equation (2.2) as follows:

$$\frac{d\varphi}{d\tau} + \sin \varphi = i_B \; . \qquad (2.3)$$

The above equation also represents [16] the dynamics of an over-damped simple pendulum. Therefore, starting from this analogy [15], [2], [3], [17], we consider the static and dynamic solutions of Eq. (2.3) referred to a simple pendulum with a constant forcing term, trying to grasp some physical insight from these expressions. Successively, we derive [16] the curve of the driving torque versus the time average of the angular frequency. Finally, the analogy between the two systems is utilized to discuss the current-voltage characteristics of over-damped Josephson junctions.

2.2 An over-damped pendulum

Let us consider [16] the pendulum hinged in O and consisting of a massless rod of length l and a spherical body of mass m, as shown in fig. 2.2. Let us also assume that the sphere of mass m has radius R. This sphere is moving in a fluid of density ρ_F, so that it is subjected to the buoyance force of intensity $F_B = \dfrac{4\pi R^3}{3} g \rho_F$, where g is the acceleration due to gravity. In addition, by

assuming validity of Stokes' law, the sphere is taken to be subject to a viscous force, opposing its velocity and of intensity $F_S = 6\pi\eta R(l+R)\dfrac{d\theta}{dt}$, η being the coefficient of viscosity of the medium, and, of course, $(l+R)\dfrac{d\theta}{dt}$ is the sphere velocity. The spherical body is also subject to the tension in the massless rod of length l and to its weight.
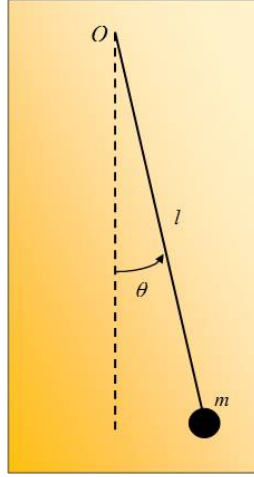

Figure 2.2. *Schematic representation of a pendulum of mass m and length l displaced of an angle θ with respect to the vertical direction. Under certain conditions, the pendulum can be considered over-damped. This system realizes a mechanical analogue of an over-damped Josephson junction.*

By taking moments about point O, we may write:

$$I_0 \frac{d^2\theta}{dt^2} = -F_S(l+R) - m^* g(l+R)\sin\theta + M_0(t) \,. \tag{2.4}$$

where I_0 is the moment of inertia, $m^* = m\left(1 - \dfrac{4\pi R^3}{3m}\rho_F\right)$ is the effective mass of the sphere, when buoyancy is taken into account, and $M_0(t)$ is the applied torque.

The (2.4) follows from the theorem of angular moment, expressed, as it is well known, into the form $\dfrac{dL}{dt} = M_{ex}$, where $L = I_0 \dfrac{d\theta}{dt}$ is the angular moment, and M_{ex} is the total moment of the external forces. Considering the finite dimensions of the sphere, the moment of inertia I_0 can be calculated by means of the parallel axes theorem [18], so that:

$$I_0 = \frac{2}{5}mR^2 + m(l+R)^2 \,. \tag{2.5}$$

By dividing [16] both members of Eq. (2.4) by $m^* g(l+R)$, by defining $\tau = \dfrac{m^* g}{6\pi\eta R(l+R)}t$ as a new dimensionless time variable, and by setting $m_0(\tau) = \dfrac{M_0(\tau)}{m^* g(l+R)}$, we may write

$$\frac{m^*mg\left(l^2 + 2Rl + \dfrac{7R^2}{5}\right)}{(6\pi\eta R)^2 (l+R)^3}\frac{d^2\theta}{d\tau^2} + \frac{d\theta}{d\tau} + \sin\theta = m_0(\tau).\tag{2.6}$$

We may consider that both τ and $m_0(\tau)$, being ratios of same dimensions quantities, are dimensionless. The proof of equation (2.6) is given in Appendix 2.1. We immediately notice that equation (2.6) is equivalent to equation (2.3) for very small values of the pre-factor of the second

derivative in equation (2.6), i. e. for $\dfrac{m^*mg\left(l^2 + 2Rl + \dfrac{7R^2}{5}\right)}{(6\pi\eta R)^2 (l+R)^3} \ll 1$. In this way, the dynamical

equation of an over-damped pendulum becomes formally equal to equation (2.3), reading:

$$\frac{d\theta}{d\tau} + \sin\theta = m_0(\tau).\tag{2.7}$$

Therefore, the analytic and experimental study of an over-damped pendulum allows us to derive important properties of an over-damped Josephson junction. Naturally, in performing experimental studies, one needs to have negligible values of the pre-factor of the second derivative in equation (2.6). This can be obtained, for example, by using a fluid with high enough values of the coefficient of viscosity η. In the following sections we shall consider the forcing term as constant, obtaining a full analytic solution of the problem.

2.3 Constant driving moment

Let us take [16] a constant forcing term of the over- damped pendulum in fig. 2.2. In this case we can obtain analytic solutions for the differential equation (2.7). We start by noticing that, for $m_0 < 1$, we obtain two constant solutions, one stable and one unstable, as it can be argued by means of the phase-plane analysis, shown in figure 2.3.
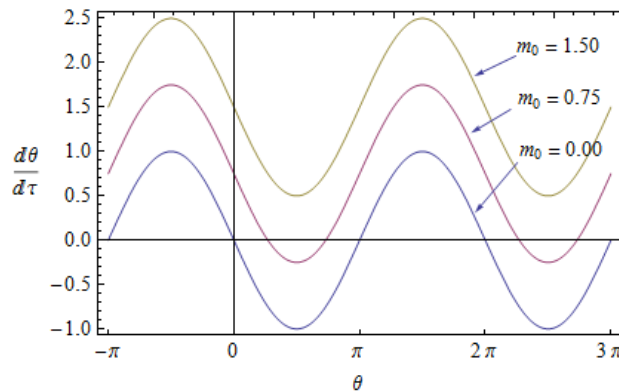

Figure 2.3. *Phase-plane analysis for the over-damped pendulum. The constant forcing term is $m_0 = 0.0$ (bottom curve), $m_0 = 0.75$ (middle curve), and $m_0 = 1.50$ (top curve).*

The stable solution of the stationary form of equation 2.7, i.e. $\sin\theta = m_0$, where, as just considered $m_0 < 1$, is given by:

$$\theta^* = \sin^{-1} m_0,$$ (2.8)

while the unstable solution is:

$$\theta = \pi - \theta^*.$$

The stability regime changes as the angle crosses the value $\theta = \dfrac{\pi}{2}$, as it can be noticed by analyzing the sign of the derivative $\dfrac{d\theta}{d\tau}$ about these fixed points. For $m_0 = 1$ we have an half-stable solution: the pendulum may swirl around O whenever an arbitrary small positive perturbation arises. In fact, for $m_0 = 1$ we get: $\sin\theta = m_0 = 1 \Rightarrow \theta = \dfrac{\pi}{2}$. Thus, in this condition, also an arbitrary small perturbation determines a displacement of the pendulum from its equilibrium position.

We may finally notice that, for $m_0 > 1$, the function $\theta = \theta(\tau)$ is monotonically increasing, given that the curves in fig. 2.3 lie above the θ-axis and the derivative $\dfrac{d\theta}{d\tau}$ is always positive. In this "running state", i.e. the situation in which $\dfrac{d\theta}{d\tau} \neq 0$ (in this case $\dfrac{d\theta}{d\tau} > 0$), we solve the ordinary differential equation (2.7) by the method of separation of variables, as done in reference [15], by writing:

$$\int_{\theta_0}^{\theta(\tau)} \frac{d\theta}{m_0 - \sin\theta} = \tau,$$ (2.9)

where $\theta_0 = \theta(0)$. By the substitution $x = \tan\dfrac{\theta}{2}$, we can write [16] the integral in (2.9) as follows:

$$\frac{2}{m_0} \int_{\tan\frac{\theta_0}{2}}^{\tan\frac{\theta(\tau)}{2}} \frac{dx}{x^2 + 1 - \dfrac{2}{m_0}x} = \frac{2}{m_0} \int_{\tan\frac{\theta_0}{2}}^{\tan\frac{\theta(\tau)}{2}} \frac{dx}{\left(x - \dfrac{1}{m_0}\right)^2 + 1 - \dfrac{1}{m_0^2}},$$ (2.10)

where we have completed the square in the denominator. The integral on the right hand side of Eq. (2.9) can now be solved. By substituting this solution into (2.9) and by defining

$$\alpha_0 = \tan^{-1}\left[\frac{m_0}{\sqrt{m_0^2 - 1}}\left(\tan\frac{\theta_0}{2} - \frac{1}{m_0}\right)\right], \text{ we may write:}$$

$$\frac{2}{\sqrt{m_0^2 - 1}}\left\{\tan^{-1}\left[\frac{m_0}{\sqrt{m_0^2 - 1}}\left(\tan\frac{\theta(\tau)}{2} - \frac{1}{m_0}\right)\right] - \alpha_0\right\} = \tau.$$ (2.11)

By finally extracting $\theta(\tau)$ from equation (2.11), we have:

$$\theta(\tau) = 2\tan^{-1}\left[\frac{1}{m_0} + \frac{\sqrt{m_0^2-1}}{m_0}\tan\left(\frac{\sqrt{m_0^2-1}}{2}\tau + \alpha_0\right)\right] + 2k\pi,\qquad(2.12)$$

where k is an integer. The above expression is represented in figure 2.4, as obtained from numerical solution of equation (2.7) with initial condition $\theta_0 = 0$, and for $m_0 = 1.5$.
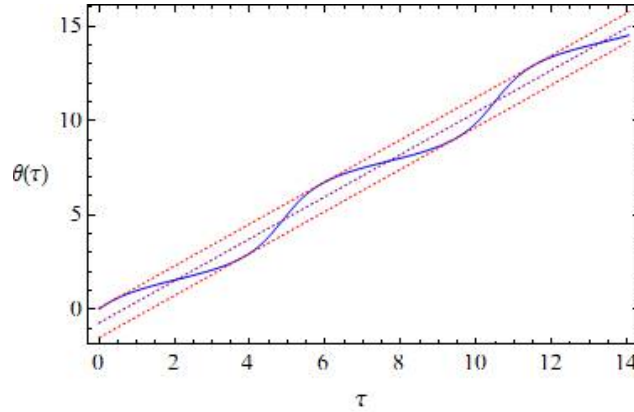

Figure 2.4. *Normalized time dependence of the angular variable θ of an over-damped pendulum (full-line curve). The constant forcing term is m₀=1.5. The top and bottom dashed lines enclose the undulatory behavior of θ, whose oscillations take place about the middle dashed line.*

We notice that the numerical solution is easier to report on a graph, given the necessity of combining different pieces of the solution (2.12), one for each 2π shift of the angular variable $\theta(\tau)$. We also notice that this function oscillates within the two lines of equation $\theta_{1,2}(\tau) = \sqrt{m_0^2-1} + \gamma_{1,2}$, where: $\gamma_{1,2} = \theta(\tau_{1,2}) - \sqrt{m_0^2-1}\,\tau_{1,2}$, $\tau_{1,2}$ being the times in which the lines are tangent to the oscillating curve $\theta(\tau)$ in the interval $[0, 2\pi]$. The quantities $\tau_{1,2}$ can be found by a straightforward, but rather cumbersome, calculation.

In order to determine $\tau_{1,2}$ we impose the equality between the curve represented by equation (2.12) and the straight line considered before, of course for $\tau = \tau_{1,2}$. This condition of equality corresponds also to the equality of the first derivatives of the same functions, always for $\tau = \tau_{1,2}$. Thus, the latter condition is so expressed:

$$\frac{m_0^2-1}{m_0}\frac{1}{\cos^2\left(\frac{\sqrt{m_0^2-1}}{2}\tau_{1,2}+\alpha_0\right)}\frac{1}{1+\left[\frac{1}{m_0}+\frac{\sqrt{m_0^2-1}}{m_0}\tan\left(\frac{\sqrt{m_0^2-1}}{2}\tau_{1,2}+\alpha_0\right)\right]^2} = \sqrt{m_0^2-1}\ ,$$

where in the first member we have the first derivative of the curve represented by equation (2.12), while in the second member there is the derivative of the straight line. With the position $\gamma = \dfrac{\sqrt{m_0^2 - 1}}{m_0}\tau_{1,2} + \alpha_0$, and by knowing that $\cos^2 \gamma = \dfrac{1}{1 + \tan^2 \gamma}$, we get:

$$\frac{\sqrt{m_0^2 - 1}}{m_0}\frac{1}{\cos^2 \gamma}\frac{1}{1 + \left[\dfrac{1}{m_0} + \dfrac{\sqrt{m_0^2 - 1}}{m_0}\tan\gamma\right]^2} = 1.$$

In this way, we obtain:

$$\frac{1 + \tan^2 \gamma}{1 + \left[\dfrac{1}{m_0} + \dfrac{\sqrt{m_0^2 - 1}}{m_0}\tan\gamma\right]^2} = \frac{m_0}{\sqrt{m_0^2 - 1}}$$

$$1 + \tan^2 \gamma = \frac{m_0}{\sqrt{m_0^2 - 1}}\left[1 + \left(\frac{1}{m_0} + \frac{\sqrt{m_0^2 - 1}}{m_0}\tan\gamma\right)^2\right] \Rightarrow$$

$$1 + \tan^2 \gamma = \frac{m_0}{\sqrt{m_0^2 - 1}} + \frac{1}{m_0\sqrt{m_0^2 - 1}} + \frac{\sqrt{m_0^2 - 1}}{m_0}\tan^2 \gamma + \frac{2}{m_0}\tan\gamma \Rightarrow$$

$$\left(1 - \frac{\sqrt{m_0^2 - 1}}{m_0}\right)\tan^2 \gamma - \frac{2}{m_0}\tan\gamma + 1 - \frac{m_0}{\sqrt{m_0^2 - 1}} - \frac{1}{m_0\sqrt{m_0^2 - 1}} = 0$$

By solving this algebraic equation, we get:

$$\tan\gamma = \frac{\dfrac{2}{m_0} \pm \sqrt{\left(\dfrac{2}{m_0}\right)^2 - 4\left(1 - \dfrac{\sqrt{m_0^2 - 1}}{m_0}\right)\left(1 - \dfrac{m_0}{\sqrt{m_0^2 - 1}} - \dfrac{1}{m_0\sqrt{m_0^2 - 1}}\right)}}{2\left(1 - \dfrac{\sqrt{m_0^2 - 1}}{m_0}\right)} = y_\pm(m_0).$$

Once obtained the two values of $\tan\gamma(\tau_{1,2}) = y_\pm(m_0)$, we can write: $\gamma(\tau_{1,2}) = \tan^{-1}[y_\pm(m_0)]$.

As we know that: $\gamma = \dfrac{\sqrt{m_0^2 - 1}}{m_0}\tau_{1,2} + \alpha_0$, we obtain: $\dfrac{\sqrt{m_0^2 - 1}}{2}\tau_{1,2} + \alpha_0 = \tan^{-1}[y_\pm(m_0)]$. So that:

$$\tau_{1,2} = \frac{2}{\sqrt{m_0^2 - 1}}\left\{\tan^{-1}[y_\pm(m_0)] - \alpha_0\right\} \tag{2.13}$$

Therefore, the curves of $\theta(\tau)$ are seen to oscillate about a central line $\theta_A(\tau) = (\sqrt{m_0^2 - 1})\tau + \gamma_A$, whose intercept γ_A is the average value of γ_1 and γ_2. The solution of Eq. (2.7) is represented in

figure 2.5, for various values of the constant forcing term m_0, along with the central lines $\theta_A(\tau)$ obtained by the procedure described above.
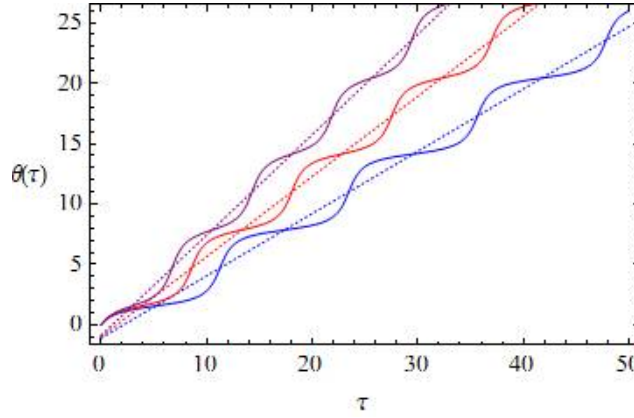

Figure 2.5 *Normalized time dependence of the angular variable θ of an over-damped pendulum (full-line curves) represented together with the central dashed line about which oscillations take place. The constant forcing terms are as follows: m₀=1.125 (lower curve), m₀=1.200 (middle curve), m₀=1.300 (upper curve).*

2.4 Time average of the angular frequency

Let us study the time average $\left\langle \dfrac{d\theta}{d\tau} \right\rangle$ of the angular frequency $\dfrac{d\theta}{d\tau}$ [16] as a function of the constant

forcing term m_0. This analysis is important, given that the m_0 versus $\left\langle \dfrac{d\theta}{d\tau} \right\rangle$ curves correspond to

the normalized current i_B versus average voltage $\left\langle \dfrac{d\varphi}{d\tau} \right\rangle$ characteristics of an over-damped

Josephson junction.

We may start by considering the function $\dfrac{d\theta}{d\tau}$, represented in figure 2.6 for $m_0 = 1.5$ along with

the value of the slope $\sqrt{m_0^2 - 1}$ of the central line running through the solution as seen in details in figure 2.4. This slope corresponds to the average value of the curve in figure 2.6.

We notice that this function is periodic with period equals to

$$T = \frac{2\pi}{\sqrt{m_0^2 - 1}} \tag{2.14}$$

as can be formally proven by calculating the derivative with respect to τ of $\theta(\tau)$ in Eq. (2.12).
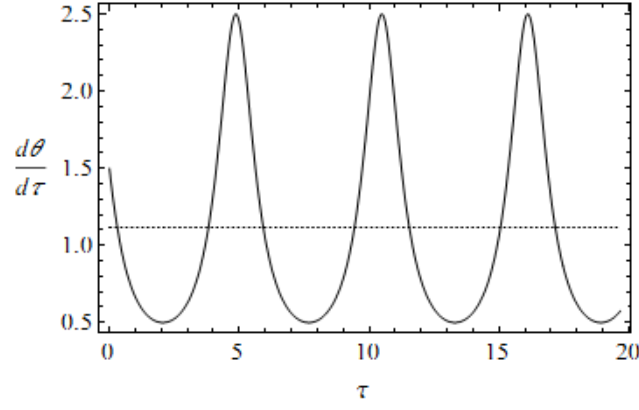
Figure 2.6. *Normalized time dependence of the angular frequency (full line) of an over-damped pendulum subject to a constant forcing equal to $m_0=1.50$. Notice that the curve is periodic and the period is $T = \dfrac{2\pi}{\sqrt{m_0^2-1}}$. The dashed line represents the slope $\sqrt{m_0^2-1}$ of the central dashed line of the primitive curve in figure 2.4 and, at the same time, the average value of the full-line curve.*

In fact, we have:

$$\frac{d\theta}{d\tau} = \frac{d}{d\tau}\left\{2\tan^{-1}\left[\frac{1}{m_0} + \frac{\sqrt{m_0^2-1}}{m_0}\tan\left(\frac{\sqrt{m_0^2-1}}{2}\tau_{1,2}+\alpha_0\right)\right]\right\} =$$

$$2\frac{\sqrt{m_0^2-1}}{m_0}\frac{1}{\cos^2\left(\frac{\sqrt{m_0^2-1}}{2}\tau+\alpha_0\right)}\frac{\sqrt{m_0^2-1}}{2}\frac{1}{1+\left[\frac{1}{m_0}+\frac{\sqrt{m_0^2-1}}{m_0}\tan\left(\frac{\sqrt{m_0^2-1}}{2}\tau+\alpha_0\right)\right]^2},$$

or $\dfrac{d\theta}{d\tau} = \dfrac{m_0^2-1}{m_0}\dfrac{1}{\cos^2\left(\frac{\sqrt{m_0^2-1}}{2}\tau+\alpha_0\right)\left\{1+\left[\frac{1}{m_0}+\frac{\sqrt{m_0^2-1}}{2}\tan\left(\frac{\sqrt{m_0^2-1}}{2}\tau+\alpha_0\right)\right]^2\right\}}.$

In order to determine the period T we can use the property for which the cosine squared and tangent functions are periodic with the same period π, and considering also that these functions have the same argument, i.e. $\gamma(\tau) = \dfrac{\sqrt{m_0^2-1}}{2}\tau+\alpha_0$, we get: $\gamma(\tau+T)=\gamma(\tau)+\pi$. In this way, we obtain:

$$\frac{\sqrt{m_0^2-1}}{2}(\tau+T)+\alpha_0 = \frac{\sqrt{m_0^2-1}}{2}\tau+\alpha_0+\pi \Rightarrow \frac{\sqrt{m_0^2-1}}{2}T = \pi$$

Thus we have:

33

$$T = \frac{2\pi}{\sqrt{m_0^2 - 1}} \, .$$

According to the above result, the slope of the central line can be written as $\frac{2\pi}{T}$. On the other hand, by recalling that the period of the function $\theta(\tau)$ is 2π, the time-averaged value of $\frac{d\theta}{d\tau}$ can be calculated as follows:

$$\left\langle \frac{d\theta}{d\tau} \right\rangle = \frac{1}{T} \int_0^T \frac{d\theta}{d\tau} d\tau = \frac{\theta(T) - \theta(0)}{T} = \frac{2\pi}{T} \, , \tag{2.15}$$

so that it is proven that the average value of the angular frequency curves is $\sqrt{m_0^2 - 1}$. From equation (2.14) and (2.15) we can then argue that

$$m_0 = \sqrt{1 + \left\langle \frac{d\theta}{d\tau} \right\rangle^2} \tag{2.16}$$

The m_0 versus $\left\langle \frac{d\theta}{d\tau} \right\rangle$ curve is represented in figure 2.7.
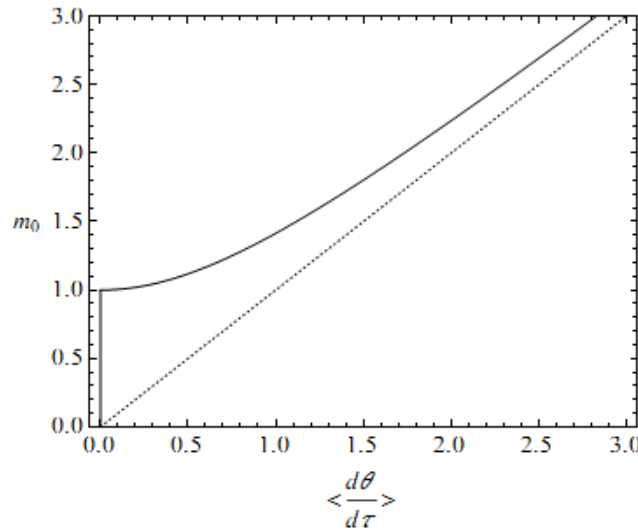
Figure 2.7 *Normalized forcing term versus the time average of the angular frequency (full line) of an over-damped pendulum. Notice that the curve is anchored at null angular frequency if $m_0 \leq 1$. On the other hand, for $m_0 > 1$, the values of the curve tend toward the asymptote, given by the dashed line, as the abscissa increases.*

We soon notice the role played by the static solution in Eq. (2.8). In fact, for $m_0 < 1$, the pendulum is in static equilibrium, so that $\left\langle \frac{d\theta}{d\tau} \right\rangle = 0$. In fact, for $m_0 < 1$, we have the same number of negative

and positive values of $\dfrac{d\theta}{d\tau}$, so that the mean value of this quantity is negligible, a we can see in figure 2.3. The same happens in a Josephson junction: when the value of the normalized bias current i_B is less than one, the junction is said to be in the superconducting or zero-voltage state. In fact, for $i_B < 1$, we have from equation (2.3): $\dfrac{d\varphi}{d\tau} = -\sin\varphi \Rightarrow \left\langle \dfrac{d\varphi}{d\tau} \right\rangle = -\langle \sin\varphi \rangle = 0$, so that we know that the average value of the trigonometric functions is zero. In this way, from the second Josephson equation, we get: $\langle v \rangle = \left\langle \dfrac{d\varphi}{d\tau} \right\rangle = 0 \Rightarrow v = \dfrac{V}{RI_0} = 0 \Rightarrow V = 0$. Therefore, we notice that the electric current I_R flowing inside the resistor, in the RSJ model, is negligible, as we have: $I_R = \dfrac{V}{R} = 0$. On the other hand, inside the Josephson junction, according to the first Josephson equation, we have: $I = I_{j,0} \sin\varphi$. This current is non zero, so that a superconducting or zero-voltage state is realized. In this state no current flows in the resistive branch of the RSJ model in figure 2.1, so that the curve climbs vertically from 0 to 1 just as shown in figure 2.7.

When $i_B > 1$, the resistive branch is activated and a finite voltage appears across the junction, in the way described in figure 2.7. In fact, in this case, we have $\dfrac{d\varphi}{d\tau} \neq 0 \Rightarrow V \neq 0 \Rightarrow I_R \neq 0$, so that the resistive branch is not anymore inactive. We also notice that the m_0 versus $\left\langle \dfrac{d\theta}{d\tau} \right\rangle$ curve presents the oblique asymptote $m_0 = \left\langle \dfrac{d\theta}{d\tau} \right\rangle$. In fact, for large enough values of m_0, this driving moment becomes predominant with respect to the nonlinear sine term in Eq. (2.7), thus justifying the observed asymptotic behavior. This consideration can be proven starting from equation (2.7), that in this case is approximated as follows:

$$\frac{d\theta}{d\tau} = m_0 \Rightarrow \left\langle \frac{d\theta}{d\tau} \right\rangle = m_0 .$$

Notice that the above equation is valid as long as m_0 is constant.

2.5   The washboard potential

Very useful physics [16] can be finally recovered by writing down the energy balance equation for the system.
We start by noticing that energy is furnished from the externally applied moment at a rate
$P_{ex} = M_0 \dfrac{d\theta}{dt}$. This analytic expression follows from the simple mechnicl properties. In fact, along a circular trajectory, i.e. the one followed by the simple pendulum during its motion, the applied force is tangential to this trajectory, and so to the infinitesime displacement of the pendulum, that is $ds = rd\theta$, where ds is the arch of circumference, and so the considered infinitesime displacement, r is the circumpherence radius, and $d\theta$ is the angle insisting on this circumpherence arch. So, the infinitesime work of this force can be represented as follows: $dW = \vec{F} \cdot d\vec{s} = Frd\theta = M_0 d\theta$, where

M_0 is the module of the torque acting on the considered particle. The externally supplied power is therefore given by: $P_{ex} = \dfrac{dW}{dt} = M_0 \dfrac{d\theta}{dt}$. This energy is in part dissipated because of the presence of the viscous force $F_S = 6\pi\eta R(l+R)\dfrac{d\theta}{dt}$ at a rate $P_d = -6\pi\eta R(l+R)^2 \left(\dfrac{d\theta}{dt}\right)^2$, the minus sign meaning that energy is flowing out from the system. Therefore, the mechanical energy E_M, being the sum of the kinetic energy $\dfrac{1}{2}I_0\left(\dfrac{d\theta}{dt}\right)^2$ and of the potential energy $m^*g(l+R)(1-\cos\theta)$, varies in time according to the following energy balance equation:

$$\frac{dE_M}{dt} = P_d + P_{ex} \tag{2.17}$$

By explicitly writing down all terms, we have:

$$\frac{d}{dt}\left[\frac{1}{2}I_0\left(\frac{d\theta}{dt}\right)^2 + m^*g(l+R)(1-\cos\theta) - M_0\theta\right] = -6\pi\eta R(l+R)^2\left(\frac{d\theta}{dt}\right)^2, \tag{2.18}$$

where we have taken M_0 constant and have included the external forcing term under the derivative operator on the left hand side. Of course, we can obtain the dynamical equations (2.4) from equation (2.18) by factoring out the angular frequency. In fact, if we calculate the derivative in the first member of the latter relation, we get:

$$I_0\frac{d^2\theta}{dt^2} + m^*g(l+R)\sin\theta - M_0 = -6\pi\eta R(l+R)^2\left(\frac{d\theta}{dt}\right).$$

After simplifying the term $\dfrac{d\theta}{dt}$ in both members, we have:

$$I_0\frac{d^2\theta}{dt^2} = -F_S(l+R) - m^*g(l+R)\sin\theta + M_0,$$

that is just the relation (2.4).

However, we are here interested in highlighting the role of the forcing term in the system. Therefore, we consider a normalized effective potential u_{eff} defined as follows:

$$u_{eff} = \frac{U_{eff}}{m^*g(l+R)} = 1 - \cos\theta - m_0\theta \tag{2.19}$$

This normalized potential, called washboard potential because of its shape, is represented in fig. 2.8 as a function of the variable θ and for various values of the parameter m_0.
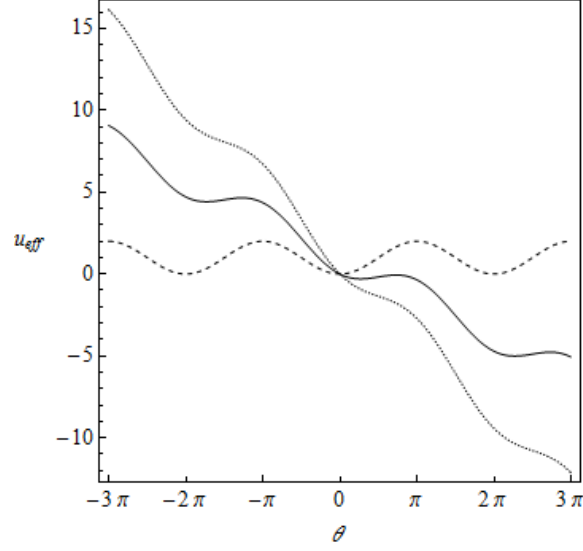
Figure 2.8. *Normalized effective potential as a function of the angle θ for the following three values of the parameter m_0: 0.0 (dashed line); 0.75 (full line); 1.5 (dotted line). Notice that the parameter m_0 determines the degree of tilting and stretching of the undulating curves.*

Some comments on the origin [16] of the term "washboard potential" are in order. By looking at the tilted full-line curve in fig. 2.8, we have the impression to see the board used by our great-grandmother to wash clothes, before the washing machine came into use. The above representation is useful, since it clarifies, once more, the crossover from static to dynamic solutions of the system. In fact, by looking at figure 2.8, we first notice that the parameter m_0 affects the degree of tilting and stretching of the washboard potential. This can be seen by starting from the dashed curve obtained for $m_0 = 0.0$ and by considering the remaining curves obtained for increasing values of this parameter. In the horizontal washboard all minima fall exactly at $2k\pi$, with k integer. The number of minima fitting in the graph shown in fig. 2.8 are three. The same number of minima, though their abscissa are slightly displaced with respect to the above specified positions, are still present in the stretched and tilted curve for $m_0 = 0.75$ (full line in figure 2.8). Therefore, a point-like body could still be in static equilibrium in the angular positions corresponding to the minima and given by equation (2.8) in the interval $[0, 2\pi]$. Static equilibrium is not anymore possible for point-like particles on the washboard potential for $m_0 = 1.5$ (dotted curve), because of excessive tilting and stretching. In fact, for values of m_0 larger than one, the tilting of the curves become very high, as the slope of the straight line $\theta_A(\tau) = \sqrt{m_0^2 - 1}\,\tau + \gamma_A$ becomes higher, so that it does not allow the presence of minima of the potential u_{eff}, which are positions of stable equilibrium of the considered system. This property is due to the fact that by applying a very high momentum of force to our system, this external momentum is not compensated by the other terms present at the second member of relation (2.4), so it is not reached the condition of stable equilibrium.

This feature can be also derived analytically from equation (2.19), by just taking the derivative with respect to θ and by setting it to zero. Of course, this corresponds to finding the fixed point of the dynamical equation (2.7) and brings us to the same results as in Section 2.3). In fact we get:

$$\frac{\partial u_{eff}}{\partial \theta} = 0 \Rightarrow \frac{\partial}{\partial \theta}(1 - \cos\theta - m_0\theta) = 0 \Rightarrow \sin\theta - m_0 = 0$$

So we obtain $\sin\theta = m_0$, that is, we get the relation just found for the so-called fixed points, for which $\dfrac{d\theta}{d\tau} = 0$, as previously determined.

2.6 Conclusions

The properties of an over-damped Josephson junction have been analyzed by means of a mechanical analogue: an over-damped pendulum. The strict analogy between the dynamical equations of the two systems [15], [2], [3], [17], has been first reviewed. Being the physical properties of a simple pendulum more familiar to students, the Josephson junction dynamics in the over-damped limit may be derived by analogy. Therefore, we have analyzed [16] some interesting features of an over-damped Josephson junction, by means of the corresponding physical properties of the over-damped pendulum. As an example, we have noticed that the current-voltage characteristics of the superconducting device can be obtained by means of an analytical expression derived for the normalized driving moment as a function of the time average of the angular frequency. Finally, by considering the energy balance equation for the system, we have seen that it is possible to describe the effect of the driving moment on the pendulum through the tilting and stretching of the washboard potential.

Apart from the analogy between the over-damped Josephson junction and the over-damped pendulum, this work can be adopted as a lecture for first-year college physics students, in order to integrate the usual description of the pendulum made by means of the small oscillations approximation. In addition, starting from a mechanical system devised in such a way that the pre-factor of the second derivative in Eq. (2.6) is negligible, teachers may experiment on the effect of a constant applied torque on the pendulum, adding to direct observation the simple comment that similar response is expected in an over-damped Josephson junction. In the future, experimental work based on the present analysis will be performed, after a careful fabrication of the mechanical system. Extension of the present analysis to non-constant applied torque will also be sought.

Appendix 2.1

Proof of the relation 2.6

Starting from the equation (2.14) and dividing both members for $m^* g(l+R)$, we get:

$$
\frac{I_0}{m^* g(l+R)}\frac{d^2\theta}{dt^2} = -\frac{F_S}{m^* g} - \sin\theta + \frac{M_0(t)}{m^* g(l+R)} \Rightarrow
$$

$$
\frac{I_0}{m^* g(l+R)}\frac{d^2\theta}{dt^2} = -\frac{6\pi\eta R(l+R)}{m^* g}\frac{d\theta}{dt} - \sin\theta + m_0(t)
$$

(2.1.1)

where we have used the expression $F_S = 6\pi\eta R(l+R)\dfrac{d\theta}{dt}$ and $m_0(t) = \dfrac{M_0(t)}{m^* g(l+R)}$.

By defining $\tau = \dfrac{m^*g}{6\pi\eta R(l+R)}t \Rightarrow d\tau = \dfrac{m^*g}{6\pi\eta R(l+R)}dt$, we obtain:

$$\frac{6\pi\eta R(l+R)}{m^*g}\frac{d\theta}{dt} = \frac{d\theta}{d\tau}.$$

As we know that: $I_0 = \dfrac{2}{5}mR^2 + m(l+R)^2$, we have:

$$\frac{I_0}{m^*g(l+R)} = \frac{m(\frac{2}{5}R^2 + l^2 + R^2 + 2lR)}{m^*g(l+R)} = \frac{m(\frac{7}{5}R^2 + l^2 + 2lR)}{m^*g(l+R)}. \tag{2.1.2}$$

By considering that

$$d\tau^2 = \left(\frac{m^*g}{6\pi\eta R(l+R)}\right)^2 dt^2, \text{ and also}$$

$$m^*g(l+R) = m^*g(l+R)\frac{(6\pi\eta R)^2(l+R)^2}{(m^*g)^2}\frac{(m^*g)^2}{[6\pi\eta R(l+R)]^2} = \frac{(6\pi\eta R)^2(l+R)^3}{m^*g}\frac{(m^*g)^2}{[6\pi\eta R(l+R)]^2},$$

we get the following expression:

$$\frac{I_0}{m^*g(l+R)}\frac{d^2\theta}{dt^2} = \frac{m(\frac{7}{5}R^2 + l^2 + 2lR)m^*g}{\dfrac{(6\pi\eta R)^2(l+R)^3}{m^*g}\dfrac{(m^*g)^2}{[6\pi\eta R(l+R)]^2}}\frac{d^2\theta}{dt^2} = \frac{m(\frac{7}{5}R^2 + l^2 + 2Rl)m^*g}{(6\pi\eta R)^2(l+R)^3}\frac{d^2\theta}{d\tau^2}. \tag{2.1.3}$$

Therefore, by (2.1.1), we get the additional expression:

$$\frac{m^*mg(l^2 + 2lR + \frac{7}{5}R^2)}{(6\pi\eta R)^2(l+R)^3}\frac{d^2\theta}{d\tau^2} = -\frac{d\theta}{d\tau} - \sin\theta + m_0(\tau).$$

In this way, we may set:

$$\frac{m^*mg(l^2 + 2lR + \frac{7}{5}R^2)}{(6\pi\eta R)^2(l+R)^3}\frac{d^2\theta}{d\tau^2} + \frac{d\theta}{d\tau} + \sin\theta = m_0(\tau),$$

that is just equation (2.6), which we have so proven.

Chapter 3

Double and triple- barrier Josephson junctions

A generalization of the semiclassical model describing the Josephson dynamics of trilayer superconducting systems is given by assuming a constant nonnull arbitrary superconducting phase for the inner electrode, and the presence of inhomogeneities in the superconducting coupling between electrodes. Extension of the model to triple-barrier Josephson junctions is proposed.

3.1 Introduction

Considering the simplicity and the efficacy of Feynman's and Ohta's models [2-3] in describing the dynamics of a Josephson junction (JJ), F. Romeo and R. De Luca have recently developed a semiclassical model for SISIS (S standing for Superconsutor and I for Insulator) trilayer superconducting systems [14]. Similar models had already been adopted by Carapella et al. [19] by considering a voltage bias across each one of the two Josephson junctions in the trilayer system. In the latter work, however, the trilayer system could not be seen as a single JJ across which a superconducting phase difference φ is detected. Instead, three-layer systems in which an external electromotive force is applied only to the outer electrodes are denoted as Double-Barrier JJs (DBJJs). These systems have been experimentally investigated by Nevirkovets et al. [20, 21, 22]. Integer and fractional shapiro steps were detected by the latter authors, so that deviations from the simple sinusoidal dependence of the current-phase relation (CPR) can be hypothesized. In fact, the same authors introduced the idea of a modified CPR for the SISIS structure, to take account of the additional channel of Josephson tunnelling between the two outer electrodes. A microscopic theory of DBJJs confirming the existence of non-sinusoidal CPRs in DBJJs has been developed by Brinkmann et al. [23].

In reference [14], however, only the case of homogeneous JJ coupling and of zero values of the superconducting phase of the inner electrode was treated. In this way, the current I vs. superconducting phase φ relation of the system can be shown to be given by:

$$I = I_0\left[\gamma \sin\varphi + \text{sgn}\left[\cos\frac{\varphi}{2}\right]\sin\left(\frac{\varphi}{2}\right)\right], \tag{3.1}$$

where I_0 and γ are proportional to the coupling energies between two adjacent electrodes and the two outermost electrodes in the JJ, respectively. In equation (3.1) we clearly see two contributions.

In fact, the first addendum represents the weak Josephson coupling between the outermost electrodes. On the other hand, the second addendum takes into account the strong coupling (Kulik and Omel'yanchuk limit [24]) between the adjacent layers.

In this way, we may say that the relation (3.1) is the superposition of two different simultaneously present contributions originated by the heterogeneous nature of the Josephson coupling [25]. In case

the maximum Josephson currents, I_1 and I_2, in the JJs of the trilayer system are different, we have [26]

$$I = I_0 \left[\gamma + \frac{\left(1 - \varepsilon^2\right)}{2\sqrt{1 - \left(1 - \varepsilon^2\right)\sin^2\left(\dfrac{\varphi}{2}\right)}} \right] \sin \varphi \, , \tag{3.2}$$

where I_0 is the average value of I_1 and I_2, and where $\varepsilon = \dfrac{I_2 - I_1}{2I_0}$.

In the present chapter we show that the choice of an arbitrary superconducting phase, supposed to be constant, for the inner electrode and the presence of inhomogeneities in the JJ coupling leads to the same Current Phase Relation (CPR) found in ref. [26], here reported in Eq. (3.2). Therefore, in the absence of inhomogeneities in the JJ coupling, the CPR of the system can be shown to be the same as in espression (3.1), in the limit of $\varepsilon = 0$. We finally propose a generalization of the semiclassical model to triple-barrier JJs (TBJJs) arising from SISISIS structures. Therefore, the present chapter is organized as follows.

We further release the assumption made in previous works, where a strictly null superconducting macroscopic phase was associated to the inner electrode. In this way, we consider the semiclassical Ohta's analysis for a inhomogeneous three-layer system, obtaining a CPR for this system equal to Eq. (3.2). Successively, we propose an extension of this model to triple-barrier Josephson junctions, deriving the related CPR. The Shapiro steps for these systems are then calculated, as experimentally related quantities able to indirectly confirm the particular expression of the CPR derived.

3.2 Semiclassical analysis of a inhomogeneous DBJJ

First of all, let us consider a schematic representation [8] of this particular superconducting three-layer system, where, taking into account the inhomogeneities in the couplings of the junctions, we may enumerate three coupling constants: K_1 and K_2 between the electrodes 2-1 and 2-3, and $\tilde{K}$ between 1 and 3. The system is schematically shown in figure 3.1.
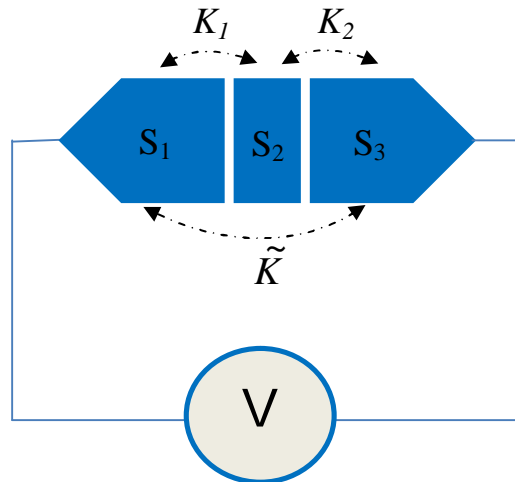

Figure 3.1. *Schematic representation of an inhomogeneous three-layer SISIS system, where the coupling constants for adjacent layers, K_1 and K_2 are assumed to be different. The constant $\tilde{K}$, on the other hand, couples the outermost layers to which a voltage V is applied.*

We may start our analysis by considering the Hamiltonian function H_0 of the trilayer system, called the semiclassical Hamiltonian, that is the expectation value of the Hamiltonian operator H_0. In this way, we write:

$$H_0 = (\psi_1^* \ \psi_2^* \ \psi_3^*) \begin{pmatrix} E_1 & -K_1 & -\tilde{K} \\ -K_1 & E_2 & -K_2 \\ -\tilde{K} & -K_2 & E_3 \end{pmatrix} \begin{pmatrix} \psi_1 \\ \psi_2 \\ \psi_3 \end{pmatrix} \tag{3.3}$$

In the above expression ψ_k and E_k (for $k = 1, 2, 3$) are the wave function and the ground state energy of the k-th superconductor S_k, respectively. Moreover, as shown in figure 3.1, K_1, K_2 are the coupling constants between adjacent layers, and $\tilde{K}$ is the coupling constant between the two outer junction electrodes. In this way, we have:

$$H_0 = E_1 |\psi_1|^2 + E_2 |\psi_2|^2 + E_3 |\psi_3|^2 - K_1(\psi_1^* \psi_2 + \psi_2^* \psi_1) - K_2(\psi_2^* \psi_3 + \psi_3^* \psi_2) - \tilde{K}(\psi_1^* \psi_3 + \psi_3^* \psi_1). \tag{3.4}$$

The superconducting wave functions ψ_1, ψ_2 and ψ_3 may be written as follows:

$$\psi_1 = \sqrt{N_1} e^{-i\theta_1} \ ; \ \psi_2 = \sqrt{N_2} e^{-i\theta_2} \ ; \ \psi_3 = \sqrt{N_3} e^{-i\theta_3} \tag{3.5}$$

where N_k is the numerical density of Cooper pairs, and θ_k is the superconducting phase of the k-th electrode ($k = 1, 2, 3$). We may now consider $\theta_2 = \alpha = \text{constant} \neq 0$. By substituting the three definitions (3.5) in the relation (3.4), and by carrying out the calculations, we get:

$$H_0 = E_1 N_1 + E_2 N_2 + E_3 N_3 - 2K_1 \sqrt{N_1 N_2} \cos(\theta_1 - \alpha) - 2K_2 \sqrt{N_2 N_3} \cos(\theta_3 - \alpha)$$
$$- 2\tilde{K} \sqrt{N_1 N_3} \cos(\theta_3 - \theta_1) \tag{3.6}$$

or also:

$$H_0 = \sum_{k=1}^{3} E_k N_k + W_C \tag{3.7}$$

where:

$$W_C = -2K_1 \sqrt{N_1 N_2} \cos(\theta_1 - \alpha) - 2K_2 \sqrt{N_2 N_3} \cos(\theta_3 - \alpha) - 2\tilde{K} \sqrt{N_1 N_3} \cos(\theta_3 - \theta_1) \tag{3.8}$$

Let's now introduce the energy W_{ext} of the external circuit in the semiclassical Hamiltonian H_0:

$$W_{ext} = \int VIdt , \tag{3.9}$$

where V is the voltage of the e.m.f. source, I is the electric current, and the integral is carried out over time t. In this way, we get the complete Hamiltonian H as follows:

$$H = H_0 - W_{ext} \tag{3.10}$$

Following Ohta's semiclassical model, we can now consider the Hamilton's equations for the quantities θ_k and $\hbar N_k$, which are conjugated variables:

$$\hbar \dot{N}_k = -\frac{\partial H}{\partial N_k}, \tag{3.11}$$

$$\dot{\theta}_k = \frac{1}{\hbar}\frac{\partial H}{\partial N_k}, \tag{3.12}$$

for $k = 1, 2, 3$.

In the above expressions the dot stands for the derivative with respect to time. Under the assumption of thermal bath, we get $\dot{N}_1 = \dot{N}_2 = \dot{N}_3 = 0$, because temperature is uniform and constant, and we can also consider that there is energy conservation of the whole thermodynamic system, because it is not dissipative. Under these hypotheses, we may thus write:

$$\dot{H} = \dot{W}_C - \dot{W}_{ext} = 0. \tag{3.13}$$

By these assumptions, equation (3.11) becomes an identity and equation (3.12) gives:

$$\dot{\theta}_k = \frac{E_k}{\hbar}, \qquad (k = 1, 2, 3). \tag{3.14}$$

Knowing that a voltage difference V across the first and the third electrode is present, we may consider $E_1 = -\frac{eV}{\hbar}$, $E_3 = \frac{eV}{\hbar}$ and $E_2 = 0$, because $\theta_2 = \alpha = $ constant. Therefore, by equation (3.14), we get:

$$\dot{\theta}_3 - \dot{\theta}_1 = \frac{2eV}{\hbar}. \tag{3.15}$$

If we now set $\varphi = \theta_3 - \theta_1$, we obtain:

$$\frac{d\varphi}{dt} = \frac{2eV}{\hbar}. \tag{3.16}$$

The above equation is the strict Josephson voltage phase relation.

3.3 Current Phase Relation

In order to obtain the first Josephson equation [11], or CPR, for this particular superconducting three-layer system, we may make use of equation (3.13) and write:

$$\dot{W}_C = \dot{W}_{ext} = IV \Rightarrow I = \frac{\dot{W}_C}{V}.$$

By calculating $\dot{W}_C$ we have:

$$\dot{W}_C = 2K_1\sqrt{N_1N_2}\left[\sin(\theta_1-\alpha)\right]\dot{\theta}_1 + 2K_2\sqrt{N_2N_3}\left[\sin(\theta_3-\alpha)\right]\dot{\theta}_3 +$$
$$2\tilde{K}\sqrt{N_1N_3}\left[\sin(\theta_3-\theta_1)\right]\left(\dot{\theta}_3-\dot{\theta}_1\right) \tag{3.17}$$

In this way, we obtain:

$$IV = 2K_1\sqrt{N_1N_2}\left[\sin(\theta_1-\alpha)\right]\left(-\frac{eV}{\hbar}\right) + 2K_2\sqrt{N_2N_3}\left[\sin(\theta_3-\alpha)\right]\left(\frac{eV}{\hbar}\right) + 2\tilde{K}\sqrt{N_1N_3}\left[\sin(\theta_3-\theta_1)\right]\left(\frac{2eV}{\hbar}\right).$$

Considering that $\varphi = \theta_3 - \theta_1$ and putting the term $\dfrac{2eV}{\hbar}$ in evidence, we have:

$$I = \frac{2e}{\hbar}\left[-K_1\sqrt{N_1N_2}\sin(\theta_1-\alpha) + K_2\sqrt{N_2N_3}\sin(\theta_3-\alpha)\right] + \frac{4e\tilde{K}}{\hbar}\sqrt{N_1N_3}\sin\varphi \tag{3.18}$$

It is more useful to represent the expressions (3.8) and (3.16) in terms of the following superconducting phases:

$$\theta_A = \frac{\theta_1+\theta_2}{2} \quad ; \quad \varphi = \theta_3 - \theta_1 \; .$$

We therefore have:

$$\theta_1 = \theta_A - \frac{\varphi}{2} \quad ; \quad \theta_3 = \theta_A + \frac{\varphi}{2} \; ;$$

so that:

$$I = \frac{2e}{\hbar}\left[-K_1\sqrt{N_1N_2}\sin\left(\theta_A-\frac{\varphi}{2}-\alpha\right) + K_2\sqrt{N_2N_3}\sin\left(\theta_A+\frac{\varphi}{2}-\alpha\right)\right] + \frac{4e\tilde{K}}{\hbar}\sqrt{N_1N_3}\sin\varphi \; , \tag{3.19}$$

$$W_C = -2K_1\sqrt{N_1N_2}\cos\left(\theta_A-\frac{\varphi}{2}-\alpha\right) - 2K_2\sqrt{N_2N_3}\cos\left(\theta_A+\frac{\varphi}{2}-\alpha\right) - 2\tilde{K}\sqrt{N_1N_3}\cos\varphi \; . \tag{3.20}$$

In order to determine θ_A, we minimize W_C, according to the principle of energy minimum. Therefore, we write:

$$\frac{\partial W_C}{\partial \theta_A} = 0 \Rightarrow 2K_1\sqrt{N_1N_2}\sin(\theta_A-\frac{\varphi}{2}-\alpha) + 2K_2\sqrt{N_2N_3}\sin(\theta_A+\frac{\varphi}{2}-\alpha) = 0.$$

By the aboe, we get:

$$K_1 \sqrt{N_1 N_2} \sin(\theta_A - \frac{\varphi}{2} - \alpha) = -K_2 \sqrt{N_2 N_3} \sin(\theta_A + \frac{\varphi}{2} - \alpha). \tag{3.21}$$

In this way, the expression for the current I becomes:

$$I = \frac{4eK_1}{\hbar} \sqrt{N_1 N_2} \sin(\frac{\varphi}{2} - \theta_A + \alpha) + \frac{4eK}{\hbar} \sqrt{N_1 N_3} \sin\varphi.$$

Let us now set $\tilde{\theta} = \theta_A - \frac{\varphi}{2}$. With this position we have the more simplified expression:

$$I = \frac{4eK_1}{\hbar} \sqrt{N_1 N_2} \sin(\frac{\varphi}{2} - \tilde{\theta}) + \frac{4e\tilde{K}}{\hbar} \sqrt{N_1 N_3} \sin\varphi. \tag{3.22}$$

We also can express W_C through $\tilde{\theta}$ and φ in this way:

$$W_C = -2K_1 \sqrt{N_1 N_2} \cos(\frac{\varphi}{2} - \tilde{\theta}) - 2K_2 \sqrt{N_2 N_3} \cos(\frac{\varphi}{2} + \tilde{\theta}) - 2\tilde{K} \sqrt{N_1 N_3} \cos\varphi. \tag{3.23}$$

We now set:

$$I_1 = \frac{4eK_1}{\hbar} \sqrt{N_1 N_2}; \quad I_2 = \frac{4eK_2}{\hbar} \sqrt{N_2 N_3}; \quad \tilde{I} = \frac{4e\tilde{K}}{\hbar} \sqrt{N_1 N_3};$$

In this way, eq. (3.23) can be rewritten as follows:

$$W_C = -\frac{\hbar}{2e} \left[I_1 \cos(\frac{\varphi}{2} - \tilde{\theta}) + I_2 \cos(\frac{\varphi}{2} + \tilde{\theta}) + \tilde{I} \cos\varphi \right]. \tag{3.24}$$

By now taking:

$\frac{I_1 + I_2}{2} = I_0$, we may consider:

$I_1 = I_0 (1 - \varepsilon)$
$I_2 = I_0 (1 + \varepsilon)$

Therefore:

$$W_C = -\frac{\hbar I_0}{2e} \left[(1 - \varepsilon) \cos(\frac{\varphi}{2} - \tilde{\theta}) + (1 + \varepsilon) \cos(\frac{\varphi}{2} + \tilde{\theta}) + \gamma \cos\varphi \right] \tag{3.25}$$

where $\gamma = \frac{\tilde{I}}{I_0}$. By now recalling basic trigonometric relations, we have:

$$\cos(\frac{\varphi}{2} + \tilde{\theta}) + \cos(\frac{\varphi}{2} - \tilde{\theta}) = 2\cos\tilde{\theta}\cos\frac{\varphi}{2}$$

$$\cos(\frac{\varphi}{2} + \tilde{\theta}) - \cos(\frac{\varphi}{2} - \tilde{\theta}) = -2\sin\tilde{\theta}\sin\frac{\varphi}{2}$$

and thus:

$$W_C = -\frac{\hbar I_0}{2e}\left(2\cos\tilde{\theta}\cos\frac{\varphi}{2} - 2\varepsilon\sin\tilde{\theta}\sin\frac{\varphi}{2} + \gamma\cos\varphi\right). \tag{3.26}$$

In the same way, eq. (3.20), according to these positions, can be rewritten as follows:

$$I = I_1\sin\left(\frac{\varphi}{2} - \tilde{\theta}\right) + \tilde{I}\sin\varphi \Rightarrow$$

$$I = I_o(1-\varepsilon)\sin\left(\frac{\varphi}{2} - \tilde{\theta}\right) + \gamma I_0\sin\varphi \Rightarrow \tag{3.27}$$

$$I = I_0\left[(1-\varepsilon)\sin\left(\frac{\varphi}{2} - \tilde{\theta}\right) + \gamma\sin\varphi\right]$$

Now we must find the relation between $\tilde{\theta}$ and φ, in order to express $\tilde{\theta}$ in function of φ, and so to obtain the expression of W_C in function of φ, and the expression of I in function of φ (the latter being the CPR). By therefore considering equation (3.19), and by using the expressions of I_1 and I_2, we have:

$$I_1\sin\left(\frac{\varphi}{2} - \tilde{\theta}\right) = I_2\sin\left(\frac{\varphi}{2} + \tilde{\theta}\right) \Rightarrow$$

$$(1-\varepsilon)\sin\left(\frac{\varphi}{2} - \tilde{\theta}\right) = (1+\varepsilon)\sin\left(\frac{\varphi}{2} + \tilde{\theta}\right)$$

or also:

$$\sin\left(\frac{\varphi}{2} + \tilde{\theta}\right) - \sin\left(\frac{\varphi}{2} - \tilde{\theta}\right) = -\varepsilon\left[\sin\left(\frac{\varphi}{2} + \tilde{\theta}\right) + \sin\left(\frac{\varphi}{2} - \tilde{\theta}\right)\right] \Rightarrow$$

$$2\sin\tilde{\theta}\cos\frac{\varphi}{2} = -2\varepsilon\sin\frac{\varphi}{2}\cos\tilde{\theta}$$

The above relation is equivalent to the following:

$$\tan\tilde{\theta} = -\varepsilon\tan\frac{\varphi}{2}. \tag{3.28}$$

By now considering eq. (3.26), we can find $\cos\tilde{\theta}$ and $\sin\tilde{\theta}$ in function of φ and ε. In fact, for $\cos\tilde{\theta}$, we have:

$\dfrac{1}{\cos^2 \tilde{\theta}} - 1 = \tan^2 \tilde{\theta} = \varepsilon^2 \tan^2 \dfrac{\varphi}{2}$, so that:

$$\cos \tilde{\theta} = \pm \frac{1}{\sqrt{1 + \varepsilon^2 \tan^2 \dfrac{\varphi}{2}}} = \pm \frac{\left|\cos \dfrac{\varphi}{2}\right|}{\sqrt{\varepsilon^2 + (1 - \varepsilon^2)\cos^2 \dfrac{\varphi}{2}}} .$$

For the expression of $\sin \tilde{\theta}$, we may use eq. (3.28), and we get:

$$\sin \tilde{\theta} = -\varepsilon \tan \frac{\varphi}{2} \cos \tilde{\theta} \Rightarrow$$

$$\sin \tilde{\theta} = \frac{-\varepsilon\left(\pm \left|\cos \dfrac{\varphi}{2}\right|\right)\tan \dfrac{\varphi}{2}}{\sqrt{\varepsilon^2 + (1 - \varepsilon^2)\cos^2 \dfrac{\varphi}{2}}} = \frac{\mp \varepsilon \cos \dfrac{\varphi}{2}\, \mathrm{sgn}\!\left(\cos \dfrac{\varphi}{2}\right)\tan \dfrac{\varphi}{2}}{\sqrt{\varepsilon^2 + (1 - \varepsilon^2)\cos^2 \dfrac{\varphi}{2}}} = \frac{\mp \varepsilon \sin \dfrac{\varphi}{2}\, \mathrm{sgn}\!\left(\cos \dfrac{\varphi}{2}\right)}{\sqrt{\varepsilon^2 + (1 - \varepsilon^2)\cos^2 \dfrac{\varphi}{2}}}$$

Therefore eq. (3.23) now becomes:

$$W_C = -\frac{\hbar I_0}{2e}\left[\frac{\pm 2 \cos \dfrac{\varphi}{2}\left|\cos \dfrac{\varphi}{2}\right|}{\sqrt{\varepsilon^2 + (1 - \varepsilon^2)\cos^2 \dfrac{\varphi}{2}}} + \frac{\pm 2\varepsilon^2 \left(\sin^2 \dfrac{\varphi}{2}\right)\left(\mathrm{sgn}(\cos \dfrac{\varphi}{2})\right)}{\sqrt{\varepsilon^2 + (1 - \varepsilon^2)\cos^2 \dfrac{\varphi}{2}}} + \gamma \cos \varphi\right] =$$

$$-\frac{\hbar I_0}{2e}\left[\frac{\pm 2\,\mathrm{sgn}(\cos \dfrac{\varphi}{2})}{\sqrt{\varepsilon^2 + (1 - \varepsilon^2)\cos^2 \dfrac{\varphi}{2}}}\left(\cos^2 \dfrac{\varphi}{2} + \varepsilon^2 \sin^2 \dfrac{\varphi}{2}\right) + \gamma \cos \varphi\right]$$

According to the principle of minimum energy, we can take $\pm \,\mathrm{sgn}\!\left(\cos \dfrac{\varphi}{2}\right) = 1$, in order to minimize the expression of W_C.

We thus obtain:

$$W_C = -\frac{\hbar I_0}{2e}\left[\frac{2\left(\cos^2 \dfrac{\varphi}{2} + \varepsilon^2 sen^2 \dfrac{\varphi}{2}\right)}{\sqrt{\varepsilon^2 + (1 - \varepsilon^2)\cos^2 \dfrac{\varphi}{2}}} + \gamma \cos \varphi\right] \Rightarrow$$

$$W_C = -\frac{\hbar I_0}{2e}\left\{\frac{2\left[\varepsilon^2 + (1 - \varepsilon^2)\cos^2 \dfrac{\varphi}{2}\right]}{\sqrt{\varepsilon^2 + (1 - \varepsilon^2)\cos^2 \dfrac{\varphi}{2}}} + \gamma \cos \varphi\right\}$$

(3.29)

Similarly, the electric current I in eq. (3.27) becomes:

$$I = I_0(1-\varepsilon)\sin\left(\frac{\varphi}{2}-\tilde{\theta}\right)+\gamma I_0\sin\varphi = I_0(1-\varepsilon)\left[\sin\frac{\varphi}{2}\cos\tilde{\theta}-\cos\frac{\varphi}{2}\sin\tilde{\theta}\right]+\gamma I_0\sin\varphi =$$

$$I_0(1-\varepsilon)\left[\frac{\pm\sin\frac{\varphi}{2}\left|\cos\frac{\varphi}{2}\right|}{\sqrt{\varepsilon^2+(1-\varepsilon^2)\cos^2\frac{\varphi}{2}}}+\frac{\pm\varepsilon\sin\frac{\varphi}{2}\cos\frac{\varphi}{2}\mathrm{sgn}\left(\cos\frac{\varphi}{2}\right)}{\sqrt{\varepsilon^2+(1-\varepsilon^2)\cos^2\frac{\varphi}{2}}}\right]+\gamma I_0\sin\varphi =$$

$$I_0(1-\varepsilon)\left[\frac{\left(\pm\mathrm{sgn}(\cos\frac{\varphi}{2})\right)\left(\sin\frac{\varphi}{2}\cos\frac{\varphi}{2}+\varepsilon\sin\frac{\varphi}{2}\cos\frac{\varphi}{2}\right)}{\sqrt{\varepsilon^2+(1-\varepsilon^2)\cos^2\frac{\varphi}{2}}}\right]+\gamma I_0\sin\varphi$$

Using the relation $\pm\mathrm{sgn}\left(\cos\frac{\varphi}{2}\right)=1$ considered above, we have:

$$I = I_0(1-\varepsilon)\frac{(1+\varepsilon)\sin\frac{\varphi}{2}\cos\frac{\varphi}{2}}{\sqrt{\varepsilon^2+(1-\varepsilon^2)\cos^2\frac{\varphi}{2}}}+\gamma I_0\sin\varphi =$$

$$I_0\frac{(1-\varepsilon^2)\cos\frac{\varphi}{2}}{\sqrt{\varepsilon^2+(1-\varepsilon^2)\cos^2\frac{\varphi}{2}}}\sin\frac{\varphi}{2}+\gamma I_0\sin\varphi$$

In this way, we get:

$$I = I_0\left[\frac{(1-\varepsilon^2)\cos\frac{\varphi}{2}}{\sqrt{\varepsilon^2+(1-\varepsilon^2)\cos^2\frac{\varphi}{2}}}\sin\frac{\varphi}{2}+\gamma\sin\varphi\right] \qquad (3.30)$$

If we consider the limit for $\varepsilon\to 0$ of this expression, which corresponds to the physical situation $I_1 = I_2$, where the electric current from 2 to 1 and from 2 to 3 are the same, we get:

$$\lim_{\varepsilon\to 0}\frac{(1-\varepsilon^2)\cos\frac{\varphi}{2}\sin\frac{\varphi}{2}}{\sqrt{\varepsilon^2+(1-\varepsilon^2)\cos^2\frac{\varphi}{2}}}=\frac{\cos\frac{\varphi}{2}}{\left|\cos\frac{\varphi}{2}\right|}\sin\frac{\varphi}{2}=\mathrm{sgn}\left(\cos\frac{\varphi}{2}\right)\sin\frac{\varphi}{2}.$$

We thus obtain:

$$I = I_0\left[\mathrm{sgn}\left(\cos\frac{\varphi}{2}\right)\sin\frac{\varphi}{2}+\gamma\sin\varphi\right]$$

This result agrees with the one found getting $\theta_2 = 0$, and also considering an homogeneous coupling, analysed, as just mentioned, by F. Romeo and R. De Luca [14].

3.4 Extensions of the model to triple barrier Josephson junctions

We can now consider [8] a system made up by a triple barrier Josephson Junction, i.e., a four-layer superconducting system, with no phase difference between S_2 and S_3. A schematic representation of this physical system is given in figure 3.2, where the coupling constants K_1, K_2 and K_3 between electrodes 1-2, 2-3 and 3-4, respectively, are not taken to be equal. The remaining coupling constants $\tilde{K}_1$ and $\tilde{K}_2$ pertain to interactions between the superconducting layers 1-3 and 2-4, respectively.
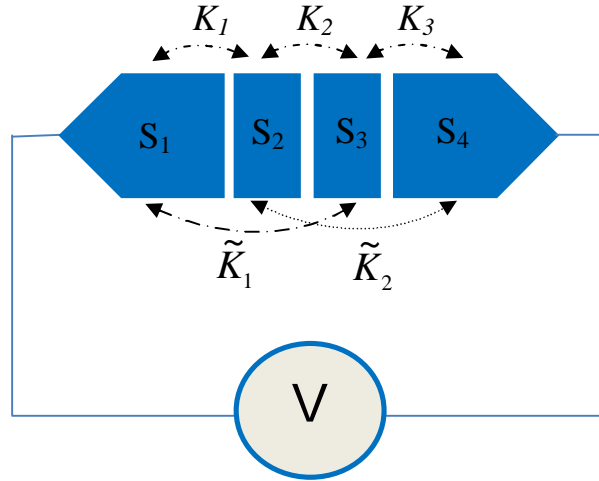

Figure 3.2. *Schematic representation of an inhomogeneous four-layer SISISIS system, where the coupling constants for adjacent layers K_1, K_2 and K_3 are assumed to be different. The constants $\tilde{K}_1$ and $\tilde{K}_2$, on the other hand, couple the next nearest neighbour layers $S_1 - S_3$ and $S_2 - S_4$, respectively. A voltage V is applied to the outermost layers S_1 and S_4.*

As before, the latter parameters are taken to be small compared to the direct coupling parameters K_1, K_2, and K_3. In what follows we shall consider the same steps illustrated in the previous section, with the hypothesis that the inner two layers S_2 and S_3 can be described by the same superconducting phase θ which we assume to be zero. Therefore, we can write the analytical expressions of the macroscopic wave functions of the various superconductors as follows:

$$\psi_1 = \sqrt{N_1}e^{-i\theta_1} \ ; \ \ \psi_2 = \sqrt{N_2} \ ; \ \ \psi_3 = \sqrt{N_3} \ ; \ \ \psi_4 = \sqrt{N_4}e^{-i\theta_4}$$

Following Ohta's semiclassical model we can first calculate the expectation value of the Hamiltonian operator $\hat{H}_0$ of the four-layer superconducting system, and then, as usual, we add the energy contribution of the external e.m.f. source. By proceeding as in the prevoious section, we therefore get:

$$H_0 = \langle \psi | \hat{H}_0 | \psi \rangle = \begin{pmatrix} \psi_1^* & \psi_2^* & \psi_3^* & \psi_4^* \end{pmatrix} \begin{pmatrix} E_1 & -K_1 & -\hat{K}_1 & 0 \\ -K_1 & E_2 & -K_2 & -\hat{K}_2 \\ -\hat{K}_1 & -K_2 & E_3 & -K_3 \\ 0 & -\hat{K}_2 & -K_3 & E_4 \end{pmatrix} \begin{pmatrix} \psi_1 \\ \psi_2 \\ \psi_3 \\ \psi_4 \end{pmatrix} \tag{3.31}$$

By straightforward calculations, we have:

$$H_0 = \sum_{K=1}^{4} E_K N_K + W_C = \sum_{K=1}^{4} E_K N_K - 2K_1\sqrt{N_1 N_2}\cos\theta_1 - 2\hat{K}_2\sqrt{N_1 N_3}\cos\theta_3 - 2K_2\sqrt{N_2 N_3} +$$
$$-2K_3\sqrt{N_3 N_4}\cos\theta_4 - 2\tilde{K}_2\sqrt{N_2 N_4}\cos\theta_4.$$

Therefore, by inspection, we may see that:

$$W_C = -2(K_1\sqrt{N_1 N_2} + \tilde{K}_1\sqrt{N_1 N_3})\cos\theta_1 - 2K_2\sqrt{N_2 N_3} - 2(K_3\sqrt{N_3 N_4} + \tilde{K}_2\sqrt{N_2 N_4})\cos\theta_4. \tag{3.32}$$

Adding the external energy contribution $W_{ext} = \int VI dt$ we have:

$$H = \sum_{K=1}^{4} E_K N_K + (W_C - W_{ext}) = \sum_{K=1}^{4} E_K N_K + (W_C - \int VI dt). \tag{3.33}$$

With the usual assumption of thermal bath, we may write: $\dot{N}_1 = \dot{N}_2 = \dot{N}_3 = \dot{N}_4 = 0$, so that $\dot{W}_C - \dot{W}_{ext} = 0 \Rightarrow IV = \dot{W}_C$. By now using the classical Hamilton's equations for the conjugate variables θ_k and $\hbar N_k$, we obtain:

$$\dot{\theta}_k = \frac{1}{\hbar}\frac{\partial H}{\partial N_k} \Rightarrow \dot{\theta}_k = \frac{E_k}{\hbar} \quad \text{for } k = 1, 2, 3, 4. \tag{3.34}$$

From (3.34), using the previous hypotheses, we get:

$$E_2 = E_3 = 0.$$

In this way, we may write:

$$\dot{\theta}_1 = \frac{E_1}{\hbar} \quad ; \quad \dot{\theta}_4 = \frac{E_4}{\hbar}.$$

Let now: $E_1 = -eV$; $E_4 = eV$; by substituting the latter expressions in (3.34), we have:

$$\dot{\theta}_4 - \dot{\theta}_1 = \frac{eV - (-eV)}{\hbar} = \frac{2eV}{\hbar} \quad \Rightarrow \quad \frac{d\varphi}{dt} = \frac{2eV}{\hbar} \qquad \text{with} \quad \varphi = \theta_4 - \theta_1 \tag{3.35}$$

Equation (3.35) is the Josephson's voltage- phase relation (VPR) for the whole four-layer system. In order to obtain the current-phase relation (CPR), we may again use the expression: $I = \dfrac{\dot{W}_C}{V}$. With the thermal bath assumption considered above we have that the only quantities depending on time, in the expression of W_C, are $\cos\theta_1$ and $\cos\theta_4$. In this way, by straightforward calculation, we get:

$$\dot{W}_C = 2\left(K_1\sqrt{N_1 N_2} + \tilde{K}_1\sqrt{N_1 N_3}\right)(\sin\theta_1)\dot{\theta}_1 + 2\left(K_3\sqrt{N_3 N_4} + \tilde{K}_2\sqrt{N_2 N_4}\right)(\sin\theta_4)\dot{\theta}_4 =$$
$$\frac{2eV}{\hbar}\left[\left(-K_1\sqrt{N_1 N_2} - \tilde{K}_1\sqrt{N_1 N_3}\right)(\sin\theta_1) + \left(K_3\sqrt{N_3 N_4} + \tilde{K}_2\sqrt{N_2 N_4}\right)(\sin\theta_4)\right],$$

and so:

$$I = \frac{1}{V}\dot{W}_C = \frac{2e}{\hbar}\left[-\left(K_1\sqrt{N_1 N_2} + \tilde{K}_1\sqrt{N_1 N_3}\right)\sin\theta_1 + \left(\tilde{K}_2\sqrt{N_2 N_4} + K_3\sqrt{N_3 N_4}\right)\sin\theta_4\right].$$

By now defining the following quantities:

$$I_1 = \frac{4e}{\hbar}\left(K_1\sqrt{N_1 N_2} + \tilde{K}_1\sqrt{N_1 N_3}\right) \ ; \ I_2 = \frac{4e}{\hbar}\left(K_3\sqrt{N_3 N_4} + \tilde{K}_2\sqrt{N_2 N_4}\right),$$

we can rewrite I as follows:

$$I = -\frac{1}{2}I_1\sin\theta_1 + \frac{1}{2}I_2\sin\theta_4 = \frac{1}{2}\left(I_2\sin\theta_4 - I_1\sin\theta_1\right).$$

By introducing the average current , we can define the additional following quantities:

$$I_1 = I_0(1-\varepsilon) \ ; \ I_2 = I_0(1+\varepsilon) \quad \text{so that} \quad I_0 = \frac{I_1 + I_2}{2}$$

Finally, we have:

$$I = \frac{I_0}{2}\left[(1+\varepsilon)\sin\theta_4 - (1-\varepsilon)\sin\theta_1\right].$$

Let us now set: $\theta_A = \dfrac{\theta_1 + \theta_4}{2} \ ; \ \varphi = \theta_4 - \theta_1$, so that: $\theta_1 = \theta_A - \dfrac{\varphi}{2}$; $\theta_4 = \theta_A + \dfrac{\varphi}{2}$. The quantities I and W_C can thus be rewritten as follows:

$$I = \frac{I_0}{2}\left[(1+\varepsilon)sen\left(\theta_A + \frac{\varphi}{2}\right) + (1-\varepsilon)sen\left(\frac{\varphi}{2} - \theta_A\right)\right] \tag{3.36}$$

$$W_C = -2\left[\left(K_1\sqrt{N_1 N_2} + \tilde{K}_1\sqrt{N_1 N_3}\right)\cos\left(\theta_A - \frac{\varphi}{2}\right) + K_2\sqrt{N_2 N_3} + \left(K_3\sqrt{N_3 N_4} + \tilde{K}_2\sqrt{N_2 N_4}\right)\cos\left(\theta_A + \frac{\varphi}{2}\right)\right].$$

We can simplify the latter expression by multiplying it by $\frac{2e}{\hbar}$, and by using the previous definitions of I_1 and I_2, so that:

$$\frac{2e}{\hbar}W_C = -\left[I_1\cos\left(\theta_A - \frac{\varphi}{2}\right) + \frac{4eK_2}{\hbar}\sqrt{N_2 N_3} + I_2\cos\left(\theta_A + \frac{\varphi}{2}\right)\right] =$$

$$-\left[I_0(1-\varepsilon)\cos\left(\theta_A - \frac{\varphi}{2}\right) + \frac{4eK_2}{\hbar}\sqrt{N_2 N_3} + I_0(1+\varepsilon)\cos\left(\theta_A + \frac{\varphi}{2}\right)\right]. \tag{3.37}$$

According to the Minimum Energy Principle, we can consider that:

$$\frac{\partial}{\partial\theta_A}\left(\frac{2e}{\hbar}W_C\right) = 0.$$

From this equation we obtain a very useful relation; in fact, we have:

$$\frac{d}{d\theta_A}\left[(1-\varepsilon)I_0\cos\left(\theta_A - \frac{\varphi}{2}\right) + (1+\varepsilon)I_0\cos\left(\theta_A + \frac{\varphi}{2}\right)\right] = 0 \Rightarrow$$

$$I_0(1-\varepsilon)\sin\left(\theta_A - \frac{\varphi}{2}\right) + I_0(1+\varepsilon)\sin\left(\theta_A + \frac{\varphi}{2}\right) = 0 \Rightarrow$$

$$(1-\varepsilon)\sin\left(\frac{\varphi}{2} - \theta_A\right) = (1+\varepsilon)\sin\left(\frac{\varphi}{2} + \theta_A\right). \tag{3.38}$$

By using (3.36), we can simplify the expression for I; in fact, we have:

$$I = I_0(1+\varepsilon)\sin\left(\theta_A + \frac{\varphi}{2}\right). \tag{3.39}$$

We can now use equation (3.38) to obtain the expression of $\cos\theta_A$ and of $\sin\theta_A$ in function of ε and φ. In this respect, we can first use the following basic trigonometric relations:

$$\sin\left(\frac{\varphi}{2} - \theta_A\right) = \sin\frac{\varphi}{2}\cos\theta_A - \cos\frac{\varphi}{2}\sin\theta_A;$$

$$\sin\left(\frac{\varphi}{2} + \theta_A\right) = \sin\frac{\varphi}{2}\cos\theta_A + \cos\frac{\varphi}{2}\sin\theta_A;$$

So that Eq. (3.38) can be rewritten as follows:

$$\left(\frac{1-\varepsilon}{1+\varepsilon}\right)\left(\sin\frac{\varphi}{2}\cos\theta_A - \cos\frac{\varphi}{2}\sin\theta_A\right) = \sin\frac{\varphi}{2}\cos\theta_A + \cos\frac{\varphi}{2}\sin\theta_A \Rightarrow$$

$$\left(1 - \frac{1-\varepsilon}{1+\varepsilon}\right)\sin\frac{\varphi}{2}\cos\theta_A + \left(1 + \frac{1-\varepsilon}{1+\varepsilon}\right)\cos\frac{\varphi}{2}\sin\theta_A = 0 \Rightarrow$$

$$2\varepsilon\sin\frac{\varphi}{2}\cos\theta_A + 2\cos\frac{\varphi}{2}\sin\theta_A = 0 \Rightarrow$$

$$\tan\theta_A = -\varepsilon\tan\frac{\varphi}{2}.$$

By now using the latter expression, we therefore have:

$$\cos\theta_A = \pm\frac{1}{\sqrt{1 + \varepsilon^2\tan^2\frac{\varphi}{2}}} = \pm\frac{1}{\sqrt{1 + \varepsilon^2\left(\frac{\sin^2\frac{\varphi}{2}}{\cos^2\frac{\varphi}{2}}\right)}} = \pm\frac{\left|\cos\frac{\varphi}{2}\right|}{\sqrt{\varepsilon^2 + (1-\varepsilon^2)\cos^2\frac{\varphi}{2}}} \; ;$$

$$\sin\theta_A = \tan\theta_A\cos\theta_A = \mp\frac{\tan\frac{\varphi}{2}\left|\cos\frac{\varphi}{2}\right|}{\sqrt{\varepsilon^2 + (1-\varepsilon^2)\cos^2\frac{\varphi}{2}}} \; .$$

By considering the analytic expression of W_C, and requiring that it must attain its minimum value, it can be shown that this condition is met when $\pm\operatorname{sgn}\left(\cos\frac{\varphi}{2}\right) = 1$. In this way, we have:

$$\begin{cases} \cos\theta_A = \dfrac{\cos\dfrac{\varphi}{2}}{\sqrt{\varepsilon^2 + (1-\varepsilon^2)\cos^2\dfrac{\varphi}{2}}}, \\[4ex] \sin\theta_A = \dfrac{-\varepsilon\sin\dfrac{\varphi}{2}}{\sqrt{\varepsilon^2 + (1-\varepsilon^2)\cos^2\dfrac{\varphi}{2}}}. \end{cases} \qquad (3.40)$$

By now considering Eq. (3.39), and by using Eq. (3.40), we get:

$$I = I_0(1+\varepsilon)\left(\sin\theta_A\cos\frac{\varphi}{2} + \cos\theta_A\sin\frac{\varphi}{2}\right) = I_0(1+\varepsilon)\left(\frac{-\varepsilon\sin\frac{\varphi}{2}\cos\frac{\varphi}{2}}{\sqrt{\varepsilon^2 + (1-\varepsilon^2)\cos^2\frac{\varphi}{2}}} + \frac{\sin\frac{\varphi}{2}\cos\frac{\varphi}{2}}{\sqrt{\varepsilon^2(1-\varepsilon^2)\cos^2\frac{\varphi}{2}}}\right) =$$

$$I_0(1+\varepsilon)(1-\varepsilon)\frac{\sin\frac{\varphi}{2}\cos\frac{\varphi}{2}}{\sqrt{\varepsilon^2 + (1-\varepsilon^2)\cos^2\frac{\varphi}{2}}}.$$

Therefore, we finally obtain:

$$I = I_0 \frac{1-\varepsilon^2}{2} \frac{\sin\varphi}{\sqrt{\varepsilon^2 + (1-\varepsilon^2)\cos^2\frac{\varphi}{2}}} . \qquad (3.41)$$

Eq. (3.41) is the CPR for this particular four-layer superconducting system. It can be represented as done in the figure 3.3.
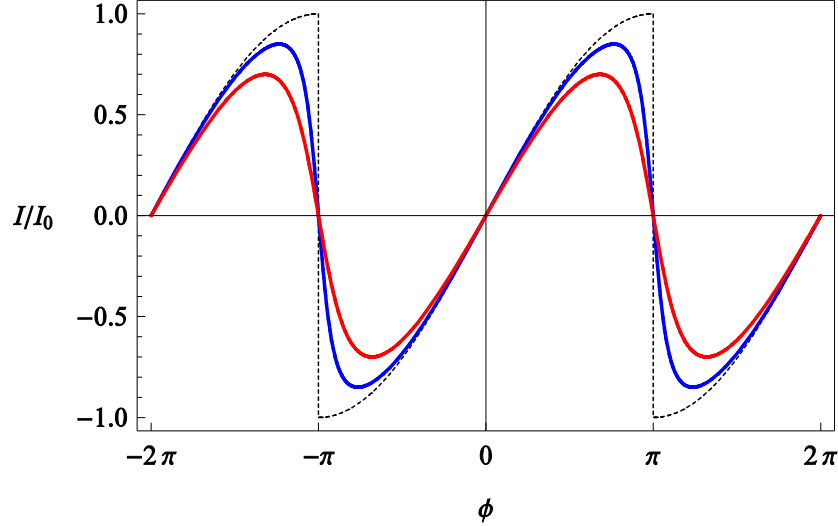

Figure 3.3. *Current-phase relation of a TBJJ for $\varepsilon = 0.00,\ 0.15,\ 0.30$ (dashed, blue, and red lines, respectively). Notice that the effect of an increasing inhomogeneity in the junction parameters gives curves with lower values of the maximum Josephson current. In fact, the maximum Josephson current I_{MAX} is found to vary according to the simple relation $\Delta I_{MAX} = -I_0 \Delta\varepsilon$.*

If we consider the limit for ε tending to zero, we have:

$$\lim_{\varepsilon \to 0} \frac{I}{I_0} = \frac{1}{2} \frac{2\sin\frac{\varphi}{2}\cos\frac{\varphi}{2}}{\left|\cos\frac{\varphi}{2}\right|} = \sin\frac{\varphi}{2}\operatorname{sgn}\left(\cos\frac{\varphi}{2}\right).$$

Therefore, under this condition, we have:

$$I = I_0 \operatorname{sgn}\left(\cos\frac{\varphi}{2}\right)\sin\frac{\varphi}{2}.$$

This CPR is similar to the one found for a simmetric trilayer homogeneous superconducting system, except for the remaining term, that is $I_0 \beta \sin\varphi$, in which, as we know, $I_0 = \dfrac{4e\tilde{K}\sqrt{NN_2}}{\hbar}$, where $\tilde{K}$ is the coupling constant of the first neighbour electrodes, N_2 is the number of Cooper pairs in

electrode 2, and N is the number of Cooper pairs in electrodes 1, 3, and $\beta = \dfrac{K}{\tilde{K}}\sqrt{\dfrac{N}{N_2}}$ gives the ratio

between the coupling constants K and $\tilde{K}$ of the second and the first neighbour electrodes. Therefore, in the limit $\varepsilon \to 0$, the coupling between the second neighbour electrodes is negligible, and so we can consider the two superconducting layers S_2 and S_3 as a whole superconducting system, which interacts with S_1 and S_4; we can also consider the interaction between the outermost electrodes. However, this is only a limiting behaviour for the CPR, because the true CPR for this particular four-layer superconducting system is given by the eq. (3.41).

We can end this section by considering the effective potential for this particular quadrilayer superconducting system. Starting from the eq. (3.37), we can rewrite the expression of W_C as follows:

$$W_C = -\frac{\hbar}{2e}\left[I_0(1-\varepsilon)\cos\left(\theta_A - \frac{\varphi}{2}\right) + I_0(1+\varepsilon)\cos\left(\theta_A + \frac{\varphi}{2}\right) + \frac{4eK_2}{\hbar}\sqrt{N_2 N_3} \right]. \tag{3.42}$$

In the above expression we notice that the latter term is independent from φ, and so we can consider, in what it follows, only the first two terms. By using some trigonometric relations, we get:

$$W_C = -\frac{\hbar I_0}{2e}\left[2\sqrt{\varepsilon^2 + (1-\varepsilon^2)\cos^2\frac{\varphi}{2}} + \frac{4eK_2}{\hbar}\sqrt{N_2 N_3} \right]. \tag{3.43}$$

By knowing that:

$$I = \frac{1}{V}\dot{W}_C = \frac{1}{V}\frac{\partial W_C}{\partial \varphi}\frac{d\varphi}{dt} = \frac{\partial W_C}{\partial \varphi}\frac{1}{V}\frac{2eV}{\hbar} \quad ,$$

we may also write:

$$I = \frac{2e}{\hbar}\frac{\partial W_C}{\partial \varphi}. \tag{3.44}$$

The effective potential, which can be derived from the expression of W_C in (3.43) by subtracting the constant term, is defined as follows:

$$U_{eff} = -\frac{\Phi_0 I_0}{\pi}\sqrt{\varepsilon^2 + (1-\varepsilon^2)\cos^2\frac{\varphi}{2}} \quad .$$

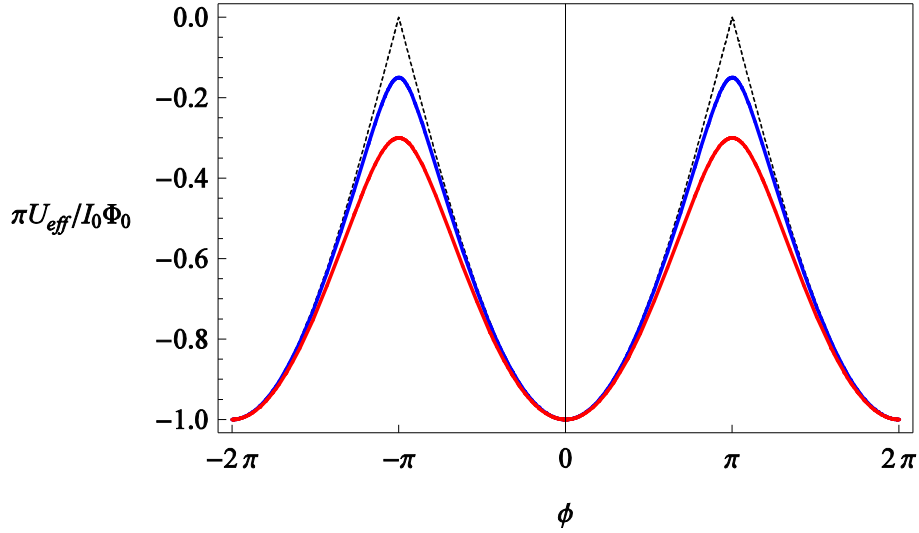In figure 3.4 we show the effective potential U_{eff} for various values of ε.

Figure 3.4. *Normalized effective potential as a function of the superconducting phase difference ϕ across a TBJJ for $\varepsilon = 0.00$, 0.15, 0.30 (dashed, blue, and red lines, respectively). Notice that minima and maxima in the effective potential appear at $\phi_{min} = 2k\pi$ and $\phi_{max} = (2k-1)\pi$, respectively, for k integer.*

From figure 3.4 we notice that minima and maxima in U_{eff} appear at $\varphi_{min} = 2k\pi$ and $\varphi_{max} = (2k+1)\pi$, respectively, for *k* integer. The barrier height $\Delta U = U_{eff}(\varphi_{max}) - U_{eff}(\varphi_{min})$, can be seen to be:

$$\Delta U = \frac{\Phi_0 I_0}{\pi}(1-\varepsilon) .\tag{3.45}$$

3.5 Maximum Josephson current and Shapiro steps for the triple-barrier superconducting system

In this section, we calculate [8] the maximum Josephson current and the Shapiro steps for the particular superconducting system considered in the previous section. Beginning with the calculation of the maximum Josephson current, we can consider the expression of the normalized CPR:

$$\frac{I(\varphi)}{I_0} = f(\varphi) = \frac{(1-\varepsilon^2)\sin\varphi}{2\sqrt{\varepsilon^2 + (1-\varepsilon^2)\cos^2\frac{\varphi}{2}}}\tag{3.46}$$

Then, we calculate the first derivative of $f(\varphi)$ and impose it equals zero, in order to get the maximum value of it. In this way, we have:

$$f'(\varphi) = \frac{1-\varepsilon^2}{2}\left(\frac{\cos\varphi\sqrt{\varepsilon^2 + (1-\varepsilon^2)\cos^2\dfrac{\varphi}{2}} + \dfrac{\sin\varphi}{2}\cdot\dfrac{1}{2}\dfrac{2(1-\varepsilon^2)\cos\dfrac{\varphi}{2}\sin\dfrac{\varphi}{2}}{\sqrt{\varepsilon^2 + (1-\varepsilon^2)\cos^2\dfrac{\varphi}{2}}}}{\varepsilon^2 + (1-\varepsilon^2)\cos^2\dfrac{\varphi}{2}} \right) = 0 \Rightarrow$$

$$\frac{1-\varepsilon^2}{2}\frac{\left[\varepsilon^2 + (1-\varepsilon^2)\cos^2\dfrac{\varphi}{2}\right]\cos\varphi + \dfrac{1-\varepsilon^2}{4}\sin^2\varphi}{\left[\varepsilon^2 + (1-\varepsilon^2)\cos^2\dfrac{\varphi}{2}\right]^{\frac{3}{2}}} = 0 \Rightarrow$$

$$4\left[\varepsilon^2 + (1-\varepsilon^2)\cos^2\frac{\varphi}{2}\right]\cos\varphi + (1-\varepsilon^2)\sin^2\varphi = 0.$$

If we use the trigonometric expressions

$$\cos^2\frac{\varphi}{2} = \frac{1+\cos\varphi}{2} \quad ; \quad \sin^2\frac{\varphi}{2} = \frac{1-\cos\varphi}{2},$$

we obtain:

$$4(\varepsilon^2\sin^2\frac{\varphi}{2} + \cos^2\frac{\varphi}{2})\cos\varphi + (1-\varepsilon^2)\sin^2\varphi = 0 \Rightarrow$$
$$2\left[\varepsilon^2(1-\cos\varphi) + 1 + \cos\varphi\right]\cos\varphi + (1-\varepsilon^2)\sin^2\varphi = 0 \Rightarrow$$
$$2\left[\varepsilon^2 + 1 + (1-\varepsilon^2)\cos\varphi\right]\cos\varphi + (1-\varepsilon^2) - (1-\varepsilon^2)\cos^2\varphi = 0 \Rightarrow$$
$$2(\varepsilon^2+1)\cos\varphi + 2(1-\varepsilon^2)\cos^2\varphi + 1 - \varepsilon^2 - (1-\varepsilon^2)\cos^2\varphi = 0 \Rightarrow$$
$$(1-\varepsilon^2)\cos^2\varphi + 2(1+\varepsilon^2)\cos\varphi + (1-\varepsilon^2) = 0 \Rightarrow$$
$$\cos^2\varphi + 2\frac{1+\varepsilon^2}{1-\varepsilon^2}\cos\varphi + 1 = 0 \Rightarrow$$
$$\cos\varphi = -\frac{1+\varepsilon^2}{1-\varepsilon^2} \pm \sqrt{\left(\frac{1+\varepsilon^2}{1-\varepsilon^2}\right)^2 - 1} = -\frac{1+\varepsilon^2}{1-\varepsilon^2} \pm \frac{\sqrt{4\varepsilon^2}}{1-\varepsilon^2} = \frac{-1-\varepsilon^2 \pm 2\varepsilon}{1-\varepsilon^2}.$$

If we consider the solution with the sign minus, that we can denote as $\cos\varphi_-$ we get:

$$\cos\varphi_- = -\frac{(\varepsilon+1)^2}{1-\varepsilon^2} = -\frac{\varepsilon+1}{1-\varepsilon}.$$

We know that $\varepsilon + 1 > 1 - \varepsilon$ for $\varepsilon > 0$ (in this case $0 < \varepsilon < 1$). Therefore, we have:

$$\cos\varphi_- = -\frac{\varepsilon+1}{1-\varepsilon} < -1$$

Therefore, we can conclude that this solution is not admitable,, because it doesn't agree with the definition of the cosine function.

Instead, the solution with the sign +, is written as follows:

$$\cos\varphi_+ = -\frac{1-\varepsilon}{1+\varepsilon},$$

since we have $1-\varepsilon < 1+\varepsilon \Rightarrow \frac{1-\varepsilon}{1+\varepsilon} < 1 \Rightarrow \cos\varphi_+ = -\frac{1-\varepsilon}{1+\varepsilon} > -1$. Therefore, according to the definition of this function, this solution is admitable. We can now calculate the corresponding value

of the sine by setting: $\sin\varphi_+ = \pm\sqrt{1-\cos^2\varphi_+} = \pm\sqrt{1-\left(\frac{1-\varepsilon}{1+\varepsilon}\right)^2} = \pm\frac{\sqrt{4\varepsilon}}{1+\varepsilon} = \frac{2\sqrt{3}}{1+\varepsilon}$. As we are interested

at the maximum value taken by the function $f(\varphi)$, we consider only the positive sign in the expression of $\sin\varphi_+$. We can express the function $f(\varphi)$ in a more appropriate form for the maximization:

$$f(\varphi) = \frac{1-\varepsilon^2}{2}\frac{\sin\varphi}{\sqrt{\varepsilon^2 + (1-\varepsilon^2)\left(\frac{1+\cos\varphi}{2}\right)}} = \frac{1-\varepsilon^2}{2}\frac{\sin\varphi}{\sqrt{\varepsilon^2 + \frac{1-\varepsilon^2}{2} + \frac{1-\varepsilon^2}{2}\cos\varphi}} =$$

$$\frac{1-\varepsilon^2}{2}\frac{\sin\varphi}{\sqrt{\frac{1+\varepsilon^2}{2} + \left(\frac{1-\varepsilon^2}{2}\right)\cos\varphi}} = \frac{1-\varepsilon^2}{\sqrt{2}}\frac{\sin\varphi}{\sqrt{1+\varepsilon^2 + (1-\varepsilon^2)\cos\varphi}}.$$

(3.47)

By substituting the values of $\cos\varphi_+$, $\sin\varphi_+$ into the analytic expression of the function $f(\varphi)$, we obtain the maximum value taken by this function, denoted as f_{MAX}. In this way, we get:

$$f_{MAX} = \frac{1-\varepsilon^2}{\sqrt{2}}\frac{\frac{2\sqrt{\varepsilon}}{1+\varepsilon}}{\sqrt{1+\varepsilon^2 - (1-\varepsilon^2)\frac{1-\varepsilon}{1+\varepsilon}}} = \frac{(1-\varepsilon)\sqrt{2\varepsilon}}{\sqrt{1+\varepsilon^2 - (1+\varepsilon^2 - 2\varepsilon)}} = \frac{(1-\varepsilon)\sqrt{2\varepsilon}}{\sqrt{2\varepsilon}} = 1-\varepsilon.$$

So, we have obtained the important result that the maximum value of the function $f(\varphi)$ considered is:

$$f_{MAX} = 1-\varepsilon.$$

(3.48)

Therefore, the maximum value I_{MAX} of the Josephson current for this particular quadrilayer superconducting system is:

$$I_{MAX} = I_0 f_{MAX} = I_0(1-\varepsilon),$$

(3.49)

with $I_0 = \frac{I_1 + I_2}{2} = \frac{2e}{\hbar}\left(K_1\sqrt{N_1 N_2} + \tilde{K}_1\sqrt{N_1 N_3} + K_3\sqrt{N_3 N_4} + \tilde{K}_2\sqrt{N_2 N_4}\right).$

Let us now turn our attention to the Shapiro steps for this particular four-layer superconducting system. First of all, we can consider, as in the previous chapter about the three-layer superconducting system, that, also in this case, the whole four-layers superconducting system is driven by an external oscillating voltage of this form:

$$V(t) = V_0 + V_1 \cos(w_r t) \,,$$
(3.50)

where V_0 is the dc component, and V_1 is the amplitude of the oscillating part, having angular frequency w_r. If we normalize this voltage V to the quantity RI_0 , in which R is the overall resistance parameter of this quadrilayer superconducting system, and make a rescaling of the time variable, defining $\tau = \dfrac{2\pi RI_0}{\Phi_0} t$, we can show that:

$$\varphi(\tau) = \varphi_0 + v_0 \tau + a \sin(\tilde{w}_r \tau) \,,$$
(3.51)

in which $v_0 = \dfrac{V_0}{RI_0}$; $a = \dfrac{2\pi V_1}{\Phi_0 w_r}$; $\tilde{w}_r = \dfrac{\Phi_0}{2\pi RI_0} w_r$.

In order to prove Eq. (3.51) we can start from the second Josephson equation:

$$\frac{d\varphi}{dt} = \frac{2eV}{\hbar} \Rightarrow V = \frac{\hbar}{2e} \frac{d\varphi}{dt} = \frac{\hbar}{2e} \frac{1}{2\pi} \frac{d\varphi}{dt} = \frac{\Phi_0}{2\pi} \frac{d\varphi}{dt} \Rightarrow V = \frac{\Phi_0}{2\pi} \frac{d\varphi}{dt} \,.$$

If we consider the change of variable:

$$\tau = \frac{2\pi RI_0}{\Phi_0} t \,,$$

we get:

$$V = \frac{\Phi_0}{2\pi} \frac{d\varphi}{d\tau} \frac{1}{\Phi_0} 2\pi = RI_0 \frac{d\varphi}{d\tau} \Rightarrow \frac{V}{RI_0} = \frac{d\varphi}{d\tau} \,.$$

Considering that the new variable used is τ , we notice that:

$$v(\tau) = \frac{V(\tau)}{RI_0} = \frac{d\varphi}{d\tau} \,.$$
(3.52)

As a starting hypothesis, we set:

$$V(t) = V_0 + V_1 \cos(w_r t) \Rightarrow V(\tau) = V_0 + V_1 \cos\left(\frac{w_r \Phi_0}{2\pi RI_0} \tau \right) \Rightarrow V(\tau) = V_0 + V_1 \cos(\tilde{w}_r \tau) \,,$$

with $\tilde{w}_r = \dfrac{w_r \Phi_0}{2\pi RI_0}$.

By now dividing the voltage V by RI_0, we get:

$$v(\tau) = \frac{V(\tau)}{RI_0} = \frac{V_0 + V_1\cos(\widetilde{w}_r\tau)}{RI_0} = \frac{V_0}{RI_0} + \frac{V_1}{RI_0}\cos(\widetilde{w}_r\tau). \qquad (3.53)$$

Therefore:

$$\frac{d\varphi}{d\tau} = v_0 + \frac{V_1}{RI_0}\cos(\widetilde{w}_r\tau) \Rightarrow$$

$$\frac{d\varphi}{\varphi} = v_0\frac{d\tau}{\tau} + \frac{V_1}{RI_0}\cos(\widetilde{w}_r\tau) \Rightarrow \int\limits_{\varphi_0}^{\varphi} d\varphi = \int\limits_0^{\tau} v_0 d\tau + \frac{V_1}{RI_0}\int\limits_0^{\tau}\cos(\widetilde{w}_r\tau)d\tau \Rightarrow$$

$$\varphi - \varphi_0 = v_0\tau + \frac{V_1}{RI_0}\frac{1}{\widetilde{w}_r}\int\limits_0^{\tau}\cos(\widetilde{w}_r\tau)d\tau \Rightarrow \varphi = \varphi_0 + v_0\tau + \frac{V_1}{RI_0}\frac{1}{\widetilde{w}_r}\sin(\widetilde{w}_r\tau)$$

$$\Rightarrow \varphi = \varphi_0 + v_0\tau + \frac{2\pi V_1}{w_r\Phi_0}\sin(\widetilde{w}_r\tau).$$

If we now set $a = \dfrac{2\pi V_1}{w_r\Phi_0}$, we get:

$$\varphi(\tau) = \varphi_0 + v_0\tau + a\sin(\widetilde{w}_r\tau),$$

which is the expression (3.51), that we have so proven.

In order to calculate the Shapiro steps, we could make a Fourier expansion of the analytic expression of the CPR function. However, its expression is rather complicated, so that we consider the same function in the limit of $\varepsilon \to 0$, that we can denote as $f_0(\varphi)$. In this limit the normalized CPR becomes:

$$f_0(\varphi) = \frac{\cos\dfrac{\varphi}{2}}{\left|\cos\dfrac{\varphi}{2}\right|}\sin\frac{\varphi}{2} = \operatorname{sgn}(\cos\frac{\varphi}{2})\sin\frac{\varphi}{2}. \qquad (3.54)$$

We can now make a Fourier expansion of this function, which has the same analytic expression of the function present inside the CPR for the particular trilayer superconducting system analysed in the previous paper. Therefore, we can consider that, for very small values of ε (*i.e.* $\varepsilon \ll 1$) we can approximate

$$f(\varphi) \cong f_0(\varphi) = \operatorname{sgn}(\cos\frac{\varphi}{2})\sin\frac{\varphi}{2}, \qquad (3.55)$$

and we can expand this function in Fourier series for $\dfrac{\varphi}{2}$ comprised between $-\dfrac{\pi}{2}$ and $\dfrac{\pi}{2}$, or in the same way for φ comprised between $-\pi$ and π, so that:

$$\cos\frac{\varphi}{2} > 0 \Rightarrow \text{sgn}(\cos\frac{\varphi}{2}) = 1 \Rightarrow f_0(\varphi) = \sin\frac{\varphi}{2}.$$

We now notice that we already know [8] the Fourier expansion of the function $f_0(\varphi)$, because it has been calculated in the previous chapter. In particular, we therefore have:

$$f_0(\varphi) = \frac{I_0(\varphi)}{I_0} = \sum_{k=1}^{+\infty} b_k \sin(kx) \quad,$$

with $b_k = \frac{1}{\pi}\int_{-\pi}^{\pi} f_0(\varphi)\sin\varphi d\varphi = -\frac{8}{\pi}\frac{(-1)^k k}{4k^2-1}$. $\hspace{2cm}$ (3.56)

So we have:

$$f_0(\varphi) = \sum_{k=1}^{+\infty} \frac{8}{\pi}\frac{(-1)^{k+1}k}{4k^2-1}\sin k\varphi \Rightarrow$$

$$I_0(\varphi) = I_0 \,\text{Im}\left(\sum_{k=1}^{+\infty}\frac{8}{\pi}\frac{(-1)^{k+1}k}{4k^2-1}e^{ik\varphi}\right). \hspace{2cm} (3.57)$$

By using the expression (3.44), we obtain:

$$I_0(\varphi) = I_0 \,\text{Im}\left(\sum_{k=1}^{+\infty}\frac{8}{\pi}\frac{(-1)^{k+1}k}{4k^2-1}e^{ik(\varphi_0+v_0\tau+a\sin(\tilde{w}_r\tau))}\right) \Rightarrow$$

$$I_0(\varphi) = I_0 \,\text{Im}\left(\sum_{k=1}^{+\infty}\frac{8}{\pi}\frac{(-1)^{k+1}k}{4k^2-1}e^{ik\varphi_0}e^{ikv_0\tau}e^{ika\sin(\tilde{w}_r\tau)}\right). \hspace{1cm} (3.58)$$

We can now use some properties of the Bessel functions. In particular, it can be shown [27] that:

$$\exp\left[ika\sin(\tilde{w}_r\tau)\right] = \sum_m J_m(ka)\exp(im\tilde{w}_r\tau). \hspace{2cm} (3.59)$$

By using this expression, we get:

$$I_0(\varphi) = I_0 \,\text{Im}\left[\sum_{k=1}^{+\infty}\left(\frac{8}{\pi}\frac{(-1)^{k+1}k}{4k^2-1}e^{ik\varphi_0}\sum_m J_m(ka)e^{i(kv_0+m\tilde{w}_r)\tau}\right)\right] \hspace{1cm} (3.60)$$

As it is well known, the *I-V* characteristics of the Josephson junctions [8] show the so called Shapiro current steps, which are well defined values intervals of electric current *I*, having the property that they show a variation in *I* at a fixed voltage value. In particular, these steps can be obtained at well defined value $V = V_0$ which is constant in time (d.c. voltage):

$$V_0 = n\frac{h}{2e}v, \hspace{2cm} (3.61)$$

in which $n \in N$. In the expression (3.61), we note that h is the Planck constant, e is the absolute value of the electron charge, and ν is the frequency of the oscillating part of the considered voltage signal. In this way, we get:

$$V_0 = n \frac{\Phi_0}{2\pi} w, \qquad (3.62)$$

where $w = 2\pi\nu$, and $\Phi_0 = \dfrac{h}{2e}$ is the elementary magnetic flux quantum, or also called London fluxoid. If we divide the expression (3.62) by RI_0, we get:

$$v_0 = \frac{V_0}{RI_0} = n \frac{\Phi_0}{2\pi} \frac{w_r}{RI_0}.$$

By using the expression $\widetilde{w}_r = \dfrac{\Phi_0 w_r}{2\pi RI_0}$, we obtain:

$$v_0 = n\widetilde{w}_r, \quad \text{with } n \in N. \qquad (3.63)$$

Equation (3.63) expresses the values of voltage at which we may have Shapiro current steps. Therefore, considering our expression of $I_0(\varphi)$, we may have Shapiro steps when $kv_0 + m\widetilde{w}_r = 0$, because, in this way, there is no dependence of this expression on V. So we have:

$$kv_0 + m\widetilde{w}_r = 0 \Rightarrow v_0 = -\frac{m}{k}\widetilde{w}_r \text{ and, comparing this result with the one of equation (56), we get:}$$

$$-\frac{m}{k} = n \Rightarrow m = -nk.$$

Therefore, the analytic expression of $I_0(\varphi)$ becomes:

$$I_n = I_0 \operatorname{Im} \sum_{k=1}^{+\infty} \left(\frac{8}{\pi} \frac{(-1)^{k+1} k}{4k^2 - 1} e^{ik\varphi_0} J_{-nk}(a) \right) \qquad (3.64)$$

and, by using the following property of Bessel functions:

$$J_{-nk}(a) = (-1)^{nk} J_{nk}(a),$$

we have:

$$I_n = I_0 \operatorname{Im} \sum_{k=1}^{+\infty} \frac{8}{\pi} \frac{\left[(-1)^{k+1+nk} \right] k}{4k^2 - 1} J_{nk}(a) e^{ik\varphi_0}. \qquad (3.65)$$

The semiamplitude of Shapiro steps can be determined by calculating the maximum value of the function I_n with respect to φ_0, which varies between 0 and 2π. In this way, the semiamplitude of the Shapiro steps is:

62

$$\Delta I_n = \max_{\varphi_0 \in [0, 2\pi]} I_0 \sum_{k=1}^{+\infty} \frac{8}{\pi} \frac{(-1)^{k+1+nk} k}{4k^2 - 1} \sin k\varphi_0 \tag{3.66}$$

In particular, for $n = 1$, we get:

$$\Delta I_1 = \max_{\varphi_0 \in [0, 2\pi]} I_0 \sum_{k=1}^{+\infty} \frac{8}{\pi} \frac{\left[(-1)^{k+1+k}\right] k}{4k^2 - 1} J_{1k}(a) \sin(k\varphi_0) \Rightarrow$$

$$\frac{\Delta I_1}{I_0} = \max_{\varphi_0 \in [0, 2\pi]} \sum_{k=1}^{+\infty} \frac{8}{\pi} \frac{(-1)^{2k+1}}{4k^2 - 1} k \sin(k\varphi_0). \tag{3.67}$$

Taking only the first two terms in the sum considered, i.e. the terms for $k = 1$ and $k = 2$, because the other ones are always smaller, for the quantity $4k^2 - 1$ present at the denominator, we obtain:

$$\frac{\Delta I_1}{I_0} \cong \max_{\varphi_0 \in [0, 2\pi]} \left[\frac{8}{\pi} \frac{(-1)^3 J_1(a)}{3} \sin \varphi_0 + \frac{8}{\pi} \frac{(-1)^5 J_2(a)}{15} 2 \sin 2\varphi_0 \right] \Rightarrow$$

$$\frac{\Delta I_1}{I_0} \cong \max_{\varphi_0 \in [0, 2\pi]} \left[-\frac{8}{3\pi} J_1(a) \sin \varphi_0 - \frac{16}{15\pi} J_2(2a) \sin 2\varphi_0 \right]. \tag{3.68}$$

In these expressions the maximum value of the function $\dfrac{\Delta I_1}{I_0}$ is just calculated on the interval $\varphi_0 \in [0, 2\pi]$, as the other quantities, present in the expression of the function, are constant. So, we must determine the maximum value of the function:

$$f(x) = A \sin x + B \sin 2x \tag{3.69}$$

in which the variable x is, in our case, represented by φ_0, and the coefficients A and B are defined in the following way:

$$A = -\frac{8}{3\pi} J_1(a) \quad ; \qquad B = -\frac{16}{15\pi} J_2(a). \tag{3.70}$$

As we know, the maximum must satisfy the condition:

$$f'(x) = 0 \Rightarrow$$

$$A \cos x + 2B \cos 2x = 0 \Rightarrow A \cos x + 2B(\cos^2 x - \sin^2 x) = 0 \Rightarrow$$
$$4B \cos^2 x + A \cos x - 2B = 0 \Rightarrow$$
$$\cos^2 x + \frac{A}{4B} \cos x - \frac{1}{2} = 0$$

By solving this equation we obtain:

$$\cos x = \frac{-\dfrac{A}{4B} \pm \sqrt{\left(\dfrac{A}{4B}\right)^2 + 2}}{2} = -\frac{A}{8B} \pm \sqrt{\frac{A^2}{64B^2} + \frac{1}{2}} \ .$$

We can notice, in the latter expression, that the square-root term is larger than the first term; so, in order to maximize the function *f(x)*, we can take only the positive values of $\cos x$, and then substitute them inside the expression of *f(x)*. In this way, we get:

$$\cos x = -\frac{A}{8B} + \sqrt{\frac{A^2}{64B^2} + \frac{1}{2}} = \frac{A}{8B}\left(\sqrt{1 + \frac{32B^2}{A^2}} - 1\right) = X \ .$$

Therefore, we can re-express the function *f(x)* in a more adequate form, in order to maximize it:

$$f(x) = A\sin x + 2B\sin x\cos x = \sin x(A + 2B\cos x) = \sqrt{1 - \cos^2 x}(A + 2B\cos x) \ .$$

In order to maximize *f(x)*, we notice that, in the expression of $\sin x = \pm\sqrt{1 - \cos^2 x}$, we may take only the positive solution, so that $\sin x = \sqrt{1 - \cos^2 x}$. In this way, by substituting X with $\cos x$, and by taking the absolute value of the coefficients A and B, we obtain the maximum value of the function *f(x)*, that we denote as f_{MAX}:

$$f_{MAX} = \sqrt{1 - X^2}\left(|A| + 2|B|X\right) = \sqrt{1 - X^2}\left[|A| + \frac{|A|}{4}\left(\sqrt{1 + 32\frac{B^2}{A^2}} - 1\right)\right] =$$

$$\sqrt{1 - X^2}\left[|A| - \frac{|A|}{4} + \frac{|A|}{4}\sqrt{1 + \frac{32B^2}{A^2}}\right] = \sqrt{1 - X^2}\left[\frac{3}{4}|A| + \frac{|A|}{4}\sqrt{1 + \frac{32B^2}{A^2}}\right] =$$

$$\frac{\sqrt{1 - X^2}}{4}\left(3|A| + |A|\sqrt{\frac{A^2 + 32B^2}{A^2}}\right) = \frac{\sqrt{1 - X^2}}{4}\left(3|A| + \sqrt{A^2 + 32B^2}\right)$$

Finally, we have:

$$f_{MAX} = \frac{\sqrt{1 - X^2}}{4}\left(3|A| + \sqrt{A^2 + 32B^2}\right) \ . \tag{3.71}$$

Knowing now that $f_{MAX} = \dfrac{\Delta I_1}{I_0}$, by taking into account the expression (3.68), we obtain:

$$\frac{\Delta I_1}{I_0} \cong \frac{\sqrt{1 - X^2}}{4}\left(3|A| + \sqrt{A^2 + 32B^2}\right) \Rightarrow$$

$$\Delta I_1 \cong I_0\frac{\sqrt{1 - X^2}}{4}\left(3|A| + \sqrt{A^2 + 32B^2}\right) \ . \tag{3.72}$$

In this expression we consider that:

$$A = -\frac{8}{3\pi} J_1(a) \quad ; \quad B = -\frac{16}{15\pi} J_2(a) \quad ; \quad X = \frac{A}{8B}\left(\sqrt{1 + 32\frac{B^2}{A^2}} - 1\right).$$

Also, we notice that ΔI_1 depends, through the coefficients A and B, on the quantity $a = \frac{2\pi V_1}{\Phi_0 w_r}$.

In the same way, we can calculate the maximum value of I_n, that we can denote as ΔI_2, in the case of $n = 2$. Always starting from the expression (3.65), we get:

$$\frac{\Delta I_2}{I_0} = \max_{\varphi_0 \in [0, 2\pi]}\left[\sum_{k=1}^{+\infty} \frac{8}{\pi} \frac{(-1)^{3k+1} k}{4k^2 - 1} J_{2k}(a)\sin(k\varphi_0)\right].$$

Also in this case, we can take only the first two terms of the sum, for $k = 1$, and $k = 2$, as the others are smaller because of the presence of the term at denominator. So we get:

$$\frac{\Delta I_2}{I_0} \cong \max_{\varphi_0 \in [0, 2\pi]}\left[\frac{8}{3\pi} J_2(a)\sin\varphi_0 - \frac{16}{15\pi} J_4(a)\sin 2\varphi_0\right]. \tag{3.73}$$

As before, we must determine the maximum value of the following function:

$$f(x) = C\sin x + D\sin 2x \tag{3.74}$$

in which:

$$C = \frac{8}{3\pi} J_2(a) \quad ; \quad D = -\frac{16}{15\pi} J_4(a). \text{ In this way, we write:}$$

$$f'(x) = 0 \Rightarrow C\cos x + 2D\cos 2x = 0 \Rightarrow C\cos x + 2D(2\cos^2 x - 1) = 0 \Rightarrow$$

$$4D\cos^2 x + C\cos x - 2D = 0.$$

So we obtain:

$$\cos^2 x + \frac{C}{4D}\cos x - \frac{1}{2} = 0. \tag{3.75}$$

By now solving the above equation, we have:

$$\cos x = -\frac{C}{8D} \pm \sqrt{\frac{C^2}{64D^2} + \frac{1}{2}} = -\frac{C}{8D} + \sqrt{1 + \frac{32D^2}{C^2}}. \tag{3.76}$$

In (3.69), we consider only the positive solution, in order to maximize the function $f(x)$.

So we have:

$$\cos x = \frac{C}{8D}\left(\sqrt{1+\frac{32D^2}{C^2}}-1\right) = Y.$$

As before, we can re-express $f(x)$ in the following way:

$$f(x) = C\sin x + D\sin 2x = \sqrt{1-\cos^2 x}\left(C+2D\cos x\right), \tag{3.77}$$

where, also in this case, we take only the positive solution of the sine function (i.e., $\sin x = \sqrt{1-\cos^2 x}$), in order to get a maximum for $f(x)$. Finally, by substituting Y with $\cos x$, and by taking, as before, the absolute value of the coefficients C and D, we get the maximum value, f_{MAX}, of the function $f(x)$:

$$f_{MAX} = \sqrt{1-Y^2}\left(|C|+2|D|Y\right) = \sqrt{1-Y^2}\left[|C|+\frac{|C|}{4}\left(\sqrt{1+\frac{32D^2}{C^2}}-1\right)\right]. \tag{3.78}$$

After the same calculations of the previous case, we therefore have:

$$f_{MAX} = \frac{\sqrt{1-Y^2}}{4}\left(3|C|+\sqrt{C^2+32D^2}\right). \tag{3.79}$$

In the above expression we recall that the quantities Y, C, and D are:

$$C = \frac{8}{3\pi}J_2(a) \quad ; \quad D = -\frac{16}{15\pi}J_4(a) \quad ; \quad Y = \frac{C}{8D}\left(\sqrt{1+\frac{32D^2}{C^2}}-1\right).$$

Therefore, knowing that $\dfrac{\Delta I_2}{I_0} = f_{MAX}$, and taking into account the expression (3.66), we get:

$$\frac{\Delta I_2}{I_0} \cong \frac{\sqrt{1-Y^2}}{4}\left(3|C|+\sqrt{C^2+32D^2}\right). \tag{3.80}$$

We notice that also that the current step in Eq. (3.73) depends on the quantity $a = \dfrac{2\pi V_1}{\Phi_0 w_r}$, through the coefficients C and D.

Therefore, in figure 3.5a we show the profile of $\dfrac{\Delta I_1}{I_0}$ and $\dfrac{\Delta I_2}{I_0}$ as the quantity a varies, together with the numerical evaluation of the first twenty terms in the expressions of ΔI_1 and ΔI_2. We can notice a rather good agreement between the results obtained by the above analysis and by a computer-assisted numerical approach in which more terms in the summations in (3.67) and (3.73) are retained.
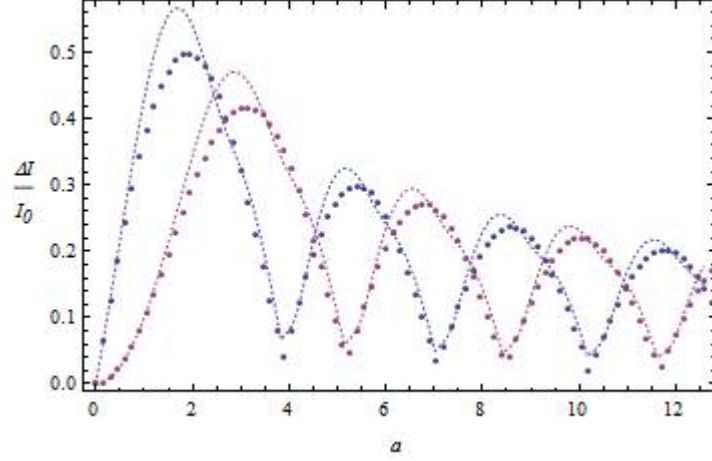
Figure 3.5a. *Approximate analytical evaluation of ΔI_1 and ΔI_2 (blue and purple dashed lines, respectively) calculated by retaining only the two leading addends in their expression. Numerical evaluation of ΔI_1 and ΔI_2 (blue and purple scattered points) utilizing the first twenty terms in their expression is also shown.*

We summarize our results saying that the quantities represented by $\dfrac{\Delta I_1}{I_0}$, $\dfrac{\Delta I_2}{I_0}$ are, for $n=1$ and $n=2$, the approximate normalized semiamplitudes of Shapiro current steps in the *I-V* characteristics of the Josephson Junctions devices (in this case we have a superconducting four-layer non homogeneous system, in which the phase angles are $\theta_2 = \theta_3 = 0$). In fact, as we have aòready said, in correspondence of the voltage values $v_{0,n} = n\widetilde{w}_r$ we obtain an expression of I_n given by:

$I_n = I_0(-1)^n J_n(a)\sin\varphi_0 \Rightarrow \dfrac{I_n}{I_0} = (-1)^n J_n(a)\sin\varphi_0$. Therefore, we notice that the maximum value of

this expression is: $\left| J_n(a) \right|$, which represents the semiamplitude of the Shapiro steps, with *n* varying

in the set of integer numbers, and $a = \dfrac{2\pi V_1}{\Phi_0 \widetilde{w}_r}$. Thus, the quantities $\dfrac{\Delta I_n}{I_0}$ represent the normalized

(because they have been divided by I_0) and approximate (because they have been calculated only considering the first two terms, in particular for $k = 1$, and $k = 2$) Shapiro current steps. We notice

also that they depend also on $a = \dfrac{2\pi V_1}{\Phi_0 w_r}$, through the coefficients present in their expression, in

particular through the argument of the Bessel function.

In addition to integer Shapiro steps, we may also find fractional Shapiro steps, by considering the

ratio $\dfrac{m}{k} = -q$, where q is a positive rational number, if we analyse, as done before, only the positive

voltage branch of the *I-V* characteristics. In this case, we may set:

$$I_q = \frac{8I_0}{\pi} \operatorname{Im}\left\{ \sum_{\substack{k=1 \\ \text{with } kq \\ \text{integer}}}^{+\infty} \frac{(-1)^{k+1+kq} k}{4k^2 - 1} e^{ik\phi_0} J_{kq}(ka) \right\}, \tag{3.81}$$

where the summation on *k* is extended to all those integers for which the product qk is an integer. As before, the semi-amplitude of the step can be written formally as follows:

$$\Delta I_q = \frac{8I_0}{\pi} \max_{\phi_0 \in [0,\, 2\pi]} \left\{ \sum_{\substack{k=1 \\ \text{with } kq \\ \text{integer}}}^{+\infty} \frac{(-1)^{k+1+kq}\, k}{4k^2 - 1} J_{kq}(ka) \sin k\phi_0 \right\}. \tag{3.82}$$

In fig. 3.5b we show the numerical evaluation of ΔI_q, for q=1/4, 1/3, 1/2, 2/3, for the first ten terms in the summation in (3.82). We may notice that the semi-amplitude of the half-integer Shapiro steps (q=1/2), while having lower peaks than ΔI_1 and ΔI_2, show larger peak values than $\Delta I_{1/4}$, $\Delta I_{1/3}$, and $\Delta I_{2/3}$.
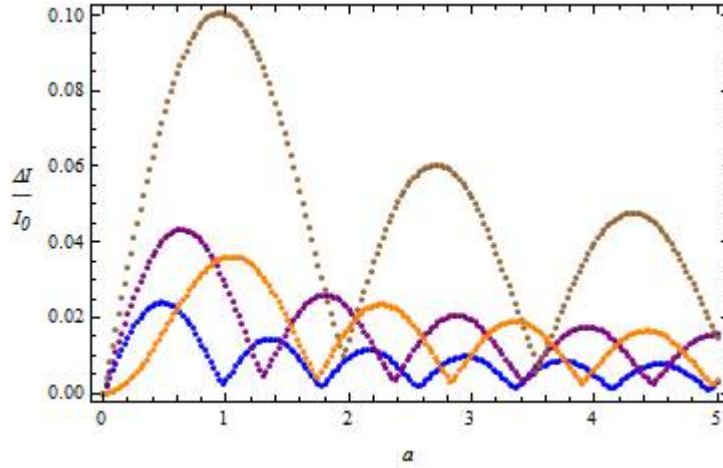

Figure 3.5b. *Numerical evaluation of $\Delta I_{1/4}$, $\Delta I_{1/3}$, $\Delta I_{1/2}$, and $\Delta I_{2/3}$ (blue, purple, brown, orange scattered points) utilizing the first ten terms in their expression.*

3.6 Conclusions

In this chapter, we have analysed two particular superconducting systems: an inhomogeneous three-layer characterized by a constant non-null phase of the inner electrode, and an inhomogeneous four-layer with null phases of the inner two electrodes.

In the first case (inhomogeneous DBJJ), we have calculated the CPR, in terms of the inhomogeneity parameter ε and of the parameter describing the coupling between the two outermost electrodes γ, obtaining an expression which reduces, for ε =0, to the current-phase relation found by Romeo and De Luca for a homogeneous DBJJ in ref. [14].

In the second case (inhomogeneous TBJJ), we have found that the term describing the interaction between the outermost electrodes is absent, so that the CPR is formally identical to the expression for the DBJJ, provided one sets γ =0. In fact, when considering nearest and next nearest neighbour interactions, the two superconducting layers S_2 and S_3 in a TBJJ act as a single quantum system assumed to be described by the same superconducting phase. When sandwiched between S_1 and S_4, however, the intermediate layers S_2 and S_3 do not allow direct coupling between the outermost layers as it happens in a DBJJ, so that the $\sin\phi$ term disappears in the CPR of a TBJJ.

We have noticed that the maximum Josephson current I_{MAX} in TBJJs depends on the inhomogeneity parameter ε as follows: $I_{MAX} = I_0(1-\varepsilon)$, where I_0 is a constant which depends on the

superconducting properties of the four layers. Furthermore, by means of a Fourier expansion of the CPR, we have calculated the Shapiro steps for a homogeneous ($\varepsilon = 0$) TBJJ. In this respect, we have noticed appearance of integer and fractional Shapiro steps in the *I-V* characteristics of these systems. We were able to determine, by a standard analytic procedure, at least for the homogeneous case, the semi-amplitudes of these quantities, both for the case of integer and fractional Shapiro steps.

Chapter 4

I-V characteristics of triple-barrier Josephson Junctions

In this chapter, we start to consider the *I-V* characteristics of two particular kinds of Josephson junctions: the simple Josephson junction (SJJ), and the triple-barrier Josephson Junction (TBJJ), in this latter case with the simplification of $\varepsilon = 0$, both in the presence of a constant bias current. The results obtained for these two particular devices are the same, i.e., the *I-V* characteristics is the same for both them. In particular, it takes the following analytic form:

$$I = \pm I_0 \sqrt{\langle v \rangle^2 + 1} \, ,$$

where I_0 is a constant with the dimension of an electric current, assuming different values for the two considered cases, and $\langle v \rangle$ is the time mean value of ratio $\dfrac{V}{RI_0}$, with *V* that is the voltage applied to the outermost junction electrodes, and *R* is the electric resistance of the overall considered device.

In particular, in TBJJs, deviation from this behaviour is found for inhomogeneous Josephson coupling between different layers in the device, always considering a constant bias of electric current. Appearance of integer and fractional Shapiro steps is predicted in the presence of r.f. frequency radiation. The amplitudes of these steps are also calculated in the homogeneous case, as clear footprints of the non-canonical current-phase relation in these systems.

4.1 Introduction

Josephson junctions (JJs) have a great variety of applications [15]. The most diffuse use of these superconducting elements can probably be recognized in the realization of quantum interference devices [28]. Usually the latter ultra-sensitive magnetic field sensors are fabricated utilizing conventional JJs. However, double or multi-barrier JJs have been also proposed as elements of Superconducting Quantum Interference Devices (SQUIDs) [9, 10]. It is therefore important to study the properties of the latter types of junctions and, in particular, the current-voltage (*I-V*) characteristics of triple-barrier Josephson junctions (TBJJs).

In this chapter, we begin to determine [29] the current-voltage (*I-V*) characteristic of a single-barrier Josephson junction with negligible capacitive parameter, by using the Resistively Shunted Junction (RSJ) model. We next analyse the *I-V* characteristics of TBJJs, by starting with their current-phase relation (CPR) derived in the previous chapter.

We first consider a homogeneous system ($\varepsilon = 0$) and analytically determine that, in this case, the *I-V* characteristics of TBJJs are given by Eq. (3.1) in the presence of a constant current bias. For inhomogeneous Josephson coupling ($\varepsilon \neq 0$) numerical evaluation of *I-V* characteristics are made;

deviations of these curves from the analytically determined characteristics for $\varepsilon = 0$ are seen to be compatible with the expression of maximum Josephson current $I_{MAX} = (1-\varepsilon)I_0$. In the presence of a r. f. radiation integer and fractional Shapiro steps arise in the *I-V* characteristics. Expressions of the semi-amplitudes of these steps for $\varepsilon = 0$ are determined by means of a semi-analytic approach. Numerical evaluation of *I-V* curves are performed.

4.2 I-V characteristic for a simple Josephson junction

Let us begin by considering [29] the case of the SJJ, and let us determine its *I-V* characteristics. From Josephso equations, the current-phase relation (CPR), and the voltage-phase relation (VPR) are:

$$I_J(\varphi) = I_{J,0} \sin \varphi, \qquad (4.1)$$

$$V(\varphi) = \frac{\Phi_0}{2\pi} \frac{d\varphi}{dt}. \qquad (4.2)$$

In Eq. (4.1), $I_{j,0} = \frac{4eK}{\hbar}\sqrt{N_1 N_2}$, where K is the coupling constant between the two layers of the SSJ, N_1 is the numerical density of Cooper pairs in layer 1, N_2 in layer 2, and $\hbar = \frac{h}{2\pi}$, where h is the Planck's constant. In Eq. (4.2), on the other hand, we consider the so called elementary quantum flux $\Phi_0 = \frac{h}{2e}$, where e is the electric charge of electron.

Also, we know that relation (4.2) can be rewritten as:

$$V = \frac{\hbar}{2e} \frac{d\varphi}{dt} \Rightarrow \frac{d\varphi}{dt} = \frac{2eV}{\hbar}$$

Let us consider the "Resistively Shunted Junction" (RSJ) model [15], that is a SJJ connected in parallel with a resistor, of electric resistance R, which can be so schematized:
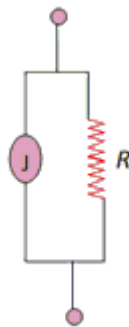

Figure 4.1. *Resistively shunted model for a Josephson junction. The junction is described by a parallel connection of a resistor with resistance R and an ideal Josephson element J: this model can be adopted also for multi-barrier Josephson junctions.*

From this figure [29] we notice that, by applying the first Kirchhoff's law to the electric circuit considered in figure 4.1), we get:

$$I_B = I_R + I_J ,$$
(4.3)

where I_R is the electric current circulating inside resistor R, and I_J the one circulating inside SJJ, while I_B is the so called bias electric current, that is provided by the source of electromotive force, applied from outside to the same electric circuit. Knowing that $I_R = \dfrac{V}{R}$, where V is the voltage applied to the two electrodes of the SJJ, and so also to the resistor, from (4.1) we get:

$$I_B = \frac{V}{R} + I_{J,0} \sin \varphi .$$
(4.4)

Now, by using (4.2), we have:

$$I_B = \frac{\Phi_0}{2\pi R} \frac{d\varphi}{dt} + I_{J,0} \sin \varphi .$$

Dividing all by $I_{J,0}$, we get:

$$\frac{I_B}{I_{J,0}} = \frac{\Phi_0}{2\pi R} \frac{d\varphi}{dt} + \sin \varphi .$$

Defining now the quantities:

$$\frac{I_B}{I_{J,0}} = i_B \quad \text{and} \quad \tau = \frac{2\pi R I_{J,0}}{\Phi_0} t ,$$

we get:

$$\frac{d\varphi}{d\tau} + \sin \varphi = i_B .$$
(4.5)

In order to solve Eq.(4.5), we can consider that:

$$\frac{d\varphi}{d\tau} = i_B - \sin \varphi ,$$ and by using the method of separation of variables:

$$\frac{d\varphi}{i_B - \sin \varphi} = d\tau .$$
(4.6)

Therefore, it is possible to integrate this relation, and so we get:

$$\int_{\varphi_0}^{\varphi(\tau)} \frac{d\varphi}{i_B - \sin\varphi} = \int_0^\tau d\tau = \tau,$$

where φ_0 is the angle of initial phase difference, corresponding to time 0, and $\varphi(\tau)$ corresponds to time τ. We must thus calculate the integral at first member, by using the method of substitution. In particular, we can make the following change of variable:

$$t = \tan\frac{\varphi}{2} \Rightarrow \frac{\varphi}{2} = \tan^{-1} t \Rightarrow \varphi = 2\tan^{-1} t \Rightarrow d\varphi = \frac{2dt}{1+t^2}$$

Furthemore: $\cos^2\frac{\varphi}{2} = \frac{1}{1+\tan^2\frac{\varphi}{2}} = \frac{1}{1+t^2} \Rightarrow \cos\frac{\varphi}{2} = \frac{1}{\sqrt{1+t^2}}$

In the same way, knowing that $\sin^2\frac{\varphi}{2} = 1 - \cos^2\frac{\varphi}{2} = \frac{t^2}{1+t^2} \Rightarrow \sin\frac{\varphi}{2} = \frac{t}{\sqrt{1+t^2}}$,

we get:

$$\sin\varphi = 2\sin\frac{\varphi}{2}\cos\frac{\varphi}{2} = \frac{2t}{1+t^2}.$$

Therefore, we have:

$$\int \frac{d\varphi}{i_B - \sin\varphi} = \int \frac{\dfrac{2dt}{1+t^2}}{i_B - \dfrac{2t}{1+t^2}} = 2\int \frac{dt}{i_B(1+t^2) - 2t} = \frac{2}{i_B}\int \frac{dt}{(1+t^2) - \dfrac{2t}{i_B}} = \frac{2}{i_B}\int \frac{dt}{1+t^2 + \dfrac{1}{i_B^2} - \dfrac{1}{i_B^2} - \dfrac{2t}{i_B}} =$$

$$= \frac{2}{i_B}\int \frac{dt}{\left(t - \dfrac{1}{i_B}\right)^2 + 1 - \dfrac{1}{i_B^2}}.$$

Considering the positions:

$$1 - \frac{1}{i_B^2} = A^2 \;;\; t' = t - \frac{1}{i_B} \Rightarrow dt' = dt,$$

we obtain:

$$\frac{2}{i_B}\int \frac{dt'}{(t')^2 + A^2} = \frac{2}{i_B}\frac{1}{A^2}\int \frac{dt'}{1 + \left(\dfrac{t'}{A}\right)^2} = \frac{2}{i_B A}\int \frac{\dfrac{dt'}{A}}{1 + \left(\dfrac{t'}{A}\right)^2} = \frac{2}{i_B A}\tan^{-1}\left(\frac{t'}{A}\right).$$

Knowing that $A^2 = \dfrac{1 - i_B^2}{i_B^2} \Rightarrow A = \dfrac{1}{i_B}\sqrt{i_B^2 - 1}$, as we assume that A > 0,

we get:

$$\frac{2}{i_B A}\tan^{-1}\left(\frac{t^{'}}{A}\right) = \frac{2}{\sqrt{i_B^2-1}}\tan^{-1}\left[\frac{i_B\left(t-\frac{1}{i_B}\right)}{\sqrt{i_B^2-1}}\right] = \frac{2}{\sqrt{i_B^2-1}}\tan^{-1}\left(\frac{i_B t-1}{\sqrt{i_B^2-1}}\right) = \frac{2}{\sqrt{i_B^2-1}}\tan^{-1}\left(\frac{i_B\tan\left(\frac{\varphi}{2}\right)-1}{\sqrt{i_B^2-1}}\right).$$

In this way, we have determined the value of integral, that is:

$$\int_{\varphi_0}^{\varphi(\tau)}\frac{d\varphi}{i_B-\sin\varphi} = \frac{2}{\sqrt{i_B^2-1}}\left[\tan^{-1}\left(\frac{i_B\tan\left(\frac{\varphi(\tau)}{2}\right)-1}{\sqrt{i_B^2-1}}\right) - \tan^{-1}\left(\frac{i_B\tan\left(\frac{\varphi_0}{2}\right)-1}{\sqrt{i_B^2-1}}\right)\right] = \tau .$$

Carrying out the calculations, we obtain:

$$\tan^{-1}\left(\frac{i_B\tan(\frac{\varphi}{2}(\tau))-1}{\sqrt{i_B^2-1}}\right) - \tan^{-1}\left(\frac{i_B\tan\left(\frac{\varphi_0}{2}\right)-1}{\sqrt{i_b^2-1}}\right) = \frac{\sqrt{i_B^2-1}}{2}\tau .$$

Because the second addendum present at the first member is constant, it can be considered equal to a constant a_0, so that:

$$\tan^{-1}\left(\frac{i_B\tan(\frac{\varphi}{2})-1}{\sqrt{i_B^2-1}}\right) = a_0 + \frac{\sqrt{i_B^2-1}}{2}\tau . \qquad (4.7)$$

By applying the tangent function to both members, we get:

$$\tan\left[\tan^{-1}\left(\frac{i_B\tan(\frac{\varphi}{2})-1}{\sqrt{i_B^2-1}}\right)\right] = \tan\left(a_0 + \frac{\sqrt{i_B^2-1}}{2}\tau\right).$$

Recalling that $\tan(\tan^{-1}x)= x$, we get:

$$\frac{i_B \tan(\frac{\varphi}{2}) - 1}{\sqrt{i_B^2 - 1}} = \tan\left(a_0 + \frac{\sqrt{i_B^2 - 1}}{2}\tau\right) \Rightarrow$$

$$i_B \tan(\frac{\varphi}{2}) - 1 = \sqrt{i_B^2 - 1}\tan\left(a_0 + \frac{\sqrt{i_B^2 - 1}}{2}\right) \Rightarrow$$

$$i_B \tan(\frac{\varphi}{2}) = \sqrt{i_B^2 - 1}\tan\left(a_0 + \frac{\sqrt{i_B^2 - 1}}{2}\right) + 1 \Rightarrow$$

$$\tan\frac{\varphi}{2} = \frac{\sqrt{i_B^2 - 1}}{i_B}\tan\left(a_0 + \frac{\sqrt{i_B^2 - 1}}{2}\tau\right) + \frac{1}{i_B}.$$

Since the tangent is a periodic function, of period equal to π, we get:

$$\tan\left(\frac{\varphi}{2} + k\pi\right) = \tan\frac{\varphi}{2} = \frac{1}{i_B}\left[\sqrt{i_B^2 - 1}\tan\left(a_0 + \frac{\sqrt{i_B^2 - 1}}{2}\tau\right) + 1\right] \qquad (4.8)$$

with $k \in Z$, where Z is the set of integer relative numbers . From the above relation, we get:

$$\frac{\varphi}{2} + k\pi = \tan^{-1}\frac{1}{i_B}\left[\sqrt{i_B^2 - 1}\tan\left(a_0 + \frac{\sqrt{i_B^2 - 1}}{2}\tau\right) + 1\right].$$

Therefore, we have:

$$\varphi = 2\tan^{-1}\frac{1}{i_B}\left[\sqrt{i_B^2 - 1}\tan\left(a_0 + \frac{\sqrt{i_B^2 - 1}}{2}\tau\right)\right] - 2k\pi. \qquad (4.9)$$

This result can also be expressed with the last term $2k\pi$ being preceded by a sign + , according to the fact that k is an integer relative number. By this result, we obtain that the period in φ is of 2π, that is:

$$\varphi(T) - \varphi(0) = 2\pi.$$

Therefore, if we calculate [29] the average value of normalized voltage $v = \dfrac{V}{RI_{J,0}}$ on time τ, by using the relation:

$$v = \frac{V}{RI_{J,0}} = \frac{\Phi_0}{2\pi RI_{J,0}}\frac{d\varphi}{dt} = \frac{d\varphi}{d\tau}, \qquad (4.10)$$

we get:

$$\langle v \rangle = \frac{1}{T}\int_0^T v(\tau)d\tau = \frac{1}{T}\int_0^T \frac{d\varphi}{d\tau}d\tau = \frac{1}{T}\left(\varphi(T) - \varphi(0)\right) = \frac{2\pi}{T}$$

In this way, we may write:

$$\langle v \rangle = \frac{2\pi}{T}. \qquad\qquad (4.11)$$

We must now calculate the value of T. Knowing that the tangent is a periodic function, of period π, we have:

$$\tan(\varphi + k\pi) = \tan\varphi,$$

with $k \in Z$ (set of integer relative numbers). Therefore:

$$\tan\left(a_0 + \frac{\sqrt{i_B^2 - 1}}{2}\tau\right) = \tan\left(a_0 + \frac{\sqrt{i_B^2 - 1}}{2}\tau + \pi\right) = \tan\left(a_0 + \frac{\sqrt{i_B^2 - 1}}{2}\tau'\right),$$

where, in the latter equation, we consider a second time τ'. We thus have:

$$a_0 + \frac{\sqrt{i_B^2 - 1}}{2}\tau' = a_0 + \frac{\sqrt{i_B^2 - 1}}{2}\tau + \pi \Rightarrow (\tau' - \tau)\frac{\sqrt{i_B^2 - 1}}{2} = \pi.$$

By defining $\tau' - \tau = T$, we finally obtain:

$$T = \frac{2\pi}{\sqrt{i_B^2 - 1}}. \qquad\qquad (4.12)$$

By substituting this value in (4.10), we get:

$$\langle v \rangle = \frac{2\pi}{T} = \frac{2\pi}{2\pi}\sqrt{i_B^2 - 1} = \sqrt{i_B^2 - 1} \Rightarrow \langle v \rangle = \sqrt{i_B^2 - 1}$$

By squaring this expression, and doing some other algebraic steps, we get:

$$\langle v \rangle^2 = i_B^2 - 1 \Rightarrow i_B^2 = 1 + \langle v \rangle^2 \Rightarrow$$
$$i_B = \pm\sqrt{1 + \langle v \rangle^2}.$$

Knowing that $i_B = \frac{I_B}{I_{J,0}}$, we finally have:

$$I_B = \pm I_{J,0}\sqrt{1 + \langle v \rangle^2}. \qquad\qquad (4.13)$$

Equation (4.13) represents the *I-V* characteristic of a SJJ. The double sign $\pm$ indicates the presence of two branches in the graph of I_B in function of *V*: one for $I_B < 0$, V < 0, in the third quadrant, and the other one for $I_B > 0$ and V > 0 in the first quadrant. In the next paragraph we will notice that the *I-V* characteristic of a SJJ is equal to the one of a homogeneous TBJJ.

4.3 I-V characteristic for a homogeneous triple-barrier Josephson junction in the presence of a constant current bias

In this section, we consider [29] the *I-V* characteristic of a homogeneous Triple-Barrier Josephson Junction (TBJJ), for which we have $\varepsilon = 0$. Let us recall [8] that the CPR for a TBJJ is:

$$I = I_0 \frac{1 - \varepsilon^2}{2} \frac{\sin \varphi}{\sqrt{\varepsilon^2 + (1 - \varepsilon^2) \cos^2 \frac{\varphi}{2}}} \ . \tag{4.14}$$

Therefore, in the particular case of $\varepsilon = 0$, we obtain [29]:

$$I(\varepsilon = 0) = I_0 \sin \frac{\varphi}{2} \operatorname{sgn}\left(\cos \frac{\varphi}{2}\right), \tag{4.15}$$

where $\operatorname{sgn}\left(\cos \dfrac{\varphi}{2}\right) = \begin{cases} 1 & if \ \cos \dfrac{\varphi}{2} > 0 \\ -1 & if \ \cos \dfrac{\varphi}{2} < 0. \end{cases}$

If we consider the interval of values of φ given by

$$\varphi \in \left[-\pi, \pi\right],$$

we notice that, whithin this interval, $\cos \dfrac{\varphi}{2} > 0$, and so we have:

$$\operatorname{sgn}\left(\cos \frac{\varphi}{2}\right) = 1. \tag{4.16}$$

In this way, we get:

$$I(\varepsilon = 0) = I_0 \sin \frac{\varphi}{2} \quad \forall \varphi \in \left[-\pi, \pi\right]. \tag{4.17}$$

Following now the same considerations of the previous section, in particular adopting the "Resistively Shunted Josephson model", or also called, for simplicity, RSJ model, we describe the junction dynamics by the following equation:

$$\frac{d\varphi}{d\tau} + \sin\frac{\varphi}{2} = i_B , \tag{4.18}$$

where φ is phase difference between the outermost superconductors of the TBJJ, and $i_B = \dfrac{I_B}{I_o}$, where I_B is the electric current flowing inside the considered superconductor device, and where I_0, in the case of a TBJJ, is defined as follows:

$$I_0 = \frac{2e}{\hbar}\left(K_1\sqrt{N_1 N_2} + \tilde{K}_1\sqrt{N_1 N_3} + K_3\sqrt{N_3 N_4} + \tilde{K}_2\sqrt{N_2 N_4}\right). \tag{4.19}$$

In Eq. (4.19) K_1 is the coupling constant between the electrodes 1 and 2, $\tilde{K}_1$ is the one between the electrodes 3 and 4, $\tilde{K}_2$ is the one between 2 and 4, and N_1 , N_2 , N_3 , N_4 are the numerical densities of the Cooper pairs inside the considered electrodes 1, 2, 3, 4. We can now solve Eq. (4.14) with the method of variable separation, and so we get:

$$\int_{\varphi_0}^{\varphi(\tau)} \frac{d\varphi}{i_B - \sin\dfrac{\varphi}{2}} = \int_0^\tau d\tau \Rightarrow \int_{\varphi_0}^{\varphi(\tau)} \frac{d\varphi}{i_B - \sin\dfrac{\varphi}{2}} = \tau , \tag{4.20}$$

where we take the integration interval $[\varphi_0, \varphi(\tau)]$ inside the interval $[-\pi, \pi]$ so that the relation (4.18) holds. In order to solve the integral on the left hand side of Eq. (4.18), we can make the following substitution: $t = \tan\dfrac{\varphi}{4}$. In this way:

$$\frac{\varphi}{4} = \tan^{-1} t \Rightarrow \varphi = 4\tan^{-1} t \Rightarrow d\varphi = \frac{4dt}{1+t^2} .$$

We may also write:

$$\sin^2\frac{\varphi}{4} = \frac{\tan^2\dfrac{\varphi}{4}}{1+\tan^2\dfrac{\varphi}{4}} = \frac{t^2}{1+t^2} \Rightarrow \sin\frac{\varphi}{4} = \frac{t}{\sqrt{1+t^2}} \; ;$$

$$\cos^2\frac{\varphi}{4} = \frac{1}{1+\tan^2\dfrac{\varphi}{4}} = \frac{1}{1+t^2} \Rightarrow \cos\frac{\varphi}{4} = \frac{1}{\sqrt{1+t^2}} \; ;$$

$$\sin\frac{\varphi}{2} = 2\sin\frac{\varphi}{4}\cos\frac{\varphi}{4} = \frac{2t}{1+t^2} .$$

So we get:

$$\int \frac{d\varphi}{i_B - \sin\dfrac{\varphi}{2}} = \int \frac{\dfrac{4dt}{1+t^2}}{i_B - \dfrac{2t}{1+t^2}} = \int \frac{4dt}{i_B(1+t^2) - 2t} = \frac{4}{i_B}\int \frac{dt}{1+t^2 - \dfrac{2t}{1+t^2}} . \tag{4.21}$$

By repeating the same considerations of the case of SSJ, we get:

$$\int_{\varphi_0}^{\varphi(\tau)} \frac{d\varphi}{i_B - \sin\frac{\varphi}{2}} = \frac{4}{\sqrt{i_B^2 - 1}} \left[\tan^{-1}\left(\frac{i_B \tan(\frac{\varphi}{4}) - 1}{\sqrt{i_B^2 - 1}} \right) \right]_{\varphi_0}^{\varphi(\tau)} \Rightarrow$$

$$\int_{\varphi_0}^{\varphi(\tau)} \frac{d\varphi}{i_B - \sin\frac{\varphi}{2}} = \frac{4}{\sqrt{i_B^2 - 1}} \left[\tan^{-1}\left(\frac{i_B \tan(\frac{\varphi}{4}) - 1}{\sqrt{i_B^2 - 1}} \right) - \tan^{-1}\left(\frac{i_B \tan(\frac{\varphi_0}{4}) - 1}{\sqrt{i_B^2 - 1}} \right) \right].$$

The second addendum in the above expression is a constant, as it is made up by all constant quantities; therefore, it can be indicated as a_0, and so:

$$\tan^{-1}\left(\frac{i_B \tan(\frac{\varphi_0}{4}) - 1}{\sqrt{i_B^2 - 1}} \right) = a_0.$$

As we have shown, in relation (4.20), that the integral at first member equals τ, we get:

$$\frac{4}{\sqrt{i_B^2 - 1}} \left[\tan^{-1}\left(\frac{i_B \tan(\frac{\varphi}{4}) - 1}{\sqrt{i_B^2 - 1}} \right) - a_0 \right] = \tau \Rightarrow \tan^{-1}\left(\frac{i_B \tan(\frac{\varphi}{4}) - 1}{\sqrt{i_B^2 - 1}} \right) = \frac{\sqrt{i_B^2 - 1}}{4}\tau + a_0. \qquad (4.22)$$

By applying the tangent function to both members of the latter equation, we get:

$$\tan \tan^{-1}\left(\frac{i_B \tan(\frac{\varphi}{4}) - 1}{\sqrt{i_B^2 - 1}} \right) = \tan\left(a_0 + \frac{\sqrt{i_B^2 - 1}}{4}\tau \right).$$

Knowing that $\tan(\tan^{-1} x) = x$, we get:

$$\frac{i_B \tan(\frac{\varphi}{4}) - 1}{\sqrt{i_B^2 - 1}} = \tan\left(a_0 + \frac{\sqrt{i_B^2 - 1}}{4}\tau \right) \Rightarrow i_B \tan(\frac{\varphi}{4}) - 1 = \sqrt{i_B^2 - 1}\,\tan\left(a_0 + \frac{\sqrt{i_B^2 - 1}}{4}\tau \right) \Rightarrow$$

$$\tan\frac{\varphi}{4} = \frac{1}{i_B}\left[\sqrt{i_B^2 - 1}\,\tan\left(a_0 + \frac{\sqrt{i_B^2 - 1}}{4}\tau \right) + 1 \right].$$

As the tangent is a periodic function, of period of π, we get:

$$\tan\left(\frac{\varphi}{4}+k\pi\right)=\tan\left(\frac{\varphi}{4}\right)=\frac{1}{i_B}\left[\sqrt{i_B^2-1}\tan\left(a_0+\frac{\sqrt{i_B^2-1}}{4}\tau\right)+1\right] ,\ \text{where } k \text{ is an integer. Therefore, we}$$

get:

$$\frac{\varphi}{4}+k\pi=\tan^{-1}\left\{\frac{1}{i_B}\left[\sqrt{i_B^2-1}\tan\left(\frac{\sqrt{i_B^2-1}}{4}\tau+a_0\right)+1\right]\right\}\Rightarrow$$

$$\varphi=\varphi(\tau)=\tan^{-1}\left\{\frac{1}{i_B}\left[\sqrt{i_B^2-1}\tan\left(\frac{\sqrt{i_B^2-1}}{4}\tau+a_0\right)+1\right]\right\}+4k\pi . \tag{4.23}$$

In fact, as k is an integer relative number, this result (4.23) can also be expressed with the positive sign in the term $4k\pi$. In this way, for $k = 1$, we obtain the term 4π, which represents the value of period for the phase difference angle φ, in this case of TBJJ. Just like in the previous case, we can calculate the average value of $v(t)=\dfrac{V(t)}{RI_0}$, that is the normalized voltage, with the meaning of the various terms just discussed previously. Also, by using the relation $\tau=\dfrac{2\pi RI_0}{\Phi_0}t$, we get:

$$\langle v\rangle=\frac{1}{T}\int_0^T v(\tau)d\tau=\frac{1}{T}\int_0^T\frac{d\varphi}{d\tau}d\tau=\frac{4\pi}{T}$$

In the latter equation, we have considered the periodicity in φ, equals to 4π, as just previously considered. So, we have obtain:

$$\langle v\rangle=\frac{4\pi}{T} . \tag{4.24}$$

We must now calculate the value of the period T. By using the property, according to which the tangent function is periodic, of period π, we obtain:

$$\tan\left(\frac{\sqrt{i_B^2-1}}{4}\tau+a_0\right)=\tan\left(\frac{\sqrt{i_B^2-1}}{4}\tau+a_0+\pi\right)=\tan\left(\frac{\sqrt{i_B^2-1}}{4}\tau'+a_0\right) .$$

In this way, from the considered equation, we get:

$$\frac{\sqrt{i_B^2-1}}{4}\tau+a_0+\pi=\frac{\sqrt{i_B^2-1}}{4}\tau'+a_0\Rightarrow$$

$$\frac{\sqrt{i_B^2-1}}{4}(\tau'-\tau)=\pi\Rightarrow\frac{\sqrt{i_B^2-1}}{4}T=\pi.$$

We therefore obtain:

$$T = \frac{4\pi}{\sqrt{i_B^2 - 1}}.$$

(4.25)

By now using the relation (4.24), we have:

$$\langle v \rangle = \frac{4\pi}{T} = \frac{4\pi}{\dfrac{4\pi}{\sqrt{i_B^2 - 1}}} = \sqrt{i_B^2 - 1} \Rightarrow$$

$$i_B^2 - 1 = \langle v \rangle^2 \Rightarrow i_B^2 = \langle v \rangle^2 + 1 \Rightarrow i_B = \pm\sqrt{1 + \langle v \rangle^2}.$$

Because $i_B = \dfrac{I_B}{I_0}$, we finally get:

$$I_B = \pm I_0 \sqrt{1 + \langle v \rangle^2}$$

(4.26)

The above relation is the *I-V* characteristic of a TBJJ, in the simplified case of $\varepsilon = 0$. We can notice that it is analytically equal to the *I-V* characteristics of the SJJ, expressed by the relation (4.13), with the value of I_0 which is obviously different, as it has been previously specified.

4.4 I-V characteristics of an inhomogeneous TBJJ in the presence of a constant current bias

When the case [29] of an inhomogeneous TBJJ, so with $\varepsilon \neq 0$, is considered, we can also use the RSJ model, just like the homogeneous case, and we obtain:

$$I_B = I_R + I_J = \frac{V}{R} + I_0 \frac{1 - \varepsilon^2}{2} \frac{\sin \varphi}{\sqrt{\varepsilon^2 + (1 - \varepsilon^2)\cos^2 \dfrac{\varphi}{2}}}.$$

(4.27)

By using the second Josephson equation, and normalizing both members of the latter relation for I_0, we get:

$$\frac{d\varphi}{d\tau} + \frac{1 - \varepsilon^2}{2} \frac{\sin \varphi}{\sqrt{\varepsilon^2 + (1 - \varepsilon^2)\cos^2 \dfrac{\varphi}{2}}} = i_B,$$

(4.28)

where τ is defined as in the previous paragraphs. In order to solve the latter differential equation we recur to numerical analysis, and so, for $\varepsilon = 0.15$ and, $i_B = 0.9, 1.1, 1.3, 1.5$ we obtain numerical solutions of $\varphi(\tau)$ and $\dfrac{d\varphi}{d\tau}$.

The profiles of $\varphi(\tau)$ and $\dfrac{d\varphi}{d\tau}$ as functions of τ, for these values of the parameters ε and i_B, are represented in figures 4.2a and 4.2b respectively.
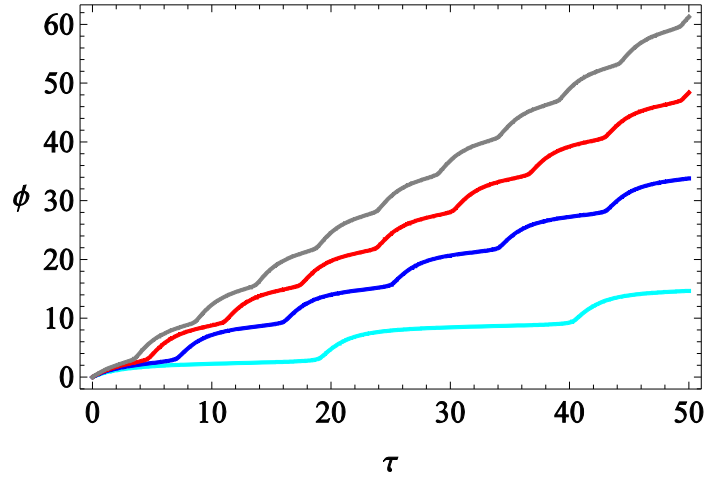

Figure 4.2a. *Numerical solution $\phi(\tau)$ of the dynamical equation of a TBJJ in the presence of a constant current bias i_B for $\varepsilon = 0.15$ and for $i_B = 0.9$ (cyan curve), $i_B = 1.1$ (blue curve), $i_B = 1.3$ (red curve), and $i_B = 1.5$ (gray curve).*

Figure 4.2b. *Time evolution of the derivative $\dfrac{d\phi}{d\tau}$ of the superconducting phase difference φ in the presence of a constant current bias i_B for $\varepsilon = 0.15$ and for $i_B = 0.9$ (cyan curve), $i_B = 1.1$ (blue curve), $i_B = 1.3$ (red curve), and $i_B = 1.5$ (gray curve).*
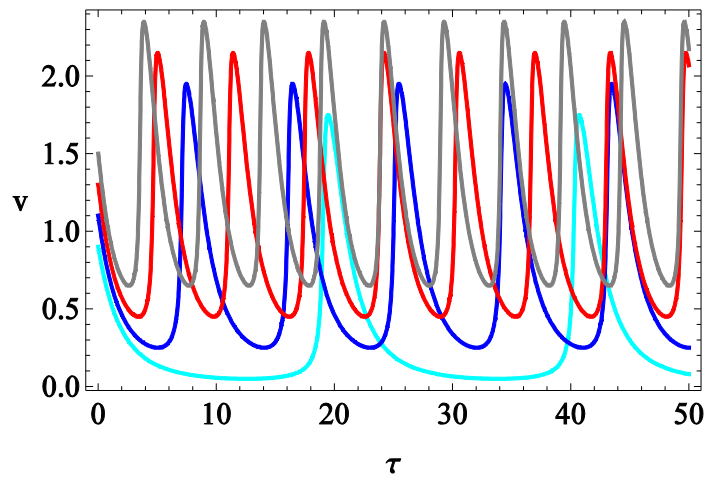
Successively, for each value of i_B, a value of $\varphi(\tau)$ is determined and, consequently, of $\dfrac{d\varphi}{d\tau}$ by the numerical resolution of (4.28). Therefore, by knowing that $\langle v \rangle = \left\langle \dfrac{d\varphi}{d\tau} \right\rangle = \dfrac{1}{T} \displaystyle\int_0^T \dfrac{d\varphi}{d\tau} d\tau$, we obtain the *I-*

V characteristics of a inhomogeneous TBJJ, i.e. the profile of i_B as a function of $\langle v \rangle$. In figure 4.3 we show the *I-V* characteristics for $\varepsilon = 0.15$ along with the *I-V* characteristics for $\varepsilon = 0$.
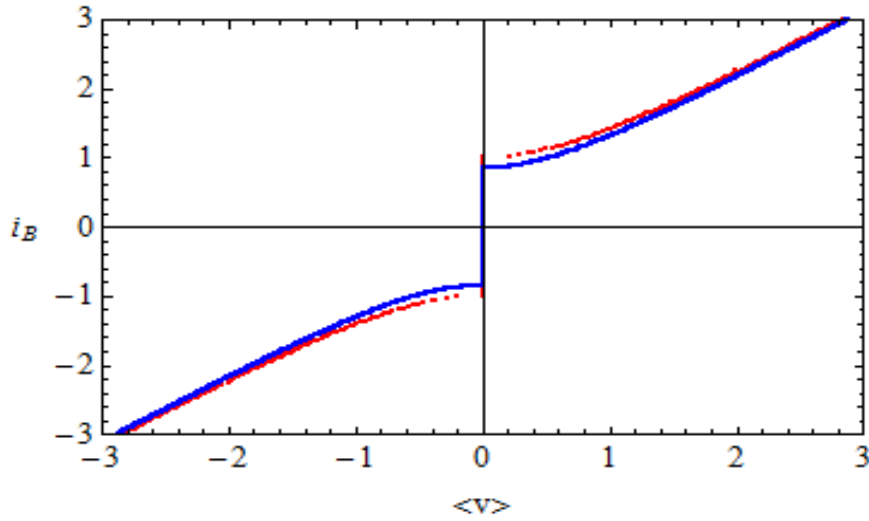

Figure 4.3. *Current-voltage characteristics of a TBJJ in the presence of a constant current bias for $\varepsilon = 0.00$ (red curve) and $\varepsilon = 0.15$ (blue curve). Notice that the red curve shows a larger maximum Josephson current I_{MAX}. In fact, it depends on ε simply as follows: $I_{MAX} = I_0 (1-\varepsilon)$, I_0 being the maximum possible value obtained at $\varepsilon = 0$.*

In the latter figure, we notice that the $\varepsilon = 0.15$ curve lies below the $\varepsilon = 0$ curve. This feature can be understood by generalizing the zero voltage case to finite voltages. In fact, we may start by noticing that the maximum value I_{MAX} of the Josephson current for the TBJJ can be expressed as follows [8]:

$$I_{MAX} = I_0 (1-\varepsilon) . \tag{4.29}$$

Because of (4.29), the normalization of the bias current [29] should be made with respect to I_{MAX}, if we were to perform analytic calculations also in this case. However, retaining the usual normalization with respect to I_0, we are left with a rescaling factor in (1) equal to $(1-\varepsilon)$. Therefore, the *I-V* curves obtained for $\varepsilon \neq 0$ are affected by the rescaling of the non-linear term in Eq. (16) and thus differ from the corresponding curves obtained for $\varepsilon = 0$.

4.5 I-V characteristics in the presence of r.f. radiation

Let us now consider [29] the *I-V* characteristics of TBJJs in the presence of r.f. radiation, in such a way that the whole four-layer superconducting system is driven by an external oscillating voltage of the following form:

$$V(t) = V_0 + V_1 \cos(\omega_r t) , \tag{4.30}$$

where V_0 is the d.c. voltage component, and V_1 is the amplitude of the oscillating part. This analysis has already been performed, in the case of a homogeneouys TBJJ, in the previous chapter,

in particular in the paragraph 3.5). We have determined, by integrating [6] the Josephson voltage-frequency relation $v = \dfrac{d\varphi}{d\tau}$ the analytic expression of $\varphi = \varphi(\tau)$:

$$\varphi(\tau) = \varphi_0 + v_0\tau + a\sin(\tilde{\omega}_r\tau),$$ (4.31)

with the meaning of the symbols just expressed into the relation (3.51). In the case of homogeneous TBJJs we have determined integer Shapiro steps and their semi-amplitudes in relations (3.65) and (3.66), respectively. Fractional Shapiro steps and their semi-amplitudes have also been determined in relations (3.81) and (3.82), respectively.

The *I-V* characteristics of a inhomogeneous device needs to be evaluated numerically, as in the previous paragraph 4.3), by means of the RSJ model, where the expression $v(\tau) = v_0 + a\tilde{\omega}_r\cos(\tilde{\omega}_r\tau)$ takes the place of the electric current i_B. The latter expression of $v(\tau)$ can be determined by the relation (3.53), in which it can be shown that, according to the symbols in relation (3.51), the coefficient $\dfrac{V_1}{RI_0}$ is equal to $a\tilde{\omega}_r$. Therefore, we take [5] the average value of i_B to correspond to v_0, as we know that the mean value of the cosine function is zero. The average value $\langle v \rangle$ can be obtained by means of the numerically determined solution $\varphi(\tau)$ of the differential equation (4.28) and its first derivative.

From (4.28) we may notice that $\langle v \rangle$ depends on ε, and from (4.31) that it also depends on the parameters a and $\tilde{\omega}_r$. In this way, the graph of i_B as a function of $\langle v \rangle$, representing the *I-V* characteristics of a TBJJ in the presence of r.f. radiation, as in this case it is considered, will depend on the parameters ε, a, and $\tilde{\omega}_r$. In figures 4.4a and 4.4b the *I-V* curves for $\varepsilon = 0$, and $\varepsilon = 0.15$ (in both cases $a = 0,6$ and $\tilde{\omega}_r = 1$) are shown; in figure 4.4c, on the other hand, we show the *I-V* curve for the following choice of the parameters: $\varepsilon = 0.0$, $a = 1.2$, $\tilde{\omega}_r = 1$.
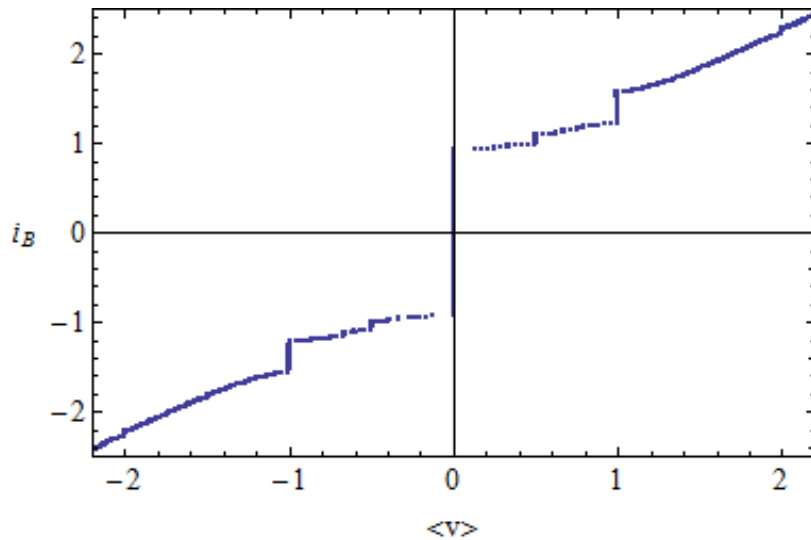

Figure 4.4a. *Current-voltage characteristics of a TBJJ in the presence of an oscillating r.f. voltage $v_0 + a\tilde{\omega}_r\cos(\tilde{\omega}_r\tau)$, obtained from (4.30) by normalizing all terms for RI_0, for the following values of the parameters: $\varepsilon = 0.00$, $a = 0.6$, $\tilde{\omega}_r = 1$.*

Figure 4.4b. *Current-voltage characteristics of a TBJJ in the presence of an oscillating r.f. voltage* $v_0 + a\tilde{\omega}_r \cos(\tilde{\omega}_r \tau)$, *obtained from (4.30) by normalizing all terms for* RI_0, *for the following values of the parameters:* $\varepsilon = 0.15$, $a = 0.6$, $\tilde{\omega}_r = 1$.
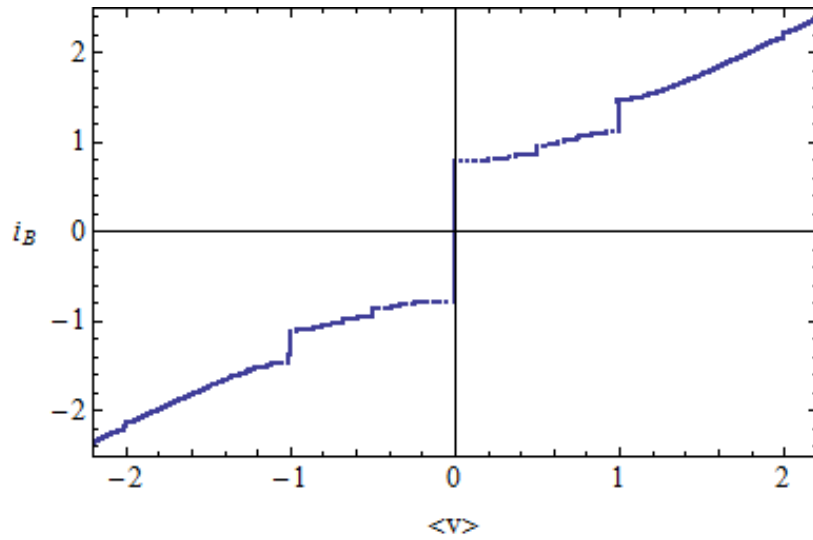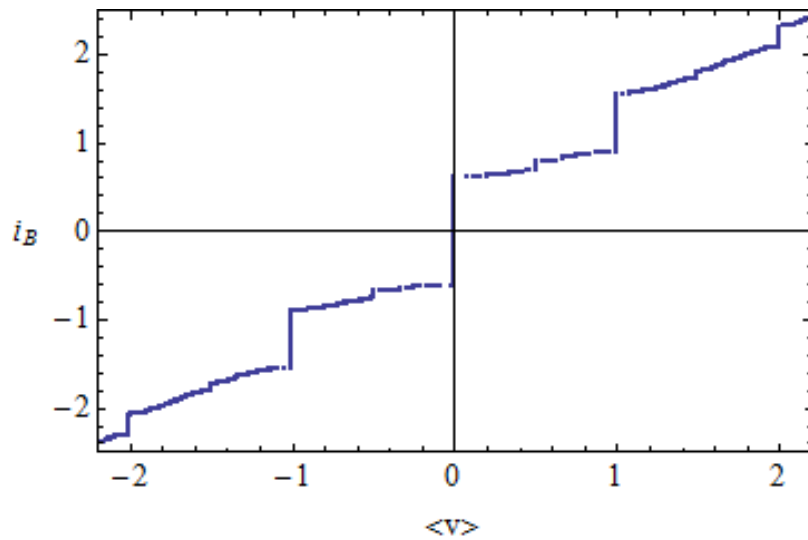

Figure 4.4c. *Current-voltage characteristics of a TBJJ in the presence of an oscillating r.f. voltage* $v_0 + a\tilde{\omega}_r \cos(\tilde{\omega}_r \tau)$, *obtained from (4.30) by normalizing all terms for* RI_0, *for the following values of the parameters:* $\varepsilon = 0.00$, $a = 1.2$, $\tilde{\omega}_r = 1$.

In figure 4.5a a comparison [29] between the results reported in figures 4.4a and 4.4b is made. In this particular figure we notice that, apart from a displacement of the curve for $\varepsilon = 0.15$ toward the bottom in comparison with the curve for $\varepsilon = 0.00$, the amplitude of the Shapiro steps appearing in these figures remain roughly unaltered. In figure 4.6b, on the other hand, we compare the curves in

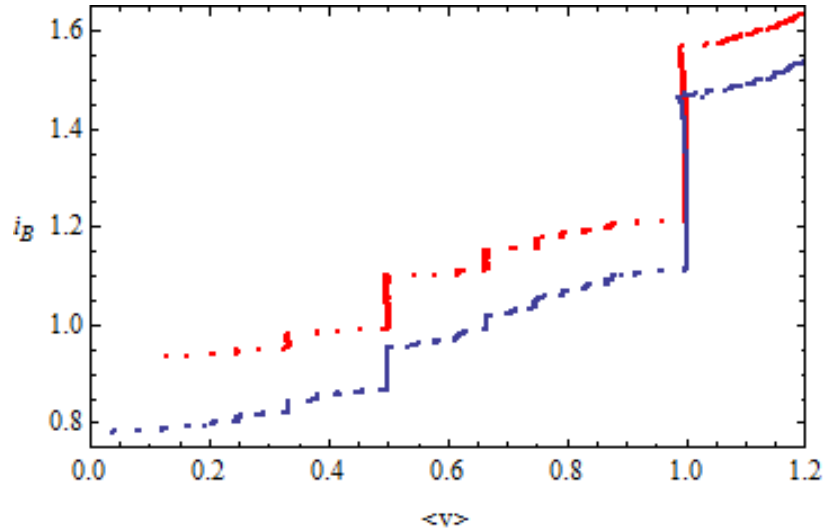figures 4.4a and 4.4c, considering that the amplitudes of the current steps vary by choosing different values of *a*.

Figure 4.5a. *Comparison between the curves in fig. 4.4a and fig. 4.4b in a restricted voltage interval: the* $\varepsilon = 0.00$ *case (red curve) and the* $\varepsilon = 0.15$ *case (blue curve) are both obtained for* $a = 0.6$ *and* $\tilde{\omega}_r = 1.0$.
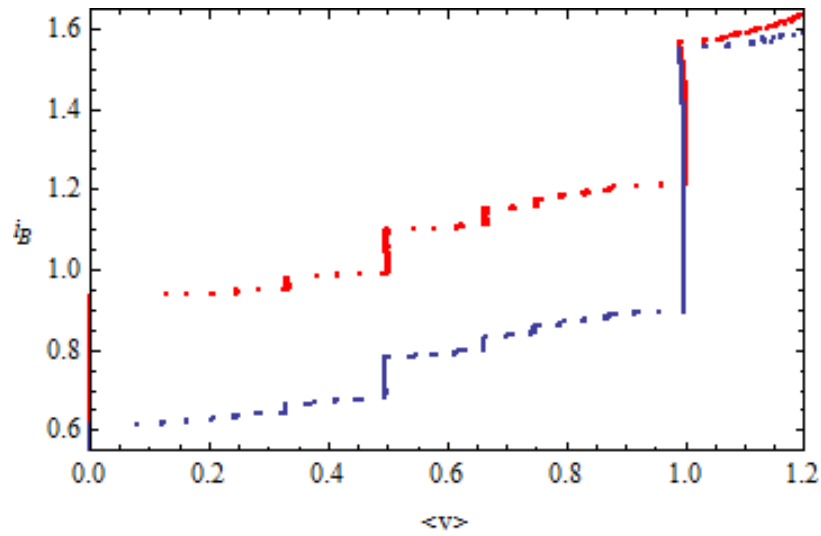
Figure 4.5b*. Comparison between the curves in fig. 4.4a and fig. 4.4c in a restricted interval of* $\langle v \rangle$. *Both the red curve (* $a = 0.6$ *) and the blue curve (* $a = 1.2$ *) are obtained for* $\varepsilon = 0.00$ *and* $\tilde{\omega}_r = 1.0$.

With respect to the Shapiro steps analysed in Chapter 3, we show the numerical evaluation of ΔI_1 and ΔI_2 for the first forty terms in the summation in relation (3.66). In this way, we get a more refined evaluation of these quantities.
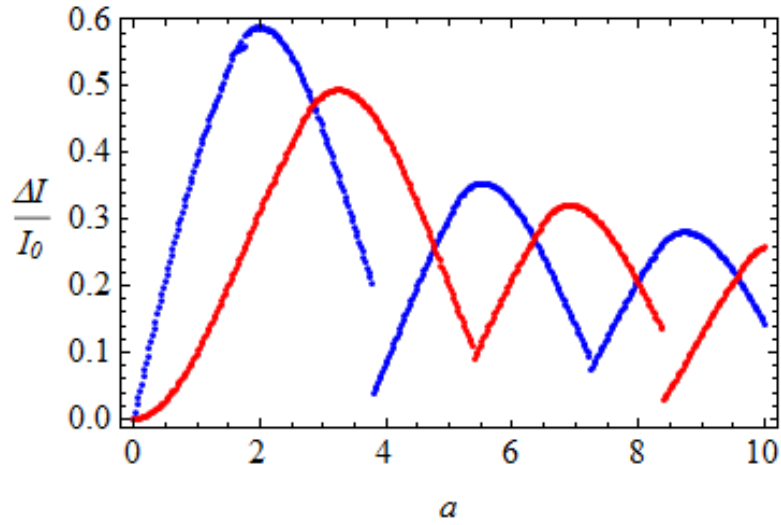
Figure 4.6a. *Numerical evaluation of* ΔI_1 *and* ΔI_2 *(blue and red curves, respectively) as a function of the parameter a for* $\varepsilon = 0$. *The first forty terms in the summation in (3.66) are considered.*

We also show the numerical evaluation of ΔI_q, for q $= \dfrac{1}{4}, \dfrac{1}{3}, \dfrac{1}{2}, \dfrac{2}{3}$, for the first forty terms in the summation in relation (3.82).
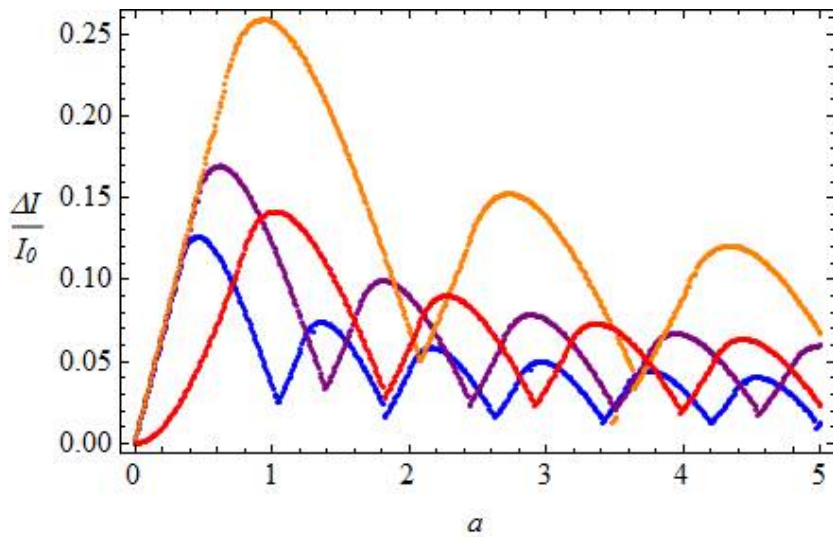
Figure 4.6b. *Numerical evaluation of* ΔI_q, *for q=1/4, 1/3, 1/2, 2/3 (blue, purple, orange, and red curves, respectively) as a function of the parameter a for* $\varepsilon = 0$. *The first forty terms in the summation in (25) are considered. We notice that the semi-amplitude of the half-integer Shapiro steps (q=1/2), while having lower peaks than* ΔI_1 *and* ΔI_2, *show much larger oscillations than* $\Delta I_{1/4}$, $\Delta I_{1/3}$, *and* $\Delta I_{2/3}$.

We can consider [29] that the semi-amplitude of Shapiro steps is calculated in a semi-analytical way, as the relations (3.66) and (3.82) have been analytically determined, while the maximum value in the summations expressed by these same relations has been calculated by using techniques of numerical analysis. Instead, figures 4.4a, 4.4b, 4.4c, and 4.5a, 4.5b have been represented only by means of numerical analysis, because they are connected with the numerical solution of (4.28). Let us now compare, at least qualitatively, the integer and fractional current step amplitudes, obtained, as just said, by numerical integration, with those obtained semi-analytically from equations (3.66) and (3.82). For example, by estimating from figure 4.5b the semi-amplitudes of the first integer step ($n = 1$) and of the rational step $q = \dfrac{1}{2}$, obtained for $\tilde{\omega}_r = 1$ and $\varepsilon = 0$, and for a = 0.6 (red curve) and $a = 1.2$ (blue curve), we might see that the $n = 1$ step almost doubles and the $q = \dfrac{1}{2}$ step is left almost unaltered. This behaviour corresponds to an increase of ΔI_1 (blue curve in fig. 4.6a) for 0.0 < a < 2.0 and to a small variation of the value of $\Delta I_{1/2}$ (orange curve in fig. 4.6b) when going from $a = 0.6$ to $a = 1.2$. In fact, we notice that for the quantity a comprised between 0.6 and 1.2 and with $n = 1$, ΔI_1 shows a larger variation almost between 0.1 and 0.5, in comparison with the case of $\Delta I_{1/2}$, that varies between 0.05 and 0.25 in the same range of the quantity a. This property agrees with the behaviour of the amplitude of i_B as a function of a varying into the range 0.6-1.2, as it is shown in the numerically determined figure 4.5b, where, for $n = 1$, this amplitude practically doubles, while for $q = \dfrac{1}{2}$ remains almost unchanged. As we have noticed, for $n = 1$ the current i_B varies about between 0.8 and 1.6, while for $q = \dfrac{1}{2}$ the current i_B only varies between 0.6 and 0.8, therefore confirming that the semi-analytical profiles of figure 4.6a and 4.6b agree with the numerical profile of figure 4.5b.

4.6 Conclusions

The *I-V* characteristics of triple-barrier Josephson junctions have been studied in the presence of a constant current bias and of a r. f. voltage radiation.
In the case of constant current bias, we have first analysed the homogeneous case ($\varepsilon = 0$) in which the Josephson coupling between superconducting regions does not depend on the particular pair of layers considered. In this case we have been able to analytically determine the *I-V* characteristics of TBJJs in the presence of a constant current bias. Adopting the RSJ model, the analytically determined *I-V* curves are seen to be formally identical to the canonical ones derived for JJs. For inhomogeneous Josephson coupling ($\varepsilon \neq 0$), on the other hand, numerical evaluation of *I-V* shows that deviations of these curves from the analytically determined characteristics for $\varepsilon = 0$ are seen to be compatible with the expression of maximum Josephson current $I_{MAX} = (1 - \varepsilon)I_0$.
In the presence of a r. f. radiation the *I-V* characteristics show integer and fractional Shapiro steps. By a standard semi-analytic approach, expressions of the semi-amplitudes of these steps have been determined for $\varepsilon = 0$. Numerical evaluation of *I-V* curves, performed for $\varepsilon \neq 0$, shows persistence of integer and fractional Shapiro steps.

Chapter 5

Semi-classical and quantum analysis of the one-junction and the two-junction Josephson interferometer

Starting from the review of the classical and quantum physical properties of one-junction interferometers, the same type of analysis is extended to two-junction interferometers. By means of this approach, the Hamiltonian of the latter system is determined in terms of the average phase difference for the two Josephson junctions in the device. Under the hypothesis of negligible loop inductance, energy and current states in two-junction interferometers in the quantum regime are found. Possible extension of the present analysis to ternary quantum computing is discussed.

5.1 Introduction

The magnetic properties of a superconducting loop interrupted by one Josephson junction are well known and give rise to interesting applications in the realm of mesoscopic [15] and quantum physics [30-31]. In fact, r. f. Superconducting Quantum Interference Devices (r. f. SQUIDs) are nowadays useful instruments in experimental research [28]. As far as the field of quantum computing is concerned, a superconducting loop containing one Josephson junction (JJ) can be shown to be equivalent to a Cooper pair box [32-33]. The former device is thus denoted as "flux box", which may be considered to be a promising candidate for elementary memory cells in quantum computing [34-39].

Equally well known are the magnetic properties of two-junction quantum interferometers [15]. Similar widespread use of d. c. SQUIDs is made in various fields [28]. The two-junction quantum interferometer, on the other hand, is not isolated from external classical systems and its quantum extension does not result to be as immediate as in the case of a flux box. Moreover, the presence of two forcing terms in the latter device, namely, the applied magnetic flux and the bias current, provide additional features, giving the possibility of operating this superconducting system in different applicative contexts. For these reasons, even though the strict quantum regime of these types of superconducting elements, directly coupled to classical circuitry, could be more difficult to attain experimentally, the study of the magnetic response of their quantum states could give new hints in conceiving devices with two control parameters. Moreover, logic circuits utilizing Josephson junctions as fundamental elements for memory cells in ternary logic computing [40-41] have already been proposed in the literature. In this respect, extension of the quantum properties of the one-junction to the two-junction interferometer may provide a way to consider quantum computing based on qutrits, rather than qubits.

According to these considerations, in this chapter, starting [42] from a semi-classical and quantum analysis of a single junction interferometer, whose main analytical properties are summarized, we extend these concepts to the analysis of the semiclassical and quantum properties of a two junction interferometer. In particular, by following a semiclassical analysis, we have considered the expression of the potential energy of a one-junction interferometer, called "parabolic washboard

potential", recalling how the dynamical equation of the phase difference in the Josephson Junction can be derived. We have thus calculated the current states, showing the presence of a diamagnetic and a paramagnetic behaviour in two different states. We have also considered the quantum analysis of the same device, determining the expression of the Hamiltonian operator, calculating its eigevalues and the current states corresponding to them, showing that an alternating diamagnetic and paramagnetic behaviour still exists.

The extension of semiclassical and quantum analysis to a two-junction interferometer has also been considered. By using a semiclassical analysis we have recalled, with the condition of negligible loop inductance, how the dynamical equation for the phase difference, taken as the mean value of the phase differences in the Josephson Junctions, can be derived. In addition, we have calculated the persistent current flowing inside this system, as a function of the external magnetic flux. Successively, just as in the previous case, we have extended to the quantum analysis of a two-junction interferometer, determining its Hamiltoninan operator, calculating its eigenvalues and the related expression of the current states.In the quantum regime we still notice the characteristic alternating occurrence of diamagnetic and paramagnetic states, in the same way they appear in their classical counterpart. The classical and quantum properties of the two-junction interferometer are compared and possible extension of these concepts to ternary or higher order computing are discussed. Some specific calculations, connected to the main arguments, have been reported in Appendixes 5.1, 5.2, 5.3, 5.4, 5.5.

5.2 Semi-classical analysis of the one-junction interferometer

The one-junction quantum interferometer [42] can be described, on semiclassical ground, by means of the following potential energy function:

$$E(\varphi, \Phi) = \frac{(\Phi - \Phi_{ex})^2}{2L} + \frac{I_{j,0}\Phi_0}{2\pi}(1 - \cos\varphi) \qquad (5.1)$$

where, Φ is the magnetic flux threading the superconducting loop, Φ_{ex} is the applied flux, L is the loop inductance, $I_{J,0}$ is the maximum Josephson current, and φ is the superconducting phase difference across the single Josephson junction considered. Equation (5.1) can be obtained considering that in the total potential energy we have two terms: the first one is the interaction energy between the superconducting loop and the external magnetic field, and the second one is the energy of the simple Josephson Junction (SJJ). In fact, the first term is a magnetic energy of the form:

$$E_M = \frac{1}{2}LI^2 \qquad (5.2)$$

where L is the loop inductance, and I is the electric current flowing in the loop, that can be expressed by using the relation:

$$\Phi = \Phi_{ex} + LI \implies I = \frac{\Phi - \Phi_{ex}}{L}. \qquad (5.3)$$

Substituting this expression in Eq. (5.2), we get:

$$E_M = \frac{(\Phi - \Phi_{ex})^2}{2L}, \tag{5.4}$$

which gives the analytic expression of the first term. The energy associated to the SJJ can be obtained starting from the relation, that is proved in the theory of the Josephson Junctions:

$$I = \frac{dW_C}{dt} \frac{1}{V},$$

where I is the electric current made up by the Cooper pairs (Josephson current), W_C is the potential coupling energy between the two superconductors constituting the SJJ, and V is the voltage applied at the electrodes of the considered Josephson junction. By using the second Josephson equation $\frac{d\varphi}{dt} = \frac{2eV}{\hbar}$, we get:

$$I = \frac{dW_C}{d\varphi} \frac{d\varphi}{dt} \frac{1}{V} = \frac{2e}{\hbar} \frac{dW_C}{d\varphi}$$

In this way, identifying the variation of W_C with the variation of the total energy of the Josephson Junction $E_J(\varphi)$, with varying φ, we get:

$$I = \frac{2\pi}{\Phi_0} \frac{dE_J(\varphi)}{d\varphi}, \tag{5.5}$$

where $\Phi_0 = \frac{h}{2e}$, and h is the Planck's constant. So, by integrating Eq. (5.4), we obtain:

$$E_J(\varphi) = \frac{\Phi_0}{2\pi} \int_0^\varphi I(\varphi')d\varphi' = \frac{\Phi_0 I_{j,0}}{2\pi} \left[-\cos\varphi'\right]_0^\varphi = \frac{\Phi_0 I_{J,0}}{2\pi}(1 - \cos\varphi),$$

where we have used the Current Phase Relation (CPR) of a Single Josephson Junction (SJJ):

$$I = I_{J,0} sen\varphi .$$

In this way, considering $E(\varphi,\Phi) = E_M(\varphi) + E_J(\varphi)$ we get the expression (5.1).
By means of the fluxoid quantization condition:

$$\varphi + 2\pi \frac{\Phi}{\Phi_0} = 2\pi k , \tag{5.6}$$

with k integer, we can express the potential energy $E(\varphi,\Phi)$ exclusively in terms of the magnetic flux Φ. Therefore, we get:

$$W_P(\Phi) = \frac{(\Phi - \Phi_{ext})^2}{2L} + \frac{I_{J,0}\Phi_0}{2\pi}\left[1 - \cos\left(\frac{2\pi\Phi}{\Phi_0}\right)\right], \tag{5.7}$$

where the trigonometric property: $\cos\left(2\pi k - 2\pi\dfrac{\Phi}{\Phi}\right) = \cos\left(2\pi\dfrac{\Phi}{\Phi_0}\right)$ has been used. In order to make clear the link between this classical description and its quantum extension already at this stage, we can define the following quantities:

$$n = \frac{\Phi}{\Phi_0} \quad ; \quad n_{ex} = \frac{\Phi_{ex}}{\Phi_0},$$

where n represents the number of trapped fluxons in the superconducting loop of the SQUID considered, and n_{ex} the equivalent real value of applied fluxons. Let us now define:

$E_L = \dfrac{\Phi_0^2}{2L} \quad ; \quad E_{J,0} = \dfrac{I_{J,0}\Phi_0}{2\pi} \quad ; \quad \alpha = \dfrac{E_{J,0}}{E_L}$, so that the expression of W_P as a function of n, can be written as follows:

$$W_P(n) = E_L\left[(n - n_{ex})^2 + \alpha(1 - \cos(2\pi n))\right]. \tag{5.8}$$

We can report the profile of the parabolic washboard potential $W_P(n)$, normalized to E_L, as a function of n, in figure 5.1, where we have considered two different values of the applied external magnetic flux, namely $\Phi_{ex} = 0$ and $\Phi_{ex} = \dfrac{\Phi_0}{2}$, so that $n_{ex} = 0$ and $n_{ex} = \dfrac{1}{2}$, both for $\alpha = 0.25$, obtaining, for each of these values, a different shape of this potential.
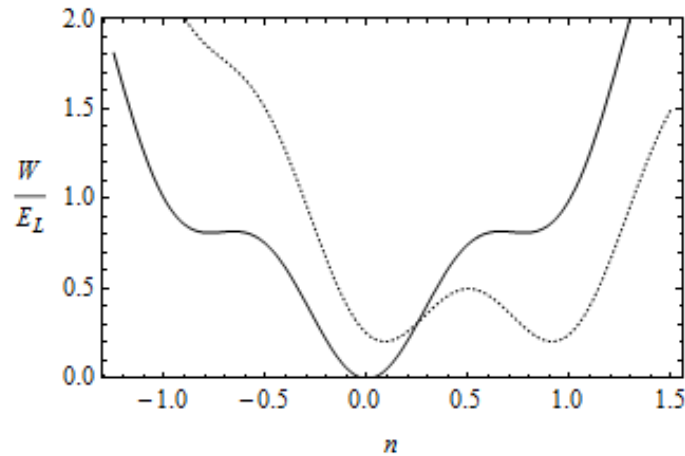

Figure 5.1. *Parabolic washboard potential of a one-junction quantum interferometer for $\alpha = 0.25$ and for normalized applied flux n_{ex} equals to 0.0 (full line) and 0.5 (dashed line).*

We can extract useful information on the flux dynamics with two different methods: the Resistively Shunted Junction (RSJ) model, and the power balance relation. Let us first consider the RSJ model. The electric current I circulating in the loop, and flowing through the Josephson Junction (JJ) divides into the two branch currents: $I_J = I_{J,0}\sin\varphi$ flowing in the ideal Josephson element, and $I_R = \dfrac{V}{R}$ flowing in the shunt resistor of electric resistance R, when a nominal voltage V is present. Therefore, by using current conservation, we have:

$$I = I_J + I_R \,, \tag{5.9}$$

where I is expressed by the relation (5.3), and $V = \dfrac{\Phi_0}{2\pi}\dfrac{d\varphi}{dt}$ according to the second Josephson equation. In this way, we obtain:

$$\frac{\Phi_0}{2\pi R}\frac{d\varphi}{dt} + I_{J,0}\sin\varphi = \frac{\Phi - \Phi_{ex}}{L} \,. \tag{5.10}$$

The relation (5.10) expresses the phase difference dynamics. In order to obtain, from Eq. (5.10), the magnetic flux dynamics, we can use the fluxoid quantization condition (5.6), so that:

$$-\frac{1}{R}\frac{d\Phi}{dt} + I_{J,0}\sin\left(2\pi k - 2\pi\frac{\Phi}{\Phi_0}\right) = \frac{\Phi - \Phi_{ex}}{L} \,.$$

Knowing that $\sin\left(2\pi k - 2\pi\dfrac{\Phi}{\Phi_0}\right) = -\sin 2\pi\dfrac{\Phi}{\Phi_0}$, and changing the sign in the first and second member in the relation (5.10), we write:

$$\frac{1}{R}\frac{d\Phi}{dt} + I_{J,0}\sin 2\pi\frac{\Phi}{\Phi_0} = \frac{\Phi_{ex} - \Phi}{L} \,. \tag{5.11}$$

Equation (5.11) expresses the magnetic flux dynamics connected with this one-junction interferometer considered. We notice that the first addendum on the left-hand side of equations (5.10) and (5.11) represents a dissipation in the system. In fact, the presence of the resistive term R, due to the insulating material present between the superconducting electrodes of the JJ, leads to energy dissipation of the electromotive force source, having considered our system insulated from the external environment. From relation (5.11) we can obtain the dinamycs for $n = \dfrac{\Phi}{\Phi_0}$ in Appendix 5.1.

The second method is based on the following power-balance relation:

$$\frac{V^2}{R} + \frac{dW(\Phi)}{dt} = 0 \,. \tag{5.12}$$

Equation (5.12) is obtained by using classical electrodynamics, namely the relations: $P = VI = \dfrac{V^2}{R}$, where P is the electric power, which represents the time variation of energy, in this case of the potential energy $W(\Phi)$. So we get:

$$\frac{dW(\Phi)}{dt} = -\frac{V^2}{R} \,,$$

where the minus sign is due to the dissipation of energy on the resistor. By Eq. (5.12), we obtain:

$$\frac{dW(\Phi)}{dt} = \frac{dW(\Phi)}{d\Phi}\frac{d\Phi}{dt} = \left\{ \frac{\Phi - \Phi_{ex}}{L} + \frac{I_{J,0}\Phi_0}{2\pi}\left[\sin\left(\frac{2\pi\Phi}{\Phi_0}\right)\right]\frac{2\pi}{\Phi_0} \right\}\frac{d\Phi}{dt} \ .$$

By using the fluxoid quantization (5.6), and knowing that $\sin(2\pi k - \varphi) = -\sin\varphi$, we have:

$$\frac{dW(\Phi)}{dt} = \left[\frac{\Phi - \Phi_{ex}}{L} - I_{J,0}\sin\varphi \right]\frac{d\Phi}{dt} \ . \qquad\qquad (5.13)$$

We can now express $\dfrac{d\Phi}{dt}$ in terms of $\dfrac{d\varphi}{dt}$ by using the relation (5.6), so that:

$$2\pi\frac{\Phi}{\Phi_0} + \varphi = 2\pi k \Rightarrow \Phi = (2\pi k - \varphi)\frac{\Phi_0}{2\pi} \Rightarrow \frac{d\Phi}{dt} = -\frac{\Phi_0}{2\pi}\frac{d\varphi}{dt} \ .$$

By replacing this term inside the expression (5.13), and by using the second Josephson equation, we obtain:

$$\left(\frac{\Phi - \Phi_{ex}}{L} - I_{J,0}\sin\varphi \right)\left(-\frac{\Phi_0}{2\pi}\frac{d\varphi}{dt} \right) = -\left(\frac{\Phi_0}{2\pi}\frac{d\varphi}{dt} \right)^2\frac{1}{R}$$

With the right simplifications, this expression becomes:

$$\frac{\Phi_0}{2\pi R}\frac{d\varphi}{dt} + I_{J,0}\sin\varphi = \frac{\Phi - \Phi_{ex}}{L} \ ,$$

which is just equation (5.11).

Purely superconducting states (S-states) are obtained by setting $\dfrac{d\varphi}{dt} = 0$, and thus correspond to the minima of $W(\Phi)$. In fact, if we consider the second Josephson equation $\dfrac{d\varphi}{dt} = \dfrac{2eV}{\hbar}$ we have:

$$\frac{d\varphi}{dt} = 0 \Rightarrow V = 0 \ .$$

Therefore, from equation (5.12) we get: $\dfrac{dW(\Phi)}{dt} = 0$, according to energy conservation of the system considered. The minima of $W(\Phi)$, on the other hand, are obtained by setting its first derivative to zero, since:

$$\frac{dW(\Phi)}{dt} = \frac{dW(\Phi)}{d\Phi}\frac{d\Phi}{dt} = 0 \ .$$

Now, knowing that the magnetic flux and its time derivative can be different from zero, we have:

$\dfrac{dW(\Phi)}{d\Phi} = 0$. The latter expression is the condition to obtain the minima of the function $W(\Phi)$ considered, as we can notice in figure (5.1). Therefore, the states for which $\dfrac{d\varphi}{dt} = 0$ are the ones

corresponding to the minima of $W(\Phi)$. The superconducting state (or S state) is thus characterized by the minimum energy values of $W(\Phi)$. We may thus say that the superconducting states are obtained by the condition $\dfrac{d\varphi}{dt} = 0$. The above semiclassical description of a single- junction quantum interferometer allows us to predict the physical properties of a r.f. SQUID. However, we are here interested on one particular aspect of this system, namely, the realization of different current states (or flux states) for different values of Φ_{ex}. In particular, let us consider two metastable states: one realized in the well of the parabolic washboard potential, near $\Phi = 0$, for $n \cong 0$, and the other one realized on the adjacent well to the right, approximtely at $\Phi = \Phi_0$, so for $n \cong 1$. By normalizing the electric current I to $\dfrac{\Phi_0}{L}$, where the latter quantity has the physical dimensions of an electric current, we may rewrite the expression of I as follows:

$$i = (n - n_{ex}).\qquad(5.14)$$

The relation (5.14) follows from the expression:

$$I = \frac{\Phi - \Phi_{ex}}{L} \Rightarrow \frac{I}{\dfrac{\Phi_0}{L}} = L\frac{\Phi - \Phi_{ex}}{L\Phi_0} \Rightarrow i = \frac{\Phi - \Phi_{ex}}{\Phi_0} = n - n_{ex}.$$

Therefore, according to the definitions (5.3) we obtain the relation (5.14). In this way, considering the $n_{ex} = \dfrac{1}{2}$ curve, we may see that we are in the presence of two current states, corresponding to the $n \cong 0$ and $n \cong 1$ minima, namely:

$$i_- = -\frac{1}{2} \quad ; \quad i_+ = \frac{1}{2}.\qquad(5.15)$$

We can show, in Appendix 5.2, that the $n \cong 0$ well, in the parabolic washboard potential, represents a diamagnetic state, while the $n \cong 1$ well represents a paramagnetic state.

We would like to remark that the classical case is obtained for temperatures which are sufficiently low to maintain the superconducting state (in order to not overcome the critical temperature) but also sufficiently high for fluxons to overcome the barrier height separating two adjacent minima in the parabolic washboard potential. When temperatures are low enough to confine fluxons inside a single well, quantum tunnelling gives the appropriate description of the system dynamics. In fact, if the thermal energy $k_B T$ is larger than, or at least equal to the potential barrier energy, which is of magnetic origin, we can have, from a classical point of view, the transition of fluxons from a minimum position in the parabolic washboard potential to another one.

Instead, for $k_B T$ smaller than the potential barrier energy, the passage of fluxons may hppen only by tunnel effect, that is a typical quantum phenomenon. We shall consider the quantum behaviour of this system in the following section.

5.3 Quantum analysis of one-junction interferometers

Let us now give a quantum description [42] of one-junction interferometers, starting from what stated in the previous section. We are going to show the strict parallelism between the classical and

quantum behaviour of the single junction interferometer. We thus start by giving the role of quantum operators to the conjugate variables φ and $n = \dfrac{\Phi}{\Phi_0}$. These newly defined operators obey to the following commutation relation:

$$[\hat{\varphi}, \hat{n}] = i , \qquad\qquad (5.16)$$

where $\hat{\varphi}$ is the operator corresponding to the angular position, and $\hbar\hat{n}$ (in which we have taken $\hbar = 1$) is the operator corresponding to the action, which is the product of an energy for a time, and we have to consider, in the second member, the identity operator $\hat{I}$ multiplied by the imaginary unity i. Therefore, the relation (5.16) is the ordinary commutation relation between the angle-action variables.

The Hamiltonian operator, which can be deduced directly from equation (5.1), is so defined:

$$\hat{H} = E_L \left[(\hat{n} - n_{ex}\hat{I})^2 - \alpha \cos\hat{\varphi} \right]. \qquad\qquad (5.17)$$

In the above expression, n_{ex} and $\alpha = \dfrac{E_{J,0}}{E_L}$ must be considered c-numbers. This analytic expression of the Hamiltonian operator is obtained considering that the parabolic washboard potential, like all the forms of potential energy, is characterized by an arbitrary additive constant, which, in this case, is just the term $\dfrac{I_{j,0}\Phi_0}{2\pi}$. Nevertheless, we can neglect this term when we pass from the parabolic washboard potential to the Hamiltonian operator, in order to obtain a simpler analytic expression of this quantum operator and of its matrix form.

In order to express the Hamiltonian operator in matrix form, we start by defining the Hilbert space on which this operator acts. Therefore the two states $|0\rangle$ and $|1\rangle$, that constitutes an orthonormal set, i.e. $\langle i | j \rangle = \delta_{i,j} = \begin{cases} 1 & for\ i = j \\ 0 & for\ i \neq j \end{cases}$ where $i, j = 0, 1$, are taken to span the entire Hilbert space. The physical meaning of the two states is as follows: the absence ($|0\rangle$) or the presence ($|1\rangle$) of a flux quantum in the superconducting loop interrupted by the Josephson junction. We can consider that the number operator $\hat{n}$ on the kets $|n\rangle$, counts the flux quanta in the superconducting loop; namely:

$$\hat{n}|n\rangle = n|n\rangle .$$

By using the commutation relation (5.16), it can be shown (we report this proof in Appendix 5.3) that:

$$e^{\pm i\hat{\varphi}}|n\rangle = |n \pm 1\rangle . \qquad\qquad (5.18)$$

Therefore, it is possible to define the way the operator $\cos\hat{\varphi}$ acts on the states $|0\rangle$ and $|1\rangle$, since:

$$\cos\hat{\varphi} = \frac{e^{i\hat{\varphi}} + e^{-i\hat{\varphi}}}{2} .$$

By using these relations, and by knowing that

$$\hat{H} = E_L \left[(\hat{n} - n_{ex}\hat{I})^2 - \alpha \frac{e^{i\hat{\varphi}} + e^{-i\hat{\varphi}}}{2} \right] ,$$

we get:

$$\hat{H}|0\rangle = E_L \left[(\hat{n} - n_{ex}\hat{I})^2 - \alpha \frac{e^{i\hat{\varphi}} + e^{-i\hat{\varphi}}}{2} \right]|0\rangle = E_L \left[n_{ex}^2|0\rangle - \frac{1}{2}\alpha|1\rangle - \frac{1}{2}\alpha|-1\rangle \right]; \qquad (5.19)$$

$$\hat{H}|1\rangle = E_L \left[(1 - n_{ex})^2|1\rangle - \frac{1}{2}\alpha|2\rangle - \frac{1}{2}\alpha|0\rangle \right]. \qquad (5.20)$$

The relations (5.19) and (5.20) indicate that the kets $|0\rangle$ and $|1\rangle$ are not eigenkets (or eigenvectors) of the Hamiltonian operator $\hat{H}$, as we have the presence of two more terms, in the second member which are not proportional to these kets. So, we can calculate:

$$\langle 0|\hat{H}|0\rangle = E_L n_{ex}^2 \langle 0\|0\rangle + 0 = E_L n_{ex}^2 \quad ; \quad \langle 0|\hat{H}|1\rangle = -\frac{1}{2}\alpha E_L \quad ; \quad \langle 1|\hat{H}|0\rangle = \langle 0|\hat{H}|1\rangle = -\frac{1}{2}\alpha E_L ;$$

$$\langle 1|\hat{H}|1\rangle = E_L(1 - n_{ex})^2 .$$

In the third term, we have used the fundamental property taht a Hamiltonian operator needs to be hermitian. Therefore, we have:

$$\hat{H} = \begin{pmatrix} E_L n_{ex}^2 & -\frac{1}{2}\alpha E_L \\ -\frac{1}{2}\alpha E_L & E_L(1 - n_{ex})^2 \end{pmatrix} = E_L \begin{pmatrix} n_{ex}^2 & -\frac{1}{2}\alpha \\ -\frac{1}{2}\alpha & (1 - n_{ex})^2 \end{pmatrix}. \qquad (5.21)$$

Having found the matrix form of the Hamiltonian operator $\hat{H}$, we can determine its eigenvalues through the relation:

$$\det(\hat{H} - \lambda\hat{I}) = 0 \Rightarrow \det \begin{pmatrix} E_L n_{ex}^2 - \lambda & -E_L\frac{\alpha}{2} \\ -E_L\frac{\alpha}{2} & E_L(1 - n_{ex})^2 - \lambda \end{pmatrix} = 0 , \qquad (5.22)$$

where the matrix form of the identity operator, in this 2x2 case, is:

$$\hat{I} = \begin{pmatrix} 1 & 0 \\ 0 & 1 \end{pmatrix}. \qquad (5.23)$$

By carrying out the calculations, we get:

$$[E_L n_{ex}^2 - \lambda][E_L(1 - n_{ex})^2 - \lambda] - E_L^2 \frac{\alpha^2}{4} = 0 . \qquad (5.24)$$

Therefore:

$$E_L^2 n_{ex}^2 (1-n_{ex})^2 - \lambda E_L n_{ex}^2 - \lambda E_L (1-n_{ex})^2 + \lambda^2 - E_L^2 \frac{\alpha^2}{4} = 0 \Rightarrow$$

$$\lambda^2 - \lambda E_L [n_{ex}^2 + (1-n_{ex})^2] + E_L^2 [n_{ex}^2 (1-n_{ex})^2 - \frac{\alpha^2}{4}] = 0 \Rightarrow$$

$$\lambda = \frac{E_L [n_{ex}^2 + (1-n_{ex})^2] \pm \sqrt{\{E_L [n_{ex}^2 + (1-n_{ex})^2]\}^2 - 4E_L^2 [n_{ex}^2 (1-n_{ex})^2 - \frac{\alpha^2}{4}]}}{2}.$$

From the above expression, we obtain:

$$\lambda = \frac{E_L}{2} \left\{ n_{ex}^2 + (1-n_{ex})^2 \pm \sqrt{[n_{ex}^2 + (1-n_{ex})^2]^2 - 4n_{ex}^2 (1-n_{ex})^2 + \alpha^2} \right\} \Rightarrow$$

$$\lambda = \frac{E_L}{2} \left\{ n_{ex}^2 + (1-n_{ex})^2 \pm \sqrt{n_{ex}^4 + (1-n_{ex})^4 - 2n_{ex}^2 (1-n_{ex})^2 + \alpha^2} \right\}$$

In this way, the eigenvalues $E_{\pm}$ of the Hamiltonian operator $\hat{H}$ can be written as follows:

$$E_{\pm} = \frac{E_L}{2} [n_{ex}^2 + (1-n_{ex})^2 \pm \sqrt{[n_{ex}^2 - (1-n_{ex})^2]^2 + \alpha^2}] \ . \tag{5.25}$$

The energy gap ΔE between E_+ and E_- is:

$$\Delta E = E_+ - E_- = E_L \sqrt{[n_{ex}^2 - (1-n_{ex})^2]^2 + \alpha^2} \ .$$

We notice that the gap ΔE has a minimum at $n_{ex} = \frac{1}{2}$, its value being:

$$\Delta E(n_{ex} = \frac{1}{2}) = \Delta E_{min} = \alpha E_L = E_{J,0} \ .$$

We report, in figure 5.2, the profile of these eigenvalues in function of n_{ex}, in the interval $[0,1]$, for $\alpha = 0,25$. In this figure, the E_+ and E_- eigenvalues are represented by the upper and lower full-line branches, respectively. The states $|-\rangle$ and $|+\rangle$ are eigenstates of $\hat{H}$, so that:

$$\hat{H}|\pm\rangle = E_{\pm}|\pm\rangle \ .$$

We may now look at the currents $I_{\pm}$ characterizing these same states. In particular, it is possible to show that these currents, in their normalized form to $\frac{\Phi_0}{L}$, satisfy this relation:

$$i_{\pm} = -\frac{1}{2E_L} \frac{\partial E_{\pm}}{\partial n_{ex}}, \tag{5.26}$$
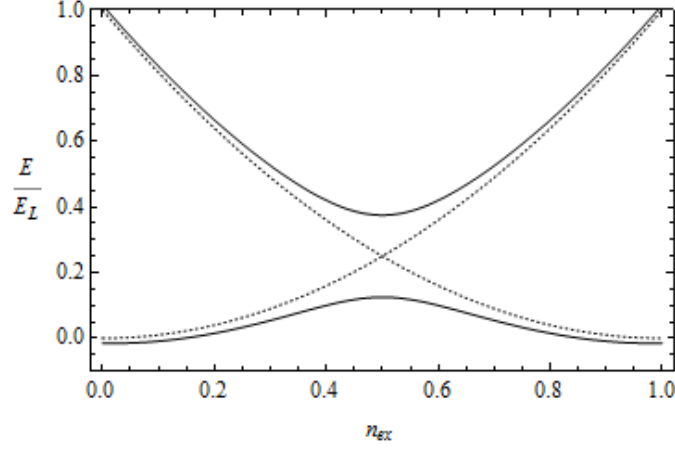
where $i_{\pm} = \dfrac{I_{\pm}}{\dfrac{\Phi_0}{L}}$.

Figure 5.2. *Eigenvalues E_+ and E_- (upper and lower full line branch, respectively) of a one-junction quantum interferometer for $\alpha = 0.25$ as a function of the normalized applied flux n_{ex}. The dashed lines represent the left branch of the parabola n_{ex}^2 and the right branch of the parabola $(1 - n_{ex})^2$, respectively.*

In fact, we can start from this relation:

$$I_{\pm} = \frac{2e}{\hbar} \frac{\partial E_{\pm}}{\partial \varphi} , \tag{5.27}$$

whose form just follows from relation (5.5). So, we get:

$$\frac{I_{\pm}}{\dfrac{\Phi_0}{L}} = \frac{1}{\dfrac{\Phi_0}{L}} \frac{1}{\dfrac{\Phi_0}{2\pi}} \frac{\partial E_{\pm}}{\partial \varphi} \Rightarrow i_{\pm} = \pi \frac{1}{E_L} \frac{\partial E_{\pm}}{\partial \varphi} . \tag{5.28}$$

By differentiating the fluxoid quantization condition, we have:

$$\varphi + 2\pi \frac{\Phi}{\Phi_0} = 2\pi n \Rightarrow d\varphi + 2\pi d\left(\frac{\Phi}{\Phi_0}\right) = 0 .$$

In this way, we obtain:

$$d\varphi = -2\pi d\left(\frac{\Phi}{\Phi_0}\right) = -2\pi dn_{ex} ,$$

where the last equation is based on the fact that $E_{\pm}$ depends, for defined values of α and E_L, only on n_{ex}. Therefore, by equation (5.28), we get:

$$i_{\pm} = -\frac{1}{2E_L}\frac{\partial E_{\pm}}{\partial n_{ex}}, \quad \text{that is just the previous relation (5.26).}$$

By carrying out the appropriate calculations according to (5.26), as it is done in details in Appendix 5.4, we get:

$$i_{\pm} = \frac{1-2n_{ex}}{2}\left[1\pm\frac{1}{\sqrt{(1-2n_{ex})^2+\alpha^2}}\right]. \tag{5.29}$$

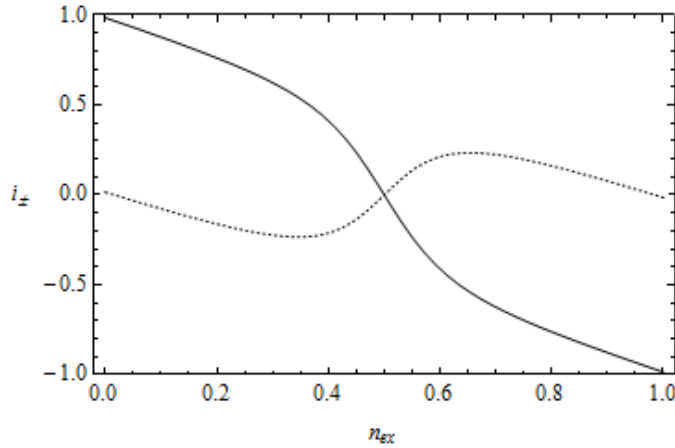We report the profile of $i_{\pm}$ as a function of n_{ex} in figure 5.3.

Figure 5.3. *Normalized currents i_+ and i_- (full line and dashed line, respectively) as a function of the applied flux number n_{ex} circulating in a one-junction quntum interferometer with $\alpha = 0.25$.*

By looking at figure 5.3, where the quantities $i_{\pm}$ are reported as a function of n_{ex}, we may argue that, in the interval [0, 1], the role of the states $|+\rangle$, $|-\rangle$ interchange. In fact, the derivatives of the energy branches are of opposite sign in this interval, both attaining the null value at $n_{ex} = \frac{1}{2}$. By now using the expression (5.26), we may show the currents $i_{\pm}$ as in figure 5.3. We may notice that in the interval $\left[0,\frac{1}{2}\right]$ of n_{ex} the state $|-\rangle$ is diamagnetic, while the state $|+\rangle$ is paramagnetic. On the other hand, in the interval $\left[\frac{1}{2},1\right]$, the magnetic character of these states is inverted, and at $n_{ex} = \frac{1}{2}$ both these states are characterized by a null value of electric current. The proof of this alternating magnetic character is reported in Appendix 5.4.

5.4 Semi-classical analysis of the two-junction interferometer

As seen for the single junction interferometer, we can describe [42] the semi-classical behaviour of the two junction quantum interferometer, by means of an effective potential energy function. We giv a schematic sketch of this device in fig. 5.4.
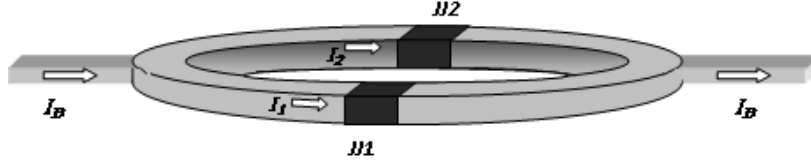
Figure 5.4. *Schematic representation of a two-junction quantum interferometer. The bias current I_B divides into two branch currents, I_1 and I_2. The applied magnetic field (not shown in the figure) is orthogonal to the plane in which the device lies.*

Considering identical JJs in the superconducting loop, so with the same value of maximum Josephson junctions and electric resistance, and neglecting the inductance of the superconducting loop, so that the flux of magnetic field Φ threading the hollow device is equal to the external applied flux Φ_{ex}, we may show that:

$$E(\varphi) = 2E_{J,0}[1 - \cos \pi n_{ex} \cos \varphi - \frac{i_B}{2}\varphi] \; . \tag{5.30}$$

In this expression $\varphi = \dfrac{\varphi_1 + \varphi_2}{2}$, where φ_1 and φ_2 are the superconducting phase differences across the first and the second JJ in the loop, respectively, and where i_B is the bias current normalized to $I_{J,0}$, i.e. $i_B = \dfrac{I_B}{I_{J,0}}$. In what follows all normalizations will be done with respect to the energy $E_{J,0}$ and the electric current $I_{J,0}$, as it is usual in the literature. The washboard potential represented by the expression (5.30) is graphically shown in figure 5.5, for $i_B = 0.0$ and $i_B = 0.5$.
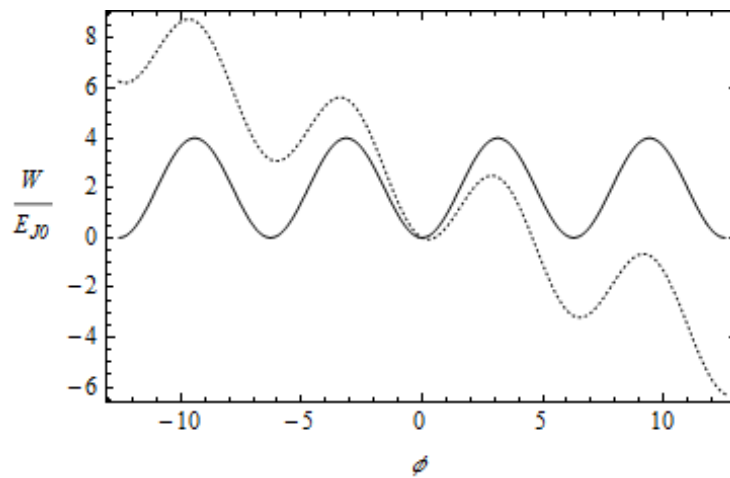

Figure 5.5. *Washboard potential of a two-junction quantum interferometer for $n_{ex} = 0.0$ and for normalized bias current i_B equal to 0.0 (full line) and 0.5 (dashed line). Notice that the degeneracy of the minima present at $i_B = 0$ is removed by applying finite bias current to the system.*

101

In order to prove the analytical expression (5.30), we begin to consider that the total potential energy in a d. c. SQUID with 2 simple Josephson Junctions is represented by:

$$E_{tot} = E_{J,1}(\varphi_1) + E_{J,2}(\varphi_2) + \frac{1}{2}LI_1^2 + \frac{1}{2}LI_2^2 - E_B. \qquad (5.31)$$

In the above expression, we notice that $E_{J,1}(\varphi_1)$ and $E_{J,2}(\varphi_2)$ are the energies corresponding, respectively, to the first and to the second Josephson junction. By considering the two JJs to be identical, as already stated before, the same values of maximum Josephson electric current $I_{J,0}$ and of the electric resistance R can be adopted for both JJs. The term E_B in (5.31) is expressed with the minus sign, because it is an energy furnished by the external environment (the source of electromotive force) to the system (the particular SQUID considered). The analytic expression for this term can be obtained by using the electromagnetic relation:

$$P_B = VI_B, \qquad (5.32)$$

where V is the voltage at the ends of the two branches of the d. c. SQUID, P_B is the electric power and I_B is the bias electric current, both of them furnished by the electromotive force. By knowing that $V = \dfrac{\Phi_0}{2\pi}\dfrac{d\varphi}{dt}$, according to the second Josephson equation, we get:

$$P_B = \frac{\Phi_0}{2\pi}\frac{d\varphi}{dt}I_B = \frac{\Phi_0 I_B}{2\pi}\frac{d\varphi}{dt}. \qquad (5.33)$$

As the power can be considered as the time variation of energy, i.e. $P = \dfrac{dE}{dt}$, in this case we get:

$$P_B = \frac{dE_B}{dt} \Rightarrow dE_B = P_B dt \Rightarrow E_B = \int_0^t P_B(t)dt = \frac{\Phi_0 I_B}{2\pi}[\varphi(t) - \varphi(0)] = \frac{\Phi_0 I_B}{2\pi}\varphi(t).$$

By assuming that the inductance of the superconducting loop is negligible, we notice that the two terms representing the magnetic energy, which are proportional to L, are also negligible. Therefore, the value of the total potential energy of this particular SQUID considered, which is made up by two simple and identical JJs, with I_B is constant, and with negligible inductance, is represented by:

$$E_{tot}(\varphi) = \frac{I_{J,0}\Phi_0}{2\pi}(1 - \cos\varphi_1) + \frac{I_{J,0}\Phi_0}{2\pi}(1 - \cos\varphi_2) - \frac{\Phi_0 I_{J,0}}{2\pi}\frac{I_B}{I_{J,0}}\varphi =$$

$$\frac{\Phi_0 I_{J,0}}{2\pi}(1 - \cos\varphi_1 - \cos\varphi_2 - i_B\varphi) = E_{J,0}[2 - (\cos\varphi_1 + \cos\varphi_2) - i_B\varphi].$$

By using the following trigonometric relation:

$$\cos\varphi_1 + \cos\varphi_2 = 2\cos\left(\frac{\varphi_1 + \varphi_2}{2}\right)\cos\left(\frac{\varphi_1 - \varphi_2}{2}\right) \quad,$$

and by adopting new variables: $\varphi = \dfrac{\varphi_1 + \varphi_2}{2}$; $\pi\psi = \dfrac{\varphi_1 - \varphi_2}{2}$, we have:

$$E_{tot}(\varphi) = E_{j,0}\left[2 - 2\cos\varphi\cos(\pi\psi) - i_B\varphi\right] = 2E_{J,0}\left(1 - \cos\pi\psi\cos\varphi - \frac{i_B}{2}\varphi\right). \qquad (5.34)$$

Knowing that for a d. c. SQUID with 2 JJs the following relation holds:

$$\Phi = \Phi_{ext} + LI_1 - LI_2 = \Phi_{ext} + L(I_1 - I_2) \,,$$

in the case of $L=0$, we may write:

$$\Phi = \Phi_{ext} \Rightarrow \Psi = \frac{\Phi}{\Phi_0} = \frac{\Phi_{ext}}{\Phi_0} = \Psi_{ext} \,.$$

Therefore, we get:

$$E_{tot}(\varphi) = E(\varphi) = 2E_{J,0}\left[1 - \cos(\pi\Psi_{ext})\cos\varphi - \frac{i_B}{2}\varphi\right],$$

that is just the relation (5.30).
It is interesting to consider that the potential energy in relation (5.30) is similar to the one of a single JJ, with a maximum Josephson current equal to $2I_{J,0}\cos(\pi n_{ex})$ in which a d.c. current i_B is injected. In order to prove this result, we can consider that the potential energy of a single JJ is:

$$E_J(\varphi) = \frac{\Phi_0 I_{J,0}}{2\pi}(1 - \cos\varphi) \,.$$

If a d.c. electric current is furnished by the external environment, we have obtained that the associated electrostatic energy is:

$$E_B = \frac{\Phi_0 I_B}{2\pi}\varphi \,.$$

So, the total energy of the single JJ is :

$$E_{tot}(\varphi) = \frac{\Phi_0 I_{J,0}}{2\pi}(1 - \cos\varphi) - E_B = \frac{\Phi_0 I_{J,0}}{2\pi}(1 - \cos\varphi) - \frac{\Phi_0 I_B}{2\pi}\varphi = \frac{\Phi_0 I_{J,0}}{2\pi}(1 - \cos\varphi) - \frac{\Phi_0 I_{J,0}}{2\pi}\frac{I_B}{I_{J,0}}\varphi =$$

$$\frac{\Phi_0 I_{J,0}}{2\pi}(1 - \cos\varphi - i_B\varphi) \,.$$

If the maximum Josephson electric current is $2I_{J,0}\cos(\pi\psi_{ext})$, by making the substitution:

$$I_{J,0} \Leftrightarrow 2I_{J,0}\cos(\pi\psi_{ext}) \qquad\qquad (5.35)$$

we obtain:

$$E_{tot}(\varphi) = 2E_{J,0}\cos\pi\psi_{ext}(1-\cos\varphi - i_B\varphi) = 2E_{J,0}[\cos(\pi\psi_{ex}) - \cos(\pi\psi_{ex})\cos\varphi - i_B\cos(\pi\psi_{ext})\varphi]. \quad (5.36)$$

If we compare this expression with the relation (5.30), we can notice that the first term is constant, being independent from φ, so it can be considered an adding constant term in the expression of the potential energy, the second term is just equal to the one of (5.30), and the third term may be considered very near the expression of the term $\dfrac{i_B}{2}\varphi$ of the (5.30), if we consider the constant term $\cos(\pi\psi_{ext})$ inside the other constant term $\dfrac{i_B}{2}$. So, the similarity between these two relations of potential energy has been proven. In this way, all the analytical results obtained for the latter device apply in our case, by simply considering this analogy.

In order to determine the value of the circulating currents in the device, we may consider the time evolution of the superconducting average phase difference φ, which can be derived, as in the case of the classical single-junction interferometer, by means of the RSJ model, or by using the power balance equation (5.11). In particular we can show, using the method of the power balance equation, that we obtain this relation:

$$\frac{\Phi_0}{2\pi R}\frac{d\varphi}{dt} + I_{J,0}\cos(\pi\psi_{ex})\sin\varphi = \frac{I_B}{2}. \quad (5.37)$$

In order to prove the (5.37), we can start by the electromagnetic relation:

$$P = VI = -\frac{V^2}{R_{eq}},$$

where the presence of minus sign is due to the energy dissipation on the equivalent resistance R_{eq} considered. It is possible to show that if R is the electric resistance of each JJ, the equivalent resistance R_{eq} is given by the relation:

$$\frac{1}{R_{eq}} = \frac{1}{R_1} + \frac{1}{R_2} = \frac{1}{R} + \frac{1}{R} = \frac{2}{R} \Rightarrow R_{eq} = \frac{R}{2}$$

having considered that $R_1 = R_2 = R$.

By knowing that $P = \dfrac{dE}{dt}$, we have: $\dfrac{dE}{dt} = -\dfrac{V^2}{\dfrac{R}{2}} = -\dfrac{2V^2}{R}$, we get:

$$\frac{dE}{dt} = \frac{dE}{d\varphi}\frac{d\varphi}{dt} = 2E_{J,0}[\cos(\pi n_{ex})\sin\varphi - \frac{i_B}{2}]\frac{d\varphi}{dt}.$$

Since now $V = \dfrac{\Phi_0}{2\pi}\dfrac{d\varphi}{dt} \Rightarrow \dfrac{2V^2}{R} = \dfrac{2}{R}\left((\dfrac{\Phi_0}{2\pi})^2(\dfrac{d\varphi}{dt})^2\right)$, from the relation $\dfrac{dE}{dt} = -\dfrac{2V^2}{R}$, knowing that

$E_{J,0} = \dfrac{\Phi_0 I_{J,0}}{2\pi}$, we get:

$2E_{J,0}[\cos(\pi n_{ex})\sin\varphi - \dfrac{i_B}{2}]\dfrac{d\varphi}{dt} = \dfrac{2}{R}(\dfrac{\Phi_0}{2\pi})^2(\dfrac{d\varphi}{dt})^2 \Rightarrow \dfrac{\Phi_0}{2\pi R}\dfrac{d\varphi}{dt} = I_{J,0}\cos(\pi n_{ex})\sin\varphi - I_{J,0}\dfrac{i_B}{2} \Rightarrow$

$\dfrac{\Phi_0}{2\pi R}\dfrac{d\varphi}{dt} + I_{J,0}\cos(\pi n_{ex})\sin\varphi = \dfrac{I_B}{2} \Rightarrow$

$\dfrac{\Phi_0}{2\pi R}\dfrac{d\varphi}{dt} + I_{J,0}\cos(\pi n_{ex})\sin\varphi = \dfrac{I_B}{2}.$

So, we have obtained equation (5.37) considered before. We can also divide both members for the maximum Josephson current $I_{J,0}$, and we get:

$$\dfrac{\Phi_0}{2\pi R I_{J,0}}\dfrac{d\varphi}{dt} + \cos(\pi n_{ex})\sin\varphi = \dfrac{i_B}{2}. \qquad (5.38)$$

If we want to determine the maxima and minima of the potential energy expressed by the relation (5.31), we can calculate its first derivative in φ, and impose ti to be zero.

Therefore, we get:

$$\dfrac{dE(\varphi)}{dt} = 0 \Rightarrow 2E_{J,0}\left[\cos(\pi n_{ex})\sin\varphi - \dfrac{i_B}{2}\right] = 0.$$

In the hypothesis in which $i_B = 0$ and $n_{ex} \neq \dfrac{1}{2} \Rightarrow \cos(\pi n_{ex}) \neq \cos\dfrac{\pi}{2} = 0 \Rightarrow \cos(\pi n_{ex}) \neq 0$, we get:

$$2E_{J,0}\cos(\pi n_{ex})\sin\varphi = 0 \Rightarrow \sin\varphi = 0 \Rightarrow \varphi = \begin{cases} 2k\pi \\ (2k+1) \end{cases} \text{ with } k \in Z.$$

For $\varphi = 2k\pi$, replacing this value in $E_{tot}(\varphi)$ we obtain:

$$E_{tot}(2k\pi) = 2E_{J,0}[1 - \cos(\pi n_{ex})\cos(2k\pi) - \dfrac{i_B}{2}2k\pi] = 2E_{J,0}[1 - \cos(\pi n_{ex}) - i_B k\pi].$$

Having considered that, for hypothesis, $i_B = 0$, we get:

$$E_{tot}(2k\pi) = 2E_{j,0}[1 - \cos(\pi n_{ex})].$$

As the maximum value of $\cos\varphi$ equals 1, and we get it for $\varphi = 2k\pi$, considering that this term has been expressed with the minus sign, we can notice that $E_{tot}(2k\pi)$ is minimum, so we have:

$$E_{min} = E_{tot}(2k\pi).$$

Instead, for $\varphi = (2k+1)\pi$, always considering that $i_B = 0$, we get:

$$E_{tot}((2k+1)\pi) = 2E_{J,0}[1 - \cos(\pi n_{ex})\cos(2k+1)\pi] = 2E_{J,0}(1 + \cos \pi n_{ex}) \Rightarrow E_{tot}((2k+1)\pi) = E_{\max}.$$

In the case of $i_B \neq 0$ but very small, and for $n_{ex} \cong 0$, the position of the minima do not vary with k ranging in Z, and it leads to a value of $E_{\min} \cong 0$.

In order to connect the phase variable to the magnetic flux Φ threading the superconducting loop, we can write, as in the previous case of the single-junction interferometer, the fluxoid quantization relation:

$$2\pi \frac{\Phi}{\Phi_0} + \varphi_1 - \varphi_2 = 2\pi k \qquad\qquad (5.39)$$

where k is an integer. This relation, whose demonstration is given in [43], can be proven by using similar argumentations just used for the case of the fluxoid quantization of the single-junction interferometer. In this way the parallelism between the single-junction and the two-junction interferometer is established.

A method for finding persistent currents (superconducting currents) in a two-junction interferometer for non negligible values of inductance of the superconducting loop of the interferometer has been given by De Luca and Romeo [44]. HEre, we make some remarks about the determination of the superconducting currents in a two-junction interferometer in the semiclassical regime, in this case of negligible inductance of the superconducting loop.

First of all, we can show that the maximum bias current which can be injected in the device at zero applied magnetic field, without destroying the superconducting state, is $2I_{J,0}$. In fact we know that in the superconducting state $V = 0$ and thus, for the second Josephson equation:

$$V = \frac{\Phi_0}{2\pi} \frac{d\varphi}{dt} \Rightarrow \frac{d\varphi}{dt} = 0.$$

Also we notice that, for zero applied magnetic field, also the external magnetic flux is zero, so

$$\Phi_{ex} = 0 \Rightarrow n_{ex} = \frac{\Phi_{ex}}{\Phi_0} = 0 \Rightarrow \cos(\pi n_{ex}) = \cos(0) = 1.$$

So from the (5.38) we get: $I_B = 2I_{J,0}\cos(0)\sin \varphi \leq 2I_{j,0}$, since $\sin \varphi \leq 1$. The normalized persistent currents can be expressed as follows:

$$i_N = -\frac{1}{2\pi E_{J,0}} \frac{\partial E}{\partial n_{ex}} = -\sin(\pi n_{ex})\cos \varphi, \qquad\qquad (5.40)$$

where we have normalized the electric current for $I_{J,0}$, as it is usually done in literature. In fact, we know that the superconductive electric current satisfies this relation: $I = \frac{2\pi}{\Phi_0} \frac{\partial E}{\partial \varphi}$, and so, by using

the condition of fluxoid quantization, we get: $I = -\dfrac{2\pi}{\Phi_0}\dfrac{dE}{2\pi dn_{ex}} = -\dfrac{1}{\Phi_0}\dfrac{dE}{dn_{ex}}$. By dividing this expression for $I_{J,0}$, we obtain:

$$i_N = \frac{I}{I_{J,0}} = -\frac{1}{\Phi_0 I_{J,0}}\frac{\partial E}{\partial n_{ex}} = -\frac{1}{2\pi E_{J,0}}\frac{\partial E}{\partial n_{ex}}$$

where we have: $E_{J,0} = \dfrac{\Phi_0 I_{J,0}}{2\pi}$. In order to find the persistent currents only in terms of the parameters i_B and n_{ex}, we may solve for the $\cos\varphi$ term by choosing the stable fixed points of the expression (5.38), which correspond to the superconductive state $V = 0 \Rightarrow \dfrac{d\varphi}{dt} = 0$. From (5.38) we notice that the stable points, and so the superconducting state, can be present only for $i_B < 2|\cos(\pi n_{ex})|$. Therefore, by knowing that $\cos\varphi = \pm\sqrt{1 - \sin^2\varphi}$ and also that, from (5.38), $\sin\varphi = \dfrac{i_B}{2\cos(\pi n_{ex})}$, we get:

$$\cos\varphi = \pm\sqrt{1 - \frac{i_B^2}{4\cos^2(\pi n_{ex})}} \; , \qquad (5.41)$$

where sign must be determined in such a way that the above expression gives a minimum in the total energy expressed by (5.30). By knowing that the positions of minimum in the expression (5.30) must satisfy the relation:

$$\frac{d^2 E(\varphi)}{d\varphi^2} > 0 \Rightarrow 2E_{J,0}\cos\varphi\cos(\pi n_{ex}) > 0 \text{, we obtain the condition:}$$

$$\cos\varphi\cos(\pi n_{ex}) > 0 . \qquad (5.42)$$

So, we may notice that $\cos\varphi$ and $\cos(\pi n_{ex})$ have the same sign. In this way, the expression (5.40) can be represented as:

$$i_N = -\text{sgn}(\cos\pi n_{ex})\sin(\pi n_{ex})\sqrt{1 - \frac{i_B^2}{4\cos^2(\pi n_{ex})}} \; , \qquad (5.43)$$

where sgn(x) denotes the sign function. The normalized current i_N is represented in figure 5.6 as a function of n_{ex} for the values of i_B represented by 0.0, 0.25, 0.50. From this figure it is possible to notice that there is a point of discontinuity of the current at half integer values of n_{ex}. Also, we may notice that the electric superconductive current I is zero for $i_B > 2|\cos(\pi n_{ex})|$, and attains its maximum value of $i_B = 2$ at integer values of n_{ex}. In fact, if the external bias electric current is larger than the maximum value of the superconductive electric current, also called critical current, i. e., if $i_B > 2|\cos(\pi n_{ex})|$, we have a phase transition inside the considered material, from the superconducting to the normal state, so that the superconductive current is negligible.

As specified in the case of a one- junction interferometer, the system lies in a classical regime as long as it is not in the very-low temperature range, in which thermal activation of excited fluxon states is not possible. When these conditions are not satisfied, we need to give a quantum description of the system.
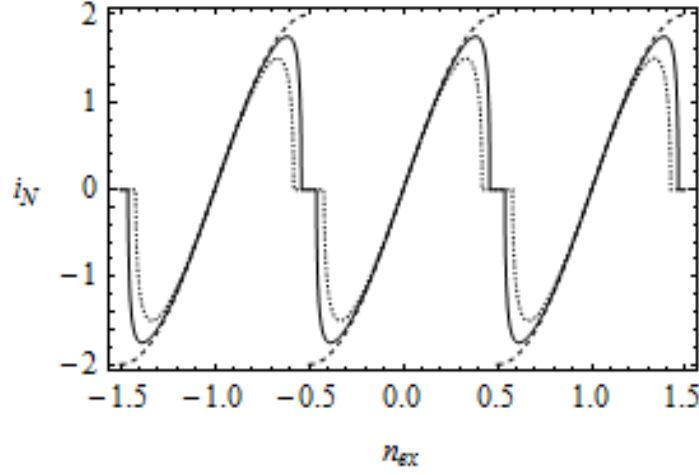

Figure 5.6. *Normalized current i_N represented in terms of n_{ex} in a classical two-junction interferometer for the following values of i_B : 0.0 (dashed line), 0.25 (full line), 0.50 (dotted line).*

In the following section we shall therefore consider the quantum behaviour of the system described by the Hamiltonian operator obtained from the relation (5.30).

5.5 Quantum analysis of the two-junction interferometer

Let us now consider [42] the following Hamiltonian operator:

$$\hat{H} = 2E_{J,0}[\hat{I} - \cos(\pi n_{ex})\cos\hat{\varphi} - \frac{i_B}{2}\hat{\varphi}] , \qquad (5.44)$$

obtained by promoting the variable φ in (5.30) to the role of an operator $\hat{\varphi}$, and by considering i_B and n_{ex} as real numbers. We already know all about the operator $\cos\hat{\varphi}$. So, we need to see how the operator $\hat{\varphi}$ acts on the single-particle Hilbert space, characterized by the states $|n\rangle$. We can express the operator $\hat{\varphi}$ in terms of the following Fourier series:

$$\hat{\varphi} = \sum_{n=1}^{\infty} b_n \sin\left(\frac{2\pi n}{T}\hat{\varphi}\right) , \qquad (5.45)$$

where the Fourier coefficients b_n are calculated in this way:

$$b_n = \frac{2}{T} \int_{-\frac{T}{2}}^{\frac{T}{2}} \varphi \sin\left(\frac{2\pi n}{T} \varphi\right) d\varphi = \frac{(-1)^{n+1} T}{n\pi} \ . \qquad (5.46)$$

These relations are proven in Appendix 5.5. So, by substituting the relation (5.46) in (5.45), and considering that the period $T = 2\pi$, we get:

$$\hat{\varphi} = \sum_{n=1}^{+\infty} \frac{2}{n} (-1)^{n+1} \sin(n\hat{\varphi}) = 2 \sum_{n=1}^{+\infty} \frac{(-1)^{n+1}}{n} \sin(n\hat{\varphi}) \ . \qquad (5.47)$$

In the summation (5.47) we may retain only the first term, as the term n is present at the denominator of this expression, and so, increasing n, $\hat{\varphi}$ decreases, so it can be considered negligible for $n > 1$. Therefore, we can express $\hat{\varphi}$ as follows:

$$\hat{\varphi} = 2 \frac{(-1)^2}{1} \sin \hat{\varphi} = 2 \sin \hat{\varphi} \ .$$

Substituting this expression of $\hat{\varphi}$ inside the relation (5.44), we get:

$$\hat{H} = 2 E_{J,0} (\hat{I} - \cos \pi n_{ex} \cos \hat{\varphi} - i_B \sin \hat{\varphi}) \qquad (5.48)$$

By using the Euler's relations:

$$\cos \hat{\varphi} = \frac{e^{i\hat{\varphi}} + e^{-i\hat{\varphi}}}{2} \quad \text{and} \quad \sin \hat{\varphi} = \frac{e^{i\hat{\varphi}} - e^{-i\hat{\varphi}}}{2i} \ ,$$

we get:

$$\hat{H} = 2 E_{J,0} \left(\hat{I} - \frac{e^{i\hat{\varphi}} + e^{-i\hat{\varphi}}}{2} \cos \pi n_{ex} - i_B \frac{e^{i\hat{\varphi}} - e^{-i\hat{\varphi}}}{2i} \right) = 2 E_{J,0} \left(\hat{I} - \frac{1}{2} e^{i\hat{\varphi}} \cos \pi n_{ex} - \frac{1}{2} e^{-i\hat{\varphi}} \cos \pi n_{ex} - i_B \frac{e^{i\hat{\varphi}}}{2i} + i_B \frac{e^{-i\hat{\varphi}}}{2i} \right)$$

$$2 E_{J,0} \left[\hat{I} - \left(\frac{1}{2} \cos \pi n_{ex} + \frac{i_B}{2i} \right) e^{i\hat{\varphi}} - \left(\frac{1}{2} \cos \pi n_{ex} - \frac{i_B}{2i} \right) e^{-i\hat{\varphi}} \right].$$

By knowing that: $i^2 = -1 \Rightarrow i = -\frac{1}{i} \Rightarrow \frac{1}{i} = -i$, we get:

$$\hat{H} = 2 E_{J,0} \left[\hat{I} - \left(\frac{\cos \pi n_{ex} - i i_B}{2} \right) e^{i\hat{\varphi}} - \left(\frac{\cos \pi n_{ex} + i i_B}{2} \right) e^{-i\hat{\varphi}} \right]. \qquad (5.49)$$

We can limit our analysis to the Hilbert space spanned by the kets $|0\rangle$ and $|1\rangle$, and so we can calculate the matrix form of the Hamiltonian operator $\hat{H}$ on these two kets. We know, from Appendix 5.3, how the operator $e^{i\hat{\varphi}}$ acts on the state $|n\rangle$:

$$e^{\pm i\hat{\varphi}} |n\rangle = |n \pm 1\rangle$$

According to the above relation, and by knowing also that $\hat{I}|n\rangle = |n\rangle$; $\langle n|m\rangle = \delta_{n,m} = \begin{cases} 1 & for \ n = m \\ 0 & for \ n \neq m \end{cases}$, we can determine the action of the Hamiltonian operator $\hat{H}$ on the two states $|0\rangle$ and $|1\rangle$. So that:

$$\hat{H}|0\rangle = 2E_{J,0}\left(|0\rangle + \frac{ii_B - \cos(\pi n_{ex})}{2}|1\rangle - \frac{ii_B + \cos(\pi n_{ex})}{2}|-1\rangle \right);$$

$$\hat{H}|1\rangle = 2E_{J,0}\left(|1\rangle + \frac{ii_B - \cos(\pi n_{ex})}{2}|2\rangle - \frac{ii_B + \cos(\pi n_{ex})}{2}|0\rangle \right).$$

From these relations we can notice that the kets $|0\rangle, |1\rangle$ are not eigenkets of the operator $\hat{H}$. So, we obtain:

$$\langle 0|\hat{H}|0\rangle = 2E_{J,0}(1+0) = 2E_{J,0};$$

$$\langle 1|\hat{H}|0\rangle = 2E_{J,0}\left(0 + \frac{ii_B - \cos(\pi n_{ex})}{2}\langle 1|1\rangle + 0 \right) = E_{J,0}(ii_B - \cos(\pi n_{ext}));$$

$$\langle 0|\hat{H}|1\rangle = 2E_{J,0}\left(0 + 0 - \frac{ii_B + \cos(\pi n_{ex})}{2}\langle 0|0\rangle \right) = -E_{J,0}(ii_B + \cos(\pi n_{ex}));$$

$$\langle 1|\hat{H}|1\rangle = 2E_{J,0}(\langle 1|1\rangle + 0 + 0) = 2E_{J,0}.$$

So, the matrix expression of the Hamiltonian operator $\hat{H}$ on the kets $|0\rangle$ and $|1\rangle$ is represented by:

$$\hat{H} = \begin{pmatrix} 2E_{J,0} & E_{J,0}(ii_B - \cos(\pi n_{ex})) \\ -E_{J,0}(ii_B + \cos(\pi n_{ex})) & 2E_{J,0} \end{pmatrix} = 2E_{J,0}\begin{pmatrix} 1 & \frac{1}{2}(ii_B - \cos(\pi n_{ex})) \\ -\frac{1}{2}(ii_B + \cos(\pi n_{ex})) & 1 \end{pmatrix} \Rightarrow$$

$$\hat{H} = 2E_{J,0}\begin{pmatrix} 1 & -\frac{1}{2}(\cos(\pi n_{ex}) - ii_B) \\ -\frac{1}{2}(\cos(\pi n_{ex}) + ii_B) & 1 \end{pmatrix} \qquad (5.50)$$

We can determine the eigenvalues λ of the Hamiltonian operator $\hat{H}$ in (5.55), which are the energy values of the particles (Cooper pairs) in the particular SQUID considered, by solving this equation:

$$\det(H - \lambda I) = 0,$$

where I is the 2 x 2 identity matrix:

$$I = \begin{pmatrix} 1 & 0 \\ 0 & 1 \end{pmatrix} \Rightarrow \lambda I = \begin{pmatrix} \lambda & 0 \\ 0 & \lambda \end{pmatrix}.$$

So, we get:

$$\hat{H} - \lambda\hat{I} = \begin{pmatrix} 2E_{J,0} - \lambda & -\dfrac{1}{2}(\cos(\pi n_{ex}) - ii_B)2E_{J,0} \\ -\dfrac{1}{2}(\cos(\pi n_{ex}) + ii_B)2E_{J,0} & 2E_{J,0} - \lambda \end{pmatrix}. \qquad (5.51)$$

By carrying out the calculation, we obtain:

$$\det(\hat{H} - \lambda\hat{I}) = (2E_{J,0} - \lambda)^2 - E_{J,0}^2(\cos(\pi n_{ex}) - ii_B)(\cos(\pi n_{ex}) + ii_B) =$$

$$4E_{J,0}^2 + \lambda^2 - 4E_{J,0}\lambda - E_{J,0}^2(\cos^2(\pi n_{ex}) - i^2 i_B^2 + ii_B\cos(\pi n_{ex}) - ii_B\cos(\pi n_{ex})) =$$

$$4E_{J,0}^2 + \lambda^2 - 4E_{j,0}\lambda - E_{J,0}^2(\cos^2(\pi n_{ex}) + i_B^2) \Rightarrow$$

$$\Rightarrow \det(\hat{H} - \lambda\hat{I}) = \lambda^2 - 4E_{J,0}\lambda - E_{J,0}^2(\cos^2(\pi n_{ex}) + i_B^2 - 4).$$

So, by the relation (5.56), we can obtain the eigenvalues of the Hamiltonian operator $\hat{H}$, by solving the second order algebraic equation:

$$\lambda^2 - 4E_{j,0}\lambda - E_{J,0}^2(\cos^2(\pi n_{ex}) + i_B^2 - 4) = 0 \Rightarrow$$

$$\lambda = 2E_{j,0} \pm \sqrt{(2E_{J,0})^2 + E_{J,0}^2(\cos^2(\pi n_{ex}) + i_B^2 - 4)} = 2E_{J,0} \pm \sqrt{4E_{J,0}^2 + E_{J,0}^2\cos^2(\pi n_{ex}) + E_{J,0}^2 i_B^2 - 4E_{J,0}^2} =$$

$$= 2E_{J,0} \pm \sqrt{E_{j,0}^2\cos^2(\pi n_{ex}) + E_{J,0}^2 i_B^2}.$$

By knowing that $E_{j,0} = \dfrac{\Phi_0 I_{J,0}}{2\pi} > 0$, we get:

$$\lambda = 2E_{J,0} \pm E_{J,0}\sqrt{i_B^2 + \cos^2(\pi n_{ex})} = E_{J,0}(2 \pm \sqrt{i_B^2 + \cos^2(\pi n_{ex})}).$$

So, we obtain the two energy values $E_\pm$, which correspond to the eigenvalues of the Hamiltonian operator in this Hilbert space:

$$E_\pm = E_{J,0}(2 \pm \sqrt{i_B^2 + \cos^2(\pi n_{ex})}). \qquad (5.52)$$

A graphical representation of the eigenvalues $E_\pm$ in terms of n_{ex} is given in figure 5.7a. It can be shown that the minimum energy gap occurs at semi-integer values of n_{ex}, and it is equals to $2i_B$. In fact, from (5.58) we have:

$$\Delta E = E_+ - E_- = 2E_{J,0} + E_{J,0}\sqrt{i_B^2 + \cos^2(\pi n_{ex})} - 2E_{J,0} + E_{J,0}\sqrt{i_B^2 + \cos^2(\pi n_{ex})} = 2E_{J,0}\sqrt{i_B^2 + \cos^2(\pi n_{ex})}.$$

The minimum value of this expression is reached for $\cos^2(\pi n_{ex}) = 0$, thus for semi-integer values of n_{ex}. So we get:

$$\Delta E_{\min} = 2E_{J,0}\sqrt{i_B^2} = 2E_{J,0}i_B \Rightarrow \frac{\Delta E_{\min}}{E_{J,0}} = 2i_B .\qquad (5.53)$$
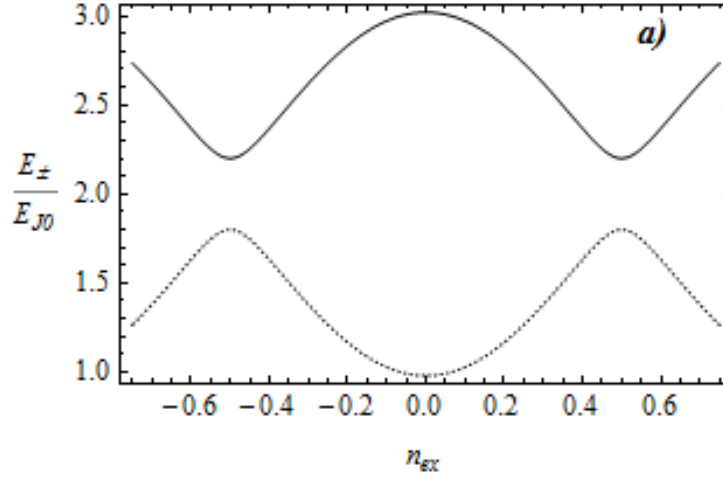

Figure 5.7a. *Energy states E_+ and E_- normalized to $E_{J,0}$ (upper and lower branch, respectively) represented in terms of n_{ex} for a two-junction interferometer in the quantum regime with $i_B = 0.20$.*

As considered before, these eigenvalues correspond to the eigenvectors $|\pm\rangle$ such that:

$$H|\pm\rangle = E_\pm |\pm\rangle$$

Let us first consider the case of persistent currents at $i_B = 0$. In this case, from relation (5.52), we have $E_\pm = E_{J,0}(2 \pm |\cos(\pi n_{ex})|)$, so that the two energy branches take the same value of $2E_{J,0}$ at $n_{ex} = \dfrac{2k+1}{2}$, with k integer, as we obtain $\cos(\pi n_{ex}) = 0$ for these particular values of n_{ex} considered. The persistent currents, at any value of i_B, can be found by equation (5.26), so that:

$$i_\pm = -\frac{1}{2\pi E_{j,0}}\frac{\partial E_\pm}{\partial n_{ex}} \qquad \text{with} \quad E_\pm = E_{J,0}(2 \pm \sqrt{i_B^2 + \cos^2(\pi n_{ex})}) .$$

So, we get:

$$\frac{\partial E_\pm}{\partial n_{ex}} = \pm\frac{E_{J,0}[2\cos(\pi n_{ex})(-\sin(\pi n_{ex})\pi]}{2\sqrt{i_B^2 + \cos^2(\pi n_{ex})}} = \pm E_{J,0}\frac{[-\pi\sin(\pi n_{ex})\cos(\pi n_{ex})]}{\sqrt{i_B^2 + \cos^2(\pi n_{ex})}} .$$

Thus, we obtain:

$$i_\pm = -\frac{1}{2\pi E_{J,0}}\frac{\partial E_\pm}{\partial n_{ex}} = \pm\frac{1}{2}\frac{\sin(\pi n_{ex})\cos(\pi n_{ex})}{\sqrt{i_B^2 + \cos^2(\pi n_{ex})}} .\qquad (5.54)$$

For $i_B = 0$, in particular, the persistent currents in the two junction-interferometer attains the following simple expression:

$$i_{\pm}(n_{ex}) = \pm\frac{1}{2}\sin(\pi n_{ex})\,sign(\cos(\pi n_{ex})) \ . \qquad\qquad (5.55)$$

These results are reported in figure 5.7b, for various values of i_B. In figure 5.7b, we may still notice the characteristic alternating occurrence of diamagnetic and paramagnetic states in the quantum system, in the same way they appear in their classical counterpart.
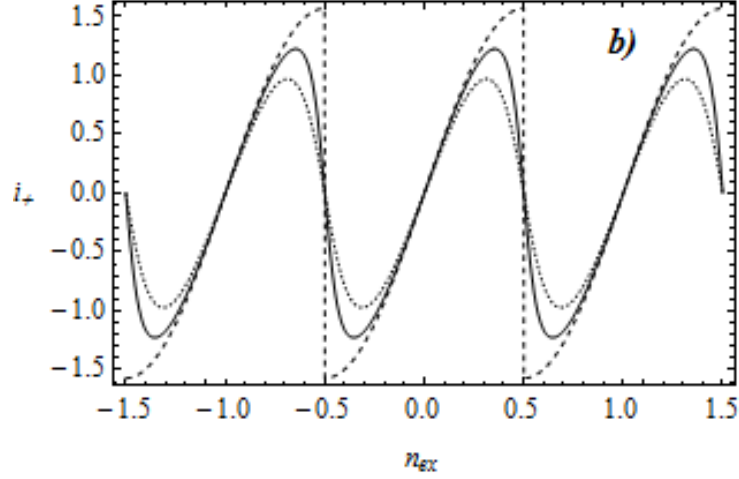

Figure 5.7b. *Normalized current i_+ plotted against n_{ex} for the following values of i_B : 0.0 (dashed line), 0.25 (full line), 0.50 (dotted line).*

In the latter figure, we may also notice the disappearance of the discontinuities present in figure 5.6, where a critical electric current must be taken into account as a discriminant of a real-valued circulating electric current. In fact, in the classical case, we consider the presence of an electric resistance between the two superconducting layers of the Josephson junction present inside the interferometer, and so a dissipation of the lectric current is created. Instead, in the quantum case, there are no dissiptions of electric current, since the Hamiltonian operator is made up by constant terms. So the energy, which is represented by its eigenvalues $E_{\pm}$, is time independent, and consequently also the superconductive electric current $i_{\pm} = -\dfrac{1}{2\pi E_{J,0}}\dfrac{\partial E_{\pm}}{\partial n_{ex}}$ is time invariant, thus the electric current is time independent. Consequently, in the quantum case, the superconductive electric current has no discontinuities, as there is no dissipation.

We can also remark that in expression (5.43) we have purposely retained only the first term, in order to limit our analysis to the Hilbert space spanned by the quantum states $|0\rangle$ and $|1\rangle$. However, the present analysis can be adopted to consider spaces with higher dimensions. This extended analysis can be implemented, for instance, when seeking a quantum system able to process numbers expressed in a ternary or higher order numeral system. For example, in the case of ternary logic, the quantum states $|0\rangle, |1\rangle, |2\rangle$, can be denoted as quantum trits or qutrits [40], which are the quantum analog of the persistent currents in semi-classical ternary systems.

5.6 Conclusions

The classical and quantum behaviour of one (Josephson) junction and two-junctions interferometers have been considered. While the classical behaviour of both systems is already well known, we have proposed a unifying approach to the study of their electrodynamic properties, suggesting an equally unified analysis in the quantum regime. Therefore, starting from the analytic expression of the washboard potential, the 2 x 2 quantum Hamiltonian acting on the quantum states $|0\rangle, |1\rangle$ is obtained by promoting the classical variables, in the classical potential, to the role of operators. The persistent electric currents in the quantum regime are seen to follow closely the qualitative behaviour of the homologous quantities in the classical system, showing alternating occurrence of diamagnetic and paramagnetic states for increments of n_{ex} equals to 1/2.

It is important to notice that the present analysis can be immediately extended to Hilbert spaces spanned by more than two quantum states. In fact, in the present analysis, we have noticed that multi-valued logic states can be obtained in the quantum regime, by generalizing the well-known classical properties of a two-junctions interferometer. In this way, quantum computing based on qutrits, rather than qubits, could be implemented by considering the properties of a two Josephson junctions interferometer, whose quantum states are generated by the orthogonal kets $|0\rangle, |1\rangle,$ and $|2\rangle$.

Appendix 5.1

Determination of the time dynamics for the normalized magnetic flux n

In this Appendix we represent the expression (5.11) as a dynamical relation for $n = \dfrac{\Phi}{\Phi_0}$. We can

start [42] by re-expressing equation (5.10) $\dfrac{1}{R}\dfrac{d\Phi}{dt} + I_{J,0}\sin\left(2\pi\dfrac{\Phi}{\Phi_0}\right) = \dfrac{\Phi_{ex} - \Phi}{L}$, as follows:

$$\frac{\Phi_0}{R}\frac{d}{dt}\left(\frac{\Phi}{\Phi_0}\right) + I_{J,0}\sin\left(2\pi\frac{\Phi}{\Phi_0}\right) = \frac{\Phi_0}{L}\frac{\Phi_{ex}-\Phi}{\Phi_0} \Rightarrow \frac{\Phi_0}{R}\frac{dn}{dt} + I_{J,0}\sin(2\pi n) = \frac{\Phi_0}{L}(n_{ex}-n),$$

where, in the latter relation, $n = \dfrac{\Phi}{\Phi_0}$. By dividing both members for $\dfrac{\Phi_0}{L}$, we obtain:

$$\frac{\Phi_0}{R}\frac{1}{\dfrac{\Phi_0}{L}}\left(\frac{dn}{dt}\right) + \frac{I_{J,0}}{\dfrac{\Phi_0}{L}}\sin(2\pi n) = n_{ex}-n \Rightarrow \frac{L}{R}\frac{dn}{dt} + \frac{\Phi_0}{2\pi}\frac{2\pi I_{J,0}}{\dfrac{\Phi_0^2}{L}}\sin(2\pi n) + n = n_{ex}. \qquad (5.1.1)$$

where, in the latter relation, we have multiplied and divided by $\dfrac{\Phi_0}{2\pi}$.

Thus, by knowing that $E_{J,0} = \dfrac{\Phi_0 I_{J,0}}{2\pi}$, $E_L = \dfrac{\Phi_0^2}{2L}$, and $\alpha = \dfrac{E_{J,0}}{E_L}$, we get:

$$\frac{L}{R}\frac{dn}{dt} + 2\pi\frac{E_{J,0}}{2E_L}\sin(2\pi n) + n = n_{ex} \Rightarrow \frac{L}{R}\frac{dn}{dt} + \pi\alpha\sin(2\pi n) + n = n_{ex}. \qquad (5.1.2)$$

We may therefore notice that the latter relation represents the time dynamics for *n*. We can also obtain the same relation by using the Power Balance Equation:

$$\frac{dW_P}{dt} + \frac{V^2}{R} = 0.$$

In fact, by using the second Josephson equation $V = \dfrac{\Phi_0}{2\pi}\dfrac{d\varphi}{dt}$, and the fluxoid quantization

$\varphi + 2\pi\dfrac{\Phi}{\Phi_0} = 2\pi k \Rightarrow \dfrac{d\varphi}{dt} = -2\pi\dfrac{dn}{dt}$, we get: $V = -\Phi_0\dfrac{dn}{dt}$.

From the relation (5.8): $W_P(n) = E_L\left[(n - n_{ex})^2 + \alpha(1 - \cos(2\pi n)\right]$, we notice that:

$$\frac{dW_P(n)}{dt} = E_L\left[2(n - n_{ex}) + 2\pi\alpha\sin(2\pi n)\right]\frac{dn}{dt}. \qquad (5.1.3)$$

So, by the Power Balance Equation, we get:

$$\frac{\Phi_0^2}{R}\left(\frac{dn}{dt}\right)^2 + E_L\left[2(n-n_{ex})+2\pi\alpha\sin(2\pi n)\right]\frac{dn}{dt} = 0. \tag{5.1.4}$$

From this relation, by doing the opportune semplifications, we obtain:

$$\frac{\Phi_0^2}{RE_L}\frac{dn}{dt} = -\left[2(n-n_{ex})+2\pi\alpha\sin(2\pi n)\right]; \text{ by knowing that: } E_L = \frac{\Phi_0^2}{2L}, \text{ we get:}$$

$$\frac{2L}{R}\frac{dn}{dt} = -2\left[(n-n_{ex})+\pi\alpha\sin(2\pi n)\right] \Rightarrow \frac{L}{R}\frac{dn}{dt} = -(n-n_{ex})-\pi\alpha\sin(2\pi n) .$$

Therefore, from the latter relation, we obtain:

$$\frac{L}{R}\frac{dn}{dt} + \pi\alpha\sin(2\pi n) + n = n_{ex}, \tag{5.1.5}$$

which is just the equation for the dynamics of n that we have previously determined.

Appendix 5.2

Diamagnetic and Paramagnetic states

We can show that, in the Washboard potential [42], the $n\cong 0$ well represents a diamagnetic state, while the n $\cong 1$ well represents a paramagnetic state. First of all we notice that: $i_- = -\frac{1}{2}$; $i_+ = \frac{1}{2}$, so that:

$$i_- < 0 \ ; \ i_+ > 0. \tag{5.2.1}$$

Then, we can consider that the diamagnetic state is characterized by a negative value of magnetic susceptibility, $\chi = \frac{\partial M}{\partial H} < 0$, so the magnetization $\vec{M}$, which is a magnetic field created inside the system, is opposed to the external magnetic field $\vec{H}$ (i.e. the response of the system, represented by the magnetization, is opposed to the excitation, represented by the external magnetic field), while the paramagnetic state is characterized by a positive value of magnetic susceptibility, $\chi = \frac{\partial M}{\partial H} > 0$ so the magnetization and the external magnetic field have the same sign (are concordant). In

practice, $n_{ex} = \frac{1}{2} \Rightarrow \frac{\Phi_{ext}}{\Phi_0} = \frac{1}{2} \Rightarrow \Phi_{ext} = \frac{1}{2}\Phi_0 = \frac{1}{2}\frac{h}{2e} > 0$; as we assume that the magnetic field is uniform on the surface of the superconducting loop, we have: $\Phi_{ext} = \mu_0 H S_0 > 0 \Rightarrow H > 0$. By knowing that the magnetization $\vec{M}$ is generated by the electric current I circulating inside the system (which in turn is created by applying the external magnetic field), we may see that $\vec{M}$ and I, according to the right hand rule, have the same sign. So, for $n = 0$, we have $I_- = i_- I_{J,0} < 0$ and so M < 0. On the other hand, for $n = 1$ we have $I_+ = i_+ I_{J,0} > 0$ and so $M > 0$. As the external magnetic field H is positive both for $n = 0$ and for $n = 1$, we can see that for $n = 0$ we have a negative magnetic susceptibility, and so a diamagnetic state, while for $n = 1$ we have a positive magnetic susceptibility and so a paramagnetic state. In this way, we have showed that the $n \cong 0$ well represents a diamagnetic state, while the $n \cong 1$ well represents a paramagnetic state.

Appendix 5.3

Proof of the relations satisfied by the exponential operator

We want to show [42] that, for a generic $|n\rangle$:

$$e^{i\hat{\varphi}}|n\rangle = |n+1\rangle \ ; \ e^{-i\hat{\varphi}}|n\rangle = |n-1\rangle.$$

Let us begin with the first relation:

$$e^{i\hat{\varphi}}|n\rangle = |n+1\rangle.$$

Let us also consider the action of the number operator $\hat{n}$ on the ket $e^{i\hat{\varphi}}|n\rangle$:

$$\hat{n}(e^{i\hat{\varphi}}|n\rangle) = \hat{n}\sum_{k=0}^{+\infty} \frac{(i\hat{\varphi})^k}{k!}|n\rangle = \sum_{k=0}^{+\infty} \hat{n}\frac{(i\hat{\varphi})^k}{k!}|n\rangle$$ where we have used the Taylor's expansion of the

exponential function $e^x = \sum_{n=0}^{+\infty} \frac{x^n}{n!}$, and the linearity of the number operator.

By knowing that $\hat{n}\hat{\varphi}^k = [\hat{n}, \hat{\varphi}^k] - \hat{\varphi}^k \hat{n}$, where $[\hat{n}, \hat{\varphi}^k] = \hat{n}\hat{\varphi}^k - \hat{\varphi}^k \hat{n}$ is the commutation operator of the two operators $\hat{n}$ and $\hat{\varphi}^k$, we get:

$$\hat{n}(e^{i\hat{\varphi}}|n\rangle) = \sum_{k=0}^{+\infty} \left\{ [\hat{n}, \hat{\varphi}^k] + \hat{\varphi}^k \hat{n} \right\} \frac{i^k}{k!}|n\rangle. \qquad (5.3.1)$$

We can now show that: $[\hat{n}, \hat{\varphi}^k] = -ik\hat{\varphi}^{k-1} \qquad (5.3.2)$

by using the commutation relation: $[\hat{\varphi}, \hat{n}] = i \Rightarrow [\hat{n}, \hat{\varphi}] = -i$, where $\hat{\varphi}$ is the angular position operator, and $\hat{n}$ is the operator representing the number of fluxons. In fact, we have:

$$[\hat{n}, \hat{\varphi}]\hat{\varphi}^{k-1} + \hat{\varphi}[\hat{n}, \hat{\varphi}^{k-1}] = \hat{n}\hat{\varphi}\hat{\varphi}^{k-1} - \hat{\varphi}\hat{n}\hat{\varphi}^{k-1} + \hat{\varphi}\hat{n}\hat{\varphi}^{k-1} - \hat{\varphi}\hat{\varphi}^{k-1}\hat{n} = \hat{n}\hat{\varphi}^{k} - \hat{\varphi}^{k}\hat{n} = [\hat{n}, \hat{\varphi}^{k}] \Rightarrow$$

$$[\hat{n}, \hat{\varphi}^{k}] = -i\hat{\varphi}^{k-1} + \hat{\varphi}[\hat{n}, \hat{\varphi}^{k-1}]$$

The second term $[\hat{n}, \hat{\varphi}^{k-1}]$ can be represented, in a similar way, as follows:

$$[\hat{n}, \hat{\varphi}^{k-1}] = -i\hat{\varphi}^{k-2} + \hat{\varphi}[\hat{n}, \hat{\varphi}^{k-2}] \qquad (5.3.3)$$

So, we get:

$$[\hat{n}, \hat{\varphi}^{k}] = -i\hat{\varphi}^{k-1} + \hat{\varphi}\{-i\hat{\varphi}^{k-2} + \hat{\varphi}[\hat{n}, \hat{\varphi}^{k-2}]\} = -i\hat{\varphi}^{k-1} - i\hat{\varphi}^{k-1} + \hat{\varphi}^{2}\{-i\hat{\varphi}^{k-3} + \hat{\varphi}[\hat{n}, \hat{\varphi}^{k-3}]\} =$$

$$-2i\hat{\varphi}^{k-1} + \hat{\varphi}^{2}\{-i\hat{\varphi}^{k-3} + \hat{\varphi}[\hat{n}, \hat{\varphi}^{k-3}]\} = -3i\hat{\varphi}^{k-1} + \hat{\varphi}^{3}[\hat{n}, \hat{\varphi}^{k-3}]$$

Going on in this way, we reach the value of k, for which we have:

$$[\hat{n}, \hat{\varphi}^{k}] = -ik\hat{\varphi}^{k-1} + \hat{\varphi}^{k}[\hat{n}, \hat{I}] \qquad (5.3.4)$$

In this expression, $\hat{I}$ represents the identity operator, which acts on a ket $|\psi\rangle$ as follows:

$$\hat{I}|\psi\rangle = |\psi\rangle.$$

In this way, we have:

$$[\hat{n}, \hat{I}]|\psi\rangle = (\hat{n}\hat{I} - \hat{I}\hat{n})|\psi\rangle = 0.$$

So, we get:

$$[\hat{n}, \hat{\varphi}^{k}] = -ik\hat{\varphi}^{k-1} \qquad (5.3.5)$$

Going back to the relation (5.46), we have:

$$\hat{n}(e^{i\hat{\varphi}}|n\rangle) = \sum_{k=0}^{+\infty}(-ik\hat{\varphi}^{k-1})\frac{i^{k}}{k!}|n\rangle + \sum_{k=0}^{+\infty}n\hat{\varphi}^{k}\frac{i^{k}}{k!}|n\rangle,$$

where we have considered the action of the number operator $\hat{n}$ on a ket $|n\rangle$ so defined:

$$\hat{n}|n\rangle = n|n\rangle.$$

So we get:

$$\hat{n}\left(e^{i\hat{\varphi}}|n\rangle\right) = \sum_{k=1}^{+\infty} i^{k-1}\frac{\hat{\varphi}^{k-1}}{(k-1)!}|n\rangle + n\sum_{k=0}^{+\infty}\hat{\varphi}^k\frac{i^k}{k!}|n\rangle = \sum_{m=0}^{+\infty}i^m\frac{\hat{\varphi}^m}{m!}|n\rangle + n\sum_{m=0}^{+\infty}i^m\frac{\hat{\varphi}^m}{m!}|n\rangle = (n+1)e^{i\hat{\varphi}}|n\rangle.$$

If we compare this relation with: $\hat{n}|n+1\rangle = (n+1)|n+1\rangle$, we can consider that:

$$e^{i\hat{\varphi}}|n\rangle = |n+1\rangle \ . \tag{5.3.6}$$

So, we have proven this relation. In order to prove the relation:

$$e^{-i\hat{\varphi}}|n\rangle = |n-1\rangle,$$

we can follow similar considerations. In particular, we can start from the relation:

$$e^{-i\hat{\varphi}} = \sum_{k=0}^{+\infty}\frac{(-i\hat{\varphi})^k}{k!} = \sum_{k=0}^{+\infty}(-1)^k\frac{(i\hat{\varphi})^k}{k!} \ . \tag{5.3.7}$$

Considering the action of the number operator, we have:

$$\hat{n}(e^{-i\hat{\varphi}}|n\rangle) = \hat{n}\left(\sum_{k=0}^{+\infty}(-1)^k\frac{(i\hat{\varphi})^k}{k!}|n\rangle\right) = \sum_{k=0}^{+\infty}(-1)^k\hat{n}\frac{(i\hat{\varphi})^k}{k!}|n\rangle = \sum_{k=0}^{+\infty}(-1)^k\frac{(-i)^k}{k!}\hat{n}\hat{\varphi}^k|n\rangle \tag{5.3.8}$$

As: $\left[\hat{n}, \hat{\varphi}^k\right] = \hat{n}\hat{\varphi}^k - \hat{\varphi}^k\hat{n} \Rightarrow \hat{n}\hat{\varphi}^k = \left[\hat{n}, \hat{\varphi}^k\right] + \hat{\varphi}^k\hat{n}$, and knowing that: $\left[\hat{n}, \hat{\varphi}^k\right] = -ik\hat{\varphi}^{k-1}$, we have:

$$\hat{n}\left(e^{-i\hat{\varphi}}|n\rangle\right) = \sum_{k=0}^{+\infty}\frac{(-1)^k}{k!}(i)^k(-ik\hat{\varphi}^{k-1})|n\rangle + \sum_{k=0}^{+\infty}\frac{(-1)^k(i)^k}{k!}\hat{\varphi}^k\hat{n}|n\rangle =$$

$$\sum_{k=1}^{+\infty}(-1)^k(i)^k(-1)i\frac{k}{k!}\hat{\varphi}^{k-1}|n\rangle + n\sum_{K=0}^{+\infty}\frac{(-1)^k(i)^k}{k!}\hat{\varphi}^k|n\rangle,$$

where we have factored out the term n from the summation, as it is independent from the summation index. By now knowing that: $\dfrac{k}{k!} = \dfrac{k}{k(k-1)!} = \dfrac{1}{(k-1)!}$, we get:

$$\hat{n}(e^{-i\hat{\varphi}}|n\rangle) = \sum_{k=1}^{+\infty}\frac{(-1)^{k+1}(i)^{k+1}}{(k-1)!}\hat{\varphi}^{k-1}|n\rangle + n\sum_{k=0}^{+\infty}\frac{(-1)^k\hat{\varphi}^k}{k!}|n\rangle =$$

$$\sum_{k=1}^{+\infty}\frac{(-1)^{k-1}(i)^{k-1}(i)^2}{(k-1)!}\hat{\varphi}^{k-1} + n\sum_{k=0}^{+\infty}\frac{(-i\hat{\varphi})^k}{k!}|n\rangle = -\sum_{K=1}^{+\infty}\frac{(-1)^{k-1}(i)^{k-1}}{(k-1)!}\hat{\varphi}^{k-1} + ne^{-i\hat{\varphi}}|n\rangle =$$

$$-\sum_{k=1}^{+\infty}\frac{(-i)^{k-1}}{(k-1)!}\hat{\varphi}^{k-1}|n\rangle + ne^{-i\hat{\varphi}}|n\rangle = -\sum_{k=1}^{+\infty}\frac{(-i\hat{\varphi})^{k-1}}{(k-1)!}|n\rangle + ne^{-i\hat{\varphi}}|n\rangle.$$

In the first addendum, we may make the following variable change:

$$k-1=m \Rightarrow \hat{n}(e^{-i\hat{\varphi}}|n\rangle) = -\sum_{m=0}^{+\infty} \frac{(-i\hat{\varphi})^m}{m!}|n\rangle + ne^{-i\hat{\varphi}}|n\rangle = -e^{-i\hat{\varphi}}|n\rangle + ne^{-i\hat{\varphi}}|n\rangle = (n-1)e^{-i\hat{\varphi}}|n\rangle .$$

So, we get:

$$\hat{n}(e^{-i\hat{\varphi}}|n\rangle) = (n-1)e^{-i\hat{\varphi}}|n\rangle . \qquad (5.3.9)$$

Since now:

$$\hat{n}|n-1\rangle = (n-1)|n-1\rangle ,$$

by comparing these two expressions, we obtain:

$$e^{-i\hat{\varphi}}|n\rangle = |n-1\rangle . \qquad (5.3.10)$$

Therefore, we have shown these two results:

$$e^{i\hat{\varphi}}|n\rangle = |n+1\rangle \; ; \; e^{-i\hat{\varphi}}|n\rangle = |n-1\rangle .$$

There is also a different way to prove these relations. In fact, we can start by using the commutation relation: $[\hat{\varphi}, \hat{n}] = i$, from which we can show that:

$$\left[\hat{\varphi}, -i\hbar\frac{\partial}{\partial\varphi}\right]\psi = i\hbar\psi . \qquad (5.3.11)$$

This commutation relation can be proven to be true from what follows:

$$\hat{\varphi}\frac{\hbar}{i}\frac{\partial}{\partial\varphi} - \frac{\hbar}{i}\frac{\partial}{\partial\varphi}(\hat{\varphi}\psi) = \frac{\hbar}{i}\varphi\frac{\partial\psi}{\partial\varphi} - \frac{\hbar}{i}\frac{\partial}{\partial\varphi}(\varphi\psi) = \frac{\hbar}{i}\varphi\frac{\partial\psi}{\partial\varphi} - \frac{\hbar}{i}\psi - \frac{\hbar}{i}\varphi\frac{\partial\psi}{\partial\varphi} = -\frac{\hbar}{i}\psi = i\hbar\psi \Rightarrow$$

$$\Rightarrow \left[\hat{\varphi}, -i\hbar\frac{\partial}{\partial\varphi}\right]\psi = i\hbar\psi ,$$

where we have used the property: $\hat{\varphi}\psi = \varphi\psi$, so that the operator $\hat{\varphi}$ is purely multiplicative. If we now apply the commutation operator $[\hat{\varphi}, \hbar\hat{n}]$ to the wave function ψ, we get:

$$[\hat{\varphi}, \hbar\hat{n}]\psi = i\hbar\psi , \qquad (5.3.12)$$

with $\psi = \psi(\varphi)$, since

$$\left[\hat{\varphi}, \frac{\hbar}{i}\frac{\partial}{\partial\varphi}\right]\psi = i\hbar\psi . \qquad (5.3.13)$$

Given that the two commutation relations lead to the same result, we may identify the number operator $\hat{n}$ with $\dfrac{1}{i}\dfrac{\partial}{\partial\varphi}$, so we get:

$$\hat{n} = \frac{\hbar}{i}\frac{\partial}{\partial\varphi} \ . \tag{5.3.14}$$

If we apply the commutation operator $\left[f(\hat{\varphi}),\hat{n}\right]$, where $f(\hat{\varphi})$ is a generic function of the operator $\hat{\varphi}$, to the wave function ψ, we get:

$$\left[f(\hat{\varphi}),\hat{n}\right]\psi = \left[f(\hat{\varphi}),\frac{1}{i}\frac{\partial}{\partial\varphi}\right]\psi = f(\hat{\varphi})\frac{1}{i}\frac{\partial}{\partial\varphi}\psi - \frac{1}{i}\frac{\partial}{\partial\varphi}(f(\varphi)\psi(\varphi)) = f(\varphi)\frac{1}{i}\frac{\partial\psi}{\partial\varphi} - f(\varphi)\frac{1}{i}\frac{\partial\psi}{\partial\varphi} - \frac{1}{i}\psi(\varphi)\frac{\partial f(\varphi)}{\partial\varphi} =$$

$$= -\frac{1}{i}\left(\frac{\partial f}{\partial\varphi}\right)\psi = i\left(\frac{\partial f}{\partial\varphi}\right)\psi.$$

In this way, we have:

$$\left[f(\hat{\varphi}),\hat{n}\right] = i\left(\frac{\partial f}{\partial\varphi}\right)\psi \ , \tag{5.3.15}$$

where we have used the property: $f(\hat{\varphi}) = \sum_{n=0}^{+\infty} a_n\hat{\varphi}^n$, with the coefficients a_n constant, and again the property according to which that the operator $\hat{\varphi}$ is purely multiplicative.

The relation (5.54) is valid for each wave function $\psi = \psi(\varphi)$ or, in the same way, for each ket $|\psi\rangle$, and also for each function of operators $f(\hat{\varphi})$, which can be expanded in Taylor's series of linear operators.

So, for $f(\hat{\varphi}) = e^{\pm i\hat{\varphi}}$, with $|\psi\rangle = |n\rangle$, we get:

$$\left[e^{\pm i\hat{\varphi}},\hat{n}\right]|n\rangle = i\frac{\partial e^{\pm i\hat{\varphi}}}{\partial\varphi} = i(\pm i)e^{\pm i\hat{\varphi}}|n\rangle = \pm i^2 e^{\pm i\hat{\varphi}}|n\rangle = \mp e^{\pm i\hat{\varphi}}|n\rangle,$$

considering that $i^2 = -1$. So, we obtain:

$$\left[e^{\pm i\hat{\varphi}},\hat{n}\right] = \mp e^{\pm i\hat{\varphi}} \ , \ \text{and from this relation, where } \hat{n} = \frac{1}{i}\frac{\partial}{\partial\varphi} \ \text{we may show that:}$$

$$e^{\pm i\hat{\varphi}}|n\rangle = |n\pm 1\rangle.$$

In fact we have:

$$e^{\pm i\hat{\varphi}}\hat{n} - \hat{n}e^{\pm i\varphi} = \mp e^{\pm i\hat{\varphi}} \Rightarrow e^{\pm i\hat{\varphi}}\hat{n} \pm e^{\pm i\hat{\varphi}} = \hat{n}e^{\pm i\hat{\varphi}} \Rightarrow e^{\pm i\hat{\varphi}}(\hat{n} \pm 1) = \hat{n}e^{\pm i\hat{\varphi}} \Rightarrow \hat{n}(e^{\pm i\hat{\varphi}}|n\rangle) = e^{\pm i\hat{\varphi}}(\hat{n} \pm 1)|n\rangle \Rightarrow$$

$$\Rightarrow \hat{n}(e^{\pm i\hat{\varphi}}|n\rangle) = (n \pm 1)(e^{\pm i\hat{\varphi}}|n\rangle).$$

If we compare this result with $\hat{n}|n \pm 1\rangle = (n \pm 1)|n \pm 1\rangle$, we can consider that:

$e^{\pm i\hat{\varphi}}|n\rangle = |n \pm 1\rangle$, so we have proven the relations considered.

Appendix 5.4

The alternating diamagnetic and paramagnetic character for the eigenstates of the Hamiltonin operator of a one-junction interferometer

In order to analytically determine [42] the alternating magnetic character of the states $|+\rangle$ and $|-\rangle$, we can consider the behaviour of the electric superconductive currents, starting from relation (5.25). By taking the derivative of this expression in n_{ex}, we obtain:

$$\frac{\partial E_\pm}{\partial n_{ex}} = \frac{E_L}{2}\left\{ 2n_{ex} + 2(1 - n_{ex})(-1) \pm \frac{[2n_{ex} - 2(1 - n_{ex})(-1)]2[n_{ex}^2 - (1 - n_{ex})^2]}{2\sqrt{[n_{ex}^2 - (1 - n_{ex})^2]^2 + \alpha^2}} \right\} \Rightarrow$$

$$= \frac{E_L}{2}\left\{ 2(2n_{ex} - 1) \pm \frac{2[n_{ex}^2 - (1 - n_{ex})^2]}{\sqrt{[n_{ex}^2 - (1 - n_{ex})^2]^2 + \alpha^2}} \right\}$$

$$\frac{\partial E_\pm}{\partial n_{ex}} = \frac{E_L}{2}\left[2(2n_{ex} - 1) \pm \frac{2(2n_{ex} - 1)}{\sqrt{(2n_{ex} - 1)^2 + \alpha^2}} \right]. \qquad (5.4.1)$$

From (5.29) we also obtain the analytic expression of the superconducting currents $i_\pm$:

$$i_\pm = -\frac{1}{2E_L}\frac{\partial E_\pm}{\partial n_{ex}} = -\frac{1}{2E_L}\frac{E_L}{2}\left[2(2n_{ex} - 1) \pm \frac{2(2n_{ex} - 1)}{\sqrt{(2n_{ex} - 1)^2 + \alpha^2}} \right] = -\frac{1}{4}\left[2(2n_{ex} - 1) \pm \frac{2(2n_{ex} - 1)}{\sqrt{(2n_{ex} - 1)^2 + \alpha^2}} \right] =$$

$$-\frac{2n_{ex} - 1}{2}\left[1 \pm \frac{1}{\sqrt{(2n_{ex} - 1)^2 + \alpha^2}} \right] = \frac{1 - 2n_{ex}}{2}\left[1 \pm \frac{1}{\sqrt{(1 - 2n_{ex})^2 + \alpha^2}} \right].$$

So we have proven that:

$$i_{\pm} = \frac{1 - 2n_{ex}}{2}\left[1 \pm \frac{1}{\sqrt{(1 - 2n_{ex})^2 + \alpha^2}}\right],$$

where $\alpha = \dfrac{E_{J,0}}{E_L}$ as considered before. Therefore, we see that:

$$i_+ = -\frac{1}{2E_L}\frac{\partial E_+}{\partial n_{ex}} = -\frac{1}{4}\left[2(2n_{ex} - 1) + \frac{2(2n_{ex} - 1)}{\sqrt{(2n_{ex} - 1)^2 + \alpha^2}}\right]. \qquad (5.4.2)$$

We notice that for $0 < n_{ex} < \dfrac{1}{2} \Rightarrow 2n_{ex} - 1 < 0$, and so the terms inside the square brackets are negative, so that i_+ is positive. Summarizing, we have:

$$i_+ > 0 \;\; for\; 0 < n_{ex} < \frac{1}{2} \Rightarrow i_+(n_{ex}) > 0 \;\;\; \forall n_{ex} \in \left[0, \frac{1}{2}\right]. \qquad (5.4.3)$$

In the same way, for $\dfrac{1}{2} < n_{ex} < 1 \Rightarrow 2n_{ex} - 1 > 0$, we have that all the terms inside the square brackets are positive, so we have:

$$i_+ = -\frac{1}{4\pi\alpha}\left[2(2n_{ex} - 1) + \frac{2(2n_{ex} - 1)}{\sqrt{(2n_{ex} - 1)^2 + \alpha^2}}\right] < 0 \Rightarrow i_+(n_{ex}) < 0 \;\;\; \forall n_{ex} \in \left[\frac{1}{2}, 1\right]. \qquad (5.4.4)$$

We can also notice that the profile of i_+ with n_{ex} is parabolic, being proportional to $(2n_{ex} - 1)^2$.

In the same way, for i_- we obtain:

$$i_- = -\frac{1}{2E_L}\frac{\partial E_-}{\partial n_{ex}} = -\frac{1}{2E_L}\frac{E_L}{2}\left[2(2n_{ex} - 1) - \frac{2(2n_{ex} - 1)}{\sqrt{(2n_{ex} - 1)^2 + \alpha^2}}\right] = -\frac{1}{4}\left[2(2n_{ex} - 1) - \frac{2(2n_{ex} - 1)}{\sqrt{(2n_{ex} - 1)^2 + \alpha^2}}\right]$$

For $0 < n_{ex} < \dfrac{1}{2} \Rightarrow 2n_{ex} - 1 < 0$, so the first addendum inside the square brackets is negative, while the second one is positive, for the presence of the minus sign. Considering the expression:

$$2(2n_{ex} - 1) - \frac{2(2n_{ex} - 1)}{\sqrt{(2n_{ex} - 1)^2 + \alpha^2}} = \frac{2(2n_{ex} - 1)(\sqrt{(2n_{ex} - 1)^2 + \alpha^2} - 1)}{\sqrt{(2n_{ex} - 1)^2 + \alpha^2}}$$

We have to show that:

$$\sqrt{(2n_{ex} - 1)^2 + \alpha^2} - 1 < 0 \Rightarrow \sqrt{(2n_{ex} - 1)^2 + \alpha^2} < 1$$

Knowing that $n_{ex} \in \left[0, \dfrac{1}{2}\right]$, we get: $2n_{ex} - 1 < 0 < 1 \Rightarrow (2n_{ex} - 1)^2 < 1$

So, we have: $\alpha = \dfrac{E_{J,0}}{E_L}$ with $E_{J,0} = \dfrac{\Phi_0 I_{J,0}}{2\pi}$ and $E_L = \dfrac{\Phi_0^2}{2L}$, and taking the inductance $L \ll 1$, we notice that $E_L \gg E_{J,0} \Rightarrow \alpha = \dfrac{E_{j,0}}{E_L} < 1 \Rightarrow \alpha^2 \ll 1$ with $L \ll 1$. So that:

$$(2n_{ex} - 1)^2 + \alpha^2 < 1 \Rightarrow \sqrt{(2n_{ex} - 1)^2 + \alpha^2} < 1 \Rightarrow \sqrt{(2n_{ex} - 1)^2 + \alpha^2} - 1 < 0$$

So, considering that:

$$i_- = -\frac{1}{4}\left[\frac{2(2n_{ex} - 1)(\sqrt{(2n_{ex} - 1)^2 + \alpha^2} - 1)}{\sqrt{(2n_{ex} - 1)^2 + \alpha^2}}\right]$$

we notice that the quantity inside the square brackets is positive, and finally:

$$\frac{1}{4}\left[f(n_{ex})\right] < 0 \Rightarrow i_-(n_{ex}) < 0 \quad \forall n_{ex} \in \left[0, \frac{1}{2}\right]. \tag{5.4.4}$$

Also for $n_{ex} \in \left[\dfrac{1}{2}, 1\right]$ we can repeat the same considerations of the previous case for

$i_- = i_-(n_{ex})$

Having obtained that $i_- = -\dfrac{1}{4}\left[\dfrac{2(2n_{ex} - 1)\sqrt{(2n_{ex} - 1)^2 + \alpha^2} - 1}{\sqrt{(2n_{ex} - 1)^2 + \alpha^2}}\right]$

we can consider the algebraic sign of the various terms present inside the square brackets.

We notice that $2n_{ex} - 1 > 0$. By knowing that $n_{ex} < 1$ we get: $2n_{ex} < 2 \Rightarrow 2n_{ex} - 1 < 1 \Rightarrow (2n_{ex} - 1)^2 < 1$; we also have:

$$\alpha = \frac{E_{J,0}}{E_L} < 1 \ \ for \ L \ll 1 \ \ \Rightarrow \sqrt{(2n_{ex} - 1)^2 + \alpha^2} < 1 \Rightarrow \sqrt{(2n_{ex} - 1)^2 + \alpha^2} - 1 < 0.$$

Considering that the term representing the denominator is always positive, that the above condition implies that the numerator is negative, so that:

$$i_-(n_{ex}) > 0 \quad \forall n_{ex} \in \left[\frac{1}{2}, 1\right]. \tag{5.4.5}$$

For $n_{ex} = \dfrac{1}{2}$, in particular, we have:

$$i_{\pm} = -\frac{1}{2\pi E_{J,0}} \frac{\partial E_{\pm}}{\partial n_{ex}} (n_{ex} = \frac{1}{2}) = 0 \qquad (5.4.6)$$

according to the analytical expression (5.26).

So, we have analytically justified the graphical behaviour of $i_{\pm} = i_{\pm}(n_{ex})$.

Appendix 5.5

Calculation of Fourier coefficients

We want to prove [42] that the operator $\hat{\varphi}$ can be expanded in Fourier series as:

$$\hat{\varphi} = \sum_{n=1}^{\infty} b_n \sin\left(\frac{2\pi n}{T} \hat{\varphi}\right),$$

where the Fourier coefficients b_n are calculated in this way:

$$b_n = \frac{2}{T} \int_{-\frac{T}{2}}^{\frac{T}{2}} \varphi \sin\left(\frac{2\pi n}{T} \varphi\right) d\varphi = \frac{(-1)^{n+1} T}{n\pi} \quad . \qquad (5.5.1)$$

In order to prove these relations, we can start by the Fourier expansion of a periodic function $f = f(x)$:

$$f(x) = \sum_{k=0}^{+\infty} a_k \cos kx + \sum_{k=1}^{+\infty} b_k \sin kx$$

where: $a_0 = \frac{1}{2\pi} \int_{-\pi}^{\pi} f(x) dx$; $a_k = \frac{1}{\pi} \int_{-\pi}^{\pi} f(x) \cos kx dx$; $b_K = \frac{1}{\pi} \int_{-\pi}^{\pi} f(x) \sin kx dx$.

If we consider the function $f(x) = x$ which is an odd function ($f(-x)=-f(x)$), knowing that the integral of an odd function between $-a$ and a, with a real number, is equals zero, we get:

$$x = \sum_{k=1}^{+\infty} b_k \sin kx . \qquad (5.5.2)$$

In fact, the term $a_k = 0$, because it is obtained by the integral of the function $f(x)\cos kx$, which is odd, as it is the product of the function $f(x)$, odd for definition, times the function cosine, even for definition. In this case, we have:

$$b_k = \frac{1}{\pi} \int_{-\pi}^{\pi} f(x)\sin kx\, dx = \frac{1}{\pi} \int_{-\pi}^{\pi} x\sin kx\, dx\,.$$

By considering that the trigonometric functions sine and cosine are periodic of period $T = 2\pi$, we notice that $\pi = \frac{T}{2}$ and so we get:

$$b_k = \frac{2}{T} \int_{-\frac{T}{2}}^{\frac{T}{2}} x\sin\left(\frac{2\pi}{T}kx\right) dx\,.$$

We can calculate this integral for parts, and so, choosing x as finite factor and $\sin\left(\frac{2\pi}{T}kx\right)$ as differential factor, we obtain:

$$b_k = \frac{2}{T}\left[\left(x\cos\frac{2\pi}{T}kx\right)\left(-\frac{T}{2\pi k}\right)\right]_{-\frac{T}{2}}^{\frac{T}{2}} - \frac{2}{T}\int_{-\frac{T}{2}}^{\frac{T}{2}} -\frac{T}{2\pi k}\cos\left(\frac{2\pi}{T}kx\right) dx\,.$$

By knowing that, for $T = 2\pi$:

$$\cos\left(\frac{2\pi}{T}k\frac{T}{2}\right) = \cos(k\pi) = \begin{cases} 1 & \text{for even } k \\ -1 & \text{for odd } k \end{cases} = (-1)^k \qquad (5.5.3)$$

and also that: $\cos(-k\pi) = \cos(k\pi) = (-1)^k$, we obtain:

$$b_k = -\frac{1}{\pi k}\left[\frac{T}{2}(-1)^k + \frac{T}{2}(-1)^k\right] + \frac{1}{\pi k}\int_{-\frac{T}{2}}^{\frac{T}{2}} \cos\left(\frac{2\pi}{T}kx\right) dx = -\frac{1}{\pi k}T(-1)^k + \frac{T}{\pi k}\frac{T}{2\pi k}\int_{-\frac{T}{2}}^{\frac{T}{2}} \cos\left(\frac{2\pi}{T}kx\right)\frac{2\pi k}{T} dx =$$

$$\frac{1}{\pi k}\left[(-1)(-1)^k\right]T + \frac{T}{\pi k}\frac{T}{2\pi k}\left[\sin\left(\frac{2\pi}{T}kx\right)\right]_{-\frac{T}{2}}^{\frac{T}{2}}\,.$$

Since $\sin(k\pi) = \sin(-k\pi) = 0 \;\; \forall k \in Z$, we notice that the second term in the previous expression is 0. Therefore, we have:

$$b_k = \frac{(-1)^{k+1}}{\pi k}T\,, \text{ which, for } T = 2\pi\,, \text{ becomes:}$$

$$b_k = \frac{(-1)^{k+1}}{\pi k} 2\pi = \frac{2}{k}(-1)^{k+1} \Rightarrow b_n = \frac{2}{n}(-1)^{n+1}, \qquad (5.5.4)$$

thus proving the relation (5.5.1).

Chapter 6

Search for a Dark Matter component

In this chapter, after reviewing some of the most important concepts about Dark Matter (DM) and methods of its registration, in particular by using SQUIDs, we focus on two main problems. First, the possible mechanism of magnetic moment origin for DM particles, in the form of neutralino, is discussed: the presence of a magnetic moment means the existence of a new kind of interaction, whose corresponding cross section is estimated. Second, a simple uniform model for DM and Dark Energy (DE) is proposed. Two types of devices based on SQUID, in particular the SQUID-paramagnetic absorber and the SQUID-magnetostrictor systems, both suitable for investigations of above problems, are considered.

6.1   Introduction

The nature of DM is one of the big challenges in modern physics, and although there are astronomical evidences for its existence, it is very hard to catch its particles.

In this chapter we start with an introduction about DM and the methods for registering its particles: since interactions between DM and baryonic particles have a very weak intensity, precise methods of registration are needed. At the same time, super-precise experimental measurements can be fulfilled by using interferometric methods, based on superconductor devices and Superconducting Quantum Interference Devices (SQUIDs). Therefore, we outline the main experimental operations and ultimate sensitivities of these devices, discuss some schemes for DM particles registration, and remark the advantages of using superconductor devices and SQUIDs. Furthermore, we consider the possible magnetic interactions of DM particles with ordinary matter and calculate the cross section of magnetic interaction, that we find to be 9 orders of magnitude larger than the conventional interactions, based on nuclear scattering. In the last part of this chapter we outline a theoretical model dealing with the unification of DM and DE, which are considered as two different manifestations of the same cosmological essence, called Dark Substance.

The detailed description of two experimental devices, one connected with DM particles detection and the other one with the registration of the pressure exerted by the flux of DM, in the theoretical model about unification DE-DM, is provided, and their results are remarked.

We also outline, in Appendix 6.1, the main features of two particular experiments, one based on Josephson junctions, the other on SQUIDs, which are able to register DM particles and their interaction with ordinary matter (working substance) of the detectors.

6.2 The problem of Dark Matter in modern cosmology

The enigma of DM (i.e. non-luminous and non-light absorbing matter) is one of the major open problems of modern science. Swiss astronomer Zwicky was the first to suggest, in 1933, the existence of DM on the basis of observation of the velocity dispersion of eight galaxies in the Coma Cluster [45]. We here show a picture of the Coma cluster of galaxies.

Figure 6.1. *The Coma cluster of galaxies.*

Credit: Springel et al., Virgo Consortium, Max-Planck-Institute for Astrophysics

In the following years other cosmological observations [46], [47], [48], [49] confirmed the existence of DM at various scales of distance from the solar system:

- The rotation curve of the spiral (and also of the elliptical) galaxies, i.e. the profile of their rotation velocity as a function of their radius;

- The ratio mass-luminosity of very far (≥ 1 Mpc) cosmic objects from the solar system;

- The comparison between the mass density of a clump of galaxies and the one of all the galaxies present in such a clump.

We also insert pictures of the rotational curves of spiral and elliptical galaxies, and of the profile of the stellar velocities as a function of their distance from the Solar System.

The discovery of DM [49] played about the same role, in cosmology, as the discovery of radioactivity phenomena by A. A. Becquerel, at the very end of the 19th century, had played in nuclear physics. In fact, as very soon after the first registrations of nuclear radiation it became clear that the well-known electromagnetic forces (actually described in the frame of Special Theory of Relativity) appeared to be much smaller than the forces of nuclear nature, in the same way the DM existence, according to modern ideas, demonstrates that the effect of gravitational curvature in

Universe, described within the General Theory of Relativity, is negligible in comparison with interactions manifested by DM.
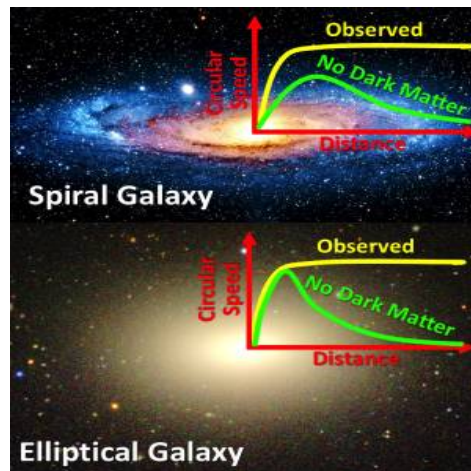

Figure 6.2. The rotational curves of spiral and elliptical galaxies.
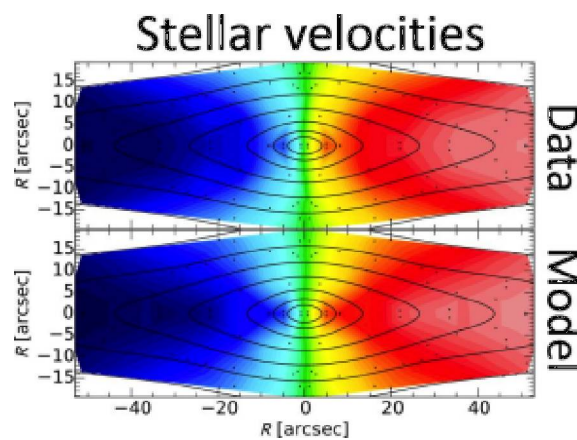*Credit: M. Cappellari and the Sloan Digital Sky Survey.*

Figure 6.3. The profile of stellar velocities as a function of distance from the Solar System.
Credit: M. Cappellari and the SLUGGS team

The nature of DM is yet obscure, but since it does not radiate light and can gravitationally interact with other celestial bodies, its elementary particles must be massive, with no electric charge, and also considering the weakness by whom they interact with common matter, with no colour charge.

At this point, we can open a parenthesis about the properties of our Universe, in order to define the role of DM. In fact, we may say that in recent years the satellite experiments WMAP (Wilkinson Microwave Anisotropy Probe) [50], SDSS (Sloan Digital Sky Survey) [51], and COBE (Cosmic Background Explorer) [52] have provided a striking picture of Universe:

- It is spatially flat;

- It is characterized by an accelerated expansion;

- It consists for 68.3% by DE, for 26.8% by DM and only for the remaining 4.9% by the ordinary luminous matter (called in cosmology baryonic matter). We can represent the contents of our Universe as in fig. 6.4.
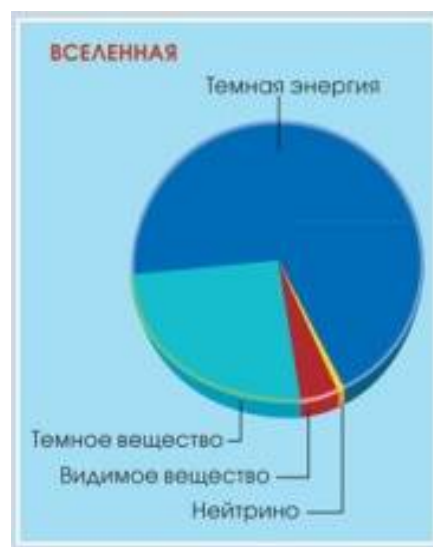

Figure 6.4. *The contents of our Universe. We notice that the yellow part represents the neutrinos, the red and the cyan parts are the visible matter (called also baryonic matter), and the Dark Matter, respectively, and the blue part is the Dark Energy.*

Courtesy of Moscow State University (MSTU) for the conference PIRT (Physical Interpretation of Relativity Theory), 29 VI- 02 VII 2015, Bauman State University (BST), Moscow, Russia.

One of the most important challenges in modern cosmology is the problem of cosmic acceleration, which is strictly connected with the comprehension of the nature of DE, the main component of our universe, which could drive the accelerated expansion. In fact, the role of the repulsive (antigravity) component is intimately related to the universal cosmological constant problem, initially appeared in the theory of general relativity (the Λ term in Einstein's equations) and currently discussed in the Superstring Theory framework [53]. Three main cosmological theories, about the problem of cosmic acceleration, have been developed:

- The ΛCDM model (also called the Concordance Model) [54], and its extension to QCDM model [55], which are two cosmological fluids models (DE and DM);

- The UDE (or UDM) models [56], where we consider only one cosmological fluid, with an energy density varying in time, which behaves as Radiation, Matter, Dark Energy in the different cosmological eras, giving rise to the cosmic acceleration [57, 58];

- An alternative approach has been proposed, based on the possibility that the cosmic acceleration is created by a fluid of curvature present inside the ordinary matter [59], so without considering the presence of exotic ingredients (DE and DM) in the cosmic pie; the analytic description of this phenomenon requires a modification of Einstein's general theory of relativity, and some theoretical models have been considered [60, 61].

After this brief description about the Universe, we can return to our main argument of DM. According to important cosmological measurements [54], [55], [56], for the constitution of DM the following results have been found:

- Only the 1% of DM is of baryonic kind (black holes, neutron stars, big planets);

- Almost the 30% is represented by Hot Dark Matter (HDM) [62], made up by relativistic particles, with mass smaller than 30 eV, so they cannot clump;

- The remaining 69% is represented by the so called Cold Dark Matter (CDM) [63], made up by non-relativistic particles, with masses comprised between GeV and TeV, so that they can clump, forming Large Scale Structure (LSS), and can be revealed by gravitational effects. Different forms of DM are shown in fig. 6.5 and in fig. 6.6.

Modern theoretical models offer a broad assortment of particles which could constitute DM (see, for example [46-49]). In any case, for its larger abundance and its non-negligible gravitational effects, the CDM is the part of DM more analyzed in the modern theoretical and experimental physical research.

Figure 6.5. *An example of the strong gravitational lensing by the Red Galaxy LRG 3-757.*
Credit: ESA / Hubble & NASA.

The most popular CDM candidates are particles generally called WIMPs (Weakly Interacting Massive Particles) with masses from a few tens of GeV to several TeV, i.e. 10-5000 times the

proton mass, speed of about $10^5 - 10^6$ m/sec and cross section σ_W of about $10^{-44} cm^2$, typical of the weak interaction processes, with no electric and colour charge.(In the context of DM, hypothetical light particles (ALPs) with masses much smaller than 1 GeV, forming a hot component of DM, are also currently considered. However, only the registration of cold nonrelativistic DM components will be discussed below.
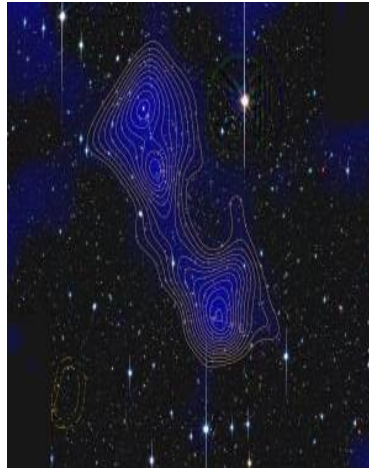

Figure 6.6. A bridge of hot matter, "shining" in X rays, connects the galaxy clusters Abell 222 and Abell 223, and so reveals part of the missing baryonic matter in the Universe. The filamentary connection between those two galaxy clusters also supports the theory that visible matter is distributed along universal filaments of Dark Matter. The mass in the filament is between $6.5 \cdot 10^{13}$ and $9.8 \cdot 10^{13}$ times the mass of the Sun. Credit: XMM- Newton X-ray telescope.

In table 6.1 we present a schematic representation for WIMP parameters and some DM particle candidates:

MASS	M_W	$10 - 5000 \, \text{GeV}/c^2$ (~ 10 – 5000 m_p)
VELOCITY	V_W	10^5 - 10^6 m/s
DENSITY	ρ_W	0,3 (GeV/c^2)/cm^3
CROSS-SECTION σ_W		$< 10^{-10}$ pbarn (~10^{-44} cm^2)
FLUX	Φ_W	~ $5 \cdot 10^4$ 1/(cm^2 s)

Table 6.1. Some significant parameters for WIMP particles. Courtesy of Moscow State University (MSTU) for the conference PIRT (Physical Interpretation of Relativity Theory), 29 VI- 02 VII 2015, Bauman State University (BST), Moscow, Russia.

Some DM particle candidates

NEUTRINO	$<30 \text{eV}/c^2$
AXION	$10 \text{ eV}/c^2$
NEUTRALINO	$> 20 \text{ GeV}/c^2$
MAJORANA FERMION	$> 20 \text{ GeV}/c^2$
FAST NEUTRONS	$> 1 \text{ MeV}/c^2$

Table 6.2. *Some possible candidate DM particles, with their corresponding mass values.* Courtesy of Moscow State University (MSTU) for the conference PIRT (Physical Interpretation of Relativity Theory), 29 VI- 02 VII 2015, Bauman State University (BST), Moscow, Russia.

The two kinds of particles which best fit these parameters are:

- The heavy neutralinos, described in the Theory of Supersymmetry (SUSY) [64], which postulates the existence of supersymmetric partners (or also called superpartners) of ordinary particles, i.e. new particles whose spins differ by ½;

- The lightest Kaluza-Klein particles (LKP), described in the String Theory [65], which postulates the existence of extra-spatial and temporal dimensions in Universe, inside whom these Kaluza-Klein particles (KK) exist as massive excited states, and the lightest of them is the appealing candidate for DM, with mass values between 40-1200 GeV. Of course, if this theoretical model of LKP is verified, we can consider a new version of Universe with extra dimensions (the so-called Multiverse) [66]. In the Minimal Supersymmetric Standard Model (MSSM) [67], the lightest neutralinos (linear combinations of four neutral fermions: Wino, Bino, and a pair of Higgsinos) are appropriate candidates.

6.3 A survey of the experiments for Dark Matter particles registration

All experimental studies on the search for DM particles can be conditionally divided into three main areas [49]:

1) experiments on colliders;

2) indirect registration of Dark Matter particles by their annihilation products in cosmic rays;

3) direct detection of Dark Matter particles of cosmic origin.

We shall here briefly describe the experimental methods adopted in each area.

1) In the colliders, the decay products of different kinds of heavy particles, created [68] in the nuclear collisions of accelerated heavy ions, are registered. Such accelerator experiments (Tevatron, LHC), may give certain results only on the basis of full kinematic analysis of visible products of *p-p* interaction, allowing to recover the value of the energy-impulse "spent" at the birth of the unknown DM particles. It is estimated [69] that only a small part (about 10%) of the total energy of *p-p* collisions is spent for the creation of supersymmetric particles, which limits the effectiveness of the experiment. So the eventual formation of a 100 GeV WIMP is supposed to be implemented with energy not less than 2 TeV. However, until now, no particles as WIMPs have been revealed in accelerator experiments. We report a picture of the LHC, and of the CMS (Compact Muon Solenoid) experiment [69] in figures 6.7, 6.8 and 6.9.

2) In the indirect methods of registration we search:

a) Particles created by the annihilation of WIMPs in the galactic halo, where we consider the presence of DM clumps: usually we may register electrons, positrons and photons through space satellite experiments, in order to avoid problems of attenuation by the terrestrial atmosphere, and deviation of charged particles by the terrestrial magnetic field.
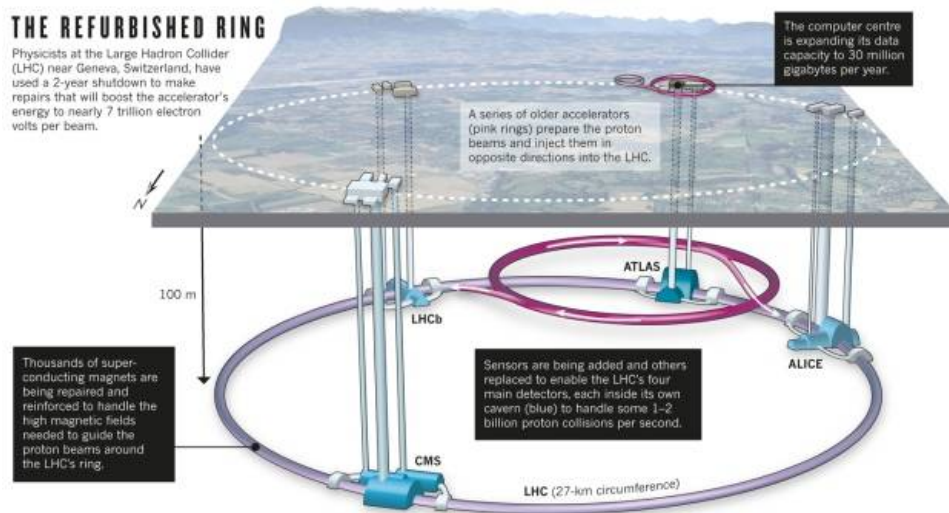
Figure 6.7. *A schematical representation of LHC.*

From: J. G. Ellis, G. Giudice, M. L. Mangano, Review of the safety of LHC collisions, Journal of Physics C, Nuclear and Particle physics, 2008.
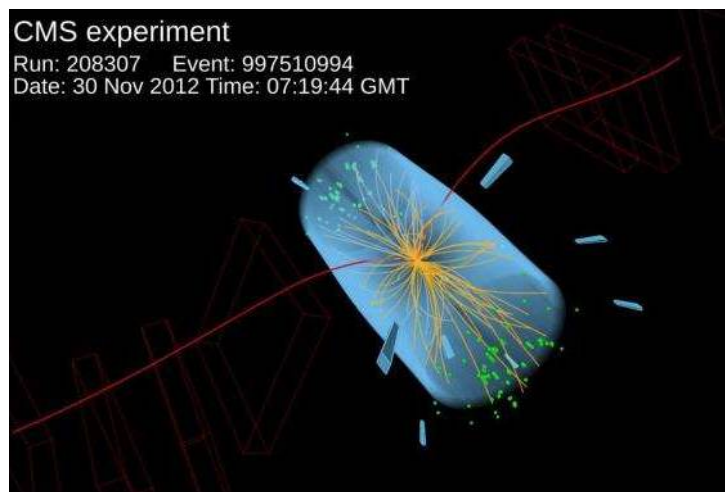

Figure 6.8. *A picture of CMS experiment, showing collisions of heavy accelerated particles.*

From: S. Chatrchyan, G. Hmyakyan, W. Adam, T. Bauer et al., The CMS experiment at CERN, JINST, S08004.

Figure 6.9. *A section of the CMS experiment.*
Credit: http:// home.cern/topics/large-hadron-collider.

One of the most recent experiments of this kind is the PAMELA (Paylod for Antimatter-Matter Exploration and Light-nuclei Astrophysics) experiment [70]. We give a sketch of PAMELA experiment in the next figure 6.10. We should say that the registered experimental photon and lepton energy spectrum can give us information about the mass and the cross section of DM particles [71]. However it is very difficult to distinguish these photons and leptons from the ones created by other cosmic sources (for example pulsars and so on).
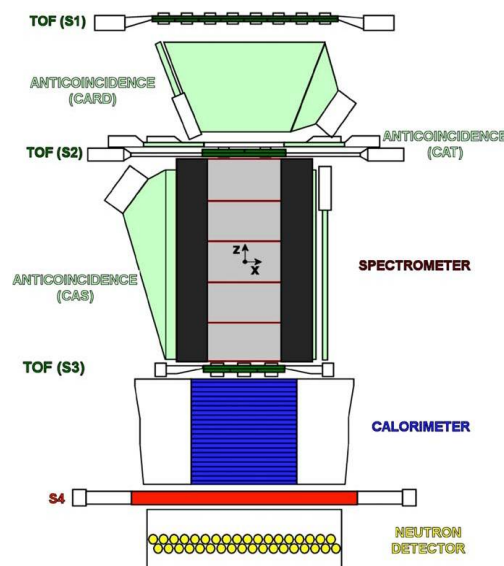

Figure 6.10. *A sketch of the PAMELA experiment, showing its detectors.*
From: W. Menn, O. Adriani, et al., The PAMELA space experiment, Advances in Space Research, 51, pp. 209-218, 2013.

b) Neutrinos, arising as final products of WIMP annihilation in the Sun or in the Earth: the registration [72] of these particles, however, is possible only in low-background underground or underwater observatories, that require very important cares and a lot of money for their handling. We have to outline [68] that indirect registration of DM particles, by their annihilation products in cosmic rays, requires the detection of TeV gamma rays (photons). However, as it is well known [73, 74], such a quantum creates in the Earth's atmosphere a wide (a few kilometers) electromagnetic air shower of secondary particles, that significantly complicates the determination of the total energy of the original photon. Among the projects for registration of $1 \div 15 \text{TeV}$ gamma rays in space-based experiments, it should be noted the project GAMMA-400, developed in P. N. Lebedev Institute [75, 76], as one of the most competitive (energy resolution of 1%, angle resolution 0.01°). This gamma-ray telescope is a stack of silicon strips and scintillation plates, and a TeV quantum, passing through it, practically loses all its energy. The system of photomultipliers allows not only to determine the initial energy of the quantum, by summing photo responses, but also to identify the point of conversion and the direction of the incident photon with the help of fiber-optic cabling.
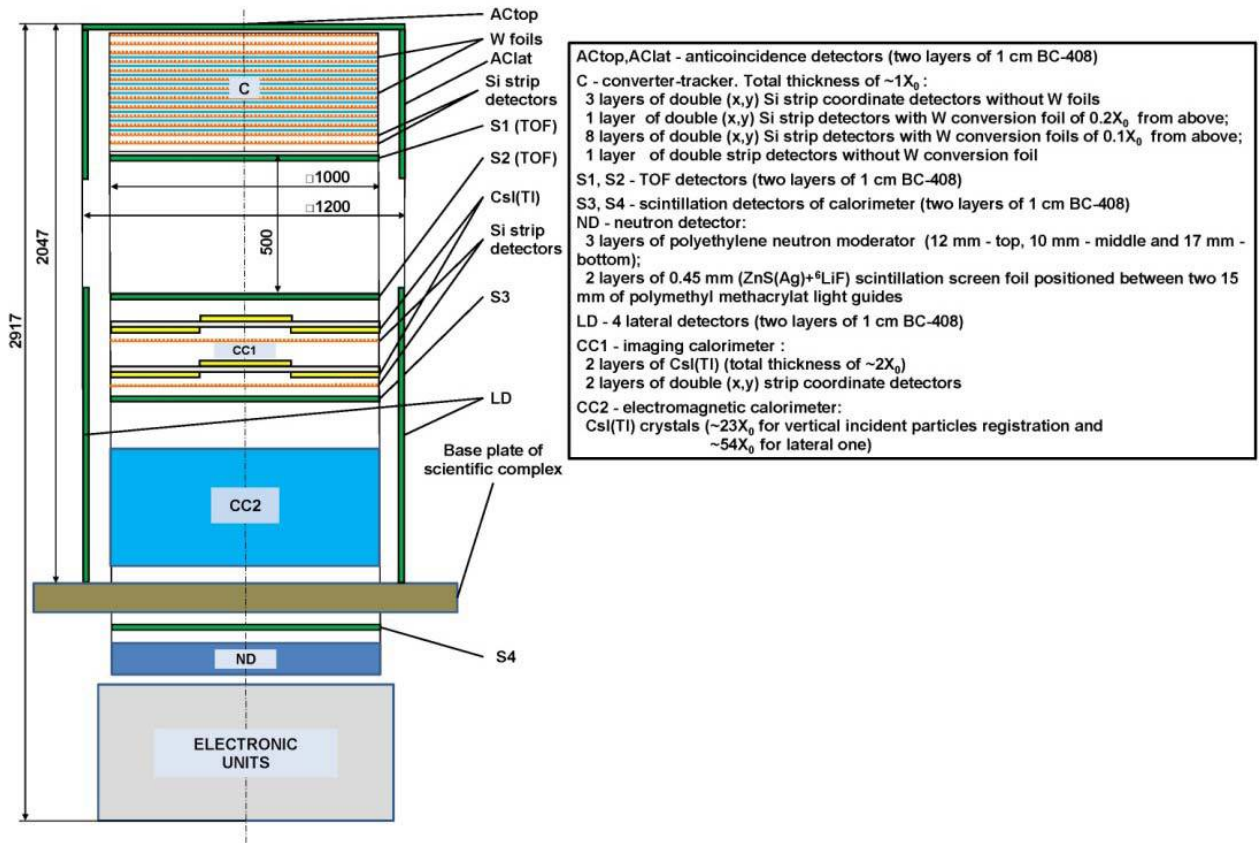
Figure 6.9. *Physical scheme of GAMMA-400 gamma telescope. All presented dimensions (in mm) are reference. From Galper, Topchiev et al., Status of the GAMMA-400 Project, Advances in Space Research 51, pp. 296-300, (2013).*

3) About the direct methods of registration [77], we may say that, as WIMPs interact with nuclear collisions, the induced effects by the process of nuclear recoil (elastic WIMP-nucleus scattering) are registered. In fact, it is possible to show [77], by using the classical theory of scattering (as WIMPs are non-relativistic particles) that the momentum and the kinetik energy exchanged during their interaction with a particle, that we can call a, are:

$$P_a = \frac{2m_a P_W}{m_W} \qquad (6.1a)$$

$$E_a = \frac{4m_a E_W}{m_W} \qquad (6.1b)$$

where m_a, P_a, E_a are the mass, impulse and kinetik energy of the particle a, while m_W, P_W, E_W are the corresponding quantities of the WIMP particle. As the previous expressions are characterized by the ratio $\frac{m_a}{m_W}$, which is usually strictly smaller than 1, we

139

may conclude that there is significant exchange of momentum and kinetik energy only for particles with big masses (for example nuclei closed to iron), and so we can neglect WIMP-electron interactions. The nuclear recoil energy, that is of about 40 eV, can induce effects of:

I) atomic ionization, or the release of an electric charge in the semiconductors;

II) scintillation phenomena (i.e. photon emission)in some liquids and solids;

III) excitation of phonons (ion vibration quanta) in lattices.

The main drawback of these experimental activities is to reject all the electrons induced by photon or lepton interactions with atomic or free electrons (also called recoil electrons) of the working substance of the detector. The rejection of background events is a very challenging and important task, because they persist despite the use of underground laboratories, protection shields and super-high pure materials. Usually, the difficulties of direct methods of registration are based on these factors:

a) A very small WIMP-nucleus scattering cross section ($<10^{-6}$ pb), necessitating a large sensitive detector mass. In fact, according to the Fermi Golden Rule:

$$W = N_1 N_2 \frac{\langle \sigma v \rangle}{V}, \qquad (6.2)$$

where W is the rate of WIMP-nucleus interactions, N_1 is the number of particles of external beam, N_2 is the number of particles of the working substance, V is the volume, and $\langle \sigma v \rangle$ is the mean value, over WIMP velocities relative to the detector, of the product of WIMP scattering cross section σ times its velocity v, we can notice that W increases by increasing the detector mass;

b) The low efficiency of small nuclear recoil energy measurements (of about 10-100 KeV), so it is needed to use detectors with several KeV threshold;

c) The location of detectors in underground or underwater laboratories, and the use of protective shields or material free from radioactive elements in order to eliminate, or at least minimize, the background noise.

Thus, the experiments [68] for direct registration of DM particles of space origin are carried out in laboratories with deep depression of cosmic background (the radiation weakening in the tunnel of Gran Sasso is characterized by the water equivalent of about 3600 m). By comparing the characteristic energy spectrum of recoil nuclei with the corresponding spectrum of known weakly interacting particles (for instance, neutrinos), also able to go through very thick defense shields, one can reach the same conclusion about detection of WIMPs. For the registration of recoil nucleus energy, a wide range of detectors is used in these experiments [49]: ionization, scintillation, phonon, heat detectors and Josephson

junction, based on the first order phase transition (such as bubble chambers or superheated superconducting microgranules) and so on. We may also consider [77] that the ratio between ionization and phonon emission have discrimination power! In fact, if there are more events of ionization, with the emission of atomic electrons, we know that they are created by the interaction of leptons and photons with ordinary atoms. On the other hand, if we register the emission of phonons, as they come from the de-excitation of nucleus, we notice that interactions with atomic nuclei occur, which are due to heavy particles, such as DM particles, according also to (6.1). In the DAMA NaI project [78], for instance, there are 9 scintillating amplitude detectors (crystals of NaI (TI), each one of 9.7 kg, so justifying the name DAMA NaI, where DAMA stays for Dark Matter) with energy resolution of about 2 keV. This project should be especially mentioned. In fact, during its seven-year-long observation period, it really fixed for the first (and in practice for the last) time the annual cycles of decreasing and increasing character of the registration rate of events. In practice, it provided clear comprehension of the coinciding/anticoinciding (June/December) direction of the velocity vector of galactic streams of Dark Matter particles with the travel line through solar system. There is now a new version of this experiment, called DAMA LIBRA (Large Iodium Bulk for Rare processes), using 25 scintillators of the same kind [79]. We report a schematical picture of DAMA NaI in the next figure 6.10.
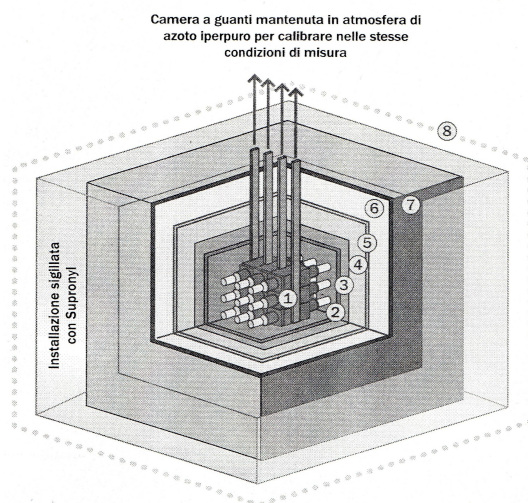

Figure 6.10. *A simplified scheme of DAMA NaI. The numbers inside the figure indicate the different parts of the experiment: 1) NaI crystals (Sodium Iodide); 2) box of copper, kept in an atmosphere of super-pure nitrogen; 3) copper; 4) lead; 5) cadmium plate of 1.5 mm; 6) poliethilene; 7) box in plexiglass, kept in an atmosphere of super-pure nitrogen; 8) about one meter of cement. From R. Bernabei et al., Searching for WIMPs by the annual modulation signature, Int. J. Mod. Phys. D 13, pp. 2128-2160, 2004.*

6.4 Focus on superconductors and SQUIDs as detectors of Dark Matter

Let us consider the processes occurring when an interaction WIMP-nucleus of an atom of a superconductor device (of first kind, so with well defined values of critical magnetic field and critical temperature) occurs:

- A number N of phonons are emitted in a region near the position of interaction, whose extension as it is possible to show [77] is:

$$d = aN^{\frac{1}{3}} \ , \qquad\qquad\qquad (6.3)$$

where a is the lattice constant, whose typical value is about 0.5 nm, and N can be expressed as: $N = \dfrac{E_W}{E_{PH}}$, with $E_W \ 10^4$ eV is the WIMP kinetic energy and $E_{PH} \cong 10^{-3}$ eV is the phonon energy, so that a numerical estimation of (6.3) is of about 0.8 nm or $0.8 \cdot 10^{-9}$ meters.

- These phonons lead to a local disruption of Cooper pairs, and the electrons so formed tend to re-arrange in new Cooper pairs, as they represent the state of minimum energy (or ground state), in a time interval typical of the electron relaxation time spin-spin, that is of about 10^{-9} seconds.

- The atomic nucleus, excited by the energy absorption due to the WIMP interaction, de-excites by emitting phonons, thermal waves, and so on, also for small values of energy, equal or smaller than 1 KeV.

Therefore, a superconducting detector has very good time response (of about 10^{-9} seconds), space resolution (of about 0.8 nm), and energy resolution (smaller than 1 KeV, also around some dozen of eV).

A SQUID (Superconducting Quantum Interference Device), whose main properties have been just presented in the previous chapter, can be used as detector of Dark Matter [80], usually in connection with another experimental device (for example a calorimeter, a thermoresistor, and so on), because it can register also very small variation in the magnetic flux (we have a resolution of $10^{-6}\Phi_0$, where $\Phi_0 = 2.08 \cdot 10^{-15}$ Weber is the quantum elementary flux) threading the experimental device with whom it is connected. Therefore, a SQUID can give very good information [80, 81] about the rate of interaction and the energy resolution of DM. We may also use SQUIDs as

amplifiers of signals (usually of electric current) [82] in the service electronics connected to the experimental apparatus. The two advantages of SQUID amplifiers are:

- No loss of signal, because there is no dissipation of electric current in a superconducting device;

- A reduction of the thermal and electric noise in comparison with the semiconductors, which made up the transistors.

We could say [68] that modern methods for Dark Matter particles direct detection make extensive use of cryogenic techniques. The evident lowering of thermal noise, along with the drifting of input stages of used electronics, allows to engage, in numerous cases, fundamentally new effects (the low-temperature phase transitions of the first order, SQUIDs, Josephson arrays [12,77], multi-barrier Josephson junctions [8], etc.) in order to increase the sensitivity of the registration process itself [49]. Recording circuitries, where the amplitude measurements of detector response are registered by means of SQUIDs [81-82], based on Josephson effect [1], have ow a widespread use. The sensitivity of a modern commercial DC-SQUID (without superconducting flux transformer) reaches the level of $10^{-6} \div 10^{-7}$ $\Phi_0/\sqrt{Hz}$ (here we have the flux quantum $\Phi_0 = \dfrac{\pi\hbar}{e} \cong 2.08 \cdot 10^{-15}$ Wb). The sensitivity of SQUIDs has allowed to apply these devices for taking such ultra-precise measurements as gravitational wave detection [83, 84] or contactless examination of bio-magnetic brain activity [83, 85]. According to the physical principles of its work, the quantum interferometer measures the magnetic flux. By using Stokes flux theorem, we can determine the interference phase difference in superconducting circuit, where Josephson junctions are included [80, 81]. However, in experiments for DM particles search, these devices are usually used merely as low-frequency picovoltmeters, registering the response of cryogenic thermoresistors. In this way, in the two-segment detectors (the project of CRESST-II [86]), the coincidence of light and thermal responses of absorber (300g of $CaWO_4$) on recoil nucleus are fixed. Two identical vanadic thermoresistors, being at a temperature near the superconducting transition, together with two DC-SQUIDs, are used as scintillating and heat recording channels of Dark Matter particles. However, alike schemes of quantum interferometer utilization, when the signal is converted according to the chain $I\delta R \rightarrow \delta U \rightarrow \delta i = \delta U/r \rightarrow \delta\Phi = L\delta i$, i. e. at first it turns into the variance of magnetic flux taken by the interferometer, and then it is directly applied at the SQUID entry, happen to be inefficient due to unavoidable losses in the conversions chain. However, two research groups [87, 88] have proposed schemes, that did not need any conversion of signal. Actually the heat response, arising in absorbers due to the interaction of a particle with matter, was transmitted directly on the signal input. In ref. [87] the possibility to measure the magnetic response of paramagnetic thermometer, by means of DC-SQUID, was tested. The signal appears here due to the

dependence of thermal sensor magnetic susceptibility according to Curie-Weiss law. In this case the sensor should be magnetized by a small magnetic field (~10 mT).

We have proposed [88] another type of scheme, where the magnetic response, registered by a SQUID, corresponds to an enhancement of the spin system entropy rather than to the change of paramagnetic absorber temperature. The operating principle of the experiment is the following. At the beginning the paramagnetic absorber is self-cooled during the process of adiabatic demagnetization [89]. After the external magnetic field is lowered down to zero, the SQUID measures the reduction of residual magnetization of the paramagnetic absorber. The latter step corresponds to the measurement of the entropy increase due to the release of energy caused by the interaction between a particle and the paramagnetic absorber. Various modes of operation of the SQUID-paramagnetic absorber system are discussed in details in the following works. In reference [90] direct measurement of the entropy growth using the method of adiabatic demagnetization is considered. In reference [91] the measurement sensitivity is increased by replacing atom paramagnetism by nuclear one, with cooling produced by a dissolution refrigerator He^3 - He^4. In reference [92] a dual-channel mode is adopted to eliminate lepton processes. In reference [93] an estimate of the sensitivity in the case of strong fields saturation using asymptotic methods of statistical mechanics is performed. Finally, in reference [94] resonance registration of THz radiation with a wavelength of about 10 mm is illustrated.

It should be noted that, among all thermal methods of Dark Matter particles registration, the magnetic ones have two essential advantages. In fact, in order to increase the probability of registration of elementary particles, which weakly interact with matter (small cross-section of interaction, approximately one event per kg per day), it is necessary to enlarge the mass of the absorber. As a consequence, the mass of real detectors of Dark Matter particles evolved from the initial value of 100 g to 100 kg [95, 96] in a short time period [49]. In common (nonmagnetic) thermal detectors [49] the enhancement of the absorber mass automatically leads to the enhancement of its thermal capacity and hence to a sufficient reduction of the thermal response. On the contrary, in cryomagnetic systems the enhancement of heat capacity is compensated by the simultaneous increase of the total number of spin-carrying particles contributing to the system's magnetic response. Another useful property of magnetic thermal detectors is connected with the growth of the magnetic part of heat capacity as the temperature decreases: $c_{\mathrm{m}} \sim T^{-2}$. This fact seems paradoxical at first glance, since it may appear inconsistent with the third law of thermodynamics. However, this dependence is true until either the total ordering due to ferromagnetic transition or the local ordering due to casual residual fields take place. We also consider that in the case a little magnetic sensor with a large magnetic heat capacity is attached to a big nonmagnetic absorber,

characterized by a small heat capacity, the whole energy released in the latter can be gathered in the former device. In fact we will see an application of this property in the second part of Appendix 6.1, where we analyse a particular version of the experimental device SQUID-paramagnetic absorber system. We also propose a second type of experimental device, the SQUID-magnetostrictor system, in order to register DM fluxes. In addition, a model of unified DE-DM providing definition of this flux is given.

6.5 Cross section estimate of the magnetic interaction of DM particles for SQUID registration

In this section we consider [68] the possible magnetic interaction of DM particles with common matter. We shall deal with a new kind of interaction, different from the conventional WIMP-nucleus scattering. In fact, this interaction is an action at distance, and its analysis is very interesting in trying to open new horizons on DM search. One of the most recent experiment, Xenon 100 [98], performed in the underground laboratory of Gran Sasso, has excluded hidden WIMP-electrons interactions. In reference [98] the sharp difference between values of cross sections for spin dependent (SD) interactions and spin independent (SI) ones (the former are nine orders of magnitude bigger than the latter), is remarked. It is noted that an adequate model of such SD interaction for DM detection is still needed.

We start by considering that one of the most realistic candidate particle for CDM is the lightest supersymmetric particle, the so called neutralino [64], whose wave function is a linear combination of fermionic super-partners of photon, of W-neutral boson and of Higgs boson. This wave function can be thus denoted as $\aleph = N_{1,1}\hat{B} + N_{1,2}\hat{W}_3 + N_{1,3}\hat{H}_1^0 + N_{1,4}\hat{H}_2^0$, where $N_{1,1}$ $N_{1,2}$, $N_{1,3}$, $N_{1,3}$, $N_{1,4}$ are some opportune constants (being the lightest supersymmetric particle, neutralino should be stable). Of course, being "neutral in all respects", neutralino has no electric charge; however, electro-neutral elementary particles can possess a magnetic moment [99]. In general, a magnetic moment might occur for two main reasons: first, because of the reversible virtual transformation of the original "non-magnetic" particle (in its ground state) to one particle of the multiplet partners with an electric charge (SU(2) baryons with isospin ½: i.e. a neutron n into a proton p); second, because of the existence of a cloud of virtual charged quanta of the interaction field, involving "naked nonmagnetic" particles. According to these modern concepts, the neutron magnetic moment is (approximately) analogously formed.

Similarly, a very weak magnetic moment of the neutrino ($\mu_\nu \cong 10^{-13}\mu_B$) should occur [100] due to the electroweak processes illustrated by Feynman diagrams represented in Figure 6.11.
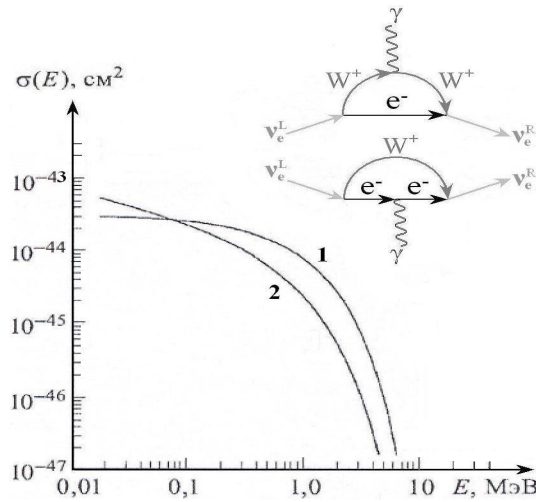

Figure 6.11. *Cross section of neutrino scattering on electron:* ***1*** *- weak interaction (the Weinberg's angle agrees with* $\sin^2\theta_W = 0.23$ *);* ***2*** *- magnetic interaction (* $\mu_\nu = 10^{-13}\mu_B$ *) [98]. In the inset, Feynman diagrams, illustrating the creation of anomalous magnetic moment of Dirac (massive) neutrino* $\nu_{(D)},$ *are given. From: A. B. Balantekin, Neutrino magnetic moment, arXiv: hep-ph, 13 January 2006.*

In the framework of Weinberg-Salam [101] electroweak interactions (Standard Model), electron neutrino ν_e has some non-zero probability to decay into an electron and a W^+ boson and then through a time interval $\Delta t \approx \hbar/(m_W c^2)$ these virtual particles annihilate, turning into another helicity neutrino. During the short ($\approx 2 \times 10^{-27}$sec) existence of electrically charged particles e$^-$ and W$^+$, they can interact with an external electromagnetic field, which is symbolized in the diagram by a photon γ. Therefore, the part of the radiative corrections, which determines the energy shift, is interpreted as the interaction energy of the neutrino magnetic moment with the magnetic field. On the other side, some astrophysical estimates [102, 103] lead to the hypothesis about a significantly larger neutrino moment value than the one given by the Standard Model. In the 90's, the search for such anomalous magnetic moment of neutrinos was engaged, in particular, by B. S. Neganov (the one who invented the dilution cryostat He^3-He^4 for obtaining temperatures below 100 mK without magnetic field) at JINR in Dubna. In his experiments [104] an attempt to observe the growth of the interaction cross section e$^-$/ν predicted for the "magnetic" neutrinos in the region of small energy was undertaken. A low-temperature calorimetric detector and a H^3 source of neutrinos were used. Similar assumptions can be considered about the presence of a magnetic moment for DM particles, also if they are beyond the Standard Model. One of the channels [105] is the reversible annihilation

of the neutralino into a pair of electrically charged gauge bosons W-type, as we can see in figure 6.12.
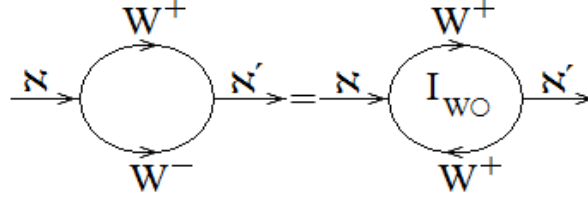

Figure 6.12. *A diagram illustration of the process showing that two branches of virtual oppositely charged W^- and W^+ form a ring current I_{W^0}, whose corresponding boson loop has the uniform charge (and effective area of S_{W^0}). From: D. A. Vasquez, P. Richardson et al., Neutralino DM in the MSSM, Phys. Rev. D 86, 2012.*

In this figure, we may notice [68] that the two diagrams are equivalent, in the sense that the motion of the W^- boson in one direction is equivalent to the motion of the W^+ boson in the opposite direction. In this way, the corresponding ring electric current of W^+ bosons is formed inside the considered loop. We can express the magnetic moment of the boson loop as $S_{W^0} I_{W^0}$, which is identified as the magnetic moment of a neutralino. (It should be noted that the specificity of magnetic interaction of DM particles with common matter is in its "tangential character", because we have an interaction with the orbital magnetic field induced by the atomic electrons, as opposed to the conventional "nuclear head on" type, that is a contact interaction WIMP-nucleus).

In order to obtain an analytic expression for it, we may consider the analytic expressions for the effective area and the ring electric current. The effective area can be represented through the square value of the Compton wavelength $S_{W^0} \cong \dfrac{\hbar^2}{(m_W c)^2}$, which is the minimum possible value, as the speed of light c is the maximum value for velocities. The loop electric current can be estimated as

$$I_{W^0} \cong \frac{e}{\tau_W} \cong \frac{e m_W c^2}{\hbar} , \qquad (6.4)$$

where τ_W is the minimum value for the time interval, according to Heisenberg's uncertainty principle, and so I_{W^0} is the maximum possible value for the considered loop of electric current. So the final expression $S_{W^0} I_{W^0} \cong \dfrac{e\hbar}{m_W} = \mu_W$ is an adequate analytic representation for the neutralino magnetic moment.

This analytic expression coincides with the structure of the standard formula of Bohr magneton μ_B and differs from the latter by replacing of the electron mass m_e with $m_W \cong 1.6 \cdot 10^5 m_e$. Accordingly, μ_W is approximately 5 orders of magnitude smaller than μ_B. This means that the magnetic interaction energy $E_\chi = \mu_W B_{orb}$ of μ_W with the magnetic induction field $B_{orb} \cong 10$ T (typical value of the field for spin-orbit effects) is about $4 \cdot 10^{-9} eV$. The probability of interaction between an atom in the absorber, whose atomic orbital current induces a magnetic field, with the magnetic moment of the boson loop, occurring during the reversible *decay* of neutralino, can be estimated by squaring the corresponding variation $\delta\psi_{W^0}$ of the amplitude of the unperturbed boson loop, defined according to the following expression [106]:

$$\psi_{W^\circ} = \psi_{W^\circ}^{(0)} + \delta\psi_{W^\circ} = \psi_{|W^\circ\rangle}^{(0)} + \sum_{\forall |W^\circ\rangle'} \frac{\mu_W B_{orb}}{E_{|0\rangle} - E_{|W^\circ\rangle'}} \psi_{|W^\circ\rangle'}^{(0)}. \qquad (6.5)$$

Thus, the required probability [68] for a typical value of the energy, eventually lost by neutralino of around 40 eV (energy quantity transferred to the absorber in case of a reliable registration), is estimated as $\left(\dfrac{\mu_W B_{orb}}{\delta E_\chi}\right)^2 \cong 10^{-20}$. Therefore, the probability sought for a typical value of energy, eventually lost by a neutralino, and coinciding with $\delta E_\chi \cong 40$ eV (that is roughly transferred to the absorber in a reliable registration), is estimated by squaring the ratio between the corresponding variation and the amplitude of the unperturbed boson loop, so we get: $\left(\dfrac{\mu_W B_{orb}}{\delta E_\chi}\right)^2 \cong 10^{-20}$.

Considering a linear chain of 10^{20} absorber atoms, and adding up all the probabilities of magnetic interaction with all atoms, as all the events of interaction are independent from one another, and also characterized by the same probability, we get the level of confidence: $\sum_{1}^{10^{20}} 10^{-20} \cong 1$. According to this expression, we have almost the certainty that a magnetic interaction event occurs between the neutralino and one of the atoms of the considered linear chain, having a length of $a \cdot 10^{20}$ where a is the lattice constant, which assumes a value of about 0.3 nm.

Let us "build" a hypothetical absorber with a large number of such chains and let its square surface area be S_0. Then the cross section of the magnetic interaction neutralino-absorber will be

$$\sigma_{\chi \leftrightarrow B_{orb}} \cong \sigma_{W^0 \leftrightarrow B_{orb}} \cong \frac{S_0}{N_A} = \frac{S_0}{S_0 \cdot a \cdot 10^{20} \cdot n_A} \cong \frac{10^{-20}}{a \cdot n_A} \cong 10^{-35} \, \text{cm}^2, \quad \text{where } n_A = a^{-3} \cong 3 \cdot 10^{22} cm^{-3} \, \text{cm}^{-3}$$

is the concentration of atoms in the absorber. Moreover, this implies that the less is the registered energy, the more such events should occur, and hence the higher is the estimated cross section.

This estimated «magnetic cross section» is at the level of 10^{-35} cm^2 and it happens to be noticeably higher than typical values at level of 10^{-44} cm^2 for the conventional interaction WIMP-nucleus.

6.6 The experimental system SQUID-paramagnetic calorimeter

In this section [68], we consider some features of optimal experimental design for search of DM particles such as the neutralino.

A calorimeter with a possibly low energy detection threshold (not higher than 40 eV) is required. In addition, a solid-state absorber made up of atoms with strong spin-orbital effect, indicating the presence of a large (not lower than $B_{orb} \approx 10$ T) orbital magnetism, is needed. The only candidate for the role of calorimetric detector with energy threshold of the order of $\delta E \approx 40$ eV is the SQUID-paramagnetic absorber system [87, 88]. This cryogenic system (Figure 6.13) consists of a paramagnetic absorber, demagnetizing as a consequence of the heat transferred by the energy δE of the detected radiation, and of a quantum interferometer, measuring the corresponding decrease of the magnetic moment δm_{abs} of the absorber.

At sufficiently low temperatures ($T \approx 1$ K), the contribution of the atomic paramagnetism [89] to the heat capacity prevails on the phonon contribution, so the following relation holds: $\delta E \cong B \delta m_{abs}$ (where B depends on the mode of operation of the system, and it may be either the induction of the external magnetizing field [87] or the residual paramagnetic field [88]). The magnetic flux variation, directly registered by the SQUID, is $\delta\Phi \cong \dfrac{\mu_0 \delta m_{abs}}{h} \cong \dfrac{\mu_0 \delta E}{hB}$, where h is the absorber length (the height of the paramagnetic cylinder), and $\mu_0 = 4\pi \cdot 10^{-7}$ H/m.

The Superconducting Quantum Interference Device (SQUID) [80-82]), due to the sensitivity of its Josephson junctions, to the difference between the Cooper condensates quantum phases [1] and to the detected magnetic field flux inside the superconducting ring, fixes flux variations as a fraction of the basic period, that is the flux quantum $\Phi_0 = \dfrac{\pi\hbar}{e} \cong 2.08 \cdot 10^{-15}$ Wb (which corresponds to a phase change $\delta\varphi = 2\pi$). At the same time [68] a good, but not record sensitivity, of the modern interferometer is considered to attain the value $\delta\Phi \approx 10^{-6}\Phi_0/\sqrt{\text{Hz}}$. This value corresponds to the

energy resolution $\delta E \cong \dfrac{hB\delta\Phi}{\mu_0} \cong 2\times10^{-18}$ J/Hz ≈ 15 eV/Hz , if $h \approx 0.1$ m and $B \approx 0.01$ T, that makes it possible to fix $\delta E_\chi \approx 40$ eV, with maximal frequency nearly 10 events per second.

However, real conditions of experiment on the Earth correspond to the density of DM particle flux at the level of no more than 200 km/s $\times$ 1500 particles/m^3=3×10^8 s^{-1}m^{-2} with respect to the absorber. If we use as an absorber a paramagnetic material with strong atomic orbital magnetism with volume $h\times S\approx0.1$m$\times0.01$m^2, it would contain approximately 0.15 kmole $\approx10^{26}$ atoms. With the optimistic assumption of a cross section of magnetic interaction of $\sigma \approx 10^{-35}$cm^2, by using the Fermi Golden Rule, just mentioned in section 6.3, we get a maximum registration rate of $3\cdot10^{-5}$ events/s ≈ 4 events/day. Therefore, the margin of recording rate of about 6 orders of magnitude ($10/3\times10^{-5}$) can be used to compensate the loss of sensitivity of the system, associated with a low transmission coefficient of the superconducting flux transformer ($K < 1$, depending on the design [82]). This transformer provides [68] communication between the macroscopic working body of the absorber with the microscopic phase-sensitive ring of the SQUID, where the Josephson junctions are allocated (such compensation is possible up to the level of K $\approx (3\times10^{-5}/10)^{\frac{1}{2}} \approx 0.0017$). In fact, we should notice that, considering the size difference between the macroscopic calorimeter and the microscopic SQUID, a part of the magnetic flux is lost during the passage along the flux transformer.

Therefore, if we define the coefficient $K = \dfrac{\delta\Phi_{SQUID}}{\delta\Phi_{ABS}}$, where $\delta\Phi_{SQUID}$ is the variation of the magnetic flux registered by the SQUID, and $\delta\Phi_{ABS}$ is the variation of the magnetic flux inside the paramagnetic calorimeter, we notice that $K \ll 1$. The numerical value of this coefficient can be obtained by following these considerations:

- The real signal measured by the experimental apparatus is just the intensity of electric current, corresponding to the variation of magnetic flux registered by the SQUID;
- The intensity of electric current is proportional to the square of the amplitude of magnetic flux, and so also to its variation;
- The experimental quantity measured is, in reality, the squared value of the coefficient K.

According to these considerations, in order to calculate the considered coefficient, we can impose this relation of proportionality:

$K^2 : 1 \cong 3\cdot10^{-5} : 10$.

In fact, all these quantities can be directly registered by the experimental device. Therefore, we get:

$K \cong (3 \cdot 10^{-6})^{\frac{1}{2}}$ as it has been previously considered. We present a sketch of the SQUID-paramagnetic absorber in figure 6.13.
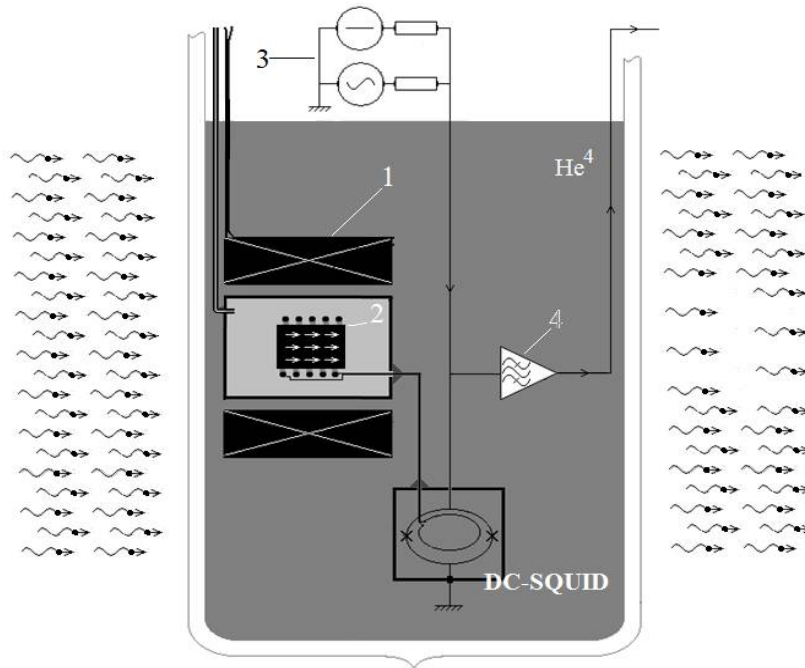

Figure 6.13 *Scheme [68] of the SQUID-paramagnetic absorber system: 1) – the superconducting solenoid magnetization; 2) the paramagnetic absorber; 3) current generators; 4) narrow–band low-frequency amplifier.*

6.7   Non-corpuscular "ether wind" and possible registration of its pressure by the SQUID-magnetostrictor system

In this section, we consider [68] a new approach for DM description, based on the possibility that DM and DE (the latter, as we have just noticed in section 6.2, could be responsible for the additional relative acceleration in the Hubble law of galaxies recession), can be considered as two different aspects of the same cosmological essence, named "Dark Substance".

According to this model DE, with its density of about 300 TeV/m^3, represents the unperturbed state of "Dark Substance", while its swings or perturbations play the role of elementary DM particles. These particles will be stable if all their decay channels into any combination of other

particles are blocked, or also, in our case, if their potential will have local minima, i.e., local traps providing metastable excited states. The Hamiltonian with metastable traps can be represented, for example, as follows:

$$\mathbf{H} = \frac{1}{2}\left(\frac{\partial \varsigma}{\partial x}\right)^2 + \frac{1}{2c^2}\left(\frac{\partial \varsigma}{\partial t}\right)^2 + \alpha \varsigma^* \varsigma - \beta \cos \gamma \sqrt{\varsigma^* \varsigma} \qquad (6.6)$$

The nonlinear wave equation, corresponding to this Hamiltonian, and describing the dynamics of perturbations to Dark Substance will be similar to the "quasi-sine-Gordon" equation, having the following analytic expression:

$$\frac{\partial^2 \varsigma}{\partial x^2} - \frac{1}{c^2}\frac{\partial^2 \varsigma}{\partial t^2} + \alpha \varsigma^* + \frac{1}{2}\beta \gamma \sqrt{\varsigma^*/\varsigma} \sin \gamma \sqrt{\varsigma^* \varsigma} = 0. \qquad (6.7)$$

Moreover, the nonlinear potential $\Pi(\varsigma) = \alpha \varsigma^* \varsigma - \beta \cos \gamma \sqrt{\varsigma^* \varsigma}$ appearing here, has the analytic structure very similar to the "parabolic washboard potential" [81] used to describe metastable states in the superconducting ring of a SQUID with one Josephson junction, namely:

$$\Pi(\varsigma) = \alpha |\varsigma|^2 - \beta \cos \gamma |\varsigma| \Leftrightarrow E(\Phi) = \frac{1}{2L}\Phi^2 - I_C \Phi_o \cos \frac{2\pi}{\Phi_o}\Phi, \qquad (6.8)$$

where Φ is the magnetic flux threading the superconducting ring and L is the inductance of the loop itself. We represent the profile [68] of the washboard potential in figure 6.14. Some comments about this figure are needed. For small ς (when the disturbance has not yet reached the first trap) swings of the Dark Substance have a quasi-harmonic character, and their quanta will have a mass

$$m = \frac{\hbar}{c}\sqrt{2\alpha + \beta\gamma^2}.$$

In order to prove this relation, we consider equation (6.7), in the limit of very small value of the perturbation. Therefore, for $\varsigma \ll 1$, we can express the last addendum in (6.7) as follows:

$$\frac{1}{2}\beta\gamma\sqrt{\frac{\varsigma^*}{\varsigma}}\sin(\gamma\sqrt{\varsigma^*\varsigma}) \cong \frac{1}{2}\beta\gamma\sqrt{\frac{\varsigma^*}{\varsigma}}\gamma\sqrt{\varsigma^*\varsigma} = \frac{1}{2}\beta\gamma^2\varsigma^*$$

where we have used the property $\sin\theta \cong \theta$, valid for $\theta \ll 1$, as it follows from Taylor's expansion of sine function. Therefore, from equation (6.7), we get:

$$\frac{\partial^2 \varsigma}{\partial x^2} - \frac{1}{c^2}\frac{\partial^2 \varsigma}{\partial t^2} + \alpha \varsigma^* + \frac{1}{2}\beta\gamma^2 \varsigma^* = 0.$$

By carrying out the opportune calculations in this expression, we obtain:

$$\frac{\partial^2 \varsigma}{\partial x^2} - \frac{1}{c^2}\frac{\partial^2 \varsigma}{\partial t^2} + \left(\frac{2\alpha + \beta\gamma^2}{2}\right)\varsigma^* = 0 \qquad\qquad (6.9)$$

If we compare the (6.9) with the Klein-Gordon equation, that can be expressed as follows:

$$\frac{\partial^2 \varsigma}{\partial x^2} - \frac{1}{c^2}\frac{\partial^2 \varsigma}{\partial t^2} + \left(\frac{c}{\hbar}m\right)^2 \varsigma = 0 , \qquad\qquad (6.10)$$

we may consider this relation: $\left(\dfrac{c}{\hbar}m\right)^2 = \dfrac{2\alpha + \beta\gamma^2}{2}$, so that:

$$m = \frac{\hbar}{c}\sqrt{\frac{2\alpha + \beta\gamma^2}{2}} \propto \frac{\hbar}{c}\sqrt{2\alpha + \beta\gamma^2} . \qquad\qquad (6.11)$$

Equation (6.11) is thus the analytic expression for the mass of these perturbations, that so coincides with the mass of DM particles for the lowest relative minimum of their energy, for which they are stable.

Nevertheless, these particles may be unstable, and the rate of decay from classical positions will correspond to the viscosity of the Dark Substance [107, 108]. At large amplitudes [68] of ς, the disturbance at some moment will "catch" the lowest energy trap. The trajectory of the oscillation ς will now be a circle in the plane {ς, ς*}, corresponding to a local minimum of the potential. The rotation around the circumference of a local minimum is similar to the mechanism of occurrence of massless Goldstone bosons in Weinberg-Salam's model. However, in this example, the mass of excitations ("zero energy") is determined by the height of the bottom of the trap with respect to the main vacuum state ς=0 ς*=0, and will be non-zero. The stability of such excitations, playing (in this example) the role of DM particles, is guaranteed by the height of the wall of the potential well, occurring in the vicinity of the local potential minimum.

$$V(\varphi) = -\,m^2(\varphi^*\varphi) + \lambda\,(\varphi^*\varphi)^2$$

$$\Pi(\varsigma) = \alpha(\varsigma^*\varsigma) - \beta\,\cos\,(\gamma\sqrt{\varsigma^*\varsigma}) \leftrightarrow E(\Phi) = \frac{1}{2L}\Phi^2 - I_C\Phi_0\cos\frac{2\pi}{\Phi_0}\Phi$$
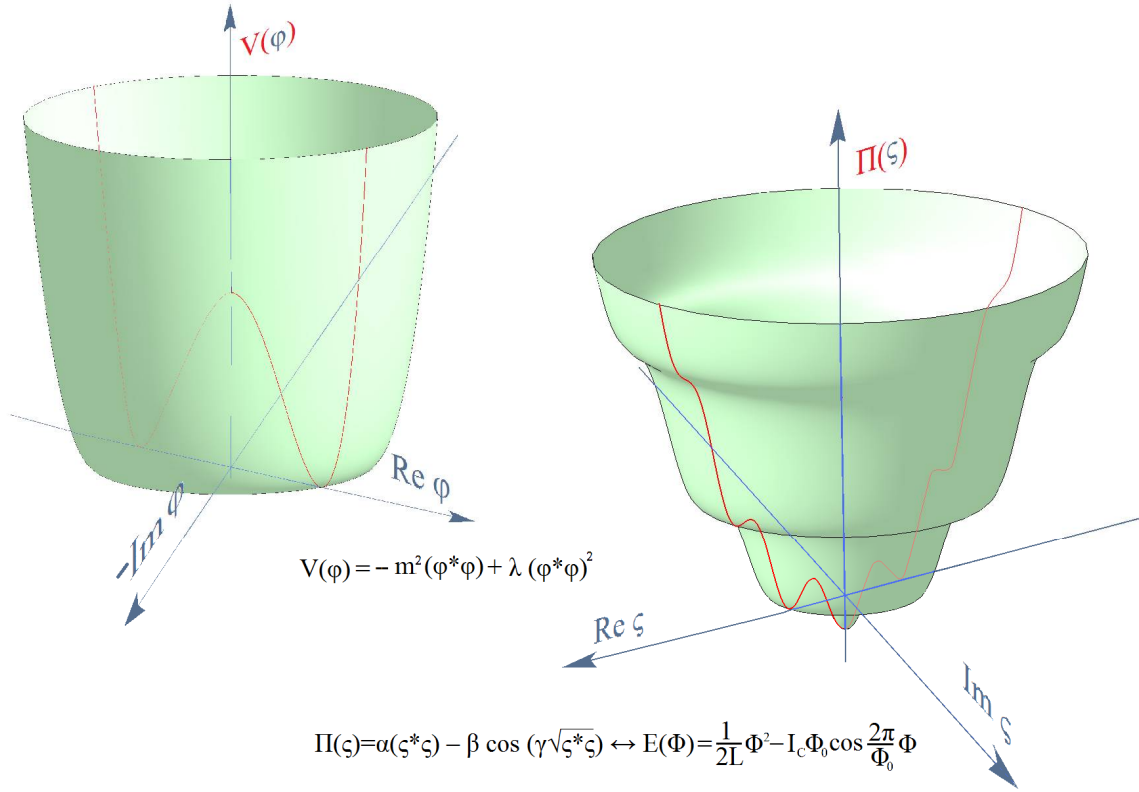
Fig 6.14. On the right, the washboard potential [68], characterized by local minimum positions, which are the metastable states of DM particles, is shown. The lower local minimum is associated with a light (or also hot) component of DM, and the top one with a heavy (or also cold) component of DM. The absolute minimum lies in the region of negative energies and is associated with antigravitational properties of DE. On the left (for comparison) [68] the potential used in models of spontaneous symmetry breaking is displayed.

According to these considerations we can do a comparison between the properties of these excitations, playing the role of DM particles, and the ones of Goldstone boson, described in the Standard Model of Particle Physics. In fact, also in the case of the Golstone boson, we have a position of stable equilibrium, coinciding with a minimum in the energy of this particle. However, it is a position of absolute minimum, where the Goldstone boson, with zero mass, is absolutely stable. Instead, the excitations (and so the DM particles) occupy positions of relative minimum of their energy, while the position of energy absolute minimum is occupied by the DE, that, according to the theoretical model we are describing, is the unperturbed state of the Dark Substance. So the mass, different from zero, of DM particles, is represented by the difference in energy between the state of energy relative minimum, where they are present, and the state of absolute minimum, occupied, according to our theoretical model, by DE.

If we provide an outside excitation to the system, the energy and so also the mass of these perturbations increase: in the lowest relative minimum these perturbations are stable, and coincide with the DM particles that we can directly register.

Therefore, the search [68] of DM particles, as stable moving excitations of Dark Substance, may be intimately connected with the research of the action of the DE non-corpuscular flux on the ordinary matter. By knowing that the free mean path is connected to the cross section of interaction by the relation $\ell^* \approx 1/(\sigma n_A)$, we may say that DE transfers to a slab of material, consisting of ordinary atoms of concentration n_A, with area S and "maximum depth" $l^* = \dfrac{1}{\sigma n_A}$, a momentum

$$q = \frac{E_{DE}}{v} = \frac{l^* S \rho_{DE}}{v}\,,$$ where E_{DE} is just the DE energy and v is the speed of DM particles relative to the substance, or equivalently, the velocity of the same material relative to DE, which is, as just considered, the unperturbed state of Dark Substance. In this way, Dark Substance exerts the pressure $p_{DE}^* = \dfrac{F}{S} = \left(\dfrac{l^* S \rho_{DE}}{v}\right)\left(\dfrac{l^*}{v}\right)\dfrac{1}{S}$ on the slab, where we have expressed the force F as the ratio between the momentum q and the time occuring in the slab crossing, i.e. $\tau = \dfrac{l^*}{v}$. As we are interested to the pressure drop on finite distance l, we can recur to the condition of mechanical equilibrium, according to which the pressure density is constant inside this slab of material, and so we get:

$$\frac{p_{DE}^*}{V^*} = \frac{p_{DE}}{V} \Rightarrow \frac{p_{DE}^*}{l^* S} = \frac{p_{DE}}{lS} \Rightarrow p_{DE} = \frac{l}{l^*}\, p_{DE}^*, \qquad\qquad (6.12)$$

where we have assumed a uniform section S throughout the material. Therefore, the effective pressure drop across the length ℓ is estimated as $p_{DE} = p_{DE}^*\, \dfrac{l}{l^*} = \rho_{DE} l \sigma n_A$.

In accordance with the generally accepted value of the average density of Dark Energy $\rho_{DE} \approx$ 300 TeV/m^3, taking into account the above-obtained "optimistic" estimation of the interaction cross section $\sigma \approx 10^{-35}$ cm^2, the pressure drop across a one-meter barrier, having a concentration of atoms $n_A \approx 3\times10^{22}$ cm^{-3}, will be of the order of $p_{DM}(l=1\,m) \approx 7\times10^{-16}$ Pa, where we have used the well-known conversion factor: $1\,eV = 1.6\cdot10^{-19}$ Joule. By considering a material of cilindrical form, of dimensions $l\;x\;S = 1\,m\;x\;0.15\,m^2$ with surface area $S = 0.15\,m^2$, the force corresponding to this pressure is so represented:

$$F = p_{DE}S = 14 \cdot 0.15 \cdot 10^{-16} Pa \cdot m^2 \cong 10^{-16} \text{N} . \qquad (6.13)$$

The above expression represents the value of the force exerted by the flux of DM particles, or equivalently, by the corresponding flux of DE.

6.8 The SQUID-magnetostrictor system

In this section we propose a second type of experimental device, the SQUID-magnetostrictor system, in order to register DM fluxes.

We start by noticing that, in order to register the pressure, and thus the force, exerted by DE or DM flux on a material, a dynamometer capable to fix the strength of 10^{-16} N at the end of the cylinder, with dimensions $l \, x \, S \approx 1\text{m}\times0.15\text{m}^2$, is required. Apparently, the only candidate for the role of the ultra-high-sensitivity dynamometer is the SQUID-magnetostrictor system [84, 109, 110]. This experimental system has been previously supposed to be used in projects for the detection of gravitational waves (Figure 6.15).
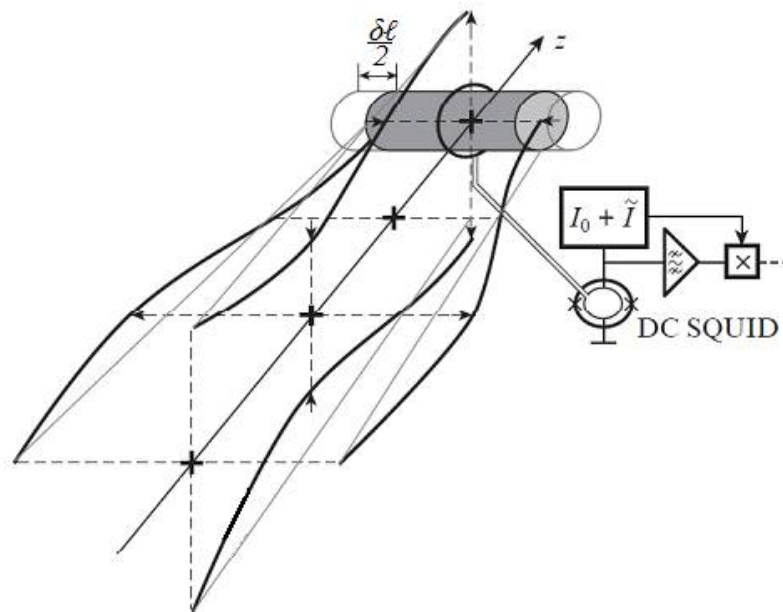

Figure 6.15. *Schematic view [68] of the SQUID-magnetostrictor system for the detection of gravitational waves (the magnetostrictive cylinder is represented in grey) [110].*

Ultra-high sensitivity is achieved by means of this system. In fact, high strain-gauge effectiveness of the sensor can be achieved, since it operates on the principle of the reverse magnetostrictive

effect, generated, in its turn, by collective quantum solid-state effects [110]. On the other hand [68], the high ("quantum scale" level) sensitivity of SQUID systems, used as measuring instruments, allows accurate registration of events. The physical quantity [68] describing the reverse magnetostrictive effect (discovered by Emilio Villari in 1865, and thus called Villari Effect) in a particular material is the ratio of the internal magnetic induction field to the growth of its outside pressure, i.e.,

$$\Lambda^{-1} = \frac{\partial B}{\partial P} . \qquad (6.14)$$

For example, an alloy made up of 54% Pt and 46% Fe, with the coefficient of magnetic permeability $\mu \approx 14000$, will have $\Lambda^{-1} \approx 10^{-4}$ T / Pa (which is basically not a record value). Thus the magnetic response, measured by the SQUID, is related to the force action δF by this expression:

$$\delta\Phi = \Lambda^{-1}\delta F . \qquad (6.15)$$

Equation (6.15) can be interpreted as the relation between the external excitation, represented by the force δF, and the response of the system, represented by the variation of the magnetic flux $\delta\Phi$. In fact, as a consequence of the force (or also of the pressure) exerted by the flux of DE (or of DM particles), there is a variation in the dimensions of the material, which determines, according to the Villari Effect, a variation in the magnetization, and so in the induction magnetic field, of the considered material, as we may notice from equation (6.14).

Accordingly, the capability to register the pressure of non-corpuscular Dark Matter flow, estimated above for $\sigma \approx 10^{-35} cm^2$ at $\delta F \approx 10^{-16}$ N, requires an "absolute" (not reduced to the time of the signal accumulation) SQUID sensitivity for the magnetic flux of the order of magnitude of 10^{-20} Wb $\approx 5\times10^{-6}\Phi_0$.

In fact, by using the equation (6.15), for $\Lambda^{-1} = 10^{-4}\frac{T}{Pa}$, and $\delta F \cong 10^{-16}$ N, we get a value of $\delta\Phi = 10^{-20}$ Wb $\cong 5\cdot10^{-6}\Phi_0$, which is independent from the time of signal accumulation. The actual value of sensitivity of a good DC-SQUID is of about $\delta\Phi \approx 10^{-6}\Phi_0/\sqrt{Hz}$, which provides the desired sensitivity with a margin of approximately 2 orders of magnitude (at least) due to the possibility of a 3-hour signal accumulation. In order to compare the numerical value of the SQUID sensitivity, which is time dependent, with the numerical value of $5\cdot10^{-6}\Phi_0$, which is, instead, time independent, we can multiply the value of SQUID sensitivity for the square root of the frequency. In this way, considering a time of three hours, we obtain a value of frequency

$$\nu = \frac{1}{T} = \frac{1}{3600\cdot3\,\text{sec}} \cong 10^{-4}\,Hz \Rightarrow \sqrt{\nu} \cong 10^{-2}\sqrt{Hz} , \text{ and so we get: } 10^{-6}\frac{\Phi_0}{\sqrt{Hz}}\cdot10^{-2}\sqrt{Hz} = 10^{-8}\Phi_0,$$

which, as just considered, provides the desired sensitivity with a margin of approximately two orders of magnitude.

6.9 Conclusions

In this chapter, starting from an introduction [68] about DM and its cosmological properties, we have focused our attention on the possible creation of neutralino magnetic moment, the estimation of its magnetic interaction cross section, and a brief description of a model unifying DE and DM.

In particular, we have found magnetic moments for neutralino to be 5 orders of magnitude smaller than the one for electrons, and a magnetic interaction cross section that is 9 orders of magnitude larger than the one corresponding to the conventional interaction WIMP-nucleus. The specificity of this magnetic-type interaction is in its "tangential character", as it is an interaction at distance with the magnetic field induced by the orbital motion of atomic electrons. So, there is a remarkable difference with the conventional DM scattering, in which only the atomic nucleus is concerned and the electron contribution is negligible. We have described the SQUID-paramagnetic absorber experimental system that, having an energy resolution of 15 eV, is very suitable for the registration of DM particles and their interactions. Technical details about this system are discussed, and several modes of its operation are briefly mentioned.

In the context of "unifying" trend, clearly dominant in the modern elementary particle physics, we have also proposed a simple model, where we try to consider the corpuscular Dark Matter and non-corpuscular Dark Energy from uniform position. In this proposed model, the Dark Energy is an absolutely continuous substance, playing the role of vacuum for metastable excitations, which can be identified as Dark Matter particles. Estimates, carried out in the framework of this model, indicate the possibility of experimental detection of the "ether wind" pressure, created by the non-corpuscular incoming flow, corresponding to the galactic orbital motion of the Earth. It is argued that these types of investigations could be performed by using the SQUID-magnetostrictor experimental system.

Appendix 6.1

Two particular experimental devices using superconducting detectors

In this appendix we consider two particular experimental devices, one that is a planar array of superconductors [77], and the other one which is the two-channel mode SQUID paramagnetic absorber system [92].

Let us begin to describe the first experimental device. A planar array of superconductors consists of several superconducting islands [77], displaced in a matrix geometrical planar form, where each superconductor is weakly coupled to the next one and so all this device constitutes a multi-channel detector of Josephson junctions. We give a sketch of this experimental device in the next figure.
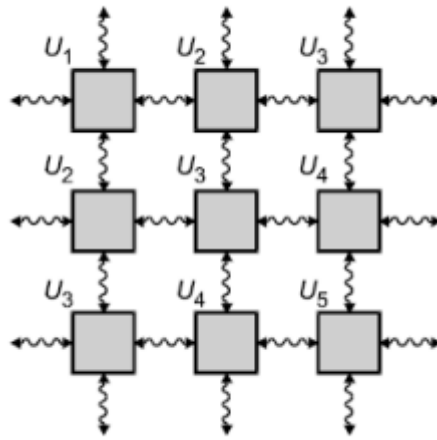

Figure 6.1.1. *Schematic representation of a detector of particles of DM. In the picture U_i is the potential on a plate of a type I superconductor; the wavy lines denote a weak coupling between plates. From G. N. Izmailov, Superconductors as detectors of particles of Dark Matter, Measurement Techniques, Vol. 51, No. 11, 2008.*

Each couple of superconductors is connected with an electro-motive force (e. m. f.) source. The interaction of a WIMP particle on this device determines the effects just considered in the beginning of section 6.4. In this case, however, we have also the presence of the e. m. f. source, which creates a potential difference U between superconductors, and so an electric current, made up by the electrons generated by the local breaking of Cooper pairs, can flow between the two coupled

superconductors if it is realized the condition $eU > \Delta$, i.e. if the electrostatic energy, determined by the e. m. f., is larger than the energy gap Δ associated to the superconducting state. This electric current is registered by using a galvanometer G. Just for sake of completeness, we may consider that this energy gap of a superconducting material is defined as the energy difference between the ground state and the Fermi level of energy, as only the electrons whose energy coincides with the Fermi level of energy can form the Cooper pairs, through the interaction of phonons [111]. When the electrons [77] arrive from the first to the second superconducting platform, they re-arrange in new Cooper pairs, because it is well known that the superconducting state is characterized by a value of energy which is lower than the one of the normal state [111]. In this process phonons are emitted from the second platform, as a consequence of the energy transition from the normal to the superconducting state, and they are registered by using a particular bolometer. We represent a sketch of a couple of superconductors of this planar structure, with the connected galvanometer and the emission of phonons in figure 6.1.2.
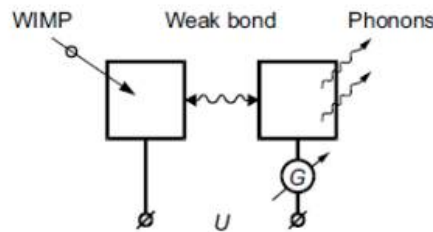

Figure 6.1.2. *Schematic depiction of a detector cell. G is the galvanometer to record the current. From G. N. Izmailov, Superconductors as detectors of particles of Dark Matter, Measurement Techniques, Vol. 51, No. 11, 2008.*

Thus, as we can also see from the figure, we have three trials at our disposal in order to register the WIMP interaction on this device:

- The passage of an electric current between two of the superconducting platforms, registered by the galvanometer G;

- The emission of phonons from one of the platform, registered by the bolometer;

- The occurrence of these events only from one of the superconductors of this planar structure, that is a phenomenon due both to the rarity of WIMP interactions, and also to the particular geometrical form of all the experimental apparatus.

For sake of completeness, we can consider [77] that by using bolometers, it is possible to register the variation of a typical physical quantity with varying temperature. In fact, the interaction of a particle on a bolometer determines an increase in temperature, and consequently a variation of a

typical observable quantity, temperature depending, such as the electric resistance, the magnetic susceptibility, and so on. In this way, it is possible to determine the rate of particle interactions, also if we cannot determine the identity of the considered particle.

Let us now consider the second experimental device [92]. It is a particular version of the SQUID-paramagnetic calorimeter system, that is based on a dual channel mode in order to eliminate, or at least to reduce, the lepton and photon processes. As it was seen in section 6.6, we have two devices, namely the magnetic calorimeter, that can be of cylindrical form, with radius R and height H, and the SQUID. In section 6.6 we have described the properties of this experimental apparatus, and also the consequences of a WIMP interaction on it. Here, we outline [92] the original experimental two channel scheme, by which it is possible to try to eliminate, or at least minimize, the electron recoil background, i.e. the lepton and photon processes of interaction on this device.

In fact, in the process of WIMP-nucleus scattering, we have to consider the two times τ_1 and τ_2:

-   τ_1 is the nuclear relaxation time spin-spin, in which the set of nuclear spins reaches the equilibrium condition, after being perturbed by the local absorption of the energy ΔE, and it is of about 10^{-3} seconds;

-   τ_2 is the relaxation time spin-phonon, in which the energy ΔE that is absorbed by nuclei, is transferred, in the form of phonons, to the crystal lattice and to the electrons, and it is of about 10 seconds.

We can notice that $\tau_2 >> \tau_1$. A schematic representation of this device is shown in figure 6.1.3. By using SQUIDs it is possible to register the ratio of the mean demagnetization rates before the condition of thermal equilibrium, that is $\dfrac{\Delta\Phi(t < \tau_1)}{\tau_1}$, and after this condition, that is $\dfrac{\Delta\Phi(t > \tau_2)}{\tau_2}$.

Each of these terms is the mean value of the magnetic flux variation in a well-defined time interval, that is τ_1 or τ_2, calculated on the local surface area of the calorimeter, interested by such energy variation ΔE. So, we get the mean demagnetization rate:

$$\eta_{WIMP} = \frac{\dfrac{\Delta\Phi(t < \tau_1)}{\tau_1}}{\dfrac{\Delta\Phi(t > \tau_2)}{\tau_2}} . \qquad (6.1.1)$$

By carrying out the opportune calculations, reported in reference [92], one obtains:

$$\eta_{WIMP} = \frac{2\pi H}{R}\frac{\tau_2}{\tau_1} . \qquad (6.1.2)$$

By taking opportune values of radius R and height H of the magnetic calorimeter, we may set:

$$\frac{2\pi H}{R} = 1 .$$

Therefore, for $\tau_1 = 10^{-3}$ seconds and $\tau_2 = 10$ seconds (typical values for sample of copper), we obtain $\eta_{WIMP} = 10^4$.
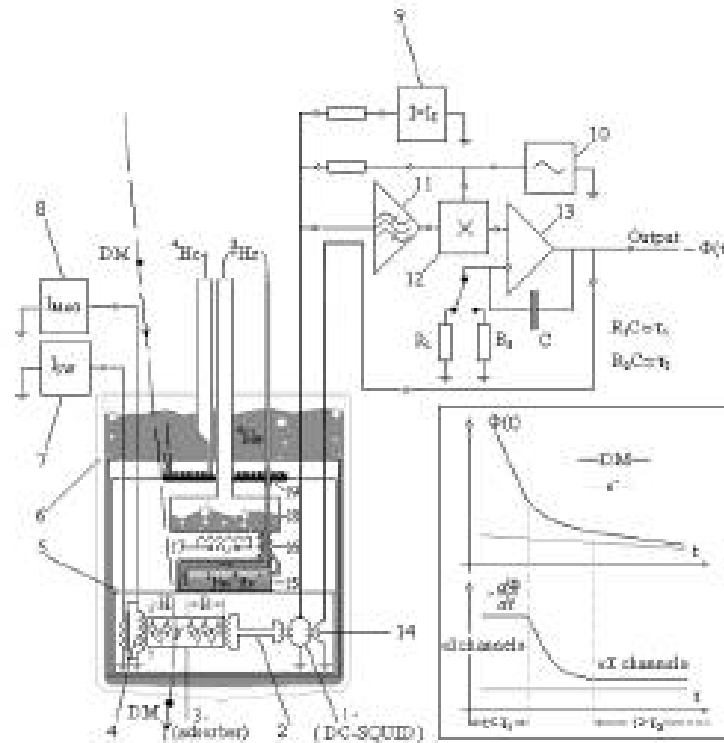

Figure 6.1.3. *The basic elements [92] of the apparatus: 1 - DC SQUID (Josephson junction are marked by crosses); 2 - superconducting flux transformer; 3 - absorber with a nuclear spin system; 4 - superconducting solenoid with a valve for the magnetic field "freezing"; 5 - superconducting screen; 6 - cryostat with liquid helium-4; 7 - current source for controlling the superconducting valve; 8 - power supply for superconducting solenoid. Components of the SQUID electronics: 9 - current source for the DC- SQUID operating- point shift above the overall critical current for the first and second Josephson junctions; 10 - alternative current generator (f =100 kHz); 11 - selective amplifier; 12 - phase detector; 13 - integrator with a variable time constant; 14 - biasing coil of the SQUID autocompensation system; analysis of the bias rate is perceived to be done by a computer after the analog-digital conversion of the output signal; analog blocks 9, 10, 12 and 13 may be also replaced by digital systems DAC and ADC under general computer control. Refrigerator for helium-3 solution in helium-4: 15 - solution chamber; 16 - counter heat exchanger; 17 - heater of the evaporation chamber; 18 - evaporation chamber (lines of the helium-3).*

In the case of leptons and photons, as they can significantly interact [77] only with the atomic or free electrons of the working substance of the considered detector, there is not a direct WIMP scattering on electrons, and consequently we only have the relaxation time spin-phonon τ_2. Therefore, one can set:

$$\eta_{e^-} = \frac{2\pi H}{R}.$$

(6.1.3)

Notice that η_{e^-} is $\dfrac{\tau_2}{\tau_1}$ times smaller than η_{WIMP}. These results can be used in order to distinguish WIMP scattering from the background events, as, if we register, by using SQUIDs, a value of $\eta \cong 10^4$, it is the sought signl for WIMPs, otherwise, if we have $\eta \cong 1$, it is the signal of electron recoil. Therefore, we have described the dual channel mode of the experimental system SQUID-paramagnetic absorber.

We can also consider another version of this experimental device, which is presented in the next figure. In this device, instead having a single absorber, with a single SQUID, we consider a set of metal cylindrical absorbers, each one directly connected to a small paramagnetic concentrator, in turn connected to a SQUID through a superconducting flux transformer. This experimental apparatus registers WIMPs by using the anticoincidence technique among the various absorbers.
In fact we notice that the rate of interaction of WIMP particles is very small (around 4 events per day [33, 68]) as a consequence of their very small values of cross section (of about $10^{-44} - 10^{-35} cm^2$ [64, 68]), and so there is not multiple scattering on the various absorbers of our device, but only one of the absorbers is hired. On the contrary, in the case of electrically neutral and massive particles, for example neutrons, which are hadrons, we may have multiple scattering, due to their higher values of cross section (in the range of $10^{-26} - 10^{-20} cm^2$ in the range of energy of $10^{-1} - 10^8 \, eV$) and so to their higher rates of interaction than the ones of WIMPs [92]. Therefore, by using the technique of anticoincidence [68], in which only one of the absorbers is hired, we have the possibility to distinguish between DM particles and electrically neutral and massive hadrons. We show this experimental apparatus in figure 6.1.4.
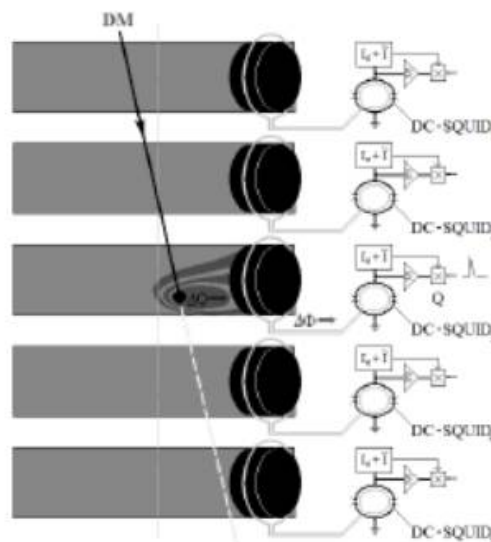

Figure 6.1.4. *The scheme [92] of magnetic multi-channel calorimeter with SQUID, destined to search DM particles, where the veto system operates at anticoincidence concept in adjacent channels: gray cylinders - separate blocks of metallic absorbers; the black cylinders - the paramagnetic concentrators of heat micro release, each concentrator is connected with separate SQUID by means of superconducting flux transformer; crosses - Josephson junctions included in SQUID.*

It is also interesting to consider [92] the structure of one of the cylindrical calorimeter in our experimental array. In fact, we notice that each calorimeter is made up by a metallic absorber and a paramagnetic concentrator, directly connected between them. The metallic absorber has bigger dimensions than the ones of the paramagnetic concentrator, in order to improve the rate of interaction of DM particles, as it has been remarked in section 6.3, so we just consider the DM interactions on this part of the calorimeter. The paramagnetic concentrator, as the same name suggests, is made up by a paramagnetic material, and it is maintained at very small temperature (of about 1 K), so that we can follow all arguments outlined in section 6.6, and so it is possible to register the variation of the magnetic flux corresponding to DM particles energy release, as it has been just considered in section 6.6. In order to minimize the magnetic flux losses during the passage along the flux transformer, connecting the paramagnetic concentrator and the SQUID, the variation in the magnetic flux, registered by the latter, is just coming from the paramagnetic concentrator. This device has the very important property to collect all the heat transferred to the absorber by the DM particles interactions. In fact, it is well known that the specific heat (and so the thermal capacity) of a metallic material, for values of temperature T tending to zero, is directly proportional to temperature, while for a paramagnetic material, as just outlined in section 6.4, is inversely proportional to the squared value of temperature. Therefore, considering the condition of thermal equilibrium inside all the calorimeter, we get:

$$T = \frac{\Delta Q}{C} = T_{conc} = \frac{\Delta Q_{conc}}{C_{conc}} \quad . \qquad (6.1.4)$$

Also, we have considered that $C = C_{abs} + C_{conc} \cong C_{conc}$, and so we obtain:

$$\Delta Q \cong \Delta Q_{conc}. \qquad (6.1.5)$$

In this way, we have proven that all the heat can be transferred to the paramagnetic concentrator. This device, having smaller dimensions than the metallic absorber, can also minimize [92] the magnetic flux losses in the passage through the flux transformer to the SQUID, so that this latter can operate with improved resolution in magnetic flux registration.

Concluding remarks

This PhD thesis consists of six chapters: the first four chapters describe theoretical properties of Josephson junctions; chapter 5 deals with one junction and two junction interferometers, analyzed from classical and also quantum positions; finally, chapter 6 is concerned with the application of superconductors and SQUIDs as detectors of Dark Matter. Let us analyse each chapter in further details.

In chapter 1 we have considered a microscopic description of N coupled superconductors in which nearest-neighbour interactions are present. Starting from the time evolution of the fermionic operators $\hat{c}$ and $\hat{c}^+$ in the Heisenberg picture, we obtain a set of coupled ordinary differential equations for the order parameters Δ_i. Since the main aim of this chapter is to show that Feynman's model for a single Josephson junction can be justified by a microscopic analysis, we have specifically written the resulting system of differential equations in the case of two coupled superconductors. In this simple case Feynman's model is obtained. In this way, one can argue that it must exist a strict correspondence between the microscopic picture described in the present chapter and the semi-classical analysis proposed by Feynman and successively refined by Ohta. Therefore, generalizations of Ohta's model to multi-barrier Josephson junctions [8] based on the semi-classical analysis developed by the latter authors can be retained to agree with a strict microscopic description of these systems.

In chapter 2, the properties of an over-damped Josephson junction have been analyzed by means of a mechanical analogue: an over-damped pendulum. The strict analogy between the dynamical equations of the two systems [15], [2], [3], [17], has been first reviewed. Being the physical properties of a simple pendulum very well known, the Josephson junction dynamics in the over-damped limit may be derived by analogy. Therefore, we have analyzed [16] some interesting features of an over-damped Josephson junction, by means of the corresponding physical properties of the over-damped pendulum. As an example, we have noticed that the current-voltage characteristics of the superconducting device can be obtained by means of an analytical expression derived for the normalized driving moment as a function of the time average of the angular frequency. Finally, by considering the energy balance equation for the system, we have seen that it is possible to describe the effect of the driving moment on the pendulum through the tilting and stretching of the washboard potential.

In chapter 3, we have analysed two particular superconducting systems: an inhomogeneous three-layer characterized by a constant non-null phase of the inner electrode, and an inhomogeneous four-layer with null phases of the inner two electrodes. In the first case (inhomogeneous DBJJ), we have calculated the CPR, in terms of the inhomogeneity parameter ε and of the parameter describing the coupling between the two outermost electrodes γ, obtaining an expression which reduces, for $\varepsilon = 0$, to the current-phase relation found by Romeo and De Luca for a homogeneous DBJJ in ref. [14]. In the second case (inhomogeneous TBJJ), we have found that the term describing the interaction between the outermost electrodes is absent, so that the CPR is formally identical to the expression for the DBJJ, provided one sets $\gamma = 0$. In fact, when considering nearest and next nearest neighbour interactions, the two superconducting layers S_2 and S_3 in a TBJJ act as a single quantum system assumed to be described by the same superconducting phase. When sandwiched between S_1 and S_4, however, the intermediate layers S_2 and S_3 do not allow direct coupling between the outermost layers as it happens in a DBJJ, so that the $\sin\phi$ term disappears in the CPR of a TBJJ. We have noticed that the maximum Josephson current I_{MAX} in TBJJs depends on the inhomogeneity parameter ε as follows: $I_{MAX} = I_0(1-\varepsilon)$, where I_0 is a constant which depends on the superconducting properties of the four layers. Furthermore, by means of a Fourier expansion of the CPR found in the present work, we have calculated the Shapiro steps for a homogeneous (ε

=0) TBJJ. In this respect, we have noticed appearance of integer and fractional Shapiro steps in the *I-V* characteristics of these systems. We were able to determine, by a standard analytic procedure, at least for the homogeneous case, the semi-amplitudes of these quantities, both for the case of integer and fractional Shapiro steps.

In chapter 4 the *I-V* characteristics of triple-barrier Josephson junctions have been studied in the presence of a constant current bias and of a r. f. voltage radiation. In the case of constant current bias, we have first analysed the homogeneous case ($\varepsilon = 0$), in which the Josephson coupling between superconducting regions does not depend on the particular pair of layers considered. In this case we have been able to analytically determine the *I-V* characteristics of TBJJs in the presence of a constant current bias. Adopting the RSJ model, the analytically determined *I-V* curves are seen to be formally identical to the canonical ones derived for JJs. For inhomogeneous Josephson coupling ($\varepsilon \neq 0$), on the other hand, numerical evaluation of *I-V* shows that deviations of these curves from the analytically determined characteristics for $\varepsilon = 0$ are seen to be compatible with the expression of maximum Josephson current $I_{MAX} = (1 - \varepsilon)I_0$. In the presence of a r. f. radiation the *I-V* characteristics show integer and fractional Shapiro steps. By a standard semi-analytic approach, expressions of the semi-amplitudes of these steps have been determined for $\varepsilon = 0$. Numerical evaluation of *I-V* curves, performed for $\varepsilon \neq 0$, shows persistence of integer and fractional Shapiro steps.

In chapter 5 the classical and quantum behaviour of one-junction and two-junction interferometers have been considered. While the classical behaviour of both systems is already well known, we have proposed a unifying approach to the study of their electrodynamic properties, suggesting an equally unified analysis in the quantum regime. Therefore, starting from the analytic expression of the washboard potential, the 2 x 2 quantum Hamiltonian acting on the quantum states $|0\rangle, |1\rangle$ is obtained by promoting the classical variables, in the classical potential, to the role of operators. The persistent electric currents in the quantum regime are seen to follow closely the qualitative behaviour of the homologous quantities in the classical system, showing alternating occurrence of diamagnetic and paramagnetic states for increments of n_{ex} equals to 1/2. It is important to notice that the present analysis can be immediately extended to Hilbert spaces spanned by more than two quantum states. Therefore, in the present analysis, we have noticed that multi-valued logic states can be obtained in the quantum regime, by generalizing the well-known classical properties of a two-junctions interferometer. In this way, quantum computing based on qutrits, rather than qubits, could be implemented by considering the properties of a two Josephson junctions interferometer, whose quantum states are generated by the orthogonal kets $|0\rangle, |1\rangle,$ and $|2\rangle$.

In chapter 6 we have analyzed the experimental techniques for the registration of Dark Matter based on superconductors and SQUIDs. Starting from an introduction [68] about DM and its cosmological properties, we have focused our attention on the possible creation of neutralino magnetic moment, the estimation of its magnetic interaction cross section, and a brief description of a model unifying DE and DM. In particular, we have found magnetic moments for neutralino to be 5 orders of magnitude smaller than the one for electrons, and a magnetic interaction cross section that is 9 orders of magnitude larger than the one corresponding to the conventional interaction WIMP-nucleus. The specificity of this magnetic-type interaction is in its "tangential character", since it is an interaction at distance with the magnetic field induced by the orbital motion of atomic electrons. A remarkable difference thus exists between this type of interaction and the conventional DM scattering, in which only the atomic nucleus is concerned and the electron contribution is negligible. We have described the SQUID-paramagnetic absorber experimental system that, having an energy resolution of 15 eV, is very suitable for the registration of DM particles and their interactions. Technical details about this system are discussed, and several modes of its operation are briefly mentioned. In the context of "unifying" trend, clearly dominant in the modern elementary particle physics, we have also proposed a simple model, where we try to consider the corpuscular Dark Matter and non-corpuscular Dark Energy from uniform position. In this proposed

model, the Dark Energy is an absolutely continuous substance, playing the role of vacuum for metastable excitations, which can be identified as Dark Matter particles. Estimates, carried out in the framework of this model, indicate the possibility of experimental detection of the "ether wind" pressure, created by the non-corpuscular incoming flow, corresponding to the galactic orbital motion of the Earth. It is argued that these types of investigations could be performed by using the SQUID-magnetostrictor experimental system.

Bibliography

[1] B. D. Josephson, *Possible new effects in superconductive tunnelling*, Phys. Lett. 1, 251-253, DOI: 10.1016/0031-9163(62)91369-0, (1963).

[2] R. P. Feynman, R. B. Leighton and M. Sands, *The Feynman's lectures on Physics*, Vol. III, *Quantum Mechanics*, paragraph 21.9, Addison-Wesley Publishing Company, 1965.

[3] H. Ohta, *A self-consistent model of the Josephson junction*, IC-SQUID 76, 35, W. De Gruyter, Berlin, 1976, pp. 35-49.

[4] J. G. Bednorz, K. A. Mueller, *Possible high T_C superconductivity in the Ba-La-Cu-O system*, Phys B, Vol. 64, pp.189-193 (1986), DOI: 10.1007/BF01303701.

[5] K. A. Mueller, M. Takashige, J. G. Bednorz, *Flux trapping and superconductive glass state in La2CuO (4-y): Ba*, Physical Review Letters (ISSN 0031-9007), vol. 58, March 16, 1987, pp. 1143-1146. DOI: 10.1103/PhysRevLett.58.1143.

[6] D. X. Chen, A. Sanchez, A. Hernando, *Magnetic properties of slablike Josephson-junction arrays*, Physical Review B (Condensed Matter), volume 50, Issue 18, November 1, 1994, pp.13735-13743.

[7] R. S. Newrock, C. J. Lobb, U. Geigenmueller, M. Octavio, *The two-dimensional physics of Josephson junctions arrays*, Solid State Physics, 2000; volume 54; pp. 263-512; Publisher: Academic Press.

[8] R. De Luca and A. Giordano, *Double and triple-barrier Josephson junctions, Superconductor Science and Technology*, 27 (2014) 115001 (8pp), DOI: 10.1088/0953-2048/27/11/115001.

[9] A. Nakayama, T. Furukawa, Y. Okabe, *Analysis and application to superconducting quantum interference devices of double barrier superconducting junctions*, Journal of Applied Physics, Volume 88, Issue 11, pp. 6605-6609 (2000), DOI: 10.1063/1.1319650.

[10] A. Nakayama, Y. Okabe et al., *Characteristics of superconducting quantum interference devices using multi-barrier superconducting junctions*, Journal of applied Physics, volume 89, Issue 11, pp. 7499-7501, (2001).

[11] R. De Luca, *Feynman's and Ohta's model of a Josephson junction*, Eur. J. Phys. 33 (2012) 1547-1554, DOI: 10.1088/0143-0807/33/6/1548.

[12] A. Giordano, R. De Luca, *From microscopic to macroscopic description of Josephson dynamics in one-dimensional arrays of weakly-coupled superconducting islands*, Results in Physics 5 (2015) 34-38, DOI: 10.1016/j.rinp.2015.01.003.

[13] B. L. Gyorffy, J. B. Staunton, G. M. Stocks, *Pairing, condensation and superconductivity described by a Hubbard model with an attractive interaction*, Physical Review B (Condensed Matter), Volume 44, Issue 10, September 1, 1991, pp. 5190-5208, DOI: 10.1103/PhysRevB.44.5190.

[14] R. De Luca, F. Romeo, *Sawtooth current-phase relation of a superconducting trilayer system described using Ohta's formalism*, Physical Review B, vol.79, Issue 9, id. 094516, (2009) DOI: 10.1103/PhysRevB.79.094516.

[15] A. Barone and G. Paternò, *Physics and applications of the Josephson Effect* (New York, Wiley, 1982), pp. 1-24.

[16] R. De Luca, A. Giordano, and I. D'Acunto, *Mechanical analog of an over-damped Josephson junction*, European Journal of Physics, 36 (2015) 055042, August 2015, DOI: 10.1088/0143-0807/36/5/055042.

[17] D. B. Sullivan, J. E. Zimmerman, *Mechanical analogs of time dependent Josephson phenomena*, Am. J. Phys. 39, 1504 (1971).

[18] F. W. Sears, M. W. Zemansky and H. D. Young, 1977, *University Physics*, 5th ed. (Reading: Addison-Wesley), pp. 301-303.

[19] C. Carapella, G. Costabile, R. De Luca, S. Pace, A. Polcari and C. Soriano, *Josephson equations for the simplest superconducting multiplayer system*, Physica C, Superconductivity 259 (3), pp. 349-355.

[20] I. P. Nevirkovets, J. B. Ketterson, M. Siegel, *Investigations of double-barrier Nb -Al-AIO$_2$ – AI-AIO$_X$ – (Al-) –Nb junctions under high-frequency irradiation*, pp. 1138-1142, IEEE Trans. Appl. Supercond. 11, 1138 (2001), DOI: 10.1109/77.919549.

[21] I. P. Nevirkovets, J. E. Evettes, M. G. Blamire, Z. H. Barber, E. Goldobin, *Investigations of the coupling between the outer electrodes in the superconducting double-barrier devices*, pp. 299-305, Phys. Lett. A 232, 299 (1997) DOI: 0375-9601 (1997) 232: 3-4 <299: IOTCBT> 2.0.Zu; 2-0.

[22] I. P. Nevirkovets, *Coherent response of two nearly identical stacked Josephson junctions to mm wave irradiation*, Appl. Supercond. 5 291, 1997.

[23] A. Brinkman, A. A. Golubov, H. Rogalla, F. K. Wilhelm, M. Yu. Kuprianov, *Microscopic non-equilibrium theory of double-barrier Josephson junctions*, Phys. Rev. B 68, 224513 (2003), DOI: http://dx.doi.org/10.1103/PhysRevB.68.224513.

[24] I. O. Kulik, A. N. Omel'yanchuk, *DC Josephson effect and Andreev reflection*, Sov. J. Low Temp. 4, 142 (1978).

[25] A. Furusaki, *Josephson current carried by Andreev levels in superconducting quantum points contacts*, Superlattices Microstruct. 25, 809 (1999).

[26] R. De Luca, *Magnetic field dependence of the maximum Josephson current in a double-barrier junction*, Physica C 470 (2010), volume 11, pp. 487-491, DOI: 10.1016/J.physC.2010.04.

[27] M. Abramowitz, I. A. Stegun, *Handbook of Mathematical Functions* (New York: Dover), 1965, paragraph 9.

[28] J. Clarke, A. I. Braginsky (Eds.), *The SQUID Handbook, volume 1*, Wiley-VCH, Weinheim, 2004.

[29] R. De Luca, A. Giordano, *Current-voltage characteristics of triple-barrier Josephson junctions*, Physica C 513 (2015) 4-8, DOI: 10.1016/j.physc.2015.03.006.

[30] D. S. Crankshaw, T. P. Orlando, *Inductance Effects in the Persistent Current Qubit*, IEEE Tans. Appl. Supercond. 11, 1006, (2001).

[31] B. Ruggiero, C. Granata, A. Vettoliere, S. Rombetto, R. Russo, M. Russo, V. Corato, P. Silvestrini, *rf SQUID system as tunable flux qubit*, Phys. Lett. A 356, 435, (2006).

[32] R. Gross, A. Marx, and D. Einzel, *From flux quantization to superconducting quantum bits*, Journal of Superconductivity and Novel Magnetism, 19, 331, (2006).

[33] J. R. Friedman, V. Patel, W. Chen, S. K. Tolpygo, and J. E. Lukens, *Quantum superposition of distinct macroscopic states*, Nature 406, 43, (2000).

[34] V. E. Manucharyan, J. Koch, L. I. Glazman, M. H. Devoret, *Fluxonium: single Cooper-Pair circuit free of charge offsets*, Science 326, 113 (2009).

[35] M. F. Bocko, A. M. Herr, A. J. Feldman, *Prospects for quantum coherent computation using superconducting electronics*, IEEE Transactions on Applied Superconductivity 7, 3638 (1997).

[36] J. E. Mooij, T. P. Orlando, L. S. Levitov, L. Tian, C. H. Van der Wal and S. Lloyd, *Josephson persistent current qubit*, Science 285, 1036 (1999).

[37] G. Blatter, V. B. Geshkenbein, L. B. Ioffe, *Design aspects of superconducting-phase quantum bits*, Phys. Rev. B 63, 174511 (2001).

[38] L. B. Ioffe, V. B. Geshkenbein, M. V. Feigel'man, A. L. Fauchere, and G. Blatter, *Environmentally decoupled SDS-wave Josephson junctions for quantum computing*, Nature, 398, (6729), 679-681 (1999).

[39] G. Wendin, V. S. Shumeiko, *Quantum bits with Josephson junctions*, Low Temp. Phys. 33, 724 (2007), http://dx.doi.org/10.1063/1.2780165.

[40] Bin Li, Zu-Huan Yu, Shao-Ming Fei, *Geometry of quantum computation with qutrits*, Scientific Reports 3, 2594, DOI: 10.1038/srep02594, (2013).

[41] M. Morisue, K. Oochi, M. Nishizawa, *A novel ternary logic circuit using Josephson junction* IEEE Trans. on Magnetics 25, 845 (1989).

[42] A. Giordano, R. De Luca, *Quantum analysis of two-junction superconducting interferometers*, work in progress.

[43] R. De Luca, *Quantum interference in Josephson junctions,* Journal of Modern Physics, http://dx.doi.org/10.4236/jmp.2015.65058, April 2015.

[44] R. De Luca, F.Romeo, *Magnetic field dependance of persistent currents in pi-SQUIDs*, Physica C 460-462, 1962 (2008).

[45] F. Zwicky, *Die Rotverschiebung von extragalaktischen Nebeln*, (The Redshift of extragalactic nebulae), Helv. Phys. Acta. 6, 110 (1933), DOI: 10.1007 / s10714-008-0707.

[46] G. Bertone, Dan Hooper, J. Silk, *Particle Dark Matter: Evidence, Candidates and Constraints*, Phys. Rept. 405: 279-391, 2004, DOI: 10.1016 / J. phys.rep.2004.08.031 (August 2004).

[47] G. Chardin, *Dark Matter Direct Detection*, arXiv: astro-ph / 0411503v3, DOI: hal-00000404v2 (28 February 2005).

[48] B. Goldmann et al., EROS Collaboration, *Limits on Galactic Dark Matter with 5 years of EROS Small Magellanic Clouds*, Astron. Astrophys. 400, 951, astro-ph / 0212176, DOI: 10.1.1.256.9525   (6 December 2002).

[49] V.A.Ryabov, V.A.Tsarev, A.M.Tskhovrebov, *The search for dark matter particles*, Phys. Usp. 51, 1091–1121, DOI: 10.1070/PU2008v051n11ABEH006599 (2008).

[50] EROS Collaboration, *Limits on Galactic Dark Matter with 5 years of EROS Small Magellanic Clouds*, Astron. Astrophys. 400, 951, astro-ph / 0212176, DOI: 10.1.1.256.9525   (6 December 2002).

[51] M. Tegmark, D. Eisenstein , M. Strauss, et al., *Cosmological Constraints from the SDSS Luminous Red Galaxies*, Phys. Rev. D 74 123507 (2006); astro-ph / 0608632.

[52] D. Leverington (2000). *New Cosmic Horizons: Space Astronomy from the V2 to the Hubble Space Telescope*. Cambridge University Press. ISBN 0521-65833-0.

[53] M. Green, J. Schwartz, E. Witten, *Superstring theory*. (Cambridge University Press, 1988), p. 436.

[54] S. Capozziello, *Dark Energy models toward observational tests and data*, arXiv: 0706.3587v1 [astro-ph], 25 June 2007.

[55] T. Padmanabhan, *Cosmological Constant - the weight of the vacuum,* Phys. Rept., 380, 235-320, 2003.

[56] S. Capozziello, V. F. Cardone, A. Troisi, *Unified Dark Energy models: a phenomenological approach*, Phys. Rev. D, 69, 083517, 2004, DOI: http://dx.doi.org/10.1103/PhysRevD.69.083316.

[57] A. Kamenshchik, U. Moschella, V. Pasquier, *An alternative to Quintessence*, Phys. Lett. B, 511, 265-268, 2001, DOI: 10.1016/S0370-2693(01)00571-8.

[58] T. Padmanabhan, *Accelerated expansion of the Universe driven by tachionic matter*, Phys. Rev. D, 66, 021301, arXiv: hep-th / 0204150v1, 2002.

[59] S. Capozziello, V. F. Cardone, V. Salzano, *Cosmography of f(R) gravity*, arXiv: 0802.1583 v2 [astro-ph], 8 July 2008.

[60] S. Carboni, P. K. Dunsby, S. Capozziello, A. Troisi, *Some observable effects of Modified Gravity in Cosmology and Astrophysics*, Class. Quant. Grav., 22,4839, 2005.

[61] H. Kleinert, H. J. Schmidt, *Flashing Dark Matter—Gamma Ray Bursts from relativistic detonations of Electro-Dilaton Stars*, Gen. Rel. Grav., 31295, arXiv: gr-qc/0206043, 2002.

[62] G. Jungmann, M. Kamiokowsky, K. Griest, *Supersymmetric Dark Matter*, Phys. Rep. 267 195 (1996); hep-ph / 95063, DOI: 10.1016/0370-1573(95)00058-5.

[63] V. Berezinsky, V. Dokuchaev, and Y. Eroshenko, *Destruction of small-scale dark matter clumps in the hierarchical structures and galaxies*, Phys. Rev. D73, 063504 (2006).

[64] E. Hagelin, D. Nanopoulos, *Supersymmetric Relics from the Big Bang*, Nucl. Phys. B 238, 453-475, (1984), DOI: 10.1016/0550-3213(84)90461-9.

[65] G. Servant, T. Tait, *Is the Kaluza-Klein particle a viable Dark Matter candidate ?*,Nucl. Phys. 650 (2003); hep-ph / 0206071, DOI: 10.1016/S0550-3213(02)01012-x.

[66] D. Hooper, J. Silk, *Searching for Dark Matter with future cosmic positron experiments*, Phys. Rev. D71, 083503, (2005),

[67] D. Smith, N. Weiner, *The status of inelastic Dark Matter*, Phys. Rev. D64 (2001), 043502, arXiv: hep-ph/0402005.

[68] A. Giordano, G. N. Izmailov, R. De Luca, A. M. Tskovrebov, L. N. Zherikhina, V. A. Ryabov, *Search for a Dark Matter component* (work in progress).

[69] A. P. De Cosa, on behalf of CMS, ATLAS collaboration, *LHC results for Dark Matter from ATLAS and CMS*, High Energy Physics-Experiment (hep-ex), arXiv: 1510.01516, (2015).

[70] W. Menn, O. Adriani, et al., *The Pamela space experiment*, Advances in Space Research, volume 51, issue 2, pp. 209-218 (2013), DOI: 10.1016 / J.asr.2011.06.030.

[71] D. Hooper, A. Stebbins, K. M. Zurek, *The PAMELA and ATIC excesses from a nearby clump of neutralino Dark Matter*, arXiv: 0812.3202v1 [hep-ph], (2008).

[72] R. Bernabei et al., *Dark Matter search*, Eur. Phys. J. C23 (2002), 61.

[73] W. R. Leo, *Techniques for Nuclear and Particle Physics experiments*, Springer-Verlag, pp. 59-63.

[74] G. B. Khristiansen, *Prospects for studying cosmic rays at ultrahigh energies (10^{15}-10^{21} eV)*, Sov. Phys. Usp. **30,** 1110–1112 (1987), DOI: 10.1070/PU1987v030n12ABEH003075.

[75] M.Fradkin, L.Kurnosova, N.Topchiev et al., *Some tasks of observational gamma-ray astronomy in the energy range 5-400 GeV*: Space Science Reviews. **49**, 215-226 (1988).

[76] A.M.Galper, N.P.Topchiev et al., *Status of the GAMMA-400 Project,* Advances in Space Research. **51** (2), 297-300, arXiv: 1507.06246, DOI: S1875389215013826, (2013).

[77] G. N. Izmailov, *Superconductors as detectors of particles of Dark Matter*, Measurement Techniques, Vol. 51, No. 11, 2008, DOI: 10.1007/s11018-009-9182-x.

[78] R.Bernabei et al., *Searching for WIMPs by the annual modulation signature*, Int. J. Mod. Phys. D **13** 2127-2160, astro-ph/0501412, (2004).

[79] R. Bernabei et al. (2012), *Performances of the new high quantum efficiency PMTs in DAMA / LIBRA*, Eur. Phys. J. C 8: 03009. arXiv: 1002.1028, Bibcode: 2012 jnst…7.3009B. DOI: 10.1088 / 1748-0221 / 7 / 03 / P03009.

[80] A.I.Golovashkin, V.G.Elenskij, K.K.Likharev, *Josephson effect and its application*, Moscow: Science (1983), pp. 38-44.

[81]A. Barone, G. Paternò, *Physics and applications of the Josephson effect*, Wiley (1982), p. 529.

[82] A. I. Braginski (Eds), *The SQUID Handbook (volume 2)*, Wiley (2006), pp. 81-94.

[83]   J. Clarke, *Small-scale analog applications of high-transiction-temperture superconductors*, Physics Today, March 1986, pp. 36-44.

[84]   A.I.Golovashkin, A.V.Gudenko, L.N.Zherikhina, O. M. Ivanenko, K.Yu.Mitsen A.M.Tskhovrebov, *Fluctuation limit of measurements of the relative elongation of a magnetostrictive cylinder*, JETP letters 60 (8), 612, 1994.

[85] J. V. Maslennikov, V. J. Slobodchikov, *Superconducting magnetometers in biomagnetic research*, Biomedical radioelectronics № 8, 2000.

[86] G.Angloher et al, *Results on low mass WIMPs using an upgraded CRESST-II*, Astropart. Phys. **23**, 325, arXiv: 1407.3146v2 [astro-ph.CO], 2005.

[87] M. Buhler, E. Umlauf, *The noise of the magnetic bolometer*, J. Low Temp. Phys. 93, 697-702 (1993), DOI: 10.1007 / BF00693498.

[88] L. N. Zherikhina, A. I. Golovashkin, V. M. Mishachev, V.F.Troitskij, A.M.Tskhovrebov *Potentialities of method of adiabatic demagnetization in low background experiments*, Journal of Applied Physics (Russia) 6, 27-34 DOI: 10.3103 / S1068335607100053, 2003.

[89] O.V.Lounasmaa, *Experimental principles and methods below 1K*, (London and New York, Academic Press 1974), p. 4.

[90] A.I.Golovashkin, G.N.Izmailov, L.N.Zherikhina, G.V.Kuleshova, A.M.Tskhovrebov, *Magnetic calorimeter with a SQUID for detecting weak radiations and recording the ultralow energy release*, Quantum Electron **36** (12), 1168–1175,
DOI: 10.1070 / QE2006v036n12ABEH013272, (2006).

[91] A.I.Golovashkin, G.N.Izmaïlov, G.V.Kuleshova, T.Q.Khánh, A.M.Tskhovrebov, L.N.Zherikhina, *Magnetic calorimeter for registration of small energy release*, Europe Physics Journal B, **58** (3), 243-249, DOI: 10.1140 / epJb /e2007-0022-4, (2007).

[92] A.I. Golovashkin, G.N.Izmaïlov, V.A.Ryabov, A.M.Tshovrebov, L.N.Zherikhina, *Dark Matter Particle Detection System SQUID-Magnetic Calorimeter*, Amer. J. of Mod. Phys. 2(4), 208-216 (2013), DOI: 10.11648 / J. ajmp. 20130204.15.

[93] G.N.Izmaïlov, L.N.Zherikhina, A.M.Tshovrebov, *Measurements of ultrasmall energy releases: adiabatic calorimeters with magnetic and dielectric absorbers*, Measurement technology (Russian) 5, pp. 3-17, (2015).

[94] M.A.Dresvyannikov, A.L.Karuzskii, A.V.Perestoronin, A.M.Tskhovrebov, L.N.Zherikhina, *Photoresponse Beyond the Red Border of the Internal Photoeffect (Designing Problems of Photon Counting Schemes in 10 Mu M Band*, Proceedings of SPIE, 9440, ed. Orlikovsky A., Spie-Int Soc. Optical Engineering, 2014, ISBN: 978-1-62841-555-1.

[95] P. Agnes, T. Alexander, G. Fiorillo, et al., *First results from the Dark Side-50 dark matter experiment at Laboratori Nazionali del Gran Sasso*, Physics Letters B, 9 April 2015, arXiv: 1410.0653 [astro-ph. CO], DOI: 10.1016 / J. physletb. 2015.03.012.

[96] C. E. Aalseth, P. Agnes, G. Fiorillo, et al., *The Dark Side Multiton detector for the direct Dark Matter Search*, Advances in high Energy Physics, vol. 2015, Article ID 541362, DOI: 10.1155 / 2015 / 541362.

[97] E. Aprile *et al.* (XENON Collaboration), *Exclusion of Leptophilic Dark Matter Models using XENON 100 electronic recoil data*, Science 2015 vol. 349 no. 6250 pp. 851, and *Search for event rate modulation in XENON 100 electronic recoil data*, Physical Review Letters 115, 091302 (2015), arxiv.1507.07748, DOI: 10.1103/PhysRevLett.115.091302.

[98] F. Ruppin, J. Billard, E. Figueroa-Feliciano, L. Strigari, *Complementarity of dark matter detectors in light of the neutrino background*, (2014).
Phys. Rev. D, 90, 083510, http://dx.doi.org/10.1103/PhysRevD.90.083510.

[99] J. Beringer et al., *Review of Particle Physics, 2013 partial update*, Phys. Rev. D 86.010001, 8 May 2015, DOI: 10.1103/PhysRevD.86.010001.

[100] A.V. Durbins, *Search of magnetic moment of neutrinos*, Elementary-particle physics and atomic nucleus 32 (3) 734-749 (2001).

[101] M. Robinson, *Symmetry and the Standard Model*, Mathematics and Particle Physics-Springer, pp. 252-264.

[102] M.B. Voloshin, M.I. Vysotskii, L.B. Okun, *Neutrino electrodynamics and possible consequences for solar neutrinos*, JETP 64 (3), 446, DOI: 10.1088/1126.6708/2007/11/055, (1986).

[103] G. Raffelt, *The Nature of Dark Matter*, arXiv: astro-ph / 951104v1, DOI: MPI-PTh / 95-115 (10 November 1995).

[104] B. S. Neganov et al., *The movable polarized target as a basic equipment for high energy spin physics experiments at the JINR-Dubna accelerator complex*, J. Low Temp. Phys. 93, 745-749, DOI: 10.1016/0168-9002(94)01445-0, (1993).

[105] M. Gozdz, W. A. Kaminsky, *Neutralino Induced Majorana Transition Magnetic Moments*, arXiv: 1201.1243 [hep-ph], DOI: 10.1142 / SO218301309013312 (2014).

[106] B. H. Bransden, C. J. Joachain, *Quantum Mechanics (second edition)* Pearson Prentice Hall, pages 435-443.

[107] H.Velten, D J.Schwarz, J.C.Fabris, W Zimdahl, *Viscous dark matter growth in neo-Newtonian cosmology*, Phys. Rev. D **88**, 103522, DOI: 10.1103/PhysRevD.88.103522, (2013).

[108] H. Velten, J. Wang, X. Meng, *Phantom dark energy as an effect of bulk viscosity*, Phys. Rev. D **88**, 123504, DOI: 10.1088/0004-638X/ (2013).

[109] G.N. Izmailov, L.N.Zherikhina, V.A. Ryabov, A.M. Tskhovrebov. *Dark Energy: The Nature and Feasibility of Laboratory Registration using SQUID-Magnetostrictor System*, in Dark " Eds: K.Lefebvre, R.Garcia. Nova Sc. Pub., DOI: 10.3103/S1068335612090048, (2010).

[110] A.I.Golovashkin, L.N.Zherikhina, A.M.Tskhovrebov, G.N.Izmailov, *Supersensitive SQUID/magnetostrictor detecting system*, Quantum Electronics   **42** (12), 1140–1146 (2012), DOI: 10.1070/QE2012v042n12ABEH000000 (13 June 2012).

[111] J. Bardeen, L. N. Cooper, J. R. Schrieffer, *Theory of Superconductivity*, Phys. Rev. 108(5): 1175-1204, December 1958.

Acknowledgements